

DURABILITY AND DIFFUSIVE BEHAVIOUR EVALUATION OF GEOPOLYMERIC MATERIAL

by

Yolandi Muntingh

*Thesis submitted in partial fulfilment of the requirements for the
Degree of:*

**MASTER OF SCIENCE IN ENGINEERING
(CHEMICAL ENGINEERING)**

*in the Department of Process Engineering
at the University of Stellenbosch*



Supervised by

Prof. Leon Lorenzen (University of Stellenbosch, South Africa);

Prof. Jannie van Deventer (University of Melbourne, Australia).

STELLENBOSCH

December 2006

DECLARATION:

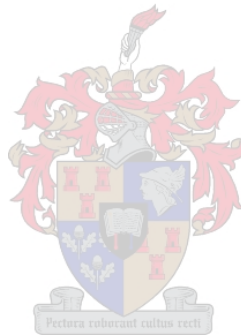
I, the undersigned, hereby declare that the work contained in this thesis is my own original work and that I have not previously in its entirety or in part submitted it at any university for a degree.

I certify that the work has been undertaken solely by the candidate, except where due acknowledgement is provided. The text of this work, inclusive of figures, references and appendices, does not exceed 40 000 words.

Signature:

YOLANDI MUNTINGH

Date:



*Copyright © 2006 Stellenbosch University
All rights reserved*

ABSTRACT:

The study presented in this thesis symbolises one of the first ever efforts to better understand and describe the durability of geopolymers used in large scale commercial applications. In terms of the construction industry, geopolymers can be seen as a value-added approach to substitute the Ordinary Portland Cement (OPC) monopoly. It is particularly the fly ash-based geopolymers that are the main attraction, due to their economic and environmental advantages, over and above the large quantities of this material that are commonly available.

Despite the fact that geopolymers have been around for thousands of years, it is only now that the accumulation of research across the globe has pooled their knowledge to broadly define this material in terms of its physical and chemical composition. The development of geopolymers for construction applications remains quite new, therefore requiring insight into the durability that can be expected from these materials, consequently leading to this work.

Concrete technology and -science is one of many techniques which can offer considerable insight into effective durability studies, in addition to acting as a reference for firm material comparisons. Thus, this work is based on a collection of concrete durability studies and recommendations which resulted from a broad range of investigations. Principally, this work aims to confirm the superiority of geopolymers in terms of corrosion resistance.

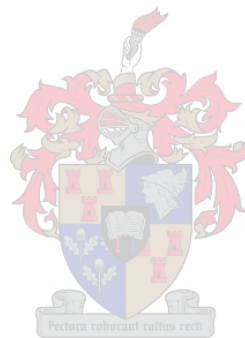
Chloride induced corrosion has been identified as being the main cause for deterioration of OPC structures and subsequently the origin of very costly, and frequent, reconstructive requirements. Geopolymers now have the opportunity to be introduced into this monopoly due to its advanced, yet credible, chloride penetration resistance. This thesis reports the development of the experimental design, as well as the associated analyses to describe the diffusive properties exhibited by fly ash-based geopolymers. Ultimately, two independent methods showed that Chloride Diffusion Coefficients (CDC) for all of the geopolymeric formulations are significantly lower (typically $1.43 \times 10^{-15} \text{ cm}^2/\text{s}$) than for cement (typically $0.5 \times 10^{-8} \text{ cm}^2/\text{s}$) or any other concrete mixture.

Furthermore, the work presented here will consider the diffusive behaviour of the geopolymer formulations in an acidic sulphate environment, presenting this material's superior resistance not only to the sulphate ion, but more so to the acid attack. Probable geopolymer applications are now further expanded to industrial applications, due to its acid resistance along with reduced Sulphate Diffusion Coefficients (SDC).

In addition, the development of a time-to-corrosion software-tool is discussed. This tool may prove to be a valuable instrument for future geopolymer durability research, as well as

commercial users in which extended material comparisons can be made. It may even assist the formulation-tailoring process where the relevant CDC/SDC can be chosen for a specific life-expectancy, reaching far beyond the limited scope of recipes covered in this work.

Finally, this thesis provides the stepping-stone in proving geopolymer durability superiority. The formulations which proved to show the best results in terms of durability and acid resistance are highlighted and valuable recommendations are made towards the selection of suitable starting materials for optimum material robustness. The findings of this work, however, can be fortified by future research and exposure.



OPSOMMING:

Hierdie tesis simboliseer die eerste probeerslag om effektief die weerstands-vermoë van geopolimere beter te verstaan en te definieer. Dit is veral belangrik om die leeftyd van dié materiale in gevorderde industriële toepassings akkuraat te voorspel en met dié van Gewone Portland Sement (GPS) te vergelyk. Klem word op vlieg-as-gebaseerde geopolimere geplaas vanweë die moontlike ekonomiese- en omgewings voordele wat hul inhou, asook die maklike toeganklikheid tot groot hoeveelhede van die stof.

Geopolimere is vermoedelik al duisende jare terug ontdek, maar dit is eers onlangs (te danke aan die versameling van navorsings-kennis reg oor die wêreld) in breër terme van sy chemiese en fisiese komposisie gedefinieer. Die gebruik van die geopolimere as konstruksie materiaal is egter nog uiters beperk; as gevolg van beperkte weerstands-vermoë kennis. Dit is juis die beperking wat eindelijk gelei het tot hierdie navorsings-projek.

Bestaande beton tegnologie- en kundigheid skep 'n goeie platform vanweë die insig in gebruikelike weerstands-metodes wat omskep is in toepaslike metodes vir die analisering van geopolimere. Die breë spektrum van bestaande literatuur in die verband het nie slegs tot die eindelike eksperimentele metodes gelei nie, maar ook as gevestigde vergelykingspunt opgetree. Dit is nou moontlik om kwalitatief die verwagte weerstand van geopolimere met beton te vergelyk.

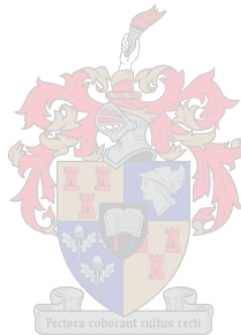
Chloried-verwante korrosie is aangewys as die hoof bydraer tot gewapende-beton strukture se agteruitgang. Die hoë-koste beton-rekonstruksie wat deurgangs geëis word, skep nou die weg vir geopolimere, as meer duursame materiaal, om sy verskyning te maak. Indien dit binne geloofwaardige perke bewys kan word dat geopolimere die deurdringing van chloriedes beter kan weerstaan, is die stryd reeds halfpad gewonne. Die klem val nou op die feit dat die werk in die tesis op twee onafhanklike maniere bewys dat geopolimere se Chloor Diffusie Koeffisiënt (CDK) aansienlik laer is as dié van enige mengsel beton of semet s'n is.

Verder, is die Sulfaat Diffusie Koeffisiënt (SDK) ook vir al die prosesse bepaal. Die verskil is in die suuragtige omgewing waarin die sulfaat blootstelling voorkom. Die metode dien 'n tweeledige doel: Eerstens om die diffusie vermoë van geopolimere met dié van beton te vergelyk en tweedens om sy weerstand teen 'n sterk suur te ondersoek. Die geopolimere monsters het uitgeblink in beide van die ondersoeke.

Die ontwikkeling van 'n sagteware pakket word ook bespreek. Die doel van die pakket is om toekomstige resepte op gelyke basisse te kan vergelyk, veral die resepte wat nie in die tesis aangeraak word nie. Die sagteware maak die omgekeerde ook moontlik, waar 'n gekose

sturktuur leeftyd die ooreenkomstige diffusie koëffisiënt sal bied. Hierdie mag 'n waardevolle instrument vir toekomstige navorsers, asook kommersiële gebruikers van geopolimere wees.

Om af te sluit: Die werk dien as die begin-punt waar geopolimere se gevorderde weerstands-vermoë teen alledaagse verwerking as konstruksie materiaal bewys word. Die resepte wat die beste in al die omstandighede gevaar het, word beklemtoon en waardevolle voorstelle vir die mees gepaste grondstowwe word uitgewys. Die sukses van die werk hang egter af van die mate van blootstelling en toekomstige navorsing wat die veld gaan geniet. Aanvanklike blootstelling het in die vorm van plaaslike konferensies geskied, asook 'n beplande publikasie in 'n geakkrediteerde joernaal.



ACKNOWLEDGEMENTS:

Hereby I would like to acknowledge and thank the following personae and entities whom have contributed to the work presented in this thesis, either directly or indirectly:

For all the hours of advice, support and the wonderful opportunity to see, live and learn in another country:

Prof. Leon Lorenzen; Prof. Jannie van Deventer

And for those who had to deal with the soaring highs and trenced lows:

Derek Muntingh; Laetetia Muntingh; Melissa Muntingh and Charl Maree

For financial support:

The financial assistance of the National Research Foundation (NRF) towards this research is hereby acknowledged. Opinions expressed and conclusions arrived at, are those of the author and are not necessarily to be attributed to the National Research Foundation.

Sincere thanks to Charl Maree for assisting in the software side of this work, and to all my friends for the laughter, wine and memorable experiences during this time.

I thank all the members of the Melbourne Geopolymer Group (in particular: Catherine, Louise, Redmond, Sindhu, Peter and Grant) for project-saving advice and the free-flow of valuable information and experiences. Sincere appreciation towards Sjoerd for technical assistance on the Dionex as well as his valuable input on finding one's way on the Australian public transport system, considering the fact that he is a born-and-bred New Zealander.

Finally, heartfelt appreciation to those assisted in the creation of some of my unusual designs:

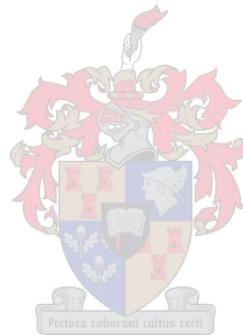
Jannie Barnard; Anton Cordier; Melbourne University Workshop

and to those playing significant roles in the analytical phase of this work:

Hanlie Botha, Riana Rossouw (Geology), Prof. W. Przybyłowicz (iThemba Labs), Chris Ryan: CSIRO (Melbourne Univeristy).

"Ability is of little account without opportunity."

-NAPOLEON BONAPARTE



"You can't build a reputation on what you're going to do."

-HENRY FORD

TABLE OF CONTENTS:

DECLARATION:	II
ABSTRACT:	III
OPSOMMING:	V
ACKNOWLEDGEMENTS:	VII
CHAPTER 1.	1
CHAPTER 2.	4
2.1. GEOPOLYMER LITERATURE	5
2.1.1. <i>Introduction to geopolymer literature</i>	5
2.1.2. <i>Geopolymerisation</i>	5
2.1.3. <i>Geopolymerisation models</i>	8
2.1.4. <i>Geopolymer recipe formulation</i>	10
2.1.5. <i>Effect of source materials on geopolymerisation</i>	11
2.1.6. <i>Effect of temperature and alkalinity on geopolymerisation</i>	12
2.1.7. <i>Immobilisation through Geopolymers</i>	13
2.1.8. <i>Geopolymeric gel-phase</i>	15
2.1.9. <i>Geopolymer applications</i>	16
2.1.10. <i>Geopolymer manufacturing</i>	17
2.1.11. <i>Geopolymer compressive strength characteristics</i>	17
2.1.12. <i>Common analytical techniques associated with geopolymers</i>	19
2.1.13. <i>Classification of fly ash</i>	21
2.1.14. <i>Expected geopolymer durability</i>	22
2.2. CEMENT AND CONCRETE LITERATURE	22
2.2.1. <i>Introduction to cement and concrete technology</i>	22
2.2.2. <i>Chloride induced corrosion</i>	23
2.2.3. <i>Corrosion determination</i>	24
2.2.4. <i>Accelerated chloride-ion diffusion test</i>	25
2.2.5. <i>Half-cell potential test</i>	27
2.2.6. <i>Chloride detection through PIXE</i>	28
2.2.7. <i>Alternative corrosion measurements</i>	29
2.2.8. <i>Relevance to geopolymers</i>	29
2.3. SUMMARY	31
CHAPTER 3.	32
3.1. INTRODUCTION	33
3.1.1. <i>Methodology</i>	33
3.1.1.a. Starting materials.....	34
3.1.1.b. Synthesis	34
3.1.1.c. Diffusion Coefficient Determination	35
3.1.2. <i>Diffusion cell</i>	36
3.1.3. <i>PIXE (Proton Induced X-Ray Emission)</i>	40
3.2. CORROSION MONITORING	41
3.2.1. <i>Copper/copper-sulphate half-cell</i>	42
3.3. PORE CHARACTERISATION	45
3.3.1. <i>Total pore volume</i>	45
3.3.2. <i>BET surface area</i>	46
3.4. EMBEDDED SENSORS	46
3.5. OSMOTIC POTENTIALS FOR GEOPOLYMERS	48
3.6. ANALYTICAL TECHNIQUES	49
3.6.1. <i>X-Ray fluorescence spectroscopy (XRF)</i>	50
3.6.2. <i>X-Ray diffraction (XRD)</i>	50
3.6.3. <i>Compressive strength testing</i>	50
3.6.4. <i>Inductively coupled plasma spectroscopy (ICP-OES)</i>	51
3.6.5. <i>Scanning electron microscopy (SEM)</i>	51
3.6.6. <i>Infrared spectroscopy (IR)</i>	52

3.6.7. Ion Chromatograph (IC).....	52
3.7. SUMMARY	53
CHAPTER 4.	54
4.1. PORE-VOLUME, -AREA AND COMPRESSIVE STRENGTH	55
4.2. THE EFFECT OF AGGREGATE ON PORE VOLUME RESULTS	59
4.3. AVERAGE HALF CELL POTENTIALS	62
4.4. GEOPOLYMER HYDROSTATIC PRESSURE POTENTIAL	64
4.4.1. <i>Sensor force readings</i>	67
4.5. SUMMARY	69
CHAPTER 5.	70
5.1. EFFECT OF CURING CONDITIONS	71
5.2. INITIAL TEST FOR CORROSION.....	72
5.3. DIFFUSION CELL CHLORIDE COEFFICIENTS.....	73
5.4. PIXE CHLORIDE DIFFUSION COEFFICIENTS	80
5.5. CHLORIDE DIFFUSION AND CORROSION.....	82
5.6. SUMMARY	87
CHAPTER 6.	89
6.1. SULPHATE DIFFUSION PROFILES AND –COEFFICIENTS	90
6.2. APPARENT GEOPOLYMER ACID RESISTANCE	95
6.3. COMPARING GEOPOLYMER SDC TO CEMENT LITERATURE.....	96
6.4. SUMMARY	97
CHAPTER 7.	98
7.1. GEOPOLYMER DIFFUSION COEFFICIENTS	99
7.1.1. <i>Chloride diffusion coefficient (CDC)</i>	99
7.1.2. <i>Acidic sulphate diffusion coefficient (SDC)</i>	100
7.2. PORE CHARACTERISATION VERIFICATION.....	100
7.2.1. <i>Varying activation concentrations</i>	101
7.2.2. <i>Varying water content</i>	102
7.2.3. <i>Varying GGBFS content</i>	103
7.2.4. <i>Varying aggregate content</i>	104
7.2.5. <i>Samples containing both aggregate and GGBFS</i>	104
7.2.6. <i>Theoretical time-to-corrosion comparisons</i>	105
7.3. SUMMARY	108
CHAPTER 8.	110
REFERENCES:	113
APPENDIX A.....	123
APPENDIX B.....	129
APPENDIX C.....	132
APPENDIX D.....	134
APPENDIX E.....	135
APPENDIX F	136
APPENDIX G	139

LIST OF SYMBOLS:

Commonly used symbols and acronyms:

Symbol	Description	Units
[Cl]	Chlorine-ion concentration	mol/litre
A	Exposed Area	cm ²
ACID	Accelerated Chlorine Ion diffusion test	-
C _{ci}	Cathode concentration	mol/litre
CDC	Chloride diffusion coefficient	cm ² /s
C _s	Surface concentration	mol/litre
CSH	Calcium silica hydrates	-
C _{th}	Threshold concentration	mol/litre
dc	Cover depth	cm
D _{ci}	Chlorine diffusion coefficient	cm ² /s
F	Faraday's Constant	C/mol
FA	Fly Ash	-
I.C.	Ion Chromatography	-
L	sample length	cm
LC	Long Curing method (28 days @ ambient T)	-
OOB	Out of Bounds (sensor/ multimeter range)	-
PPE	Personal Protective Equipment	-
PSD	Particle size distribution	-
PV	Pore Volume	m ³ /g
R	Universal Gas constant	J/mol.K
SA	Surface area	m ² /g
SC	Short Curing method (oven curing)	-
SDC	Sulphate diffusion coefficient	cm ² /s
SG	Specific gravity (basis: H ₂ O @ 25°C)	-
Slag	Ground Granulated Blast Furnace Slag	-
Std	I.C. Standard used in calibration	-
T	Absolute Temperature	K
T _i	Time to corrosion	seconds
V	Cell volume	litre
wt	Weight	-
Z _{ci}	Electrical charge	-
ΔE	Potential difference	V

Chapter 1.

INTRODUCTION

Geopolymerisation, in essence, is a relatively new technology which originated from very old principles. The durability of ancient construction materials continued to interest the development of a New Generation Material, which may even be able to provide valuable waste-management solutions. Geopolymers have been developed largely by Joseph Davidovits in Saint-Quentin, France, but the advancement of these materials to current base of knowledge has been done all over the world (**Phair, 2001**).

Often made largely out of industrial waste materials, geopolymers are a feasible and cost competitive alternative for Ordinary Portland Cement (OPC). Currently, the replacement of geopolymers into concrete technology has been slow and tedious. This may be largely due to the earlier poor understanding of the properties and durability of geopolymers, but this knowledge gap is being filled at rapid pace, thanks largely to all the work done by some of the top Universities in the world.

This thesis focusses specifically on the expected durability of fly ash-based geopolymers in an effort to improve the understanding in this field, as well as accelerating the incorporation of geopolymeric systems into cement and concrete technology. The investigation of fly ash-based geopolymers is made due to their relatively lower cost and simple synthesis procedures compared with many other geopolymer variants. Specific material properties will be determined, where chloride- and sulphide diffusion coefficients will be the predominant consideration. A selection of techniques will be employed in the determination of these coefficients, along with numerous other material property variants that will be considered (such as BET surface area, specific pore volume, compressive strengths, etc).

With the intention of effectively defining geopolymer durability as a construction material, an intensive study on existing geopolymer literature was required. **Chapter 2** introduces this large number of available literature in a concise manner with emphasis on the development towards the recent geopolymer body-of-knowledge in terms of its micro-, macrostructure and relevant chemistry. The chapter also discusses relevant cement- and concrete literature, particularly those covering durability and diffusion issues. A large proportion of the experimental design and methodology presented in **Chapter 3** originated from principles and recommendation by past cement durability investigations.

The angle of approach to the experimental design presented in **Chapter 3** was focussed on two main considerations. Firstly, seeing that fly ash is prone to batch-to-batch deviations, the exact amount required for each specific formulation for every required analysis was predetermined. Ultimately, all of the specimens used per formulation originated from a mutual batch. Secondly, the experiments had to match those used in the concrete literature in order to effectively compare results, especially in the cases of comparing chloride diffusion coefficients. Due to the extremely complex system within fly ash materials as used in this investigation, batch-to-batch deviations could lead to trivial data and effectively damage the scientific credibility of the presented results.

This work focusses on 25 geopolymer formulations; where two Class F fly ashes are compared upon varying the activation solution concentration, water content, slag content and aggregate addition. The 25th formulation is a fly ash A-based geopolymer containing both aggregate and slag. The classification of fly ash will be discussed in **Chapter 2** and two variants of fly ashes used in this work will be introduced in **Chapter 3**.

Certain distinguishing physical properties to each formulation had to be determined in order to successfully elucidate the diffusive and permeation effects exhibited by subsequent chapters. **Chapter 4** discusses these physical properties and also introduces an initial estimation of the pore characteristics upon varying the geopolymer formulation. Verifying this initial pore characterisation hypothesis was attempted through the hydrostatic potential displayed by a selection of formulations. Some extent of confirmation of the hypothesis was obtained, but the final confirmation is only achieved in **Chapter 7**.

The importance of chloride induced corrosion of OPC structures was identified fairly early in this project, shifting the focus to prove the superior chloride permeation resistance exhibited by geopolymers. The main focus in **Chapter 5** lies in the associated tests in obtaining trustworthy Chloride Diffusion Coefficients (CDC) for each geopolymer formulation. Initially, the coefficients obtained from the Accelerated Chloride Diffusion Test (ACID) are discussed and compared for each fly ash used as well as general OPC findings. Thereafter, the coefficients are weighed against CDC obtained through PIXE analyses. These two independent methods produced results in very close proximity; advocating the credibility of the ACID values. Copper/Copper-Sulphate half potential values are also discussed in **Chapter 5**, attempting to correlate the CDC values with the extent of corrosion. Some success is gained, along with deviations from the expected trends. The latter is discussed at the end of the chapter.

Sulphate diffusion, although not portrayed as the major deterioration factor by cement and concrete researchers, is considered in **Chapter 6**. The experimentation is based on the ACID tests carried out in **Chapter 5**, while the core difference lies in the acidic sulphate solution

used. The importance of including either slag or aggregate (preferably both) is highlighted, where high levels of sulphate and acid resistance are exhibited by these formulations. Similarities and differences between the two ashes, differences in formulation and sulphate diffusion coefficients measured for OPC are considered, once again highlighting the superior permeability resistance of geopolymers.

The focus of **Chapter 7** is to act dually as a “summation” tool for results presented in preceding chapters, as well as a means to clarifying the validity of the pore characterisation hypothesis pointed out in **Chapter 4**. This chapter also emphasises the fact that the majority of results throughout this project is directed towards the improved chloride-, sulphate and acid resistance by geopolymers. **Chapter 7** is concluded by considering a theoretical time-to-corrosion comparison to OPC literature. A simplistic Delphi7™ based programme is introduced, which can readily be used by future workers to evaluate geopolymer formulations not covered in this work.

This thesis covers a number of topics within the broader durability definition, with a great deal of attention driven towards comparing geopolymers to OPC data recorded by previous investigators. For this reason almost all of the chapters are written in an individually-based manner, providing rounded reading for those interested only in particular sections.



Chapter 2.

REVIEW OF GEOPOLYMER TECHNOLOGY AND RELEVANT CEMENT AND CONCRETE RESEARCH

This chapter provides an introduction to geopolymer- and the relevant cement and concrete technology, by re-evaluating the development of the Ordinary Portland Cement as well as the Geopolymer body of knowledge. Considerable attention is given to the major durability challenges facing the current concrete industry, as this forms the wider inspiration for this thesis. This chapter also serves as a preface to the main technical considerations in the development and application of concretes for industrial as well as waste management purposes. The aim is to ultimately compare the performance of geopolymer materials in replicated tests to published literature on cementitious materials.

Differences between OPC and Fly ash-based geopolymers will be discussed in broader physical, chemical and material properties by thoroughly reviewing the literature covering various aspects of OPC and geopolymers and presenting it in a Chemical Engineering adapted perspective. Due to the extensive number of accessible literature on cement and concrete technology, only the key publications will be mentioned here. Please refer to earlier works of **Mindess & Young (1981)**, **Neville (1995)** and **Popovics (1979)** for more extensive views on concrete and cement chemistry.

2.1. Geopolymer literature

This section discusses the broad geopolymer description, serving the purpose of general introduction to these materials, as well as establishing the foundation to this thesis.

2.1.1. Introduction to geopolymer literature

The literature refers to the term “geopolymer” as a matrix consisting of an aluminosilicate source (usually in the form of fly ash, metakaolin and blast furnace slag) which is activated by an alkaline sodium/potassium silicate solution at ambient conditions or slightly elevated temperatures (**Goretta et al., 2004**). The matrix is best described as a unique three dimensional amorphous to semi-crystalline network of polysialate and siloxane bonds, where sialate is a Si-O-Al bond (**Duxson et al., 2005b**) and siloxane is a Si-O-Si bond. Polysialate chemistry forms the basis tool for describing the microstructural properties of geopolymer matrices (**Phair et al., 2000b**). According to Loewenstein’s rule no two aluminium ions can occupy the centres of a tetrahedra linked by a single oxygen ion, therefore forbidding Al-O-Al links. **Duxson et al. (2005b)** together with **Provis et al. (2005c)** disproved this theory through a ^{29}Si NMR study.

It should also be noted that the term “geopolymer” has previously been used to refer to fossilised organic rock polymers consisting mainly out of kerogens and coals (**Van Jaarsveld, 2000**). This definition will be disregarded from this point onwards.

2.1.2. Geopolymerisation

Geopolymer chemistry has often been associated with that of zeolites, since they have comparable chemical compositions (**Xu & van Deventer, 2002a; Gokhale, 2001; Provis et al., 2005a; Lloyd & van Deventer, 2005**). The most significant difference between these two materials is the X-ray amorphous structure of a geopolymer in comparison with the highly crystalline structure of zeolites. It should be noted here that X-ray amorphous refers to the possible detection levels produced by instrumentation such as XRD. It should not be assumed that the matrix is completely amorphous, seeing that nanometres-sized crystalline structures can be overlooked by instrument restrictions (**Provis et al., 2005a**). Even in the earlier stages of research in this field, **Van Jaarsveld et al. (1998)** reasoned that geopolymeric binders are the synthetic analogues of natural zeolitic materials and require equivalently hydrothermal conditions for synthesis. **Lloyd & van Deventer (2005)** referred to work by **Provis et al. (2005d)** where the main difference between geopolymers and zeolites is actually the difference in amount of water present. Geopolymer synthesis is generally at ratios 10 to 100 times (solids to liquid) higher than zeolites, taking in account that the materials are synthesised from the same reactants and under very similar conditions. This may carry significant importance, seeing that there can now be a thermodynamic examination on the stability of geopolymers. In turn, the key chemical composition difference between

geopolymers and Portland cement is believed to be calcium, where calcium is not essential in any part of the basic geopolymer structure (Yip & van Deventer, 2005c).

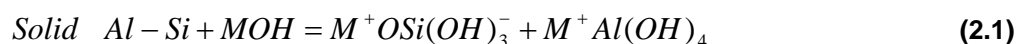
Numerous proposals for the apparent geopolymerisation mechanism have been published. None of them, however, can directly prove or describe the physical nature of the reaction. The ion-pair theory is believed to be the mechanism of mineral dissolution as well as the mechanism for geopolymerisation (Xu et al., 2001). The research, on the other hand, still lacked a precise reaction mechanism for the complex gel formation, setting and hardening phases.

One certainty is that the dissolution of the starting materials is not complete before the final hardened matrix is formed (Van Jaarsveld et al., 2004d; Xu et al., 2001) and in many cases a surface reaction binds the undissolved particles into the matrix (Phair et al., 2001b).

A more detailed chemical mechanism has been proposed for the formation of two different phases – a calcium silicate phase and a sodium aluminosilicate phase - in the presence of Ground Granulated Blast Furnace Slag (GGBFS) with alkali activation of metakaolin (Yip & van Deventer, 2003). This mechanism may even be applicable to more systems and not restricted to a GGBFS and metakaolin system.

Currently it is believed that geopolymer reaction takes place through 3 main steps (Gokhale, 2001; Van Jaarsveld et al., 2002):

1. Dissolution (described by the complexing action of hydroxide species)



Here M denotes the alkali cation Na⁺ or K⁺. The complexing reaction shown in Equation 2.1 illustrates the intricate reaction mechanism in the geopolymer system. Although this mechanism is not yet fully understood some researchers (Lee & van Deventer, 2003) have proposed that the amount of soluble silicates in the system promotes the dissolution process of the aluminosilicate species. Keyte et al. (2005) recommended that the soluble silicates increase the initial concentration of dissolved silicon, therefore resulting in faster deprotonation and consequently more dissolution. Others (Xu et al., 2004) suggested that the OH⁻ species hydrolyse the oxide bonds at the surface of the aluminosilicate source, therefore promoting the aqueous products shown in Equation 2.1. A factor one should allow for is that the dissolution process will be different in fly ash and metakaolin systems, where metakaolin is a calcinated clay and not a glass structure like fly ash (Keyte et al., 2005). The dissolution will differ due to particle size and shape, as well as the stability of the Al-Si source.

One point all the researchers agree upon, is the importance of the dissolution phase of the reaction. It is here where the initial [Al] and [Si] are generated for the reaction to start.

2. Partial orientation and partial internal restructuring of the species.

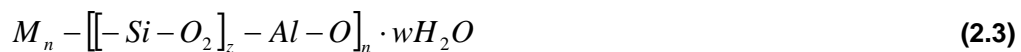


Xu & van Deventer (2002a) suggest that this is mainly a physical electrostatic reaction, where the M^+ cation reacts in a cation-anion pair condensation with the divalent-orthosilic acid and trivalent-orthosilic acid ions to balance the resulting Coulombic electrostatic repulsion. For other ceramic and zeolite materials this reaction is believed to proceed via a nucleation reaction, where the nuclei are formed and linked to commence the gel phase (**Askeland, 1998**). The presence of nucleation in the geopolymer synthesis process is yet to be proven as an accepted model, although **Provis et al., (2005a)** discussed the theoretical approach in the likelihood of this model.

3. Re-precipitation (hardening of the geopolymer matrix).

This segment of the geopolymer reaction describes the gel formation and the final hardening process. It is believed that dissolution of the raw materials continues simultaneously with the condensation reaction from the formed species in the gel (**Lee & van Deventer, 2003**). This is followed by the evaporation of water from the matrix and the final hardened geopolymer (**Lee & van Deventer, 2002c**).

The binding properties of the matrix are believed to be those of a 3-dimensional amorphous silica network, with general formula (**Yip & van Deventer, 2005**):



where: " M_n " refers to the alkali element

" z " is 1, 2, 3 or $\gg 3$

" n " is the degree of polycondensation

and

" w " refers to the water in the matrix

The monomers can also be graphically presented as shown in **Figure 2.1.1 (Gokhale; 2001)**.

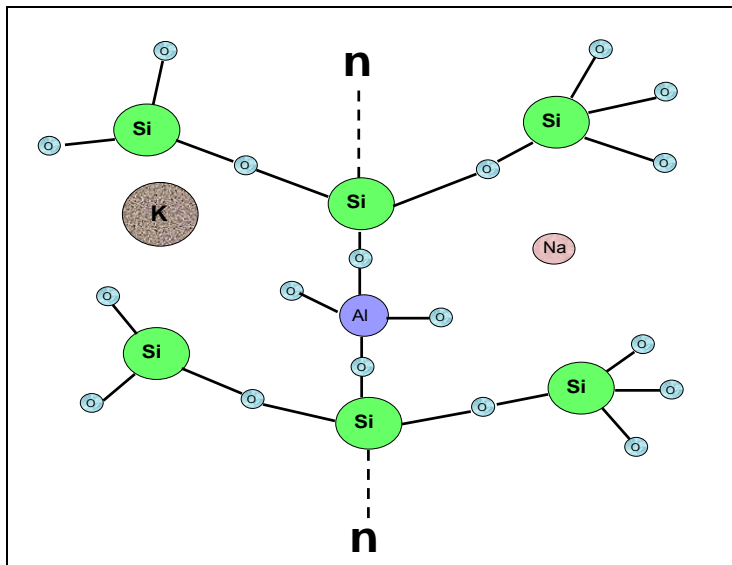


Figure 2.1.1: Graphical representation of the geopolymer monomers.

The common properties of geopolymers have been recorded as **(Goretta et al., 2004)**:

- Average density of 2.1 g/cm³
- Largely amorphous structure
- Contains aggregates of slag on addition of GGBFS
- Micro-cracks are prevalent
- Average compressive strength of 35 MPa (even though much higher strengths have been proven under specific conditions).
- Acid resistance **(Gokhale, 2001)** with approximately 7% breakdown in 5% H₂SO₄.

Conclusively, geopolymers is described as a dense material with low fracture toughness.

2.1.3. Geopolymerisation models

Several models have been proposed for the geopolymerisation of different source materials. An Ab Initio study of the dissolution reaction on five-membered Al-Si rings were investigated **(Xu et al., 2004)**, which served as the first step to model the geopolymerisation of Albite in an alkaline solution. The outcome is that the mineral can be represented by the five-membered ring model, which is part of the heulandite unit.

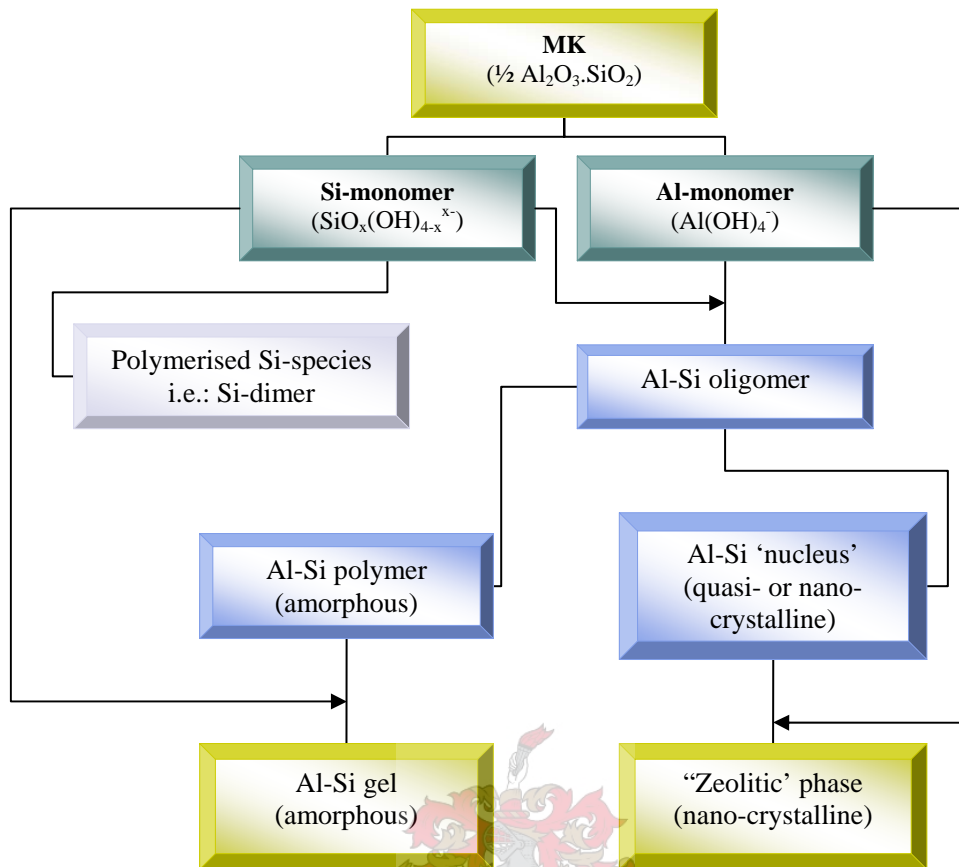


Figure 2.1.2: Schematic representation of the proposed reaction sequence found during polymerisation (Provis et al., 2005b).

The model represented in **Figure 2.1.2** was proposed by Provis et al. (2005b) and serves as an extension to that presented by Faimon (1996).

The Faimon model caters for the occurrence of the dissolution of a primary mineral into Al- and Si-monomers, the association of these monomers via either or both addition and autocatalytic polymerisation. Finally the formation of an unidentified 'secondary mineral' phase will be present. Its relevance to geopolymerisation is therefore uncomplicated, requiring only the incorporation effect of Si-oligomerisation in the concentrated Al-Si gel component of the geopolymeric binder. This must also include a second pathway by which the zeolitic material/phases are observed in the formation of geopolymers.

A thermodynamic statistical model for alumino-silicates (Provis et al., 2005c) was developed, which provides a quantitative, fundamentally based model. The latter describes the observed Gaussian trends and allows for analysis of the effects, especially when considering a change in composition and synthesis parameters on the chemical ordering of the geopolymer.

As part of the investigation by Provis, it was established that an estimation of 10% unreacted material is commonly found in the general geopolymer structure.

2.1.4. Geopolymer recipe formulation

Seeing that this work is not focussed on the basic geopolymer recipe formulation, some attention has to be on the formulations used by preceding researchers. The basic recipes ultimately used here originated from the formulations by Louise M. Keyte as part of her PhD thesis. The latter has not been published at the time of presenting of this work.

The general recipe and desired conditions for geopolymer synthesis are described in an abundance of published literature. For geopolymerisation a minimum ratio $\text{Al}_2\text{O}_3:\text{SiO}_2$ of 5.5 is needed (**Gokhale, 2001**), even though a ratio of 2.3 was used by **Duxson et al. (2005b)** and other researchers. Ultimately it was found that a Si/Al ratio of 1.90 results in metakaolin-based geopolymers with the highest compressive strength (**Duxson et al., 2006**). Generally a metakaolin to alkaline solution ratio of 1:2.5 is used, and in both Fly ash and Metakaolin systems at top strengths a Na to Al ratio close to unity in the binder phase is required. Usually the mass composition of aggregate in geopolymer mortars and alkali activator is 52% (wt) and 11.2% (wt) respectively (**Goretta et al., 2004**), even though an average of 10% (wt) alkali activator and 75% (wt) sand was used here as a more economical alternative. Finally, where GGBFS is added, its concentration is kept below 20% due to workability and strength effects (**Keyte et al., 2005; Yip & van Deventer, 2005**).

Defining a representative formulation for geopolymers is quite an impossible task, seeing that many factors alter the required recipe either independently or jointly. Factors such as desired strength for the intended application, type of aluminium source chosen (metakaolin or fly ash), addition of aggregate, curing time or temperature, type of alkali chosen, etc continuously require reformulation of the general recipe.

Lee & van Deventer (2004) used the following recipes for the geopolymer syntheses:

- *Geopolymeric binder/paste*: 9 parts fly ash (by weight) + 1 parts kaolin + 0.5 parts activation solution
- *Geopolymeric mortar*: 2 parts sand and 1 part geopolymeric binder
- *Geopolymeric concretes*: 1 part aggregates and 1 part geopolymeric mortar.

The aggregates being referred to usually are materials such as basalt, marble, siltstone, etc. It should be noted, however, that the addition of basalt presented the best results in terms of strength determination. Even though this is only one example of many variants, it aids in understanding the three most basic geopolymer classifications, consisting of -pastes, -mortars and geopolymeric concretes.

On investigating the effect of ultrasound on the geopolymerisation reaction, **Feng et al. (2003)** found that the strongest and most thermally stable system consisted of 225 g Fly ash and 25 g Metakaolin, along with a 0.5M Na₂SiO₃ and 10 M NaOH activation solution.

Lee & van Deventer (2004) suggested that a water to solid ratio of 0.25 should be used for optimum results, while **Xu & van Deventer (2002a)** suggested that a water to solid ratio of between 0.3 and 0.4 should be used. The argument is: a higher solid to liquid ratio leads to a higher degree of dissolution, but results in a lower strength geopolymer. It is therefore 'safe' to assume average water to binder ratio of 0.32 for the basic consideration in the required recipe formulation.

The physical method of synthesis for geopolymers remains fairly constant with varying recipes. Stoichiometric amounts of metakaolin, fly ash and/or other starting materials are added to activation solution (**Provis et al., 2005a; Yip & van Deventer, 2003; Yip & van Deventer, 2005**). The activation solution is pre-made by mixing the required amounts of water, alkaline-Si and alkali and leaving it to cool naturally to room temperature (**Lee & van Deventer, 2002d**). The mixture is then mechanically mixed for 15 minutes, followed by 15 minutes of vibration, which allows for the escapement of excess air. Some researchers (e.g.: **Feng et al., 2003**) found that the stirring speed has little to no effect on the final structure. The mixture is then poured into completely sealed Teflon/PVC moulds and cured at ± 40°C (and/or ambient pressure) for approximately 20 hours, depending on type of experiment, and stored until equilibrium is reached.

2.1.5. Effect of source materials on geopolymerisation

The source materials used for geopolymer synthesis were also widely researched in the past. **Duxson et al. (2005b)** found that Na⁺ affects geopolymerisation by increasing the initial dissolution rate, while K⁺ accelerates the polycondensation/gelation reactions. **Provis et al. (2005a)** stated that a broad XRD 'hump' is always present in any geopolymeric matrix, regardless of starting materials used. This XRD 'hump' or rather 'diffuse halo peak' is an indication method for a geopolymer, which in turn represents the amounts of amorphous phases present before and after geopolymerisation.

Previous research (**Xu & van Deventer, 2003b**) suggested that mixing one part calcinated source (fly ash, metakaolin, GGBFS, construction residues, etc.) with one part non-calcinated source (kaolinite, feldspars, mine tailings) one would find a final product with high initial and final strengths. The probability of these matrices cracking will also be lower.

It was suggested that a kaolinite-albite-fly ash mixture produced the strongest geopolymeric product (**Provis et al., 2005a**) with rapid solidification, high soluble components and early strength. It is believed that albite improves the hardness while kaolinite increases the final

strength by reacting slowly. Similar results have been shown for zirconia (**Phair et al., 2001b**).

The suggested ratios to be used are kaolinite: fly ash: albite of 1: 2: 4 respectively (by mass), which must be preferably activated by a 10M KOH solution (**Xu & van Deventer, 2002b**).

Another interesting observation was that the higher strength matrices were found with the following combination of source materials (**Xu & van Deventer, 2003b**):

- Fly ash + NaOH + K_2SiO_3
- Albite and KOH
- Kaolinite with an Al:Si of 1 or 2, KOH and added Ca

The highest degree of activation is found with use of monomeric silica (**Phair et al., 2001b**). **Xu et al. (2005)** completed a study on the activation of different starting materials. The result was that GGBFS is successfully activated by both high-alkaline solution and high alkaline soluble silicate solution, Class C fly ash is activated by a high alkaline soluble silicate solution and Class F fly ash can only be properly activated by a very high alkaline soluble silicate solution, where a high alkaline solution is defined by $[OH^-] > 5M$.

It should be noted that some industrial wastes such as certain mine tailings, paper sludges and naturally occurring minerals are inert to geopolymerisation. In some of the cases a calcinated source can be added to assist the geopolymerisation process.

2.1.6. Effect of temperature and alkalinity on geopolymerisation

Higher temperature implies higher rate of reaction according to the Arrhenius model, but lower degree of supersaturation (**Provis et al., 2005a**). This, however, is related to slow nucleation and crystal growth, therefore producing semicrystalline or polycrystalline products when synthesised at higher temperatures (**Van Jaarsveld et al., 2002**).

The presence of more nuclei will produce a less crystalline product with a smaller average crystal size. Conversely, fewer nuclei will produce larger crystals and induce slower solidification. The larger crystals will not be able to pack as densely with the binder phase as their smaller counterparts, thus producing a more porous geopolymer (**Provis et al., 2005a**). To avoid these porous structures and for optimum end strengths, **Van Jaarsveld et al. (2002)** recommended a curing temperature of 40°C to 60°C. This recommendation is largely based on the consideration of the significance of crystal water within the matrix, which in turn reduces cracking of the structure.

The fly ash resulting from coal burning in a coal-fired boiler contains minerals such as kaolinite, pyrite and calcite (**Keyte et al., 2005**). These minerals do not combust as they pass

through the flame, but do melt due to the adequate flame temperature. Some differences between amorphous silica sources were noted (**Van Jaarsveld et al., 2003**), which may be due to these differences in furnace temperature and coal feed composition. Ultimately, these initial differences will alter the final geopolymer product.

2.1.7. Immobilisation through Geopolymers

The possibility of utilising geopolymers as an immobilisation method for heavy contaminant metals was proposed fairly early in the development of geopolymer technology where encapsulation of Pb and Cu was considered (**Van Jaarsveld et al., 1998**). It was found that usually a geopolymeric matrix immobilises Pb better than Cu, providing that the structure can resist the disruptive effects of Pb (**Van Jaarsveld et al., 1998**).

General immobilisation of any toxic/radioactive waste is dependent on a successful mathematical modelling of particularly the geopolymer gel phase chemistry (**Provis et al., 2005b**). This type of modelling will be able to successfully predict the behaviour of the material over an extended period of time, which is essential when working with such dangerous material and where aged samples are not readily available. **Goretta et al. (2004)** also suggested that if geopolymers are used for encapsulation, the mechanical properties (e.g. abrasion, water erosion, solid-particle erosion and fracture knowledge) must be known or at least well quantified.

The mechanism of immobilisation of waste water containing Cu^{2+} and Pb^{2+} is a combination of physical and chemical interactions (**Van Jaarsveld et al., 1998**). It is believed that chemically the metals are bonded to the matrix via the Al-O or Si-O bonds or in the framework cavities to maintain electrical charge balance. Alternatively, the ions are substituted with another cation in the matrix, allowing that the surroundings favour this diffusion process.

Addition of small amounts of zirconia (**Phair et al., 2000**) improved the compressive strength of the geopolymeric matrix (approximately 3% by weight addition). The high structural resilience of zirconia to radioactive attack makes it a possible additive to the successful immobilisation of radioactive wastes. Another characteristic of interest, when considering nuclear waste immobilisation, is that of the excellent long-term chemical durability of geopolymers (**Provis et al., 2005b**).

The use of kaolinite versus metakaolinite for the development of mine tailing dam's capping was investigated resulting in a high strength geopolymer consisting of kaolinite and 0.1 (wt %) copper (**Van Jaarsveld et al., 2004**). It is therefore advised to consider the use of kaolinite when looking to use a geopolymer for immobilisation purposes. Fly ash already contains traces of heavy metals originated from the coal, therefore suggesting that a purer material such as metakaolinite and kaolinite will produce better immobilisation characteristics.

The effect of inorganic salt contamination in fly ash systems was also studied, where it was found that some salts may be detrimental (Cl^- salts) to the geopolymer structure and some may be beneficial (CO_3^{2-} salts) to the overall geopolymeric strength (**Lee & van Deventer, 2002d**). The effect of OH^- ions on a 20M KOH geopolymer was negligible.

Organic encapsulation (**Gokhale, 2001**) showed that adding 1% of phenol and 4-chlorophenol had no effect on the overall matrix compressive strength, but an addition of 5% nearly destroys the fly ash based matrix.

Waste management is directly obtained by using materials such as:

- Industrial waste
- Calcinated clays
- Melt-quenched aluminosilicates
- Natural minerals

The latter two starting materials is not yet widely used (**Provis et al., 2005a**), but mixtures of these materials is quite often found.

Fly ash is a waste produced in large quantities by all coal-firing industries, essentially power stations and Fischer-Tropsch process used by SASOL. Essential waste management can be introduced in the large scale usage of these ashes, where they are known to contain heavy metals and radionuclides which can leach into the environment unless handled correctly (**Lloyd & van Deventer, 2005**). When used as an alternative to Portland cement, the superior fire resistance of geopolymers can act dually as a solution to the housing crisis in South Africa, where huge parts of townships are devastated by annual fires. As a result the benefits are environmental, social and potentially very economical.

Phair & van Deventer (2002b) considered the effect of using Na-Al (which forms a white powder on drying) activation instead of the generally used Na-Si solutions. They found that a high strength geopolymer can be constructed from a Na-Al kaolinite activated structure. This provides a potential solution for aluminium rich wastes, such as salt cake and potliner industries, particularly when alumina is used in a caustic environment. Contamination of Al(III) in drinking water has been traced to a significant increase in Alzheimer's disease and other forms of dementia in patients in parts of Norway, Canada, the United Kingdom and south-west France (**Swaddle, 2001**).

Most of the attention for strength development and immobilisation (**Phair & van Deventer, 2002a**) was on high pH geopolymers, generally with a pH between 11 and 13. An alternative for this caustic route was researched, only to find that lower pH geopolymers are weaker with lower immobilisation characteristics.

2.1.8. Geopolymeric gel-phase

A good deal of attention has been on the geopolymer gel-phase, where the understanding of this phase may be a crucial step in the ultimate tailoring of a recipe fit for specific practical applications.

The gel-phase of a geopolymer is very difficult to analyse due to its high degree of amorphicity, where it is generally described as being 'glassy' (Provis et al., 2005a). General observations regarding the gel-phase were recorded (Phair et al., 2003) as:

- Low solid content in the gel initially produces a semi-translucent monolithic mass, which takes 24 hours for complete setting. A slight phase separation was observed in these samples.
- High solid content in the gel produced a white, thick mass. This structure seemed to harden almost instantly, forming a rock-like substance.

Inorganic salt contamination on the geopolymeric gel-phase (Lee & van Deventer, 2002b) was investigated, showing that phosphate salts are the primary gel-retarders. Chloride and oxalate salts are the second highest gel retarders. Addition of <0.4M of these salts showed no effect on the overall strength of the matrix, therefore lending the possibility of becoming geopolymeric control species (Lee & van Deventer, 2002a).

The addition of zirconia to the matrix (3% by weight) significantly increased the compressive strength of the matrix, but has an insignificant effect on the amorphous phase or gel phase (Phair et al., 2000). The addition of zirconia, nevertheless, produces high water resistant matrices.

In an effort to "tailor" the gel-phase (Feng et al., 2004), the idea of an ultrasound enhanced geopolymer was introduced. The technique is known to improve the dissolution of aluminium-silicates within the gel-phase. Ultimately, the use of ultrasound:

- Improves the strength of the matrix. A maximum exposure time is applicable in this case.
- Improves the distribution of gel phase.
- Advances the inter-linkage between Al and Si.
- Improves the thermal stability of the final geopolymer.
- Promote the transformation of semi-crystalline to crystalline phases.
- Improves the rate of dissolution of Al and Si in the gel phase, ultimately improving the extent of polymerisation between aluminium and silica species.

The solution to realistically imitate ancient construction materials is in the possibility that both the Calcium Silica Hydrate (CSH) gel as well as the geopolymeric gel are forming

simultaneously (**Yip & van Deventer, 2003**). The CHS gel formed here had significantly lower Ca to Si ratio's than what is found in OPC (Ordinary Portland Cement).

Understanding and full comprehension of the gel chemistry surrounding geopolymer technology may be the framework whereby the microstructural aspects of the matrix are presented (**Provis et al., 2005b**). This does not exclude that it may also lead to the understanding of the microstructure effect on the macroscopically measurable properties.

Thanks to the historically application-driven work in this field, most researchers focussed their time on the engineering properties exerted by geopolymers, rather than on the detailed analysis of the nanometre-level of these materials. This led to a vast amount of empirical data gathered, describing correlations between physical properties and synthesis parameters. Although there was no or little fundamental understanding of the occurring mechanisms, it provided a basis for the development of desired physical properties during the setting process. During an investigation by **Provis et al. (2005d)**, zeolitic nano-crystals were observed in the geopolymeric binder, which may be an invaluable link between the chemical composition and engineering properties of geopolymeric materials. This understanding of the nanometer-level structures can now provide for the tailoring of the desired properties fit for intended applications.

2.1.9. Geopolymer applications

Geopolymers already enjoy small scale commercial application as a construction material, but their valuable alternative qualities (fire-, acid-, thermal resistance and encapsulation medium) still need to be fully exposed. Their superiority to plastics, ceramics and other organic composites also strengthens the apparent need for geopolymer technology. These superior qualities are:

- Ease of production and handling, whereas high temperatures are not required.
- Higher heat tolerance than organic composites (resisting temperatures up to 1300 °C)
- Resistant to all organic solvents, but affected by strong HCl and H₂SO₄.
- Fast setting (especially in pre-cast applications).

In wider applications, particularly in the field of medicine, it has even been proposed that geopolymer-calcium-phosphate composites may be the answer to synthetic bone replacement (**Provis et al., 2005a**).

The production of geopolymer emits on average 5 times less CO₂ compared with that of OPC (**Gokhale, 2001**), which may possibly be a large contributing factor when looking to incorporate geopolymers into Cement and Concrete applications, seeing that CO₂ emissions

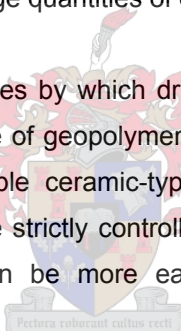
from OPC kilns play a significant role in the global greenhouse gas concentrations (**Lloyd & van Deventer, 2005**).

2.1.10. Geopolymer manufacturing

In order for geopolymers to be largely commercialised, they have to be clearly defined and the manufacturing process has to be simplified. One way of simplifying this process, is to find compositional similarities between samples (**Phair et al., 2003**). A base geopolymer has to be established and only then can it be converted to certain applications. Currently the aluminosilicate hydrogel theory (the backbone being hydrated aluminosilicate) forms the basis model for the commercial geopolymers. An important consideration according to **Van Jaarsveld et al. (2002)**, in designing a geopolymer for a specific application, is the thermal history of the source materials used.

Addition of zirconia (**Phair et al., 2000**) and other aggregates (**Lee & van Deventer, 2004; Xu & van Deventer, 2003b**) decreases the amount of alkali needed. The proposed reason for this is due to the formation of insoluble sodium polysialate species. This may prove beneficial when looking to produce large quantities of cost effective geopolymer.

A complete understanding of the routes by which drying and hardening of the gel continue after initial setting is crucial to the use of geopolymers in precast applications (**Provis et al., 2005b**), or as economically favourable ceramic-type materials, particularly in application where shrinkage upon drying must be strictly controlled to produce a product of the desired shape. This type of behaviour can be more easily predicted and controlled through mathematical modelling.



2.1.11. Geopolymer compressive strength characteristics

High compressive strength of geopolymers is one of the major tailored properties which may lead to their wide use. It is also the widest used property in current research, primarily due to the low cost and simplicity of compressive strength testing. Unfortunately the results gained from different research groups or authors can not be directly compared in any accuracy sense, due to the high variety of product sizes and geometry, strength testing apparatus and procedures followed by individuals (**Provis et al., 2005a**). It does, however, indicate how the addition of foreign species affects a specific geopolymeric system. Research where this proved valuable is the testing of a mixture of kaolinite, albite and fly ash (**Xu & van Deventer, 2002b**), addition of zirconia to the basic matrix (**Phair et al., 2000**), the effect of ionic contaminants to the matrix and many other investigations (**Lee & van Deventer, 2002d**). It is partly due to this fact that the work presented further on in this thesis does not primarily rely on compressive strength results, although included as an auxiliary comparison method within the boundaries of the investigation at hand.

Durability plays a significant role in this work. The addition of GGBFS and silica sand aggregate has been proposed by previous researchers to increase physical strength, which may possibly have a direct relation to the expected geopolymer durability. **Yip & van Deventer (2005)** investigated the effect of calcium addition to the basic geopolymer matrix. They established that the coexistence of gel and CSH phases during the early stage geopolymer activation was a major contributor to the physical strength of the samples. In order to experience the formation of both phases, an environment of low alkalinity (and high pH, >7.5 M NaOH) must be provided. A reactive source of calcium, such as GGBFS, must also be present.

An optimum ratio of metakaolin and GGBFS exists (**Yip & van Deventer, 2005**) regardless of $\text{SiO}_2:\text{Na}_2\text{O}$ ratio. A maximum strength was found for matrices introduced to 20% (wt) GGBFS after ± 7 days. Addition of 40% (wt) or more demonstrated to be destructive to the matrix strength. The improved strength is believed to originate from the extra Ca-species GGBFS brings to the geopolymeric matrix at a high pH (≈ 14). **Keyte (2005)** found that the same limit holds for fly ash based geopolymers.

Adding too much Ca to a geopolymer gel leads to the formation of CSH (cementitious based material), which in turn can contribute to a more brittle, weaker matrix. Amorphous CSH may be the major component, if correctly controlled, which contributes to the overall strength (**Yip & van Deventer, 2003**) and its formation can significantly affect the properties such as overall acid resistance (**Lloyd & van Deventer, 2005**).

Other researchers suggested that addition of granular sand increased compressive strengths (**Xu & van Deventer, 2002b; Lee & van Deventer, 2004**), enhanced density and minimised shrinkage on drying (**Provis et al., 2005d**).

It was found that the higher the amount of aqueous silica available during polymerisation (**Lee & van Deventer, 2004**), the higher the apparent compressive strength of the matrix. A matrix with silica concentration below 2.5M had the lowest compressive strengths, regardless of the alkali concentration. An important point of interest is that an optimum limit exists for the addition of soluble silica. The addition of too much aqueous silica may inhibit the dissolution of the Si-ions (**Lee & van Deventer, 2002c**), therefore SiO_2 concentrations between 5M and 10M are suggested (**Lee & van Deventer, 2003**). An early age geopolymer strength of up to 400 MPa (**Phair et al., 2003**) was recorded for a high viscosity (and high Si containing) metakaolin and sodium silicate matrix.

Generally it was found that a higher pH contributes to a geopolymer with higher compressive strengths (**Xu et al., 2001; Phair et al., 2001a**). K-geopolymers (as opposed to Na-geopolymers) in most cases exist at a higher pH, associated with higher dissolution rates and

lower amounts of unreacted material present. The experiments in this thesis make use of both cations in the quest to limit the cost associated with only potassium activation.

Although not used in this work, the addition of fibre to the matrix has been shown to significantly improve the flexural strength and fracture toughness of the geopolymer (**Provis et al., 2005b**), in comparison to a geopolymer paste.

Some nano-crystalline zeolites (**Provis et al., 2005a**) have been identified by electron microscopy to be present in geopolymer matrices, especially matrices constructed with high reaction times. Crystallisation at high silica contents also seems to be less prevalent. Crystallinity has not yet been excluded as a means of strength development in geopolymeric systems. Also, the extent of crystalline phase dissolution in the geopolymer mix (**Lee & van Deventer, 2002d**) was not promoted nor inhibited in the presence of salt contaminants, restricted to instrumentation detection limits.

Generally, high degrees of crystallinity (**Phair et al., 2001b**) are found at pH values greater than 12, while zeolite formation (**Provis et al., 2005a**) is favoured at lower activating solution ($\text{Na}_2\text{O}/\text{SiO}_2$) ratios and higher temperatures.

In fly ash systems, another interesting aspect was observed, where **Keyte et al. (2005)** found that the removal of iron from the fly ash source does not improve the compressive strength of the matrix.

Feng et al. (2004) proposed that controlled ultrasound improves the geopolymer by possibly cleaning the particle surfaces. The major defect of this technique is the creation of 'hot-spots' within the structure, therefore introducing a flawed section. Fewer cracks have been found with the use of ultrasound by forming a substantially more evenly distributed gel-phase. These are important factors when considering the eventual strength of the matrix.

2.1.12. Common analytical techniques associated with geopolymers

Past analysis of the different matrices commenced through a wide channel of technologies. At times (**Goretta et al., 2004**) the analyses are completed in a single day in order to eliminate varying environmental effects.

As previously mentioned in section **2.1.11**, compressive strengths were used in almost all of the previous investigations to compare geopolymers under varying conditions.

XRD has been used by an abundance of foregoing researchers in the quest to define the degree of amorphicity shown by the relevant starting materials and end products. Crystalline

phases are identified by comparing the found diffraction patterns to those presented by the JCPDS (Joint Committee on Powder Diffraction Standards). **Provis et al., (2005a)** re-evaluated the literature under this topic only to find that nano-sized crystals may have gone undetected in the past, due to instrumentation restrictions.

Q-XRD has been used by some authors (**Keyte et al., 2005**) as a tool to predict the reactivity of fly ash in the geopolymeric systems, by excluding the crystalline phases present in the original fly ash. The latter is believed to be un-reactive as they are resistant to alkali attack.

XRF (**Keyte et al., 2005**) is also a widely used technique by researchers to establish the oxide compositions present in the original fly ash sample. The results showed that no two ashes are similar in composition; consequently each ash will act differently during the geopolymeric reaction, producing varying products.

^{29}Si -NMR (**Duxson et al., 2005b**) showed that some degree of Al-O-Al bonding does exist, therefore contradicting Löwenstein's theory: "no two aluminium ions can occupy the centres of tetrahedra linked by a single oxygen ion", therefore forbidding Al-O-Al links. Löwenstein's 'rule' was initially based on the Pauling radius ratio rule (**Provis et al., 2005c**). It is important to note that according to Gibbs energy minimisation techniques, the bond of Al-O-Si remains energetically more favourable than that of Al-O-Al. **Duxson et al. (2005b)** found that Al-O-Al bonds will be present in prevalently potassium activated geopolymers.

MAS-NMR showed that metakaolin based geopolymers contain significant amounts of unreacted phase, while the potassium counterpart has less thereof. The tetrahedral geometry of the aluminium is not affected by the change in either the Si:Al ratio, nor the alkali cation used for activation. Analysis of these spectra, on aluminosilicate glasses and minerals, by curve fitting of Gaussian curves was established to provide critical information regarding the distribution of Si and Al tetrahedra within the geopolymeric binder (**Provis et al., 2005c**).

The most important data from calorimetric results is the determination of correspondence between the degrees of reaction and other physical properties as well as an elucidation of the reaction mechanics (**Provis et al., 2005a**). For metakaolin systems there exists a linear relationship between the geopolymer compressive strength and reaction enthalpy. All of the reactions were also observed to be exothermic.

This caloric and infrared data show the degree of formation of the crystalline materials. The degree of crystallisation increased with increased alkali concentration in NaOH activated metakaolin mixtures.

Compressional rheology was used as a means for determining the characterisation of mouldable slurries, which showed that the higher the SiO₂ to Na₂O ratio (**Phair et al., 2003**), the higher the obtained yield stress of the final product.

Infrared spectroscopy shows an identical shift of the intense peak 1090 cm⁻¹ in metakaolin towards a position at approximately 1000 cm⁻¹ in the zeolite precursor gel (**Provis et al., 2005b**). This peak has also been noted by **Lee & van Deventer (2003)**, who proposed that this may be a measure of the extent of the alkali activation reaction of the geopolymer. This finding strengthens the idea of using metakaolin based geopolymers as a model system, where the effect of fly ash on alkali activation can be understood.

ICP-OES is a common tool used to perform an elemental analysis on dilute solution composition up to trace levels.

SEM images (**Provis et al., 2005b**) provided details surrounding the physical transformation during geopolymerisation and their resulting microstructure, where a metakaolin based geopolymer structure shows a distinct transition from a porous (especially when formed under little or no soluble silicate during activation) to a more homogeneous binder phase in higher silica systems. **Lloyd & van Deventer (2005)** made use of both SEM and TEM to investigate the microstructure of fly ash-based geopolymers, mixed with GGBFS and activated with potassium silicate. The images showed that the reaction products consist of two phases, where the amorphous CSH phase was distinctively dendritic.

2.1.13. Classification of fly ash

The work presented here will focus on fly ash-based geopolymers, due to the economical, social and environmental advantages already mentioned.

When working with fly ash, it is important to be aware of the commonly used classification system (**Keyte et al., 2005**). There is currently only one classification system for coal combustion products, including fly ash, which is defined by American Society for Testing and Materials, **ASTM C618**. The ashes produced from pulverised coal are separated into two classes known as Class C and Class F, where the distinction between these two classes is based on the total amount of SiO₂, Al₂O₃ and Fe₂O₃ present. When the sum of these components is greater than 70 (mol) %, the ash is classified as a Class F. A further classification can be done on basis of iron and alkali cation content.

Seeing that most of the coal deposits contain pyrite and other iron mineral deposits, fly ash can contain as much as 20 (wt) % iron-oxides.

Another noteworthy point is that fly ash demonstrates inter and intra-particle non-homogeneous characteristics, making it a difficult material to analyse as every particle is compositionally different and will react different in the same environment. Current analytical methods are therefore very time-consuming and the results are at times hard to interpret.

Both of the ashes used in the experiments presented in this thesis are Class F ashes, sourced from Australasian resources.

The use of Coal ash instead of fly ash was considered by **Keyte et al. (2005)**. Coal ash is described as the coarse counterpart to fly ash, whereas it is melted and not combusted as found with fly ash. When considering tailoring the properties of geopolymers, it was found that fly ash produces the best results. The reasoning for this is that the reactivity of fly ash is more easily comprehended and can be modified with blends of different fly ash classes.

2.1.14. Expected geopolymer durability

Despite the increasing body of research interest in these advanced materials, little is known about the expected durability of geopolymers hold as construction material, besides the apparent need for this information. The main aspiration of this work is to contribute to this lack of knowledge and to assist in the global incorporation of geopolymer technology as a substitution to the tried-and-trusted Cement and Concrete monopoly.

2.2. Cement and concrete literature

This section focuses on literature involving durability tests previously performed on different concrete and cement blends. The techniques described here were meticulously imitated and applied to a series of geopolymeric recipes, with their relative performances being discussed later in this thesis.

2.2.1. Introduction to cement and concrete technology

Earliest findings of civilisations using cementious material date back as far as the Epipaleolithic period (somewhat 9000 years ago), but it was not until the use of Roman concrete it became widespread over Europe *ca* AD 500 (**Phair, 2001**). Roman concrete is believed to consist predominantly of limestone and pozzolans, the latter generally being volcanic- or sedimentary soils.

Long since the passing of the Roman period, Portland cement made their way into modern society, becoming the centrepiece of the current construction industry. Their demand dominates its nearest rivals of wood or bricks by nearly ten times, largely due to its low cost and relatively simple application.

In spite of its wide use, concretes and cements face some durability criticism, especially when used in structures with an expected life covering a couple of decades. Constant maintenance on existing bridges and structures due to corrosion, carbonation, alkali-silica reactions, freezing/thawing, etc may costs the American government *ca* US \$70 billion per annum. Amongst all these factors (**Liu, 1996**), the penetration of chloride-ions into concrete has been regarded as the major deterioration problem the concrete and cement technology is faced with today.

2.2.2. Chloride induced corrosion

Steel-reinforced concrete structures are in constant contact with oxygen and moisture from the atmosphere. When accessible in sufficient quantities, chloride induced corrosion can be sustained. Chloride can be introduced to the concrete via two pathways (**Liu, 1996**):

- Internal source, originated from the concrete-making. Chloride may exist as a contaminant in the raw materials.
- External source, mainly from seawater or de-icing salts. The latter consists of salts like NaCl and CaCl₂ and is commonly used to keep bridges and pavements clear of snow and ice (**Hossain & Lachemi, 2004**).

Penetration of species such as chloride from an external source, into concrete, can commence through two main pathways: capillary attraction and ionic diffusion, depending on the degree of material saturation (**Askeland, 1998**). Capillary attraction is usually associated with dry to semi-dry samples, where the ions migrate along with water. This rate of penetration of chloride ions is much faster than the penetration by ionic diffusion (**Liu, 1996**). Ionic diffusion is found in semi-wet to near saturation samples, where the migration occurs via a diffusion process following Fick's second law.

The mechanism of chloride induced corrosion is believed to be connected to chloride ions being incorporated in the passive film, replacing some of the oxygen and increasing both its conductivity and its solubility (**Liu, 1996**). The passive film refers to the high pH environment at the steel-concrete interface, where a passivating iron oxide forms on the surface of the steel (**Roskopf & Virnelson, 1985**). While this area remains basic enough, no corrosion will occur. Once corrosion has been initiated, chloride ions complex with the ferrous ions to produce soluble FeCl₂. These FeCl₂ ions now combine with the hydroxyl ions to form Fe(OH)₂ and consequently releases the chloride ions back into solution, repeating the process. Ultimately, chloride now acts as a catalyst in the corrosion process.

Corrosion delaying techniques for concrete structures have been proposed by numerous authors. Two of the most common methods remain: by coating the steel-reinforced bars (rebar) with epoxy and to increase the concrete cover depth (**Jolley, 2003**). Some success

was gained by these methods, but it is far from the perfect solution. Increasing cover depth lengthens the required time for chlorides to diffuse to the rebar, simultaneously limiting the availability of oxygen and moisture at the rebar interface. Along with this increase in concrete cover, an increase in cost and total weight of the structure is initiated. Furthermore, epoxy additionally limits the access of chlorides, oxygen and moisture to the surface of the rebar, effectively slowing down the corrosion process, but only to become brittle and to delaminate from the steel under high chloride concentrations (**Roskopf & Virnelson, 1985**). A large window of opportunity now exists for geopolymer technology to enter this field, by providing sound proof that geopolymers resist chloride induced corrosion more effectively than concrete.

2.2.3. Corrosion determination

It is increasingly important for designers to know the behaviour against corrosion of different reinforced concrete types, allowing them to take into account several aspects about durability before recommending a particular reinforced concrete type. This is a very slow and tedious task due to the test duration and the variables that could interfere when investigating natural weathering of the samples. One possibility to reduce the test time is through accelerated tests. The latter can be performed through several methods (**Castro et al., 1997**): application of electrical potential measurement, cyclic wetting and drying in 3.5% salt solution, introducing chloride content in the concrete, salt spray chamber tests, etc. Other successful methods, and those used in this thesis, involve (**Yeau & Kim, 2004**):

- Accelerated chloride-ion diffusion test (as in **Appendix D**).
- Copper/copper sulphate half-cell potential test according to **ASTM C 876** (as shown in **Figure 2.2.1**).

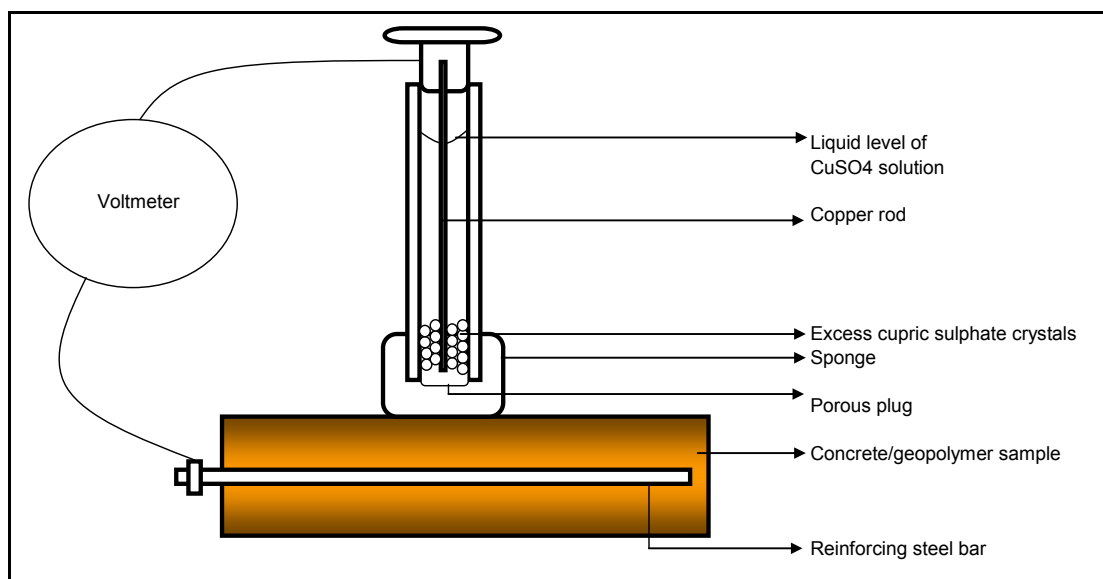


Figure 2.2.1: Copper-copper sulphate half cell testing

These tests provided the authors with diffusion coefficients, to calculate the concentration of chloride-ions permeated through the concrete specimens, as well as determining the probability of rebar corrosion.

Obviously, the reliability of these accelerated tests must be questioned. **Castro et al. (1997)** investigated the difference between the corrosion rate, the corrosion potential and the chloride content obtained for two similar samples, one being exposed to marine atmosphere 50m from the coastline, the other exposed to an accelerate salt spray chamber (ISO-9227). He found that a direct and clear correlation exists between these two tests and ultimately classifying the materials in the same order. PIXE (Proton Induced X-Ray Emission) will be used in this work as the reliability testing method due the shorter testing times associated with this technique.

Dhir et al. (1990) also made use of parallel experimentation to test the reliability of accelerated tests. They compared the results with a rapid potential difference test against those gathered from a conventional concentration difference test. A close relationship between the two methods was shown, conclusively allowing a diffusion coefficient to be determined by ASTM accelerated tests.

2.2.4. Accelerated chloride-ion diffusion test

Diffusion is temperature dependent to a certain degree, and can be quantified by the Arrhenius equation (**Askeland, 1998**). **McGrath & Hooton (1996)** established that this dependency is negligible when using voltages under 30V in the accelerated chloride-ion diffusion test, seeing that there was no significant temperature variation at these voltages.

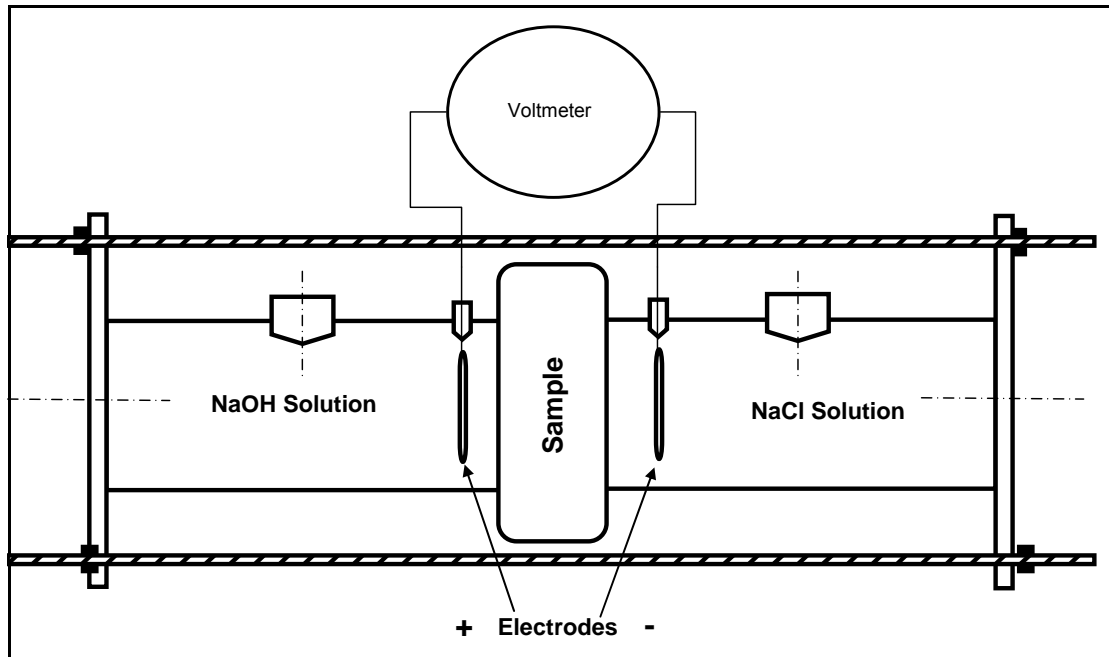


Figure 2.2.2: Experimental set up for ACID test

The experimental set up, as shown in **Figure 2.2.2**, should be done in accordance to **ASTM 1202-97 and ASTM 1202-91**. Please refer to these standards, as they provide recommendations on solute concentrations, sample thickness, applied voltage, etc.

The determination of the chloride ion diffusion coefficient from the accelerated test can be done by means of a modified version of Fick's Second law (**Halamickova & Detwiler, 1995**) and simplified to the Dhir and Sugiyama equation (**Yeau & Kim, 2005**). The latter is given in Equation 2.4:

$$D_{Cl} = \frac{R \cdot T}{Z_{Cl} \cdot F \cdot C_{Cl}} \cdot \frac{l}{\Delta E} \cdot \frac{V}{A} \cdot \frac{dC}{dt} \text{ (cm}^2 \text{/s)} \quad (2.4)$$

Where: D_{Cl} = diffusion coefficient (cm²/s)

R = universal gas constant (8.314 J/mol.K)

T = absolute temperature (K)

Z_{Cl} = electrical charge

F = Faraday's constant (96 485 J/V.mol)

C_{Cl} = cathode concentration (mol/l)

l = specimen thickness (cm)

ΔE = potential difference (V)

V = volume of the diffusion cell (litre)

A = specimen area (cm²)

dC = chloride concentration of diffusion cell (mol/l)

and

dt = elapsed time (s)

Most of the work based on this ACID (accelerated chloride-ion diffusion) test was used to compare the apparent permeability of varying concrete samples to chloride penetration (**Yeau & Kim, 2005; Halamickova & Detwiler, 1995; McGrath & Hooton, 1996**). Valuable information was gathered and the relevant alterations to the basic concrete recipe could be established. The work presented here will use this technique on geopolymeric samples, not only to verify the differences in recipes, but also to quantitatively compare the found coefficients to those found for the optimised concrete alternatives.

2.2.5. Half-cell potential test

The corrosion potential of any half-cell can be recorded against a chosen standard cell/electrode. Half-cell potentials are a function of solute concentration; therefore a solution of higher chloride concentration will be more corrosive. From this, a current will flow in a cell consisting of a single metal in two different concentrations of a common solution, implying that the corrosion of steel in concrete (or any other coating) can be considered as a concentration cell (**Jolley, 2003**). The corrosion risk in that cell can now be measured by introducing a standardised half-cell (**Ayala et al., 2000**).

Often it is important to know the extent of corrosion, without applying destructive techniques. The copper/copper sulphate test method covers the estimation of the electrical half-cell potential of uncoated reinforcing steel, therefore determining the corrosion activity of the rebar without destroying the sample. Experiments are based on **ASTM C 876-91** as shown in **Figure 2.2.1**.

Placing a half-cell on the concrete surface, connecting a voltmeter to the rebar on the one side and to the half-cell at the other, an electrical circuit is formed. The measured electrical potential difference is now a function of the iron in the pore solution environment (**Jolley, 2003**). Iron can go easily into solution at the anode side, while at the cathode side the passive layer is still strong and being strengthened by further cathodic reaction. Essentially the steel resists dissolution on the cathode side and higher corrosion potentials are associated in anodic areas.

Results from this test provide an indication of the probability that corrosion is occurring at a specific site (**Table 2.2.1**). **Yeau & Kim (2005)** and others used this technique, along with the ACID test, to optimise concrete recipes. Generally this type of investigation led to recommendations on type and quantity of typical additives like fly ash, GGBFS, etc to the basic concrete recipe.

Table 2.2.1: Guidance on interpretation of results from ASTM C 876-91

Interpretation of results from half-cell surveys	
E_{corr} (Cu/CuSO ₄)	Probability of Corrosion
>-0.20 V	Greater than 90% probability of no corrosion
-0.35 to -0.20 V	Corrosion activity uncertain
<-0.35 V	Greater than 90% probability of active corrosion

2.2.6. Chloride detection through PIXE

The problem of reinforcement corrosion has sparked a world wide quest to develop a method for reducing water absorption and permeation of chloride ions into concrete. Experimental methods as discussed in section 2.2.4 and 2.2.5 led to a limited solution to delay chloride-induced corrosion, but still a need to clarify the interaction of free chloride ions with the chemical composition and microstructure of cement pastes exists (Jenneson et al., 1998).

If this sort of microstructural understanding should be achieved, an analytical technique, capable of accurately profiling low levels of chloride, is required. This technique must further be able to trace these low levels of chloride in conjunction with other elements and chemical species present in the matrix.

Conventional measurement methods for reinforced concrete involved the extraction of a powdered sample (by drilling) and performing a wet chemical technique based on the Volhard method. These measurements are effective but exceedingly slow and tedious. EDX (Energy Dispersive X-Ray) analysis can be used, but only at concentration levels typically higher than 1 (wt) % (Auer et al., 1995).

PIXE (Particle Induced X-Ray Emission) is capable of profiling chloride levels as low as <0.05 (wt) % in cements, challenging levels for techniques such as EDX, and at physical resolution unmatched by many engineering techniques (Jenneson et al., 1998).

Chloride profiles are produced by a summation of counts versus the horizontal distance for the specific element. Diffusion coefficients are estimated through fitting the data to a semi-infinite model of Fickian diffusion.

$$\frac{c_s - c_x}{c_s - c_0} = \operatorname{erf}\left(\frac{x}{2\sqrt{D \cdot t}}\right) \quad 2.5$$

Where c_s is the constant concentration of the diffusing Cl^- atoms at the surface of the material, c_0 is the initial uniform concentration of the diffusing atoms in the material and c_x is the concentration of the diffusing atom at location x below the surface after time t . The error function can be evaluated from any standard Fickian error table (**Askeland, 1998**).

Jenneson et al. (1998) reported typical values of $(1.7 \pm 0.2) \times 10^{-7} \text{ cm}^2\text{s}^{-1}$ for OPC and values of $(9.3 \pm 0.2) \times 10^{-9} \text{ cm}^2\text{s}^{-1}$ for OPC and fly ash blends.

2.2.7. Alternative corrosion measurements

Dickerson et al. (2005) at the University of Texas, Austin, proposed a solution in determining the presence, extent and rate of corrosion without the use of invasive, expensive nor destructive techniques. The solution lies in the field of wireless sensors, developed for early detection of corrosion. These proposed sensors will be installed into new constructions or portions of rehabilitated structures, placed adjacent to the rebar just before concrete addition. Data from these sensors can now be collected either continuously or during routine inspections, resulting in early corrosion detection and prolonged structure service life.

From this study, and foregoing researchers (**Novak et al., 2003; Simonen et al., 2004**), it is clear that these type of sensors will provide constructors with a valuable corrosion-combat-device. Unfortunately these sensors were not commercially available at the time of this investigation; hence its significance to geopolymer research could not be examined.

2.2.8. Relevance to geopolymers

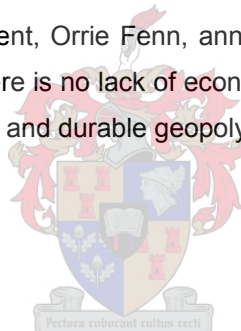
As previously mentioned, geopolymers have to show superior corrosion resistance compared with concrete, for this technology to have any hope in replacing future concrete applications. Valuable guidelines on durability tests can be found in previous concrete studies, allowing this work to be directly comparable to previous concrete research. This, in turn, excludes the need for another level of experimentation, where only geopolymers need to be investigated and compared with published data. Concrete literature does not only supply physical findings, but also valuable hints on probable test methods and means to optimise the experimentation process. The experimental design discussed in **Chapter 3** is largely based on recommendations from past cement and concrete researchers.

Lui (1996) suggested two pathways for chloride to migrate into the concrete sample (section 2.2.2). **Lee & van Deventer (2002d)** showed that incorporation of chloride into the original geopolymer was detrimental to the matrix. Combining these two facts effectively limits the investigation to external migration of chloride. All of the tests were therefore based on soaking of samples in chloride solutions or performing the ACID test. Detailed descriptions and findings are discussed later.

Lui (1996) and **Askeland (1998)** defined different mechanisms of chloride migration into the matrix, section **2.2.2**. As the geopolymer samples used in this investigation consist of ca 17% water, the mechanism of diffusion can be reduced to that of solely ionic diffusion; therefore eliminating another unnecessary level of experimentation.

Conclusively, the work presented on geopolymers and work on concrete durability can now be combined to produce plausible explanations and estimations in terms of geopolymer durability. The combination of these two research fields also led to the use of non-conventional geopolymer analytical techniques, producing a line of data not previously recorded for this type of material.

In developing countries, particularly countries like South Africa, concrete consumption is souring to European Union levels (**Engineering News, 2005**). One of the provinces in South Africa, Gauteng, is at a current per-capita consumption of 422kg/person/year, only 17% short of EU levels. The “Expanded Works Programme” currently under way, will greatly increase the concrete demand, where government-funded low-cost housing, schools, sewerage works and health care facilities are being built. The demand has grown to such an extent to where the COO of Pretoria Portland Cement, Orrie Fenn, announced a ZAR 1,36billion expansion project. From this it is clear that there is no lack of economic relevance for the introduction of a more affordable, possibly stronger and durable geopolymeric construction material.



2.3. Summary

This chapter devoted to present the reader with a sound background on the current knowledge-base in the field of geopolymers. Emphasis was on the more recent work in this field, where a better understanding on the reaction mechanisms and microstructural composition may contradict earlier publications. Very little literature was available on the expected geopolymer durability, more specifically, on the behaviour of this material in a chloride environment. It is this lack of knowledge that drove this project, where a durability definition is required for the wider commercialisation of geopolymers as construction material.

In terms of cement and concrete, a broad overview was presented, but emphasis remained on the expected durability of these materials and tests associated with the respective durability formulations. Attention has been paid to the increasing demand for knowledge and solutions regarding chloride-induced and other corrosion activities affecting concrete structures. It may just be this exact shortfall by cementitious material that will pave the way for geopolymers into the construction world, where the tried-and-trusted (or shall we say: tried-and-rusted) concrete monopoly will face competition from a more robust material.

For a complete list on available Geopolymer Literature, please refer to **Appendix A** for reference details, as well as chronological ordering.



Chapter 3.

Experimental Design and Research Methodology

The aim of this chapter is to describe the selection of experimental and analytical techniques used as basis for this thesis. No single method could effectively be used to portray the expected durability of a given geopolymeric sample, therefore a combination of techniques were used to best describe the system at hand.

The techniques used include: **PIXE** (Particle Induced X-Ray Emission), **SEM** (Scanning Electron Microscopy), **ICP-OES** (Inductively Coupled Plasma Optical Emission Spectroscopy), **IC** (Ion Chromatography), **IR** (Infrared), **XRF** (X-Ray Fluorescence Spectroscopy), **Q-XRD** (Quantitative X-Ray Diffraction), **BET** (Brunauer-Emmett-Teller) surface area, Compressive Strength testing, Diffusion Cell, Copper/Copper Sulphate Half-Cell potentials as well as commercial force sensors (FlexiForce®).

Technical background to the underlying basis for each of the techniques will not be discussed here, only discussions relevant to its use and application in this investigation. **Chapter 2** pointed out commonly used analytical techniques used by foregoing researchers. The reader is advised to refer to the stated literature for broader instrumentation definitions. Technical information regarding the atypical techniques used in this work will be discussed at its point of use when relevant to this thesis.

The methodology in combining these varying techniques, as well as interpreting the resulting data, will be discussed throughout this chapter.

3.1. Introduction

The focal point of this investigation is to develop a body of knowledge on the expected durability of geopolymers, emphasis being on the corrosion resistance and therefore the diffusion behaviour shown by ions such chloride and sulphates through a series of geopolymeric recipes.

Fly ash-based geopolymers will be the only systems considered, due to the underlying aspiration for this thesis to contribute to the future successful commercialisation of geopolymer technology. Currently the more economically viable geopolymers are the fly ash variants.

Very little work on geopolymer durability has been done, where most of the publications only touch the subject as a secondary topic. **Goretta et al. (2004)** modelled the expected erosion for geopolymers, with mechanical durability as the prominent inspiration and results showing that the matrices respond as classic brittle material. Still no direct comparison can be drawn to the proposed superiority of geopolymers to concrete as construction material. **Lee & van Deventer (2002d)** investigated the effect of inorganic salts contamination such as OH⁻, Cl⁻ and CO₃²⁻ on the measured strength of the geopolymer samples, attempting to draw a direct correlation to the expected sample durability. Results showed that the ion contaminant affected the amount of water that remained in the gel phase, which in turn determined the compressive strength of that particular sample. Even though it has now been established that an ion like chloride is detrimental to the matrix, no quantitative conclusion can be drawn.

The experimental design and conditions were chosen for the results to be directly compared with those of Ordinary Portland Cement (OPC) and other commercially used concretes.

The basis recipes used in this study were provided by **Keyte (2005)**. At this time the reader should realise that the experiments covered in this section was partly done in Melbourne, Australia, and completed in Stellenbosch, South Africa. The relevant subsections will clearly indicate where that specific experiment was conducted. It should, however, be clear that the samples used in all of the experiments were made in Australia from the same raw materials.

3.1.1. Methodology

The samples of proposed recipes by Louise Keyte were made from Australian sourced raw materials. The characterisation and classification of all these materials were done by use of XRD and XRF. The results are presented in **Appendix B**.

3.1.1.a. Starting materials

The principle source of reactive alumina and silica used in the various sample recipes was fly ash. Two types of ashes were used, labelled in this thesis as fly ash A and fly ash B. Both of these materials are classified as Class F ashes according to **ASTM C618 (Keyte et al., 2005)**. The exact origin for both of the materials is not provided owing to reasons of confidentiality.

Reagents were always purchased in bulk, ensuring that batch-to-batch deviations were minimised. The labelling and origin are:

- Hydrochloric Acid at 35.4% purity (batch IC 33 957 152 444) from Merck, Melbourne, Australia. Specific Gravity given as 1.18.
- Sodium Silicate Solution with SiO₂/Na₂O molar ratio of 2.7 and SiO₂ weight percent given as 28.7 from PQ Corporation, Australia.
- Laboratory grade NaOH (99% purity), NaCl (98.7% purity) and KOH (99% purity) from Consolidated Chemicals, Australia.
- Cement Grade washed and classified Silica (quartz) sand from Unimin Australia.
- Demineralised and distilled water was used throughout the sample make up, as well as the testing fluid make up.
- Ground Granulated Blast Furnace Slag, 95% Gypsum based.
- Cupric Sulphate from Associated Chemical Enterprises, 99% purity. Batch 9691/933.
- Sulphuric Acid from Saarchem Merck, 99% purity. Batch 588 51 24 LCA.

3.1.1.b. Synthesis

The activation solutions for each geopolymer recipe were individually made and clearly labelled, allowing for the solution to cool naturally overnight. The activation solution as described here refers to the water, sodium silicate, potassium hydroxide and sodium hydroxide mixture.

According to the recipes, as presented in **Appendix C**, the correct amount of the selected fly ash, slag (when relevant) and sand aggregate (when relevant) was weighed and dry mixed by hand for 1 minute. **Feng & van Deventer (2004)** established that mixing speed and duration does not affect the final geopolymer product. The same weighing equipment was used for all the measurements, therefore minimising experimental error as far as possible.

The activation solution was gradually introduced to the dry mixture. Care was taken to produce a smooth, lump free mixture by continuously stirring for 2 minutes. Once the desired mixing was achieved, the mixture was poured into the required mould and shaken on a mechanical shaker for a couple of seconds. This assisted in the minimisation of bubbles entrapped in the paste/mortar.

Before a batch of a specific geopolymer recipe was made, the necessary amount as determined by the experimental design was prepared and split as representative samples from the source material of each component. Once again, batch to batch variations were minimised as far as possible.

Different types of curing regimes were used for some of the experiments. The curing method chosen is clearly stated at the point of discussion in this thesis.

The two types of curing are separated by “Short Cure” (SC) and “Long Cure” (LC) methods. Short curing commences with placement of the samples in an oven at 40°C for 12 hours. After that, the samples are baked in an oven at 65°C for another 24 hours. Care, however, must be taken to seal the samples in closed containers/plastic bags to ensure a high as possible curing humidity. This curing was developed with Louise Keyte (**Figure 3.1.1**) to closely resemble the characteristics found during long curing conditions. Long curing here refers to leaving the samples to set at room temperature for 28 days.

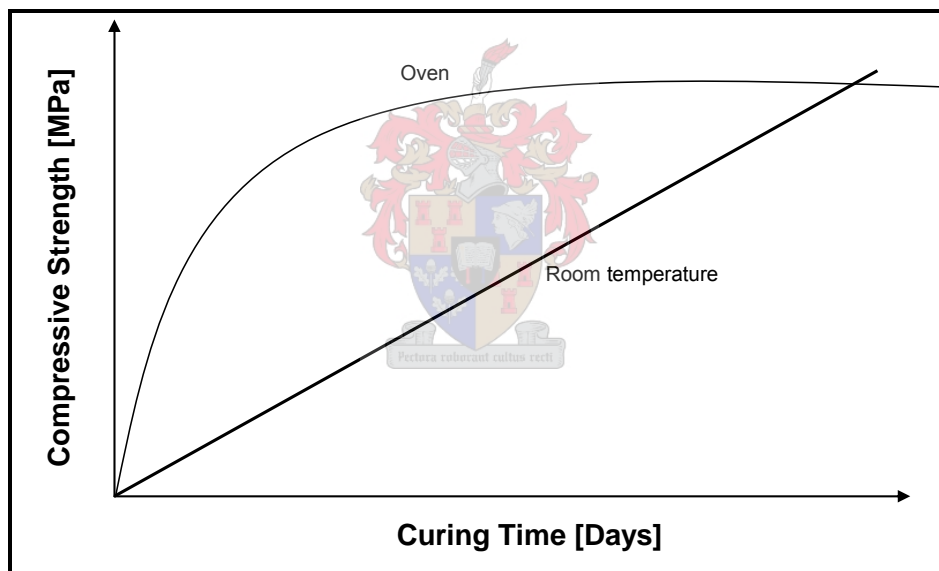


Figure 3.1.1: Conceptual chart of compressive strength versus curing time chart. The two curves represent curing in different conditions: one in an oven at the specified temperatures, the other at ambient temperature.

The samples cured in the oven were left to cool naturally to room temperature before demoulding or before any analyses were done on them.

3.1.1.c. Diffusion Coefficient Determination

The experiments discussed in this section is similar to those used in cement and concrete studies. The relevance and applicability of these techniques to geopolymers are discussed in **Chapter 2**.

In order to provide valuable information regarding geopolymer durability as construction material, it is required to successfully determine the chloride diffusion coefficient through a series of potential commercially viable geopolymer recipes. Chloride was chosen as the foundation ion, by reason of its atomic qualities, as well as the growing concern of reinforced bar corrosion linked to this chemical in concrete structures worldwide. Chloride is a relatively small ion possessing minor polarising qualities. In simple terms, the characterisation of the behaviour for such an element will provide a relative comparison for larger, more polarised elements. The latter, in time scale terms, will undoubtedly take longer to diffuse through the same thickness of a given geopolymer recipe. This hypothesis was tested by determining the sulphate-ion diffusion coefficients through similar samples. It should be noted that each sample was composed from a unique recipe and made from the same batch, but was not subjected to both tests individually. Rather, each sample was cured (to a point of maximum compressive strength) and then cut into two pieces.

3.1.2. Diffusion cell

A simple diffusion cell (**Figure 3.1.2**) was designed and constructed on the idea of a similar set-up used by **Yeau & Kim (2005)** to perform the corresponding accelerated chloride-ion diffusion (ACID) test. The original design drawing appears in **Appendix D**. The test is used to determine the chloride diffusion coefficient (CDC) passed through a given concrete specimen. Here the same principle was used for analysing the geopolymer samples, where the experimental conditions and procedures were followed as given in **ASTM C 1202**, except for the applied potential difference and test duration.

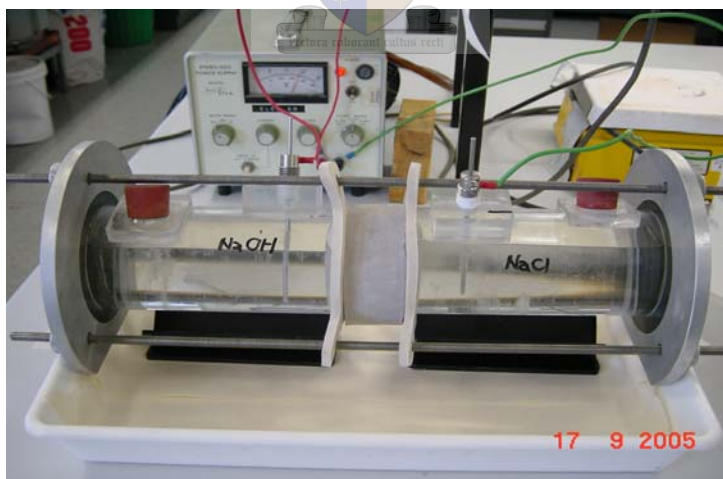


Figure 3.1.2: Diffusion cell set-up as used at the Melbourne University laboratories for determining the CDC.

Exporting issues prohibited the importing of the diffusion cell shown in **Figure 3.1.2** to South Africa. Another cell had to be made once returning to Stellenbosch University, which is presented in **Figure 3.1.3**. The cells were made from the same design and similar materials, with only minor chamber volume differences. These differences are accounted for in the relevant calculations and it is assumed for them to have a minor effect on the calculated coefficients.

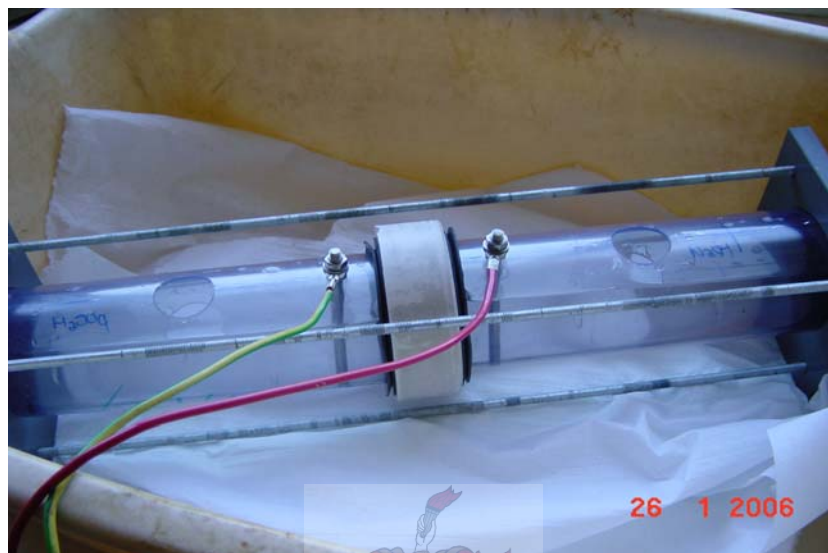


Figure 3.1.3: Diffusion cell replica as used at the University of Stellenbosch for determining the SDC.

All of the recipes shown in **Appendix C** were made up and moulded into 100mm diameter PVC pipe moulds (**Figure 3.1.4**). Plastic lids were fixed at one end of the 50mm long pipe sections. The filled moulds were then marked and sealed in individual plastic bags and cured at the specified temperatures and duration. Once the samples were fully reacted, they were cut into two radial slices, resulting in two round geopolymer “disks”.

Cutting of such large samples were quite difficult due to the amount of dust generated from the procedure. Conventional cutting methods with dry blades were not allowable in accordance with Australian Public Health and Safety Regulations. In the end, the correct instrumentation was found at the School of Earth Sciences (McCoy building) at the University of Melbourne, where a water-controlled cutter was used. It is recommended for future researchers, seeking to perform similar analyses, to rather mould two separate samples from the same batch.



Figure 3.1.4: PVC pipe moulds with geopolymer sample. The samples are carefully marked and sealed before curing and analysis.

Once the samples have been cured, cooled, de-moulded and cut, the sides were lightly polished with silicon carbide abrasive paper. This was done to ensure that all the loose surface particles are removed, and to minimise the surface effects of the samples.



Figure 3.1.5: The individual samples were lightly polished with abrasive paper. This minimised the surface effect on the samples and eliminated loose particles.

After completing the sample preparation, care was taken to clamp the samples in position in the diffusion cell. The horizontal rods (**Figure 3.1.2** and **Figure 3.1.3**) have to be tightened enough to prevent leaking and consequently significant liquid loss. The 0 – 50V power supply is now connected to the stainless steel electrodes, ensuring that the positive pole is connected to the NaOH chamber of the cell and the negative pole to the NaCl-filled chamber. For the sulphate experiments, the positive electrode was inserted in the NaOH chamber, while the H₂SO₄ chamber was connected to the negative pole.

The electrolyte solutions were prepared in bulk, at least a day before their intended use, ensuring that they have cooled and properly reached equilibrium (**Figure 3.1.6**). 5l of each solution was made and stored. The electrolytes were 3M NaOH and 3 wt% NaCl solutions made from the pure crystals/pellets dissolved in demineralised water. The sulphate diffusion experiments were performed at 3M NaOH and 3 wt% H₂SO₄ made from distilled water and laboratory grade chemicals. The specifications of the electrolyte concentrations are according to the **ASTM C 1202** standard.



Figure 3.1.6: The electrolytes were prepared in bulk and stored until required for use.

Once the power supply is switched on, clear H_2O and O_2 bubble-formation are observed at the respective electrodes (**Figure 3.1.7**). This bubble formation was used as a visual measure for the early rate of reaction/ion-migration and therefore used as an initial estimate for the sample permeability to the specific ion migration. When little to no bubbles were observed the voltage was increased and logged. The different voltage applications were considered within each diffusion coefficient calculation. The effect of the variation of voltages below 30V on the measured diffusion coefficient can be assumed to be negligible according to work done by **McGrath & Hooton (1996)**. This increased voltages proved to be essential for some of the denser geopolymer samples, where the time for ion breakthrough at lower voltages was excessive and impractical.

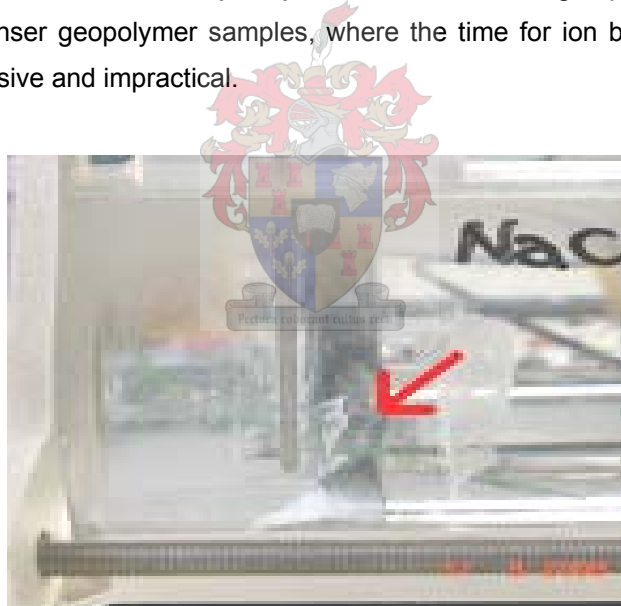


Figure 3.1.7: Bubbles appear at the electrodes once the power supply is switched on.

Hourly samples were taken for each chamber. A clean 5ml syringe was used for each sample, serving the dual purpose of preventing contamination as well as initiating mixing prior to sampling. Care was taken to minimise the volume of samples taken during each run, where a drastic change of electrolyte volume may alter the results. The aqueous samples were transferred to 10ml ICP tubes, clearly marked, sealed and used for IC and/or ICP-OES analyses.

3.1.3. PIXE (Proton Induced X-Ray Emission)

Seeing that the Diffusion Cell can detect the external/liquid concentrations of chloride, it still can not be quantitatively concluded that this number correlates to the chloride concentrations found within the matrix. **Jenneson et al. (1998)** overcame this problem by using scanning MeV proton PIXE on OPC and composite concretes. PIXE is believed to trace extremely low levels of chloride (<0.05 wt% in concrete) where other X-Ray, including EDX and WDS detector methods can only accurately identify levels above 1%. **Van Jaarsveld et al. (1998)** also used this method to trace quantities of encapsulated heavy metals.

Fortunately the Physics Department at Melbourne University (in collaboration with CSIRO Australia) was equipped with the required PIXE equipment (**Figure 3.1.8**).

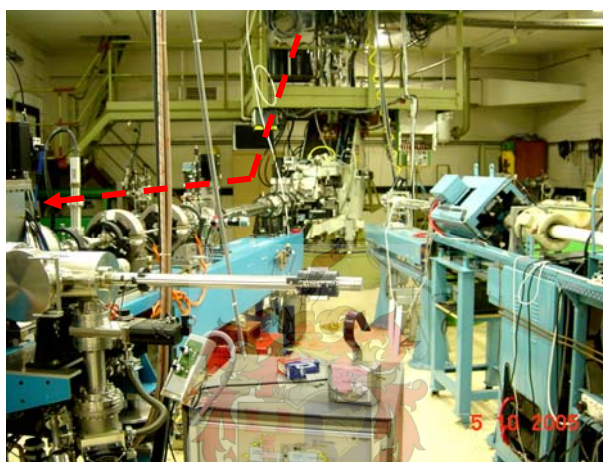


Figure 3.1.8: PIXE equipment at the Physics Department – University of Melbourne, Australia. The accelerator starts at the top of the dashed-line arrow, with the detector at the bottom.

Due to the excessive costs and time associated with PIXE analysis only one sample could be analysed. The recipe for the chosen sample is given in **Appendix C2**.

The sample was synthesised as previously discussed. The geopolymer mixture, however, was moulded in a 2cm diameter plastic phial. Curing was done at the elevated oven temperatures, then naturally cooled and de-moulded. An aqueous chloride solution was prepared, ensuring an excess as expected for coastal rain chloride content (**Brimblecombe, 1996**), estimated at 560mM. The sample was now soaked in a sealed container for a period of 3 months before running PIXE (see section 3.2 and also **Figure 3.2.1**).

Sample preparation for PIXE analysis was less intensive than required for other X-Ray methods like SEM (Scanning Electron Microscopy). The sample chosen for analysis was cut into a 2cm slice, using a diamond saw and oil based cutting lubricant (**Figure 3.1.9**). Usually water is used as coolant/lubricant for the diamond blade, but in this case the water could have

dissolved the matrix-contained chloride. A lubricant resistive to dissolving chloride was suggested by Leco®, the diamond blade suppliers.



Figure 3.1.9: Sample prepared for PIXE analysis.

The geopolymer sample was dried at 80°C for 2 days and lightly polished with silicon carbide abrasive paper, then glued onto a SEM stub with conductive carbon tape. Drying of the sample was required, seeing that the PIXE equipment operates under extreme vacuum conditions. Total carbon coating was done just prior to analysis.

PIXE equipment was fortunately also available for use on returning to South Africa. The facilities in South Africa are government owned (iThemba Labs), therefore drastically reducing analytical costs, resulting in more samples analysed. The PIXE equipment located at both Australia and South Africa was commissioned by the same company and runs from the same software program. This is extremely fortunate, seeing that the instrumentation used operates from the same basic principles and can therefore be directly compared. Samples used at iThemba Labs were shipped from Australia, introduced to an identical chloride concentration solution and left to soak for a period of 5 months in a sealed environment before analyses. The samples chosen to be analysed are also presented in **Appendix C**.

For further reading on the constraints and/or advantages of utilising PIXE as a material analysis tool, refer to **Breese & Jamieson (1996)**.

3.2. Corrosion monitoring

If this thesis is to successfully contribute to the wider commercial application of geopolymers, it has to clearly indicate or predict the behaviour of geopolymeric material in corrosive environments, especially when looking at using geopolymers in reinforced bar construction.

Also, if geopolymers are corrosive resistant it has to be clear how this material compares to the popularly used Ordinary Portland Cement (OPC).

Once the CDC for all the relevant formulations is known, one can primarily compare the measured values with those recorded for concrete. It is, nonetheless, still required to experimentally investigate the corrosion resistance for this material.

Initial tests were done to confirm that corrosion is in fact observed in some instances. Two variations of the recipe given as N1 and N25 in **Appendix C** were used for this purpose. One of the variations contained aggregate sand, while the other had no sand. The reasoning is that aggregate is believed to significantly alter the overall pore structure and density of the sample, where the amount of pores will definitely affect the diffusion of chloride through the matrix.

The two recipes were prepared as previously discussed, in 2cm diameter plastic phials, and shortened mild steel bars (3mm) were inserted in the slightly hardened geopolymer mixture. The bars were cleaned with a dilute hydrochloric acid solution prior to insertion. Care was taken to ensure that the entire bar was covered. One set of the sealed samples was left to cure at room temperature, while the others were cured in the oven. Once cured, the samples were left to soak in a 560mM chloride solution – exactly as discussed for the sample prepared for PIXE analysis.



Figure 3.2.1: Geopolymer samples were left to soak in a sodium chloride solution for an extended period of time in sealed containers.

After approximately 3 months these samples were removed from the solution, dried and prepared for SEM analysis. The sample preparation was very similar to that described for the PIXE analysis, the only difference being that more time was required to polish the samples, without destroying the matrix. Corrosion was observed at the matrix/bar interface, which now justified extensions to the investigation.

3.2.1. Copper/copper-sulphate half-cell

Chapter 2 discussed the benefits in monitoring the rate of corrosion when investigating a composite material to be used in reinforced constructions. Many authors (**Ayala et al., 2000, Yeau & Kim, 2005, etc**) made use of a copper/copper-sulphate half cell and used this standardised half-cell potential to interpret the extent of corrosion for a particular embedded rebar.

Similarly, a copper/copper-sulphate electrochemical cell (**Figure 3.2.2**) was made to perform comparable experiments on geopolymers.



Figure 3.2.2: Copper/Copper-sulphate half cell as used to determine the extent of corrosion for embedded reinforced steel bars. The method has been commonly used by concrete researchers, but was now also introduced into geopolymer research.

The cell was made from a 300 mm long, 30 mm diameter glass column, according to **ASTM C876-91** guidelines. The bottom of the sintered column is equipped with a 1 μ m porous glass plug, and both ends of the column are sealed with tight-fitting rubber plugs. The column was then filled with distilled water and an excess of cupric-sulphate crystals were gradually introduced, ensuring continuous stirring. The solution was left over night to reach equilibrium, before introducing the copper rod.

Firstly, the copper rod was lightly sanded with abrasive paper to eliminate any protective films. It was then soldered to an electrical copper wire by using a soft conductive lead alloy. The rod was carefully inserted into a snug hole in the top rubber plug (**Figure 3.2.2**).

The copper wire is now connected to a multimeter, while the other multimeter wire is connected to the sample rod (**Figure 3.2.3**).

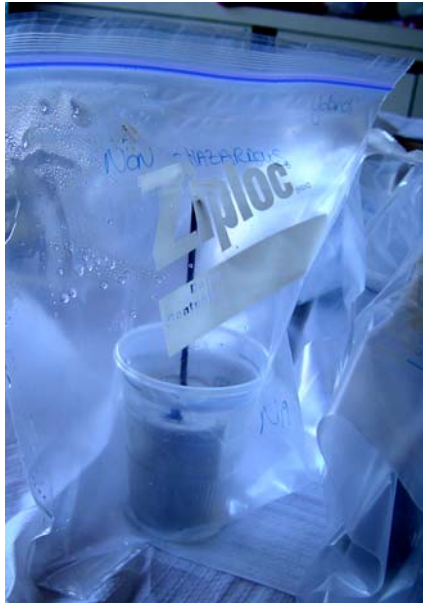


Figure 3.2.3: Copper/Copper-sulphate test samples. The samples were soaked in a 560mM NaCl solution and served a dual analytical purpose, both for PIXE (iThemba) and half cell potential testing. The samples remained sealed in plastic bags throughout the experimentation.

These samples were made by embedding Mild Steel bars (3mm diameter and ca 15cm long) into each of the geopolymer recipes (**Figure 3.2.4**) presented in **Appendix C**. The sample make-up and bar insertion were done as described for the sensors (see section 3.4). Prior to insertion, the mild steel bars were lightly cleaned with a dilute hydrochloric acid solution, which eliminated rust that might have already been on the unprotected bars. The geopolymer samples, along with the inserted bars, were sealed in plastic bags and left over night to set – allowing the bars to securely situate in their intended position. The sealed bags were then cured in an oven at the discussed temperatures and intervals.

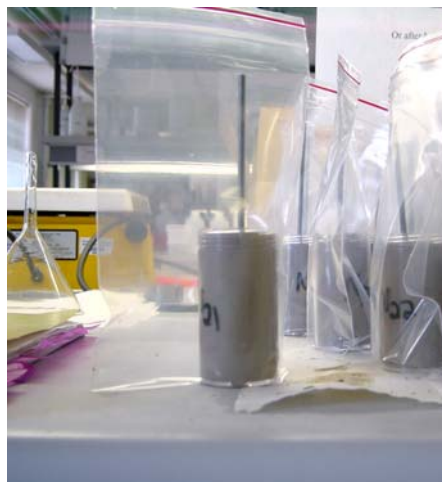


Figure 3.2.4: Mild steel bars were embedded in the respective geopolymer samples. The bars, as well as the top and bottom ends, of the geopolymer samples were coated with an epoxy coating after curing.

The cured samples were removed from the oven and left to cool naturally. Once cooled, the samples were removed from the 4cm diameter plastic phial and the top and bottom ends were also coated with an epoxy coating. Adequate time was allowed for the epoxy to harden before carefully placing the samples back into the phials and resealing them in the marked plastic bags. The epoxy coating will prevent diffusion in the longitudinal direction and restrict it to the radial direction, as well as further corrosion to the exposed mild steel bar.

Finally, the samples shown in **Figure 3.2.4** were soaked in a 560 mM NaCl solution (**Figure 3.2.3**) to become the copper half cell test samples. Half cell potentials were gathered by carefully taking the samples out of solution and connecting the rod to the multimeter, which in turn is connected to the copper/copper-sulphate half cell (**Figure 3.2.2**). Once the stabilised voltage could be read and noted, the sample was carefully placed back into its solution and the bag was tightly sealed.

3.3. Pore characterisation

Successfully modelling the diffusive, and therefore corrosive, behaviour of geopolymers relies on numerous parameters. Characterisation of the pores is an integral piece to the overall puzzle. Pore characterisation in this work relies on total pore volume, as well as total BET surface area.

3.3.1. Total pore volume

Each recipe was mixed (according to the previously discussed method) and moulded in 2cm diameter plastic phials. The phials were sealed and the samples were cured at 40°C for 12 hours and at 65°C for 24 hours. Once naturally cooled, the samples were de-moulded and ca 2-5 grams of each recipe was placed in individual weighing boats (**Figure 3.3.1**).



Figure 3.3.1: Sections of each geopolymer recipe were obtained and placed in a marked weighing boat. The samples were weighed before and after drying, therefore determining the total pore volume of each recipe. Here, the difference in colour of the two different fly ashes can be seen.

The total pore volumes were obtained by simply weighing the samples, then drying them at 100°C for 2 days. Once the samples have been cooled, they were re-weighed. The total pore volume is now simply the amount of water that evaporated during drying.

3.3.2. BET surface area

Samples for surface area analysis were prepared similarly to those shown in **Figure 3.3.1**. Samples of 1gram each were sufficient for successful analysis; therefore the samples were slightly smaller than those shown in **Figure 3.3.1**. Although it is believed that the surface area results are not affected by die geometry of the individual samples, care was taken to present a single sample of nearly 1g each.

The samples needed to be dried for the N₂ adsorption to be effective. Drying was accomplished by placing the samples in a 100°C oven for two days and 150°C for another two days.

The instrumentation used here, is classified as: ASAP 2010 (Accelerated Surface Area and Porosimetry System).

It has to be emphasised that all of the geopolymer mixture preparations discussed in this chapter were done in a single batch per recipe. In other words, the experimental design was done in such a manner that one large mixture per recipe was prepared and moulded in the variety of required moulds, conclusively eliminating some experimental errors and deviations.

3.4. Embedded sensors

The idea of an embedded sensor within a geopolymer matrix was explored. It was thought that if one can find an internal analyser/indicator one can learn more about the internal structure of a specific matrix without employing destructive methods. One area where this type of information can be extremely advantageous is with corrosion. Further exploration in the relevant literature revealed that a wireless, embedded sensor matching this description is being investigated at the University of Texas (**Dickerson et al, 2005**). It is, however, still being tested in the laboratory and not available for commercial use.

Seeing that very little is known about the osmotic potential, as well as the internal forces of the geopolymer during the re-precipitation and hardening phase, the search for an embedded force sensor began. Specification of such a sensor was increasingly difficult, where the extreme alkali environment during the sample make-up proved to be detrimental to most of the protective layers covering commercially available sensors. The sensor also had to be sensitive enough to detect a relatively low change in force readings.

Tekscan FlexiForce® sensors (**Figure 3.4.1**) seemed to be the best choice for the intended application, where it is designed to measure both static as well as dynamic force changes. One disadvantage to these sensors is that no absolute reading can be made without calibration. Calibration in this case is very difficult seeing that different geopolymer formulations are used for each application and geopolymeric material has not been tested on these sensors in the past. Relative readings are possible, therefore providing an indication of how these different geopolymer formulations perform with respect to each other. With this information it can be deduced which recipe/formulation best suit a required geopolymer function.

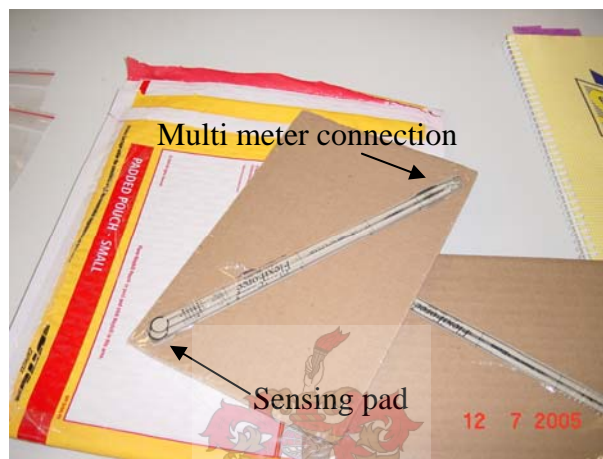


Figure 3.4.1: Tekscan FlexiForce® sensors used as embedded force sensors for the different geopolymer formulations.

The geopolymer samples for this analysis were made up as previously discussed, except that curing was not accelerated at elevated temperatures. The samples were cured at room temperature for an extended period of time.

Once the geopolymer mixture was made up, it was moulded into a 4cm diameter plastic phial. Depending on the type of formulation used, the sensor was embedded as soon as the gel began to thicken and the sensor could remain in its original inserted position. A distinctive difference between setting times are observed for formulations containing slag and aggregate. Care was taken to place the sensor as centred as possible within the cylindrically shaped sample.



Figure 3.4.2: Embedded FlexiForce® sensors. Care was taken to place all the sensors at relatively the same location in each sample.

The geopolymer recipes chosen for sensor embedment was N1, N2, N3, N4, N5, N6, N8, N10, N13, N14, N15, N16, N17, N18, N20 and N22. All of the recipes shown in **Appendix C** could not be investigated, due to the costs associated with these sensors. The justification for the recipe choice is discussed later in this thesis.

The reading of these sensors was done by use of a simple multimeter. The resistance readings ($M\Omega$ or $k\Omega$) are indirectly proportional to the force exerted by the geopolymer on the sensing pad (**Figure 3.4.1**). Readings were taken on a daily basis for a period of 44 days, which is a fair way beyond the expected 28 days for complete setting/geopolymerisation.

3.5. Osmotic potentials for geopolymers

Osmotic potentials have interested cement and concrete researchers for some time, due to the effect of capillary pressure on the fluid transportation properties during hardening (**Groot, 1993; Brocken, 1998**). It was measured that a mortar pressure of $1.2 \times 10^5 \text{ N/m}^2$ was developed by particles of *ca* $4\mu\text{m}$ and $2.5\mu\text{m}$ radii. Most of the research in this field was on the mortar/brick interface in typical buildings. Not only does fluid transportation as a whole contribute to the overall hardness of the concrete specimen, but it also plays a significant role in ion transportation when considering effects like corrosion. For this reason it is beneficial to measure the permeability of the material to water or aqueous solutions. Achieving this will require a steady-state flow conditions at a certain time, whose length depends on the period of cement curing and on the applied hydrostatic pressure (**Cioff et al., 1989**).

Seeing that non-aggregate fly ash-based geopolymers consist mainly of unreacted fly ash particles and geopolymeric gel, the pressure developed by independent particles will play an insignificant role. Osmotic potential in geopolymers can therefore be initially defined through capillary pore pressure. For the cases where aggregate is used, particulate pressure contribution should be accounted for. If one could prove that most of the pores directly link

the outside of the sample to the centre, where the rebar will commonly be placed, one may be one step closer in understanding geopolymer durability in terms of its microstructure.

The embedded sensors (section 3.4) can be used to determine if such a direct pore link exists. Experimentally it is possible to prove such a linkage if an outside hydrostatic pressure is applied to the sample and a simultaneous increased force reading is noted by the sensor.

Testing equipment had to be designed to fit the intended purpose, resulting in **(Figure 3.5.1)**. The sample is securely positioned into the detachable bottom (exposed sensor remaining outside the chamber) by use of a rubber o-ring. The chamber is then filled with water via the ball-valve, ensuring the entire sample is covered.

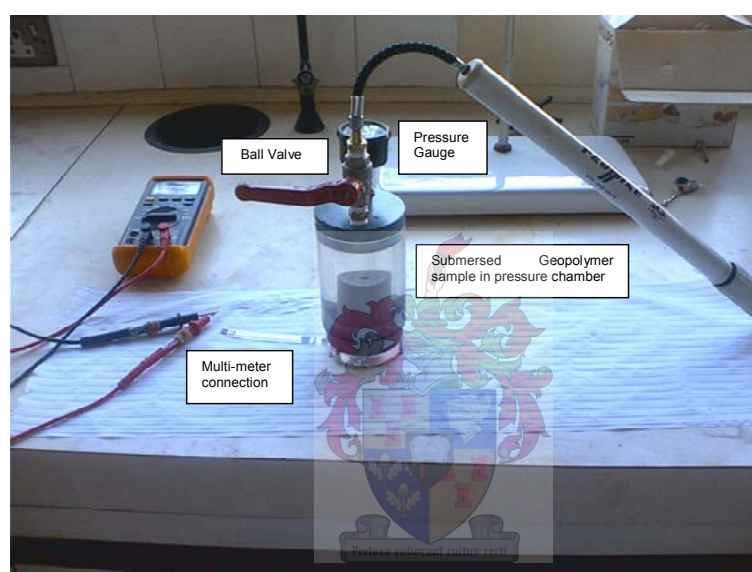


Figure 3.5.1: Test cell for determining geopolymer osmotic potential.

A portable bicycle pump is fitted to the valve outlet and the chamber is compressed up to the desired pressure (indicated by the pressure gauge). Once the desired pressure is observed, the ball valve is closed and the proper readings can be made from the exposed sensor pins.

The sensor readings were taken at fairly low pressures (typically 2.2 Bar gauge pressure), therefore not requiring compressed air through a regulator as the compression medium. A simple bicycle pump proved to be the safest and simplest option. **Cioffi et al. (1987)** and **Oh & Jang (2004)** independently investigated the effect of tortuosity (direct connected pores) on the concrete pore network by use of a 0.1 MPa hydraulic pressure.

3.6. Analytical techniques

As previously mentioned, a vast selection of analytical techniques has been employed and this section will discuss those methods used either independently or jointly in acquiring essential auxiliary information.

The techniques discussed here were mostly performed at The University of Melbourne, Australia, where it is principally accustomed to perform the analysis yourself. Adequate training, however, has been provided by the Melbourne University staff and post-graduate students.

3.6.1. X-Ray fluorescence spectroscopy (XRF)

XRF analyses were done on all the mineral based raw materials. Fortunately the data for the two ashes and GGBFS used in this thesis was available and supplied by Louise Keyte (**Appendix B**). Samples prepared for XRF was powdered, dried at 105°C and left to cool. An oxidiser, ammonium nitrate, is then added. Generally 0.5g of ammonium nitrate per 2.5g of sample is added, along with 5g of LiBO₂ (**Van Jaarsveld, 2000**). The composites were dry mixed, transferred to a platinum crucible and heated at 600°C for ca 10 minutes. During this process all the ammonium nitrate vapours are expelled. Next, the oven is heated to 1000°C which melts the LiBO₂, creating a homogenous glassy mixture. This mixture is now moulded into a disc and allowed to cool at ambient temperatures. These sample-discs were then analysed by a Siemens X-Ray fluorescence spectrometer.

3.6.2. X-Ray diffraction (XRD)

X-Ray diffraction is primarily used to identify both qualitatively and quantitatively a range of crystallographic phases. In this work XRD was used as a classification tool for the starting materials.

Fine powdered samples have to be tightly packed into the XRD sample holder. This was done with a clean microscope glass. Care should be taken to ensure a smooth, compressed sample surface. The samples (with an autosampler holding up to 12 samples) were run through a Phillips PW 1800 diffractometer. Scanning rate was set at 0.5° 2θ/min and counting times of 5 seconds. Identification of the various crystalline phases was done by use of diffraction patterns compared with the JCPDS (Joint Committee on Powder Diffraction Standards) data.

Refer to **Massa & Gould (2004)** and **Cullity & Stock (2001)** for in depth reading on XRD principles.

3.6.3. Compressive strength testing

All of the recipes were submitted to destructive compressive testing methods. Compressive testing (**Phair & van Deventer, 2001a**) is susceptible to factors such as test surface smoothness, age of the samples, internal moisture conditions, etc. It is therefore imperative that a stringent set of standards should be followed to ensure the reliability and credibility of

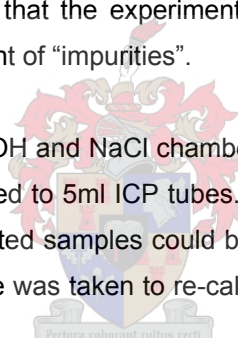
the data. The compressive strength testing methods were executed to comply with the **Australian Standards 1012.9 (1986)**.

The sample-mixtures were prepared and cast into 50mm x 50mm x 50mm cubes. All of the samples were mixed with dried sand aggregate, where pastes usually produce inaccurate compressive strength results. Cast samples were vibrated for 2 minutes on a mechanical vibrator and sealed in plastic bags. Curing commenced at 40°C for 12 hours and then 65 °C for 24 hours. The samples were left to cool at room temperature before running them through an ELE compressive strength testing apparatus. Results for the 25 recipes appear in **Appendix C**.

3.6.4. Inductively coupled plasma spectroscopy (ICP-OES)

All liquid samples, taken from both sides of the chloride diffusion cell experiments, were analysed for Pb, Si, Zn, Co, Ni, Al, Cu, Mg, Fe and K using a Perkin Elmer Optima 3000 instrument. Standards for each of these elements were prepared, covering a broad range of concentrations (0.1ppm to 50ppm). The water used in preparing these samples was from the same source throughout, ensuring that the experimental solutions as well as the standard solutions contained the same amount of “impurities”.

The aqueous samples from the NaOH and NaCl chambers were obtained by using clean 5ml syringes, which were then transferred to 5ml ICP tubes. The tubes were clearly marked and labelled for storage until all the related samples could be analysed in one run. This reduced any instrumentation deviation. Care was taken to re-calibrate the instrument between sets of 20 samples.



For the sulphate diffusion cell experiments, ICP (Agilent Octopole Reaction System 7500ce quadrupole ICP-MS) was used to determine the sulphur content in the NaOH-side chamber. This data could then be converted to the sulphates content, required for the diffusion coefficient determination. ICP had to be used here, due to the fact that the IC columns available at the University of Stellenbosch were not able to accommodate the caustic environment of the base solution and dilution would reduce the sulphate concentration below detection limits.

Further reading on ICP technical principles can be obtained from **Nölte (2003)**.

3.6.5. Scanning electron microscopy (SEM)

Instrumentation limitation and sample preparation requirements regulated the amount of samples that could be analysed. Primarily, the only samples imaged with SEM were the preliminary detecting samples for corrosion (section 3.2).

The samples were cut with a diamond saw (using an oil-based blade lubricant), dried and polished with abrasive paper. They were then affixed onto a SEM stub with conductive carbon tape and vacuum carbon coated prior to analysis. Elemental mappings were conducted using SEM-EDX. The obtained images were primarily used to establish whether or not corrosion was observed.

For supplementary technical data surrounding SEM principles, the reader is referred to **Postek (1980)**.

3.6.6. Infrared spectroscopy (IR)

Infrared spectroscopy makes use of radiation to provide information about the vibration transitions and rigidity of chemical bonds (**Stuart, 2004**). For this work, infrared spectra were used in instances where precipitate was observed on the samples during the diffusion cell analysis. The precipitate was removed with a clean spatula and compressed between two clean microscope glasses. Consideration was given to what the precipitate might consist of and spectra of relating chemicals were obtained in parallel. This proved to be a very simple method in identifying unknown compounds. The results from the obtained spectra are discussed in the relevant text.

The infrared technique of choice here was Fourier transform infrared spectroscopy using the known “potassium bromide disc sample preparation” method. The latter is done by mixing a small quantity of sample (less than 1 gram) with ca 250mg KBr. The mixture is then ground to a fine powder and compressed into a solid (translucent) material. The sample is then placed in the infrared beam and the experimentally determined spectra are compared with samples of known composition.

3.6.7. Ion Chromatograph (IC)

Ion Chromatographs were acquired by using a Dionex apparatus. Liquid samples from the diffusion cell runs were injected in 1ml volumes into the Dionex manual sampler. The samples were not diluted due to the low concentrations of the element of interest already present. The elements detected by use of this method are mainly chlorides. Prior to each analysis a calibration curve was obtained from pre-prepared standards.

The data obtained are presented as the respective diffusion profiles, which largely contributed to the generation of the respective diffusion coefficients, in the applicable text.

Ion Chromatography relies on separation principles, for further reading on this subject; please refer to **Fritz & Gjerde (2000)**.

3.7. Summary

As stated earlier, the broad investigation on geopolymer durability as construction material (or any other application) presented in this thesis can not be well defined by use of a single set of analytical techniques. In most instances the techniques are combined and integrated to produce meaningful results.

Only fly ash-based geopolymers are considered, but they were subjected to different “attack” ions and subsequently other analytical methods. The compositions of the matrices being investigated are presented in **Appendix C**, where some limited techniques were only performed on a selection of formulations. The deviations/exclusions are clearly stated where applicable.

The experimental design was clearly defined before commencing the physical experiments. This generated a situation where a single mixture of a specific geopolymer recipe could be made and moulded into the selection of required size and geometries, as set out by analytical instrumentation requirements. In the end, this method eliminated batch-to-batch deviations, as well as raw material deviations, commonly found in this type of experimentation.

Essentially, the experimental work focussed on obtaining representative diffusion coefficients for the stated geopolymer formulations. These diffusion coefficients are then combined with corrosion resistance observations and will ultimately contribute to the overall estimation of geopolymer durability. Emphasis is on the fact that the outcome must be comparable to the well-known OPC data, and in turn, establishing a basis for the incorporation of geopolymers into Cement and Concrete Technology.

Chapter 4.

INITIAL GEOPOLYMER PHYSICAL CHARACTERISATION

The durability of any brittle material relies not only on a single set of properties, e.g. its diffusive behaviour, but also often associated with numerous parameters such as: specific pore volume, BET surface area, sample compressive strength, etc.

The purpose of this chapter is to introduce some of these auxiliary physical parameters which will contribute to the diffusion coefficients covered in later chapters, eventually aiding to successfully portray the behaviour shown by certain geopolymer formulations under specific conditions. Only then can the expected durability of these materials be defined, compared or even be predicted.

Chapter 4 commences by looking at the possible correlations found between the geopolymer formulations in terms of pore characterisation and compressive strength. Although covered more extensively in later chapters, the copper/copper-sulphate half cell potentials will then be discussed with the emphasis on predicting the diffusive behaviour expected by each formulation.

The chapter will conclude by considering the hydrostatic pressure experienced by a selection of formulations, which will additionally support the pore characterisation and description sketched earlier in this chapter.

4.1. Pore-volume, -area and compressive strength

Originally a relationship between the measured pore volume and BET pore area was investigated, yielding **Figure 4.1.1**. Pore volume here refers to the total expected specific pore volume for each geopolymer formulation. The data points in this figure possess no clearly defined fit, with the closest match being a logarithmic trend line ($R^2 = 0.5455$). Through this scatter of data points a cluster of “low value” points denoted by recipe N10 to N12 and N22 to N25 can be seen. The remaining points deviate slightly from a communal Pore Volume (PV) value, but differ significantly in BET surface area, suggesting a distinctive difference in pore geometry.

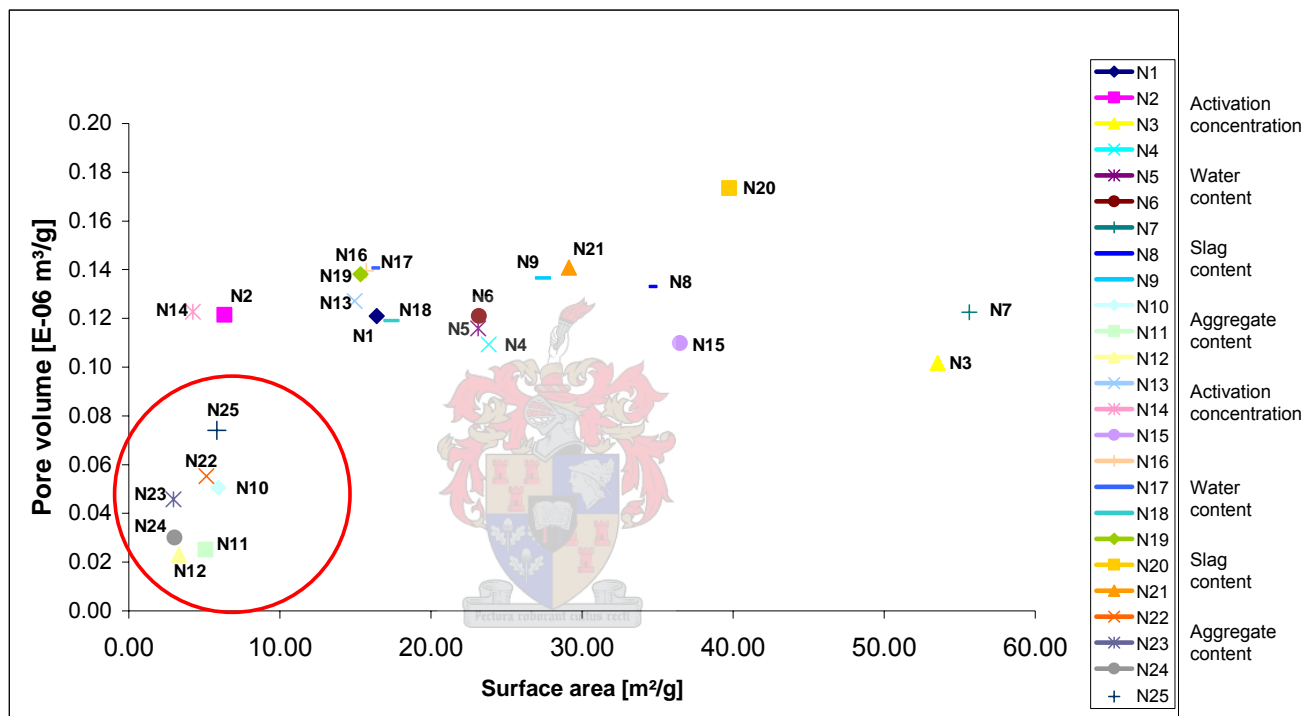


Figure 4.1.1: Pore volume vs. Surface area for the geopolymeric samples. These samples have not been exposed to any external ionic solution.

The “low value” cluster of points enclosed in **Figure 4.1.1** consists of the samples with added aggregate, except for sample N25 containing both GGBFS and aggregate. An increase in aggregate for the fly ash A samples (N10 = 2.1g sand/g fly ash, N11 = 3.15g sand/g fly ash and N12 = 4.2g sand/g fly ash) results in a decrease in pore volume vs. surface area ratio. The reverse is observed for the fly ash B- based samples (refer to **Figure 4.1.2** for formulation notation). The pore volumes as presented in **Figure 4.1.1** include the specific mass of aggregate to samples N10 to N11 and N22 to N25. The results when normalising the mass of the affected samples are discussed in section 4.2.

This phenomenon suggests that the pores with this lower value in -volume and -area generally have to be either shorter or narrower than their higher value counterparts. Deciding

which one of these characteristics is predominant, the measured compressive strength for each specimen (see **Appendix E**) needs to be considered.

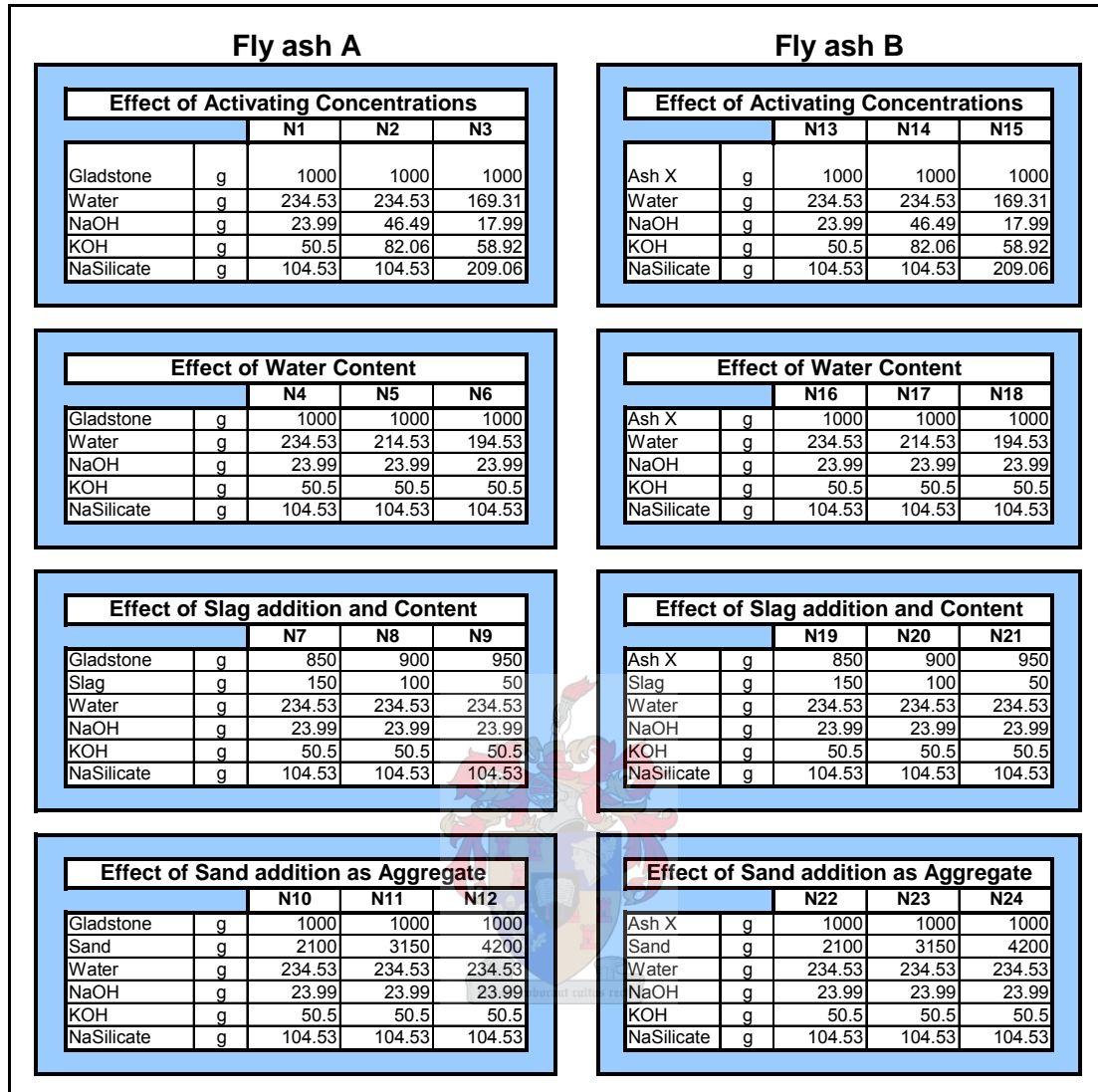


Figure 4.1.2: Geopolymer formulations and nomenclature as used in this investigation. Gladstone refers to the origin of one of the fly ashes. The other is unnamed owing to confidentiality.

Looking at the relationship of Pore Volume vs. Compressive strength for only the aggregate containing samples (**Figure 4.1.3**), another scatter of data is found. Once again, a general trend of higher compressive strengths is found for samples with higher pore volume values. According to **Askeland (1998)**, who stated that smaller pores give rise to tiny micro-cracks in brittle material, the pores in these samples have to be smaller in width, longer and more of them present per unit sample. These micro-cracks are too small to propagate by themselves and also help to blunt larger cracks trying to grow; in effect larger compressive loads can be handled by these materials.

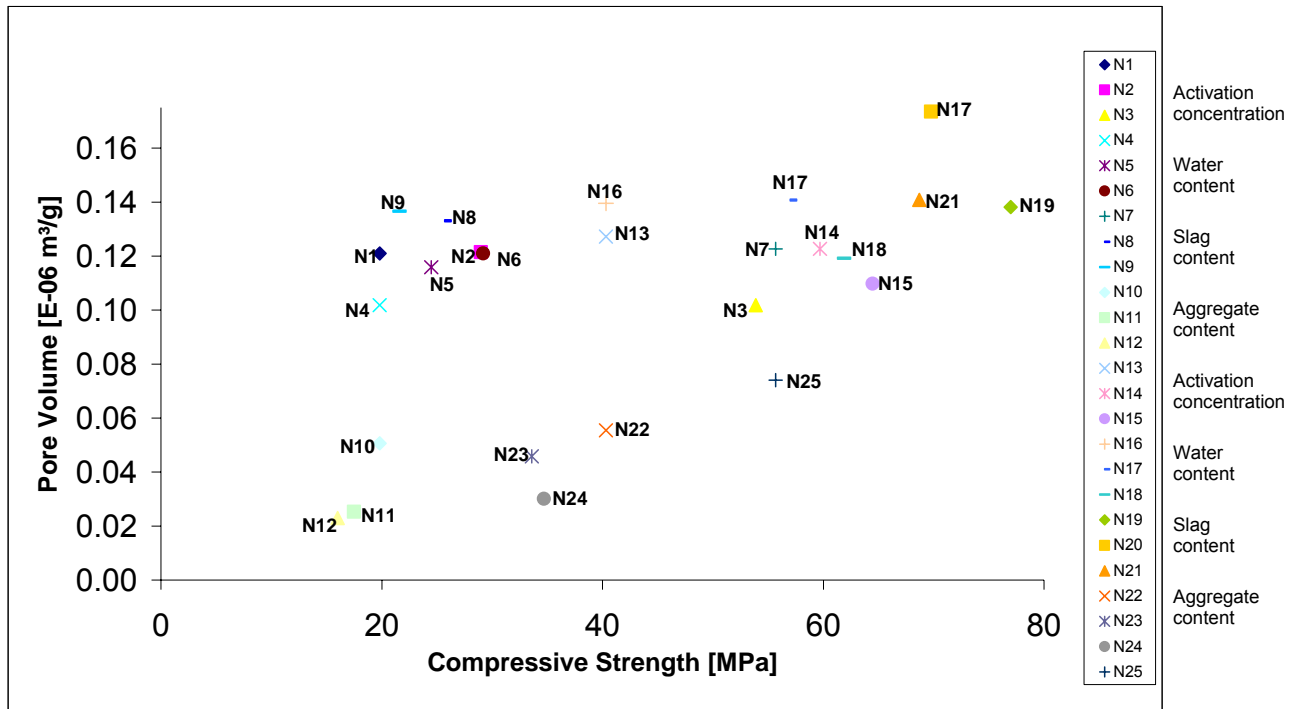


Figure 4.1.3: Specific pore volume vs. Compressive strength for the non-exposed samples.

The fly ash A-based samples indicated by the low range cluster in **Figure 4.1.1** (N10, N11 and N12) can now be characterised as being shorter, slightly broader pores with a lower count per unit sample. Expectedly so, they also form part of the lower data points in **Figure 4.1.3**. In addition, an increase in aggregate addition to these samples results in a lower pore volume to compressive strength ratio, suggesting that aggregate favours the formation of shorter, broader pores. This observation holds for the fly ash B-based samples (N22 to N24), with the exception of these samples producing larger compressive strengths; proposing that the fly ash B samples generate slightly longer, but narrower pores. This idea is supported by considering the larger surface area to pore volume ratio shown in **Figure 4.1.1**. Sample N25 presents a surprisingly high compressive strength, urging the significant effect slag has on the matrix.

An increase in activation solution concentration results in a scatter of pore volume to surface area ratios for the fly ash A specimens, where N2 produces the highest ratio and N3 the lowest. Furthermore, the pore volume to compressive strength ratios decreases with this increase in activation solution concentration. These observations suggest that sample N3 possibly consists of a network of longer, narrow pores but with a lower count per unit matrix. The suggested pore network of N2 is also a system of long/narrow pores, but possibly higher in count. The most fitting explanation for N1 is that it may consist of a combination of both long/narrow and short/broad pores, with the long/narrow pores being the dominating species.

The effect of activating solution concentration on the fly ash B specimens follows similar trends as discussed for the fly ash A specimens. A higher pore volume to surface area ratio is found for these samples, as well as a lower pore volume to compressive strength ratio. Expectedly so, the compressive strengths for these samples are significantly higher than their fly ash A equivalents: the suggested pore characteristics now being a network of increased amount of long/narrow pores. This hypothesis will be proven if the corrosive activity for these samples is higher than those found for samples N1 to N3.

Varying the water content in the fly ash A samples (N4 = 234.53g water/1000g fly ash, N5 = 214.53g water/1000g fly ash, N6 = 294.53g water/1000g fly ash) has a seemingly insignificant effect on the pore volume to surface ratios (**Figure 4.1.1**). A slight difference is observed in the pore volume to compressive strength ratio (**Figure 4.1.3**), where it decreases with a decrease in water addition. The pore structures for these samples are possibly predominantly long and narrow, with the average continuous pore length increasing with decreasing water content. In order for the similar pore volume to surface area ratios to balance for these three variants, the number of pores per unit matrix has to decrease with decreasing water content.

Fly ash B-based samples responded similarly to varying water content, where it is anticipated that a decrease in water content promotes the formation of long/narrow pores. Yet again, higher pore-volume to surface area and lower pore-volume to compressive strength ratios are found for samples N16 to N18. The resulting pores will therefore be higher in count than those found for samples N4 to N6.

Early in this chapter the unexpected performance of sample N25 revealed the significant effect of slag addition to a geopolymeric matrix. The fly ash A specimens (N7, N8 and N9) showed very similar pore volumes, but significantly different surface areas (**Figure 4.1.1**). The result being that the pore volume to surface ratios increased nearly linearly with a decrease in slag addition (N7 = 150g slag/850g fly ash, N8 = 100g slag/900g fly ash, N9 = 50g slag/950g fly ash). Also, the pore volume to compressive strength ratios increased sharply with a decrease in added slag. Combining these properties, it can be concluded that slag promotes the formation of long, narrow pores, elucidating the decrease in compressive strength with decreasing slag content where the pores will be predominantly short and broad. Research papers by **Yip & van Deventer (2003, 2005)** and **Yip et al. (2003)** discuss the effect of slag on a microscopic scale for metakaolin-based geopolymers.

Interesting results are found for the fly ash B samples upon varying the slag content. Firstly, similar to findings for samples N7 to N9, the pore volume to surface area increases with decreasing slag. The BET surface area value for N19 (N7 equivalent) seems to be too low, while re-running the sample yielded the same result. Seeing that both the ashes are Class F ashes, it is not expected for them to react to slag differently and the same trends are

anticipated. Also, the pore volume to compressive strength ratios for samples N19 to N21 are basically equal, but substantially lower than the corresponding fly ash A samples. Up to now this phenomenon has been associated with the pores becoming narrower and longer with decreasing slag addition and the higher compressive strengths recorded for these samples match up with the statement. However, later it will be shown that samples N19 to N21 resisted chloride penetration better than samples N7 to N9, which contradicts the idea that samples N19 to N21 will consist of a network of continuous, narrow pores. Although not substantiated in this thesis, it may be possible that the pore network of these samples remain to be that of a series of micro-pores (long and narrow), but they do not link into a continuous pathway as expected, rather into a series of inter-connected pores with low radii of curvature. Mercury-intrusion analyses may assist in further explaining this observation.

Essentially, the samples containing larger pore volumes to surface area ratio and compressive strength values consist of a network of increased quantity of longer but narrower pores. This hypothesis can be confirmed if it is found for the Mild Steel (MS) embedded samples possessing these characteristics to corrode more easily, due to the expected lengthened pathways for small ions like chloride to pass through. Conversely, the shorter, narrower pore structures should be more resistive to chloride penetration, where continuous pathways may be lacking.

4.2. The effect of aggregate on pore volume results

The addition of aggregate (washed and classified silica sand, particle size *ca* 2-3mm) to a specific formulation will greatly increase the sample mass for equal amounts of geopolymer paste. If it is to be assumed that the silica sand aggregate is completely inert to this system, the pore volume results will differ from those presented in section 4.1.

The samples affected by aggregate in this investigation are N10, N11, N12, N22, N23, N24 and N25. Reconstructing **Figure 4.1.1** and **Figure 4.1.3** for the normalised geopolymer paste pore volume yields **Figure 4.2.1** and **Figure 4.4.2**. The normalised pore volume is obtained by excluding the mass of aggregate from the pore volume calculations, therefore only considering the effect of the paste.

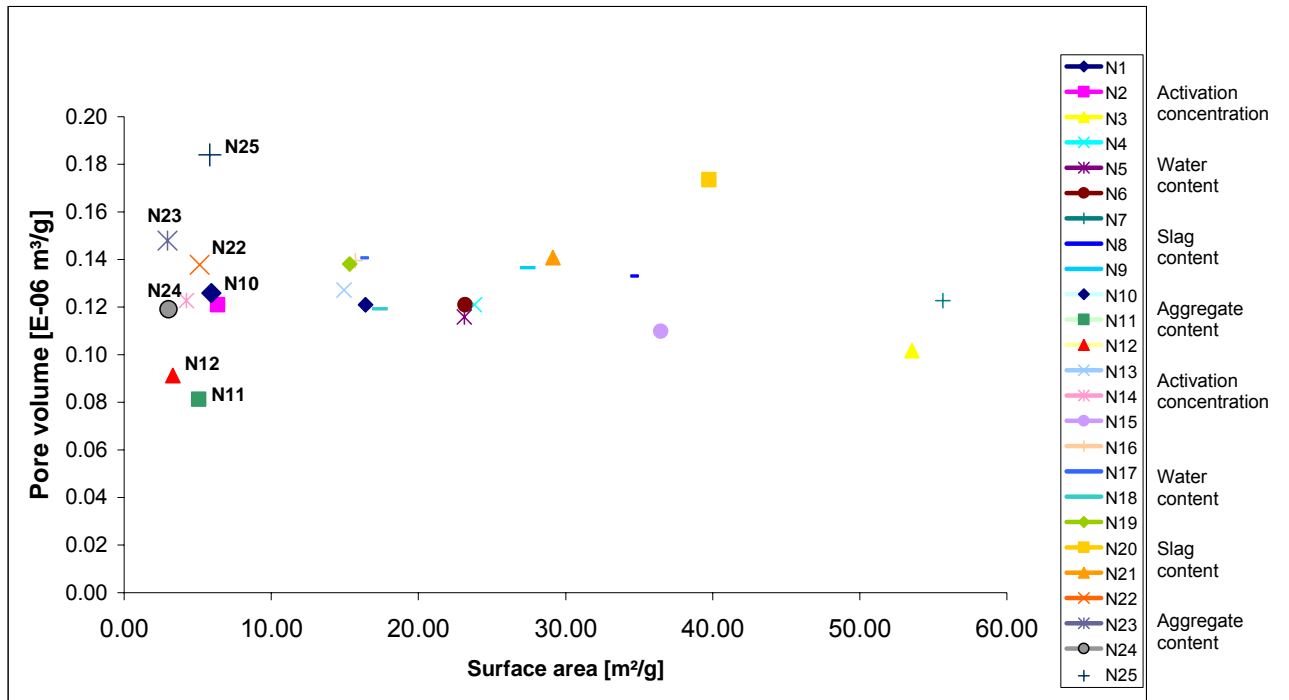


Figure 4.2.1: Pore volume vs. surface area for all the geopolymer samples. The normalised pore volume samples are labelled.

The scale presented in **Figure 4.1.1** remained constant for **Figure 4.2.1**. The differences in pore volumes for the labelled samples are evident from these figures and will significantly influence the discussions following **Figure 4.1.1** and **Figure 4.1.3**.

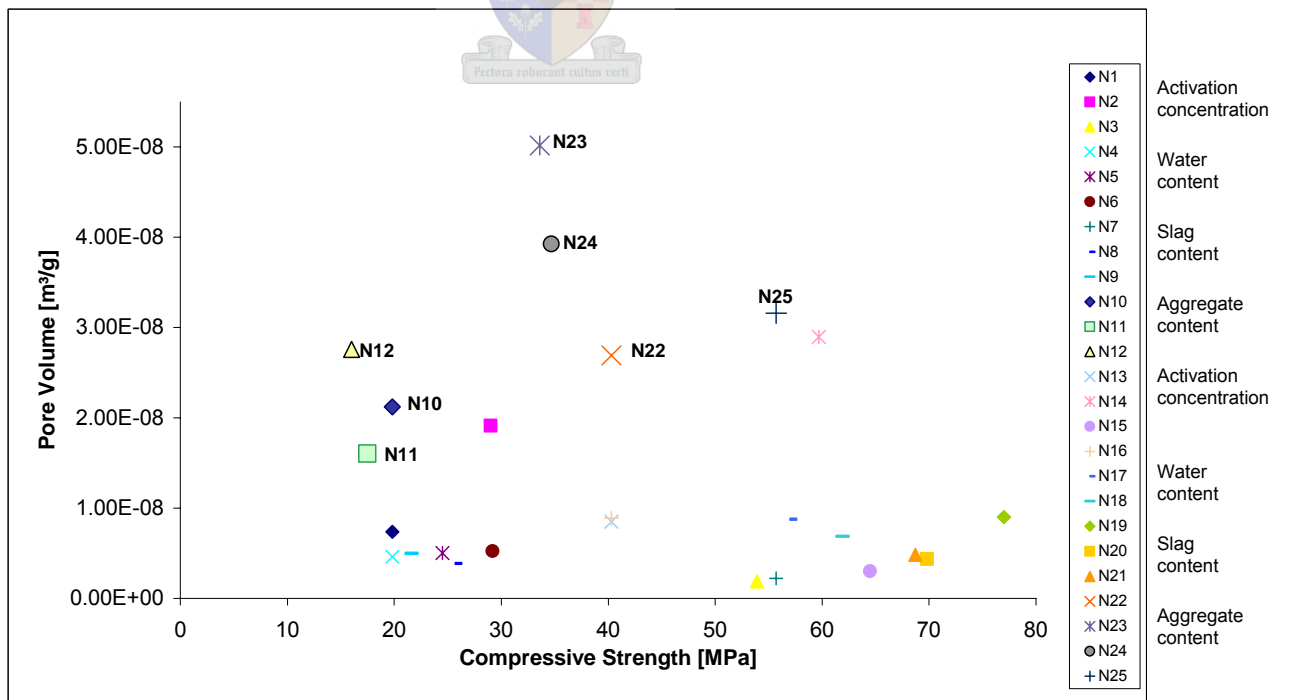


Figure 4.2.2: Pore volume vs. compressive strength values for all of the geopolymer formulations. The samples affected by aggregate are labelled.

Once more the scale presented in **Figure 4.1.3** remained constant for **Figure 4.2.2**, enabling direct comparisons. The normalised pore volume nearly contradicts the conclusions drawn in section 4.1. The resulting pore structures for samples containing aggregate are now expected to be a network of long/narrow pores (**Figure 4.2.1**), but the low values in **Figure 4.4.2** suggests the opposite. The diffusion coefficients presented in later chapters supports the hypothesis which suggests that aggregate favours the formation of shorter/broader pores.

The contradiction evident from the pore volume to surface area and pore volume to compressive strength trends, presented in this section, suggests that the silica sand aggregate is not entirely inert to this system. Visible proof of the contribution of silica sand to the overall pore network lies within PIXE maps.

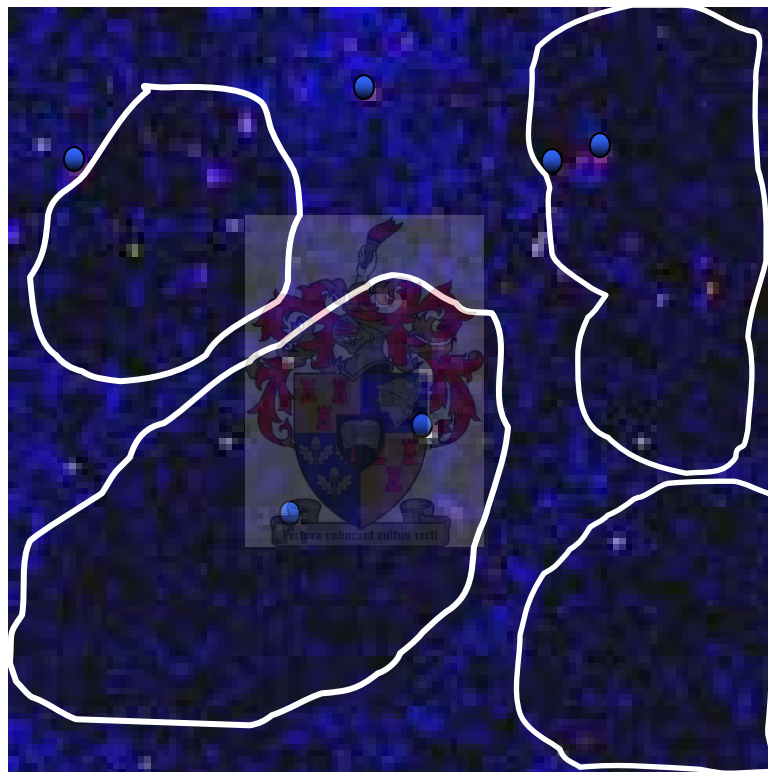


Figure 4.2.3: PIXE map tracing chloride in sample N22 containing aggregate. The aggregate particles are encircled. Although favouring the geopolymer paste, chloride is present throughout the sample.

The PIXE map presented in **Figure 4.2.3** is the equivalent to an enlarged outer rim area, as shown in **Figure 5.4.2**: Elemental map for chloride as seen by PIXE detectors.. The lighter spots in **Figure 4.2.3** represent the chloride ions diffused into the material. Chloride is present throughout this map, suggesting that the silica sand must provide a pore network for the migration of these ions within the aggregate particle. It is therefore impossible to fully exclude these particles from the discussions presented in this work. The scale to PIXE maps are generally generated in pixels, which are equivalent to $1\mu\text{m}$. The maps act only as a visual

representation to the presence of specific elements, while the GeoPIXE® software processes quantitative data.

Although not considered, future researchers in this field may find it useful to investigate the exact extent to which the silica sand aggregate contributes to the overall pore volume and therefore the resulting pore network.

4.3. Average half cell potentials

Although discussed more intensively in later chapters, the measured half cell potentials for each geopolymer formulation may confirm or disprove the suggested pore characterisation as described above.

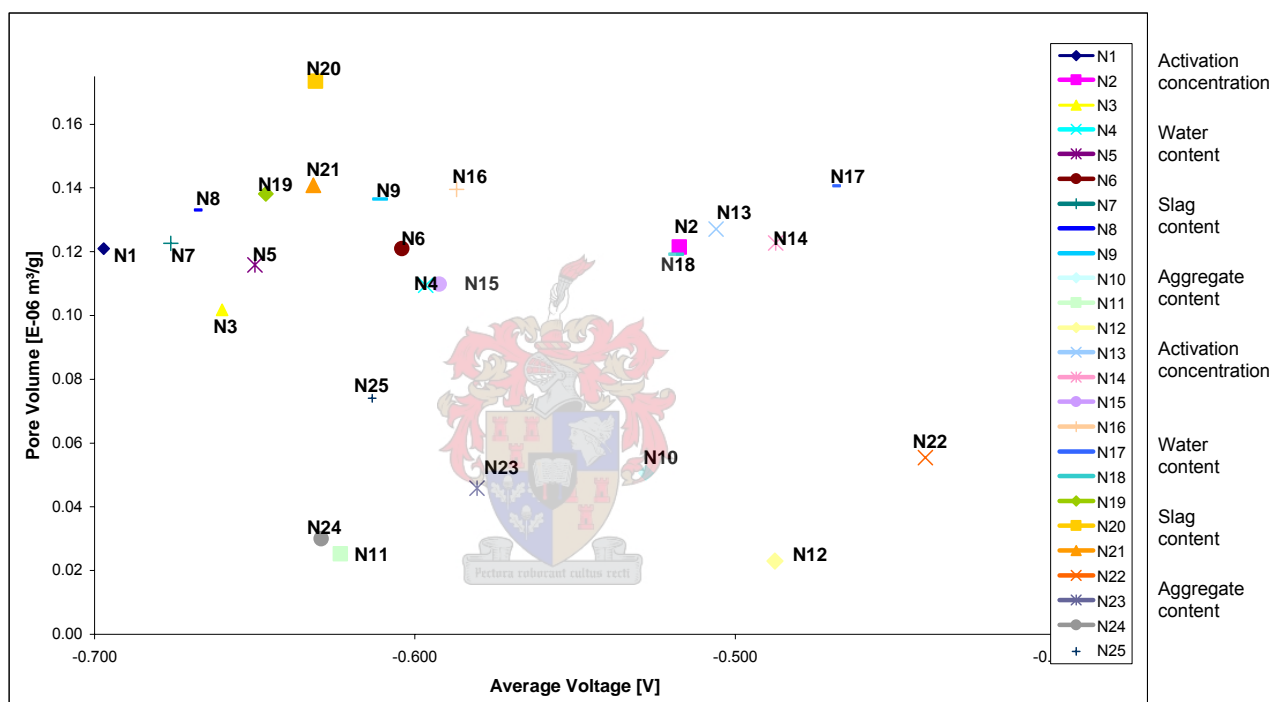


Figure 4.3.1: BET surface area vs. the Copper/Copper-Sulphate half cell potentials.

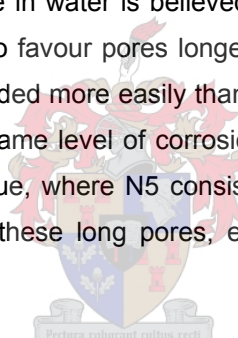
The average Copper/Copper-sulphate half cell potential values were compared with that of the measured BET surface area for each sample, as seen in **Figure 4.3.1**. All of the values are below -0.35V , suggesting a 90% probability that active corrosion is present. Comparisons to OPC literature will follow in subsequent chapters.

The data points in **Figure 4.3.1** (for the sake of clarity) may be defined in three different “groups”: The groups are separated in a low ($> -0.550\text{V}$), medium ($< -0.550\text{V}$ and $> -0.650\text{V}$) and high ($< -0.650\text{V}$) extent of corrosion. Generally it is found that those samples with a lower surface area tend to show a lower extent of active corrosion. The mid range of half cell voltages shows quite an extreme scatter and no distinct conclusion can be drawn here. The higher half cell voltage data points tend to show greater surface areas.

Section 4.1 hypothesised that an increase in activation solution concentration favoured the formation of longer, continuous and narrow pores. Sample N1 was believed to consist of a combination of short/broad and long/narrow pores. The corrosive behaviour exerted by these formulations, **Figure 4.3.1**, shows the pore characterisation hypotheses to be true. N3 with the expected continuous long/narrow pores showed severe corrosion. N2 with the shorter pores presented far less active corrosion. Sample N1 with the combined pore structure also showed aggressive corrosive activity, suggesting that the pores are predominantly long and narrow.

The fly ash B-based samples were expected to show more active corrosion than samples N1 to N3, but the surface area to half-cell voltage comparison contradicted this expectation. It may be possible that variation in activation concentration affects the pore width of the fly ash B specimens more than it does the length, concluding that the pore lengths are probably equal in both ashes, but are generally narrower for the fly ash B samples.

The amount of water added to the geopolymer mixture is believed to influence the total amount of pores, where a decrease in water is believed to result in less pores. Decreasing amount of water is also assumed to favour pores longer in length. **Figure 4.3.1** shows that sample N5 ($V_{ave} = -0.650\text{Volt}$) corroded more easily than N4 ($V_{ave} = -0.597\text{Volt}$), with N6 ($V_{ave} = -0.604\text{Volt}$) showing almost the same level of corrosion as N4. The pore characterisation can therefore be assumed to be true, where N5 consists of a network of continuously long pores, while N6 will have less of these long pores, effectively presenting lower corrosion activity.



The fly ash B specimens resulted in lower half cell voltages, suggesting that once again the pore width was more strongly affected by varying water content. The resulting pores will therefore follow the trends as discussed for fly ash A, but will be higher in count and narrower.

The effect of slag on the pore structures concluded that the addition of slag favours the formation of long and narrow pores. The corrosive activity revealed by samples N7 ($V_{ave} = -0.676\text{Volt}$), N8 ($V_{ave} = -0.669\text{Volt}$) and N9 ($V_{ave} = -0.611\text{Volt}$) in **Figure 4.3.1** shows this assumption to be true, where a decrease in slag showed a decrease in copper/copper-sulphate half cell potential.

The pore geometry resulting from fly ash B is expected to become longer and narrower with an increase in slag addition. The products from this ash presented lower half cell voltages than the fly ash A equivalents, implying that either the pores are more intertwined or they exist as shorter, but substantially narrower pores. As mentioned earlier, mercury intrusion analyses may assist in explaining the observations.

The influence of aggregate on the resulting pore structures is more prominent than the rest of the formulation variations. An increase in added aggregate will support the formation of short and broader pores. The formulations with more than 3150g sand per 1000g fly ash resulted in very porous structure, with visible macro-cracks. The corrosive behaviour therefore increased with increasing sand addition, largely due to the formation of the macro-cracks. Proof of the hypothesis now lies in the low level of active corrosion samples N10 (2.1g sand/g fly ash, $V_{ave} = -0.528\text{Volt}$) and N22 (2.1g sand/g fly ash, $V_{ave} = -0.441\text{Volt}$) showed where sample N22 was the least corroded of all the samples. The compressive strength of sample N10 is also very low, concluding that the pores had to be broad and short; therefore lacking a continuous pathway for chloride migration. The compressive strength of N22 is appreciably larger, while the corrosion activity was lower. The resulting pore geometry of this sample therefore possibly exists as narrower pores, but not long enough to link the external surface to the MS rebar. Conclusively, the addition of aggregate seems to predominantly affect the width of the resulting pores, hence an increase in pore width with increasing sand addition.

Another possible confirmation method for this hypothesis may lie in the osmotic behaviour shown by the pore network when an external hydrostatic pressure is applied.

4.4. Geopolymer hydrostatic pressure potential

Implementing the pressure cell as described in **Chapter 3**, a relative variation in applied hydrostatic pressure for a selection of geopolymer formulations could be gathered. The difference in resistance (Ohm) readings from the embedded FlexiForce® sensors served as the indication for possible internal pressure variation. Due to calibration difficulties, these values could not be converted into specific pressure values, but rather served as an indication of relative increase in sensing pressure when a constant hydrostatic load is applied. The sensing abilities between the different sensors are assumed to be consistent, thus enabling one to use the relative variations to compare the resistance to hydrostatic pressure for each sample.

The completely reacted matrix of each geopolymer sample is also believed not to subside to an external hydrostatic load of 2.2 Bar. The force sensed by the FlexiForce® sensing pad is therefore assumed to be that of the pressure exerted by the pore fluids. A larger variation in Ohm reading from the sensor will indicate a continuous pore structure where the external surface is somehow connected with the embedded sensing pad. Conversely, a low variation will indicate the robustness of that sample to an externally applied force.

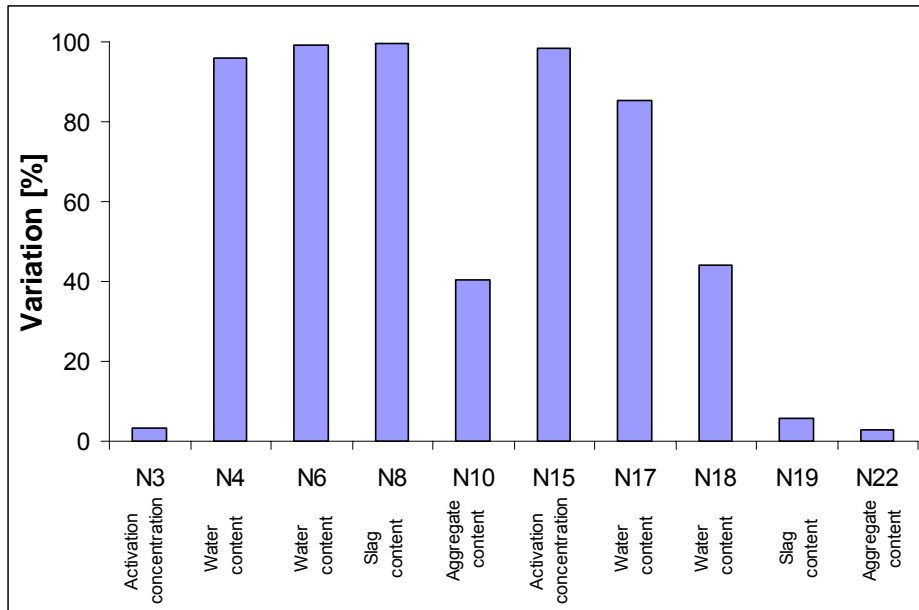
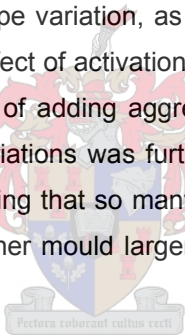


Figure 4.4.1: Percentage variation in FlexiForce® resistance readings for selected samples.

Costs associated with the use of the FlexiForce® sensors limited the experimental design to a single sample being selected per recipe variation, as well as Fly ash variation. Each of the bars in **Figure 4.4.1** represents the effect of activation solution, effect of water addition, effect of slag addition as well as the effect of adding aggregate for each Fly ash. The extent of comparison between these recipe variations was further limited by cracking of samples N1, N2, N5, N9, N13, N14 and N16. Seeing that so many samples showed destructive cracking after curing, it is recommended to either mould larger samples or replace the sensor with a smaller variant.



Sample N3, **Figure 4.3.1**, showed a high extent of corrosion, while it is associated with a low pore volume to pore area variation, a mid range compressive strength and a low variation in hydrostatic potential (**Figure 4.4.1**). The low pore volume to pore area suggests a network of broader, shorter pores. The mid range compressive strength suggests that a combination of narrow/long and broad/short pores exists, but favouring the broad and short pores. Low variation in hydrostatic potential reinforces this fact, but the high extent of corrosion contradicts it. Upon inspecting the embedded mild steel samples it was found that the bar was located very close to the bottom sample surface. It is possible that the corrosion data were greatly affected by this, therefore presenting the low half cell potentials.

Variation in hydrostatic potential for Sample N4, **Figure 4.4.1**, was large; suggesting a network of pores connecting the external surface to the sensing surface. The higher pore volume to surface area ratio reaffirms longer/narrower pores than N3. A fair amount of corrosive activity was present, but with a decrease in compressive strength. Possibly a combination of long/narrow pores and short/broad pores exists, where the longer pores are dominating, but the broad pores are sufficient to decrease the compressive load abilities.

Sample N6 (194.53 g water/1000g fly ash A) shows exactly the same characteristics as discussed for N4 (234.53g water/1000g fly ash A). Slightly higher values for the compressive strength, pore-volume to surface area ratio and corrosive activity were found. N6 consequently consists of a similar network as expected for N4, with less broad pores, elucidating the higher compressive strengths.

The corrosive activity of N8 advocates a system of long, continuous pores. The high hydraulic variation shown in **Figure 4.4.1** strengthens this proposal, but the lower compressive strength seems to be a contradiction. Sample N8 contains only 100g GGBFS per 1000g fly ash and previously it was found that a decrease in GGBFS results in a decrease in compressive strength by the formation of broader pores. The pore characterisation for this sample is therefore a mixture of long, continuous pores and with low quantities of broader pores.

Sample N10 (2.1g sand/g fly ash A) is a perfect justification to the stated pore characterisation hypothesis by presenting low hydraulic variation, compressive strength and extent of active corrosion. More so, a low pore volume to surface area is also prominent from **Figure 4.1.1**, therefore concluding that the pores will be predominantly short and broad.

Another justification of the hypothesis is found by considering the properties of sample N15. The high hydraulic variation, compressive strength and corrosion activity, along with the low pore-volume to surface area suggests a network of long, narrow and continuous pores. Consequently, the proposed geometry is strongly supported.

The high hydraulic variation, pore-volume to surface area ratio and compressive strength for sample N17 (214.53g water/1000g fly ash B) suggest a network of long, narrow pores. A low extent of corrosion opposes this idea, but once again it may be possible that a loop-like pore network, therefore lacking a continuous pathway, developed.

By investigating the properties of N18 (194.53g water/1000g fly ash B), it was found that the suggested increase in pore length with decreased water content could be substantiated. Sample N18 showed a nearly equal pore-volume to surface area ratio than N17, a slight increase in compressive strength and corrosive activity. These properties suggest a lengthened pore structure, but the lower osmotic variation contradicts it. Possibly the sensor embedded in sample N18 is faulty, producing the low variation in hydraulic potential (see section 4.4.1). Another analytical technique may be required to successfully describe the pore geometry.

The addition of slag is believed to give rise to longer/narrower pores. Sample N19 (150g slag/850g fly ash B) partly verifies this hypothesis, the exception being a low hydraulic variation. This may be the cause by either a faulty sensor or a network of distantly-spaced micro-pores which are unable to provide a sufficient pressure-transferring area for the sensor to experience an appreciable difference. The other properties, such as the compressive strength, pore-volume to surface area ratio as well as the corrosive activity resulted in higher values, therefore verifying the existence of long, continuous and now possibly very narrow pores.

The hypothesis of aggregate favouring the formation of shorter/broader pores is confirmed by observations from sample N22 (2.1g sand/g fly ash B). A low osmotic variation, along with low corrosive activity and pore-volume to surface area ratio supports this network of short/broad pores. Finally, the lower compressive strength with increasing aggregate values indicates the presence of larger pores which will readily give way for macro-cracks.

Finally, some of the pore characterisations suggested in section 4.1 can be justified by considering other physical properties typical to a particular sample. Some of the hypotheses may require other analytical techniques in order to successfully define their structure. A broader understanding, however, may be possible from discussion on the diffusive nature of both chloride and sulphate through the matrix, covered in subsequent chapters.

4.4.1. Sensor force readings

Force readings from the FlexiForce® sensors were also taken from time of insertion for a period of 44 days. Interesting results were gained from this exercise, especially when the force reading deviations was compared with the measured compressive strengths.

A general trend of decreasing Ohm readings with time (**Appendix G**) for the fly ash A recipes was observed (excluding sample N10), while the fly ash B formulations increased in Ohm readings (except N22) over time. Since the Ohm readings are inversely proportional to the force exerted on the sensor, it can be concluded that the fly ash A recipes generally increase in strength over time, while fly ash B decreases.

These findings may assist to explain the amount of dissolvable species found in each individual ash, while it simultaneously proves that a certain degree of dissolution remains after the 28 day curing period.

An average sensor reading was taken for each sample and the corresponding compressive strength result was compared with that value (**Figure 4.4.2**).

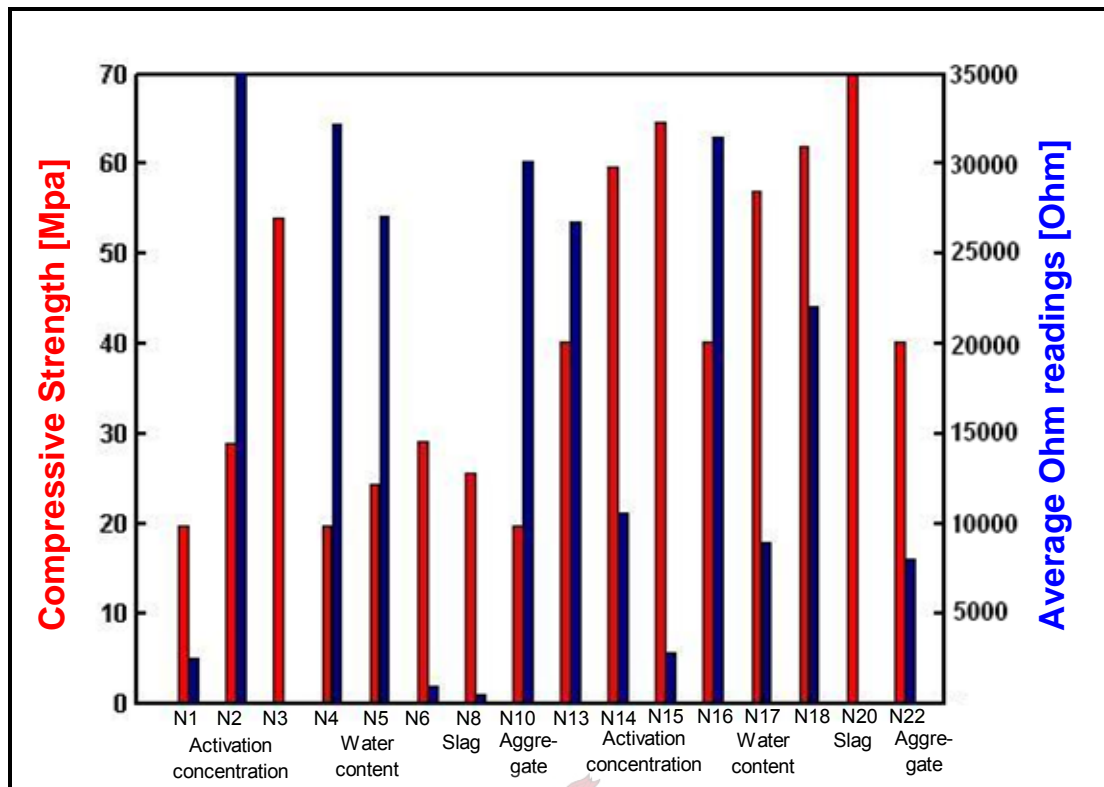


Figure 4.4.2: Comparative graph for the average sensor ($k\Omega$) readings and compressive strengths. The right-sided bars indicate the compressive strength values and the left bars the average resistance readings.

The sensor embedded in sample N2 presented an “out of bounds” value for the entire test period. Considering the fact that an increase in activation concentration results in a decrease in average sensor reading for the fly ash B formulations implies that the sensor embedded in sample N2 may have been faulty. A repetition to the sample was unattainable, hence it will be assumed that the decrease in average sensor reading is prominent for an increase in activation concentration for both ashes. This correlates to the increase in compressive strengths found for an increase in activation concentration.

The average sensor readings for sample N18 (194.53g water/1000g fly ash B) seem to be too high. Looking at the sensor readings over time presented in the sensor may have failed after 32 days of insertion. If this is true, the expected trend where a decrease in water leads to an increase in compressive strength and simultaneous decrease in sensor reading is justified. Also, disregarding the high reading from this sensor in the pore characterisation section is now justified.

Failing of some of the sensors (N2 and N18 the only ones identified) was not expected. The type of glue and polyimide/polyester coating is expected to withstand the corrosive nature of the mixture before complete hardening. For the time being the failure will be associated with the rough handling of the sensors during transit.

4.5. Summary

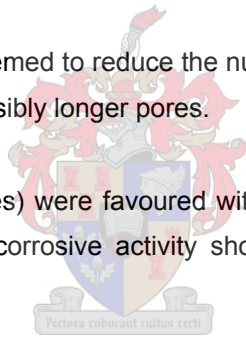
This emphasis of this chapter is to establish a basis of physical properties unique to each geopolymer formulation. Parameters such as pore-volume, specific surface area, compressive strength and later hydraulic potential and copper/copper-sulphate half cell potentials were used to initiate a pore geometry characterisation of each sample. This characterisation will then be used in subsequent chapters to elucidate the behaviour of diffusing chloride and sulphate ions through a specific geopolymer formulation.

Generally an increase in aggregate to the formulation favours the formation of shorter/broader (macro) pores. Low extents of corrosive activity are found for these samples, unfortunately linked to a significantly lower compressive strength value.

Activation solution concentration had varying effects on the two ashes, but commonly an increase in activation solution concentration was linked to longer (and for fly ash B – narrower) pores. Increasing compressive strengths, along with increased corrosion activity resulted.

Adding less water to the system seemed to reduce the number of pores, where an increase in water favoured the formation of possibly longer pores.

Long and narrow pores (micro-pores) were favoured with an increase in slag addition. The compressive strength values and corrosive activity shown by each formulation decreased readily with a decrease in slag.



Throughout this chapter two basic ratios are used to describe certain material characteristics. These ratios being: Pore-volume to surface area ratio and the pore-volume to compressive strength ratio.

Commonly it was found that an increase in pore-volume to surface area ratio results in a system of longer/narrower pores and the same holds for an increase in pore-volume to compressive strength ratios.

Finally, some of the suggested pore characterisations could be readily justified, considering the physical properties discussed in this chapter. Some extent of the hypotheses, however, could not be unboundedly justified and may require other analytical techniques in order to successfully describe the nature of their pore network. Discussion in subsequent chapters on the ionic diffusive resistance of these materials may initiate a more acceptable and defining understanding. Deviations from the expected outcome, as discussed in this chapter, may be an indication that half cell measurement is not the most effective method in determining corrosive activity.

Chapter 5.

INVESTIGATING GEOPOLYMER CHLORIDE DIFFUSION COEFFICIENTS

The importance of obtaining geopolymer Chloride Diffusion Coefficients (CDC) can not be stressed enough. It is through these values that a better understanding of the expected geopolymer corrosion resistance and durability can follow.

Initially the effect of curing methods for the total pore volumes will be investigated, thereafter testing if corrosion, and therefore chloride diffusion are present in the specimens.

This chapter looks specifically at the results from various diffusion coefficient determination methods and comparing these values to published cement and concrete material, validating the future use of geopolymeric materials. Results from different methods (Diffusion Cell and PIXE) will also be compared and the resulting discrepancies, if any, will be discussed. A broader discussion will include the copper/copper-sulphate half cell potential results where a distinct comparison between these parameters will be investigated.



Ultimately, this chapter will serve the purpose of comparing the expected corrosion resistance and durability to that of cement and concrete specimens, hence proving or disproving geopolymer superiority as construction material.

5.1. Effect of curing conditions

In order to limit the experimentation levels, it first has to be decided whether or not the curing conditions have a noteworthy effect on the total pore volume of the samples. Total pore volume was chosen as an indicative parameter due to its ease of execution, as well as the initial recognition of the importance of this variable to material permeability and diffusion resistivity.

Firstly, small samples of fly ash A were prepared from the same batch, according to recipes N1 (850g fly ash A, 150g slag, 2100g sand, 234.53g water, 23.99g NaOH, 50.5g KOH, 104.53g Na-silicate) and N25 (1000g fly ash B, 234.53g water, 23.99g NaOH, 50.5g KOH, 104.53g Na-silicate) presented in **Chapter 4**. The samples were then soaked in distilled water for a set period of time (3, 10 and 20 days), ensuring that the samples were as hydrated as possible. The pore volume determination was carried out as discussed in **Chapter 3**: Pore characterisation. The exception to the discussed method is that a sample of each recipe was independently exposed to one of the curing methods. The curing methods are described here as either the Short-Cure (SC) conditions or the Long-Cure (LC) method. The difference is discussed in **Chapter 3**: Synthesis.

The variation in weight before and after drying will now be assumed to be that of the pore water, therefore indicating the volume of the sample allocated to the respective pore voids. A dimensionless number is required to draw a direct comparison if any deviations in pore volume are found. This dimensionless number is obtained by using the measured mass of water to initial sample mass ratio. The results are shown in **Figure 5.1.1**:

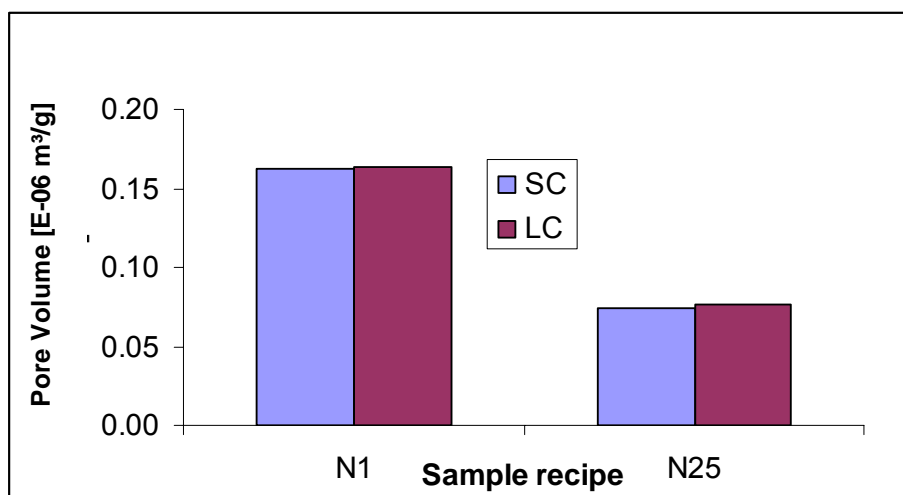


Figure 5.1.1: Comparison between pore volumes resulting from different curing conditions. The data shown here were samples soaked for 3 days in distilled water and then subjected to drying (LC denotes the long cure method, while SC denotes the short cure method).

It is evident from **Figure 5.1.1** that minor differences in the resulting pore volume exist. Upon investigating the samples soaked for an extended time, some variation were evident. These variations, however, were not significant when considering the scale of variation (**Appendix F1**). It can therefore be assumed that these two curing methods exert a minor effect on the total unit pore volume and in turn the diffusion resistivity of the individual samples. The rest of the work in this thesis will be based on the SC method, greatly reducing experimental time.

5.2. Initial test for corrosion

Prior to embarking on an extensive set of experimentation levels, it firstly needs to be established whether or not the material allows for a traceable amount of chloride ions to penetrate through a reasonable distance through the matrix. The simplest method in obtaining this initial estimation was accomplished by use of embedded Mild Steel (MS) and Stainless Steel (SS) bars into two variations of the geopolymeric recipe. The recipes chosen were N1 and N25 as shown in **Appendix C** and **Chapter 4**. These two recipes can be considered to be the two extremes in terms of expected ion-migration permeability, when considering the difference in sand-aggregate and GGBFS added to the individual sample make-up.

Sample synthesis and preparation were done as described in **Chapter 3: Corrosion Monitoring and Scanning Electron Microscopy**.

The scanned images for both of the MS containing samples showed active corrosion on the embedded bar interface (**Figure 5.2.1** and **Figure 5.2.2**) after 3 months of exposure to a chloride solution. This observation now justifies extensions to the investigation on the expected geopolymer chloride ion diffusivity.

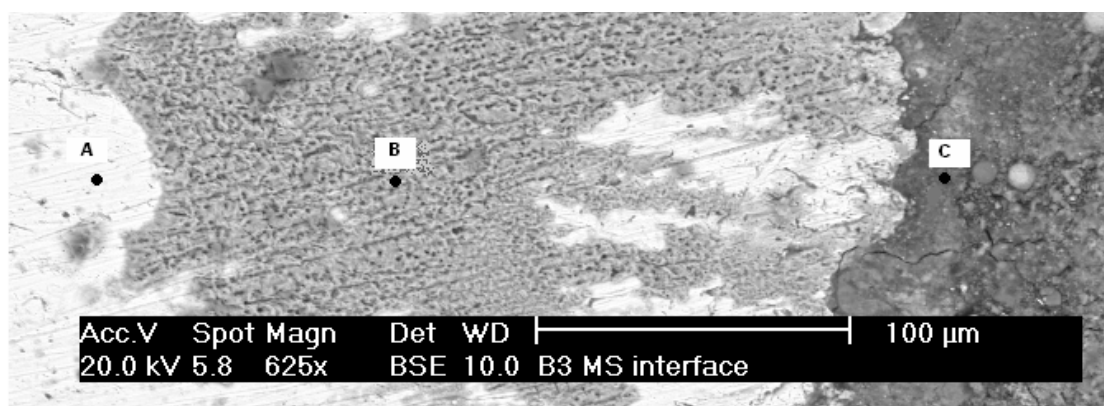


Figure 5.2.1: SEM image of a MS bar embedded in N1 sample. Three distinctive regions are present: the non-corroded bar (A), active corrosion region (B) and the geopolymer matrix (C).

Although serving as a valuable introductory step in this investigation, SEM cannot solely be used to compare the resistance of chloride diffusion between samples. Even upon considering the total area of active corrosion between these two samples, as seen in **Figure**

5.2.1 and **Figure 5.2.2**, no convincing conclusions can be drawn. The method used in obtaining distinct chloride diffusion coefficients will be presented later, where results from the PIXE analyses are discussed.

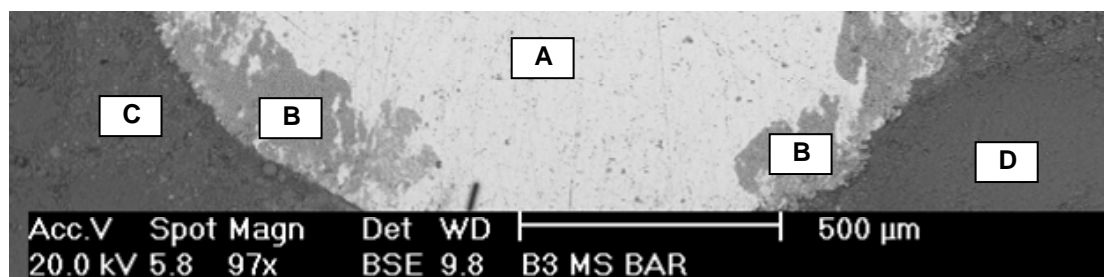


Figure 5.2.2: SEM image of a MS bar embedded in N25 sample. Four distinctive regions are visible: the non-corroded bar (A), active corrosion region (B), the geopolymer matrix (C) and sand aggregate particle (D).

Corrosion present in these two images is assumed to be predominantly chloride-induced corrosion, considering the samples were completely submerged in the concentrated chloride solution and remained sealed for the entire soaking period.

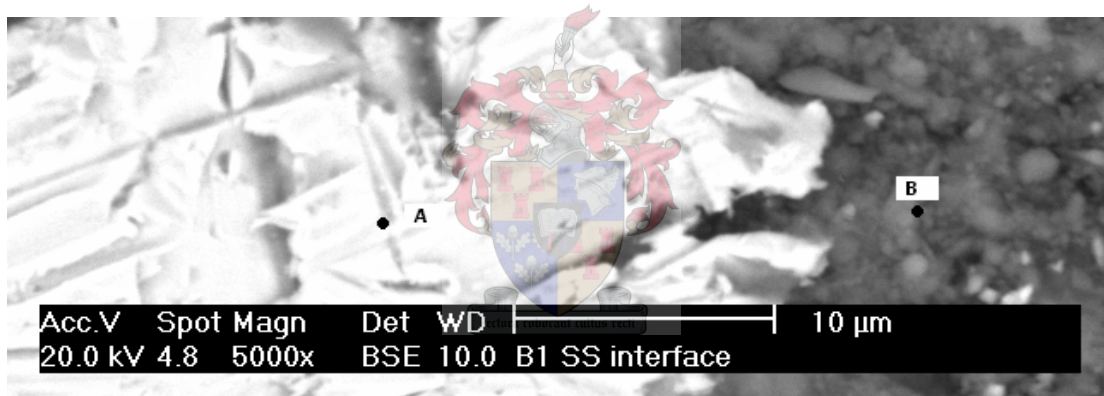


Figure 5.2.3: SEM image of a SS bar embedded in N25 sample. Two distinctive regions are visible: the non-corroded bar (A) and the geopolymeric matrix (B).

Images obtained for the samples containing SS bars, **Figure 5.2.3**, showed no signs of active corrosion. This is expectedly true, for stainless steel is known to be more resistant to chloride corrosion compared with commercially obtained MS materials. These SS images validate the conclusions drawn from **Figure 5.2.1** and **Figure 5.2.2**, where the most viable explanation for the corrosion is that of exposure to diffused chloride ions.

5.3. Diffusion cell chloride coefficients

The diffusion cell method for obtaining material diffusion coefficients relies on the variation of chloride concentrations in an external liquid. Here, as discussed in **Chapter 3**, the external basis liquid is NaOH, which was chosen on **ASTM C1202-97** guidelines.

The chloride concentrations are determined through Ion Chromatography (IC), where samples from different time intervals of electric accelerated diffusion are tested for chloride levels. The variation of concentration to time can be used along with the Dhir and Sugiyama equation (Yeau & Kim, 2005) in order to determine the independent chloride diffusion coefficient for each geopolymer recipe. Importantly so, the Dhir and Sugiyama equation is nothing more than a modified version of the Fick diffusion equations. Experimental methods were mimicked to the extent where the boundary conditions were met for direct use of the correlation.

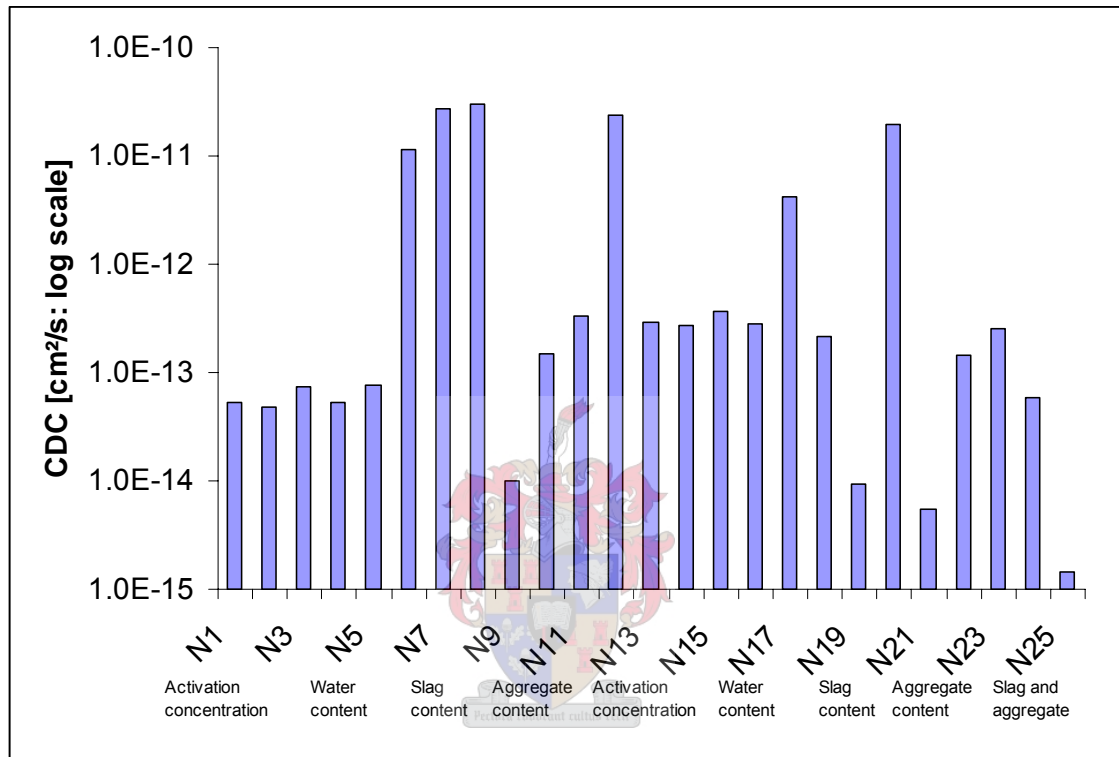


Figure 5.3.1: Chloride diffusion coefficients as determined by the diffusion cell method.

A bar graph of the resulting diffusion coefficients from the diffusion cell experiments is presented in **Figure 5.3.1**.

As seen from this graph, the highest obtained coefficient is less than 3×10^{-11} cm²/s and the lowest values are not traceable on this scale. **Figure 5.3.2** eliminates the large bars shown in **Figure 5.3.1**, therefore improving visibility by enlarging the lower region.

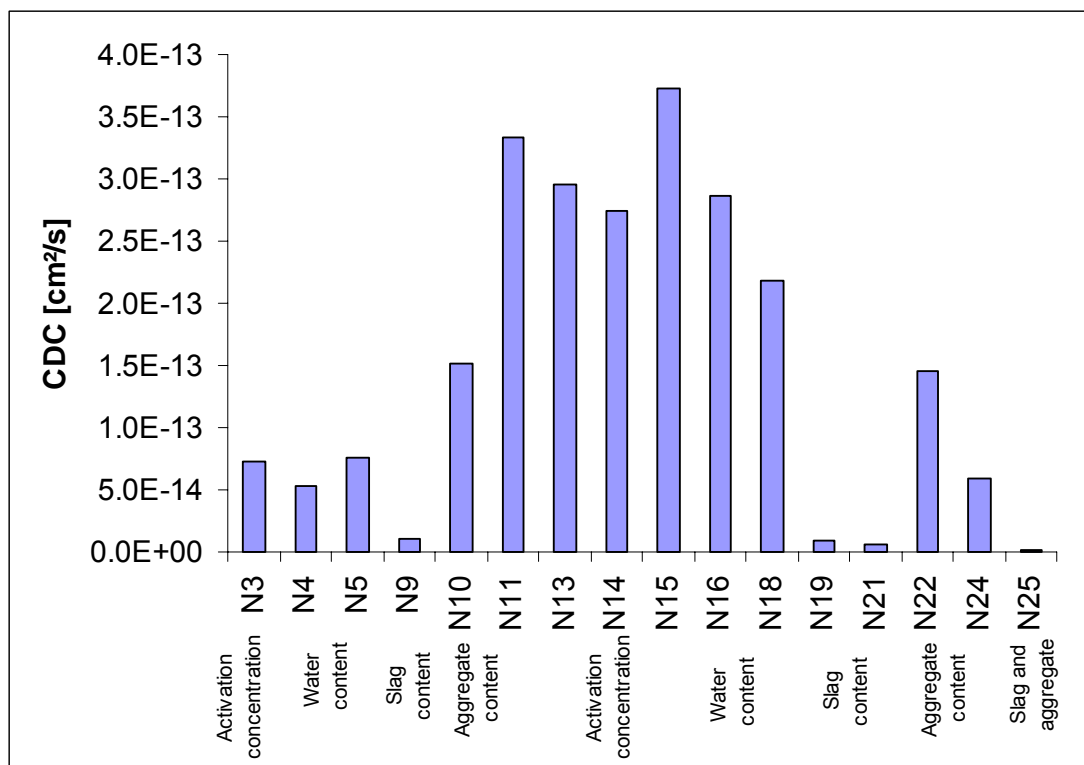


Figure 5.3.2: Lower value geopolymer diffusion coefficients. Recipe N25 produced the lowest value, therefore being the least permeable to chloride penetration.

From **Figure 5.3.2** it is evident that geopolymer N25 will most likely show the highest level of resistance to chloride penetration, hence more effectively protecting a rebar from chloride-induced corrosion. Thus, any one of the geopolymer recipes shown in **Figure 5.3.2** can be chosen as an effective medium to delay the rate of corrosion.

Investigations by **Yeau & Kim (2005)** entailed the determination of CDC for the least permeable concrete specimens. The specimens were mixed with GGBFS to levels that are comparable to that of adding fume silica, which has been confirmed by numerous researchers to greatly improve chloride penetration resistance for concrete material. The obtained diffusion coefficients over the geopolymer recipe range are substantially lower than those found in the Yeau & Kim investigation, implying that geopolymers are generally more resistive to chloride penetration. The best performing specimens in the Yeau & Kim investigation exhibited a chloride diffusion coefficient of $ca\ 0.5 \times 10^{-8}\ cm^2/s$, whereas the best performing geopolymer (N25) exhibited a coefficient of $1.4 \times 10^{-15}\ cm^2/s$, presenting a 10^7 order of magnitude improvement. Results by **Hossain & Lachemi (2004)** and **Halamickova & Detwiler (1995)**, under exactly the same conditions, showed no improvement to the results from the Yeau & Kim investigation with the highest coefficients in the order of $3 \times 10^{-8}\ cm^2/s$ and $8.4 \times 10^{-8}\ cm^2/s$, respectively. Other researchers (**Luo et al., 2003**) investigated the diffusion coefficient when sulphates are introduced to an OPC/GGBFS mixture, only to find that the CDC deteriorated from $1.95 \times 10^{-8}\ cm^2/s$ to $2.44 \times 10^{-8}\ cm^2/s$.

The time to chloride concentration profiles, as determined during the diffusion cell experiments, are presented in **Figure 5.3.3**, noting that similarly to **Figure 5.3.2** the high value outliers have been eliminated.

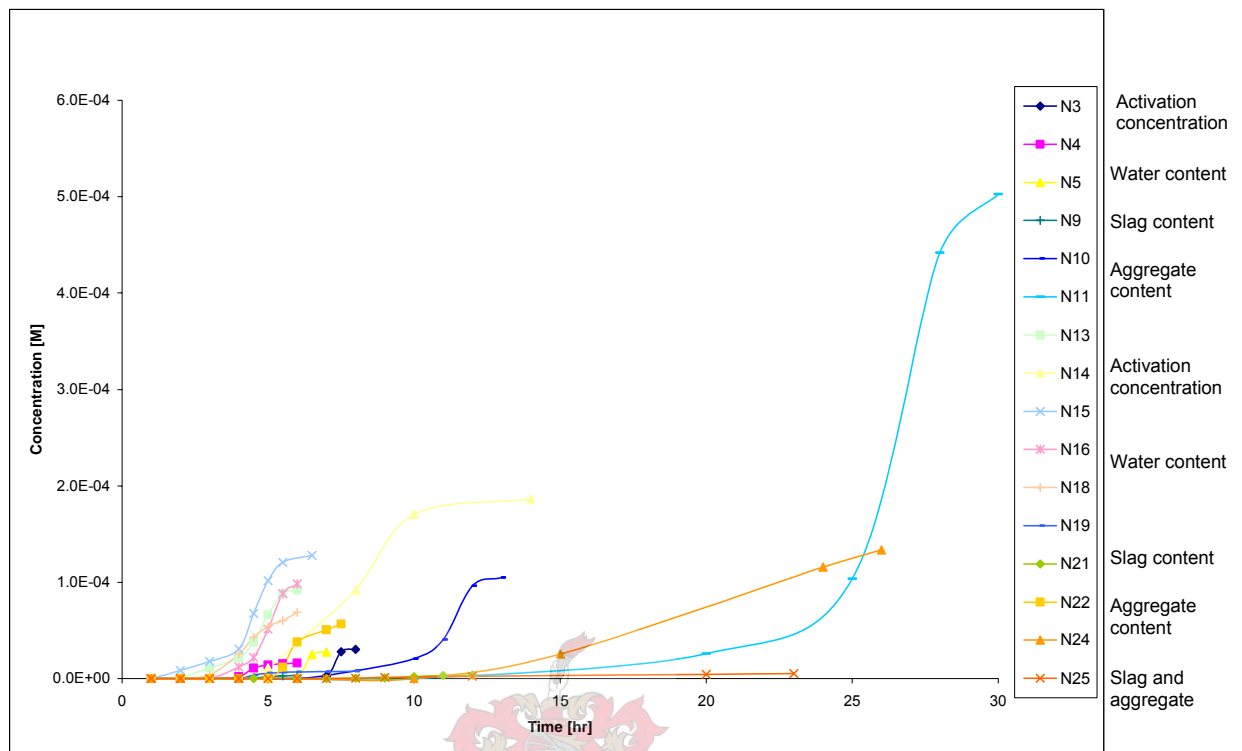


Figure 5.3.3: Chloride diffusion profiles for the least permeable geopolymer samples.

The effect of activation solution on the rate of chloride diffusion through the matrix seems to be either very slim or negligible, considering the trend lines of recipes N3 or N4 in **Figure 5.3.3**. Recipe N2 did not show traceable amounts of chloride after 8 hours and the formulation for samples N1 and N4 are one and the same (**Appendix C & Chapter 4**). The analogous recipes used for the fly ash B formulations (N13, N14 and N15) show this conclusion to be true. It does, however, tend to be more permeable than their fly ash A recipe counterparts and as will be shown later, this phenomenon can be linked to the difference in required water addition for these two fly ashes.

The amount of water added to the system has quite a significant effect on the overall geopolymer chloride. Samples N4 (234.53g water per 1000g fly ash, $CDC = 5.25 \times 10^{-14} \text{ cm}^2/\text{s}$), N5 (214.53g water per 1000g fly ash, $CDC = 7.59 \times 10^{-14} \text{ cm}^2/\text{s}$) and N6 (194.53g water per 1000g fly ash, $CDC = 1.16 \times 10^{-11} \text{ cm}^2/\text{s}$) contain decreasing amounts of water, but show an increase in chloride permeability. The difference in profiles for samples N4 and N5 is very small, but the profile of N6 lies with the higher value profiles omitted from **Figure 5.3.3** and is presented in **Figure 5.3.4**. In other words, the time to chloride concentration detection breakthrough for samples N4 and N5 is very similar, while the chloride concentrations for sample N6 was high early on. This increase in permeability with a decrease in water content

must therefore directly be linked to the pore structures and resulting pore geometries. As was seen in earlier chapters, not only does the permeability of the samples increase with decreasing water, but also a rise in pore volume, compressive strength and osmotic potential is measured. The hypothesis as set out in **Chapter 4**, where the resulting pores become longer and possibly narrower as the water content decreases, is once again justified. The fly ash B recipe analogues show similar trends to the fly ash A samples, except for sample N18 (194.53g water/1000g fly ash B, $\text{CDC} = 2.18 \times 10^{-13}$). An unexpected low diffusion coefficient is measured and it may be useful to rerun this sample (see Recommendations – **Chapter 8**). Once again the fly ash B recipes demonstrated poorer resistance to chloride penetration, suggesting differences in the required hydrating water between these two fly ashes.

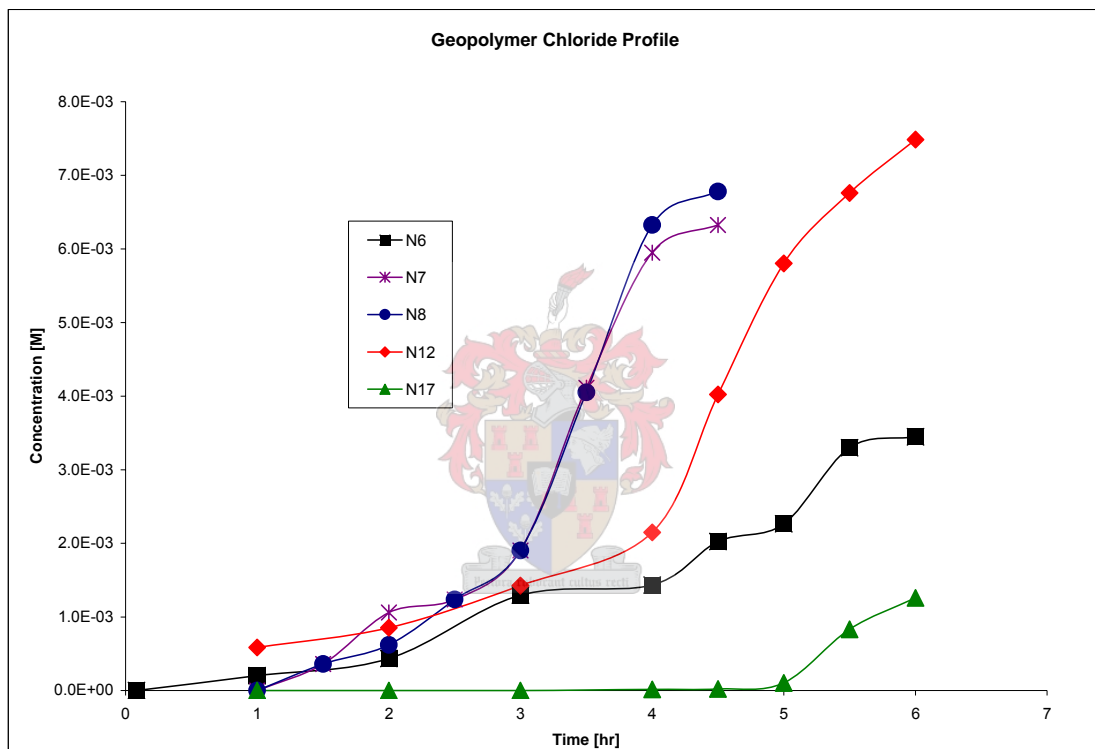


Figure 5.3.4: Chloride diffusion profiles for the higher permeable geopolymer samples.

The addition of slag to the matrix also has an unpredictable effect on the resulting chloride permeability. A jump between samples N7, N8 and N9 is observed, where samples N7 (150g slag per 850g fly ash, $\text{CDC} = 2.68 \times 10^{-11} \text{ cm}^2/\text{s}$) and N8 (100g slag per 900g fly ash, $\text{CDC} = 2.99 \times 10^{-11} \text{ cm}^2/\text{s}$) is presented in **Figure 5.3.4** and sample N9 (50g slag per 950g fly ash, $\text{CDC} = 9.93 \times 10^{-15} \text{ cm}^2/\text{s}$) in **Figure 5.3.3**. Although these samples consist of decreasing amounts of GGBFS, the permeability seems to remain constant for N7 and N8, but decreases sharply for N9. Parameters like the compressive strength and BET area decrease gradually with a decrease in added GGBFS, while the unit pore volume gradually increases. **Chapter 4** pointed out that N9 ($V = -0.611$ Volts) showed less active corrosion than N7 ($V = -0.676$ Volts) and N8 ($V = -0.669$ Volts), which produced very similar results. It may be possible that the

addition of slag encourages the formation of longer, more continuous but substantially narrower pores (micro-pores), therefore confirming the pore characterisation hypothesis set out in **Chapter 4**. From this work it can be deduced that below *ca* 7% (wt) slag addition, the pores are predominantly short and broad, lacking a continuous pathway, therefore explaining the low compressive strengths, BET area and extent of corrosion. The opposite holds for GGBFS addition above 7% (wt) slag, but although not covered in this work, **Yip & van Deventer (2003)** indicated a maximum allowable level of slag (20 wt %) addition before the geopolymer mixture becomes unworkable or even destructive to the geopolymer matrix.

Slag addition to the recipes containing fly ash B shows quite different properties. Besides the resulting chloride permeability exhibited by these samples (N19 CDC = $9.47 \times 10^{-15} \text{ cm}^2/\text{s}$, N20 CDC = $1.98 \times 10^{-11} \text{ cm}^2/\text{s}$, N21 CDC = $5.57 \times 10^{-15} \text{ cm}^2/\text{s}$), the other parameters like pore-volume, BET area and compressive strength indicates some type of threshold for N20. A decrease in slag results in a decrease in permeability, while N20 shows a sharp peak in diffusion coefficient value. This unexpected peak is found for all the stated parameters, which implies that unlike samples N19 and N21, N20 follows the trend as discussed for fly ash A. Another point of interest is that the overall comparative compressive strengths for the fly ash B samples are higher than those noted for the samples made from fly ash A (**Appendix E**). Explaining these observations no longer completely relies on the pore structure differences, but rather on the physical incorporation of the calcium from the slag into the two different matrices. Although possibly very important, the latter is not investigated in this work. Allowing for only the information at hand, it can be concluded that adding *ca* 7% (wt) slag results in a large pore count which is generally longer and narrower (N20) compared with the lower count of shorter, broader pores from the *ca* 10.6 and 3.5% (wt) slag added geopolymers (N19 and N21 respectively). Here the count of pores refer to the amount of pores per unit volume of that particular samples. This is a hypothetical base of comparison between samples and was not in any way determined numerically.

Aggregate (silica sand) undoubtedly alters the pore structure of any given geopolymer matrix, upon considering the significant difference in chloride profiles and CDC in **Figure 5.3.3** and **Figure 5.3.2** respectively. The larger the amount of added sand aggregate, the higher the measured permeability and the lower the strength, BET surface area and unit pore volume, while fly ash A presents higher diffusion coefficients than fly ash B. The explanation given in **Chapter 4** for this phenomenon is that an increase in sand addition accelerates the formation of broader pores. The decrease in unit pore volume with increasing sand aggregate may imply that the pore count decreases as they become larger. Fly ash B showed the same properties, with parameters like BET area and pore volume close in value to those measured for fly ash A. A considerable difference is found when examining the compressive strengths values, although following the same trend, the established values for fly ash B are higher than

those for fly ash A. Once again this decrease in strength for the fly ash B specimens enforce the idea of different water requirements for these two fly ashes to successfully polymerise.

Comparing the performance by these two fly ashes only in terms of their established chloride diffusion coefficients also yields interesting comparisons. Similar to **Figure 5.3.3**, **Figure 5.3.5** shows the comparative fly ash diffusion coefficients for only the lower value samples. Generally it is observed that fly ash B is significantly more permeable than fly ash A, when considering variations in activation concentration and water content. The reverse holds for varying GGBFS and silica sand aggregate, but here the measured values differ only slightly. This finding suggests that the two fly ashes differ in the required hydrating water. From previous findings where the fly ash A recipes produced compressive strengths higher in value than the fly ash B specimens, it is proposed that fly ash B requires less water for geopolymerisation than fly ash A. Hence fly ash B is more permeable than fly ash A when made from the same amount of water. This is also evident from the higher CDC values obtained for the fly ash B samples.

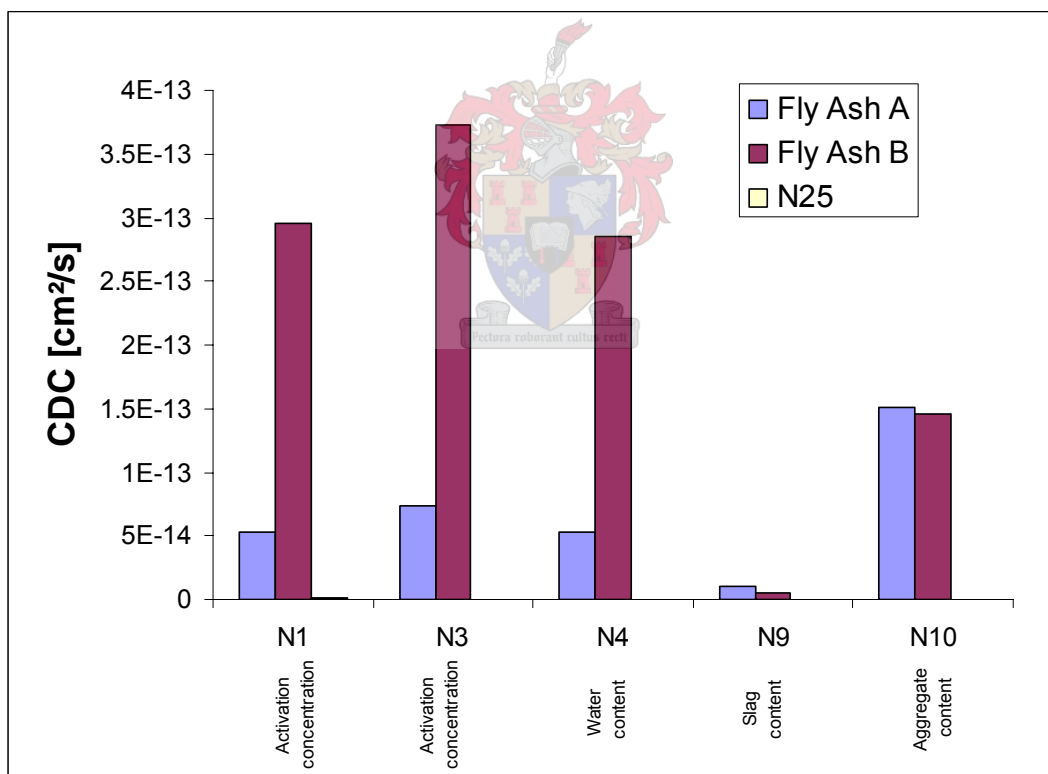


Figure 5.3.5: Diffusion coefficient comparison between fly ash A and fly ash B for the lower value samples.

Finally, this section can be concluded by stating: If chloride penetration is one of the most important parameters to consider when choosing a material for construction purposes, geopolymers unquestionably outperform the cement and concrete competition.

5.4. PIXE chloride diffusion coefficients

Chapters 2 and 3 discuss the relevant theory and required sample preparation associated with PIXE analyses. It is also pointed out that a significant cost-implication is linked with the use of this technique, and therefore limits the number of samples that can effectively be considered. It is for this reason that PIXE analysis serves the purpose of justifying the found results as discussed in section 5.3.

The basic principle in processing the PIXE data relies on the second Fick diffusion law, as shown in Equation 2.5, Chapter 2.

Discussions in section 5.3 identify sample N25 as the geopolymers formulation with the lowest chloride diffusion coefficient at $1.43 \times 10^{-15} \text{ cm}^2/\text{s}$. The aim is now to validate this value by comparing it to another analytical technique. The PIXE equipment at the University of Melbourne, Australia under Dr. Chris Ryan was used for this purpose, presenting results in Figure 5.4.1.

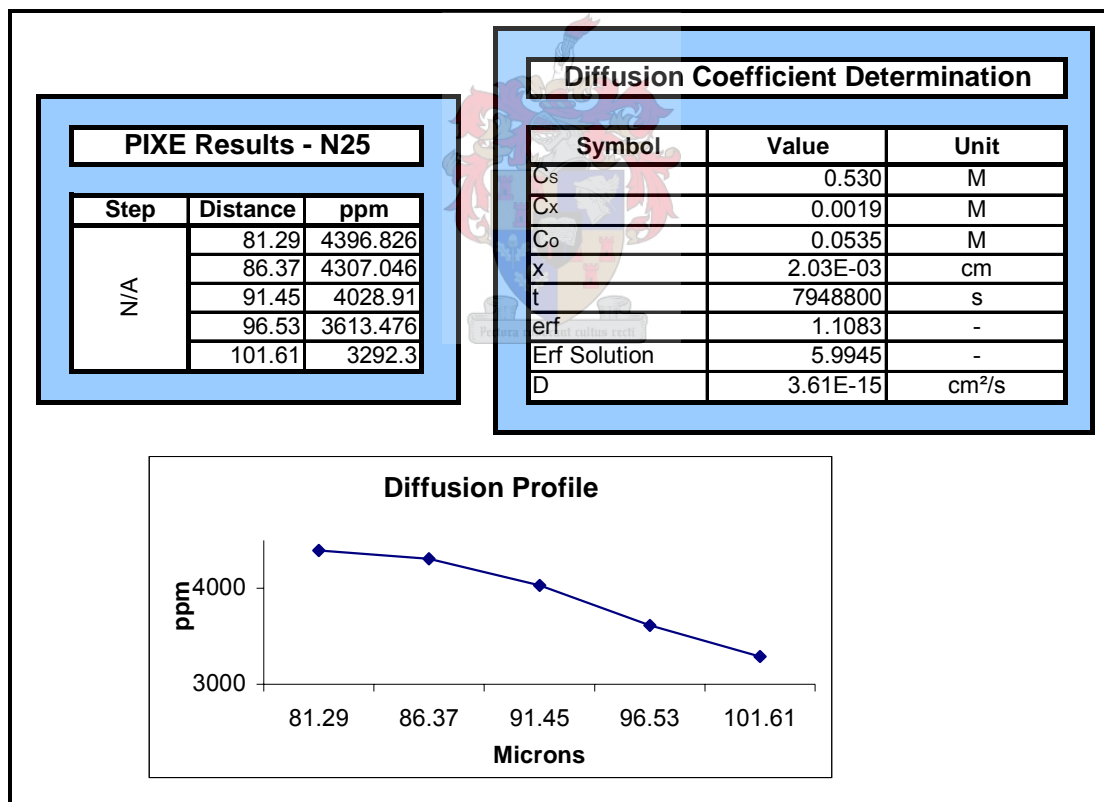


Figure 5.4.1: PIXE results for chloride diffusion coefficient for sample N25

As shown in the diffusion coefficient determination table (Figure 5.4.1) the PIXE CDC value is $3.62 \times 10^{-15} \text{ cm}^2/\text{s}$, which correlates quite closely with the value of $1.43 \times 10^{-15} \text{ cm}^2/\text{s}$ from the diffusion cell experiments. The factor (nearly 2) variation between these two values is quite common and may be the result of instrumentation errors, analytic area deviations and

calculation rounding errors. Ultimately, it can now be assumed that the value range of 10^{-15} cm^2/s is true for this sample and fit for direct comparison to published cement and concrete values.

Specimen N25 is non-homogeneous due to the large amounts of added silica sand aggregate, which can further add to calculation errors. If PIXE should be successfully used, the analytical “spots” should be picked very carefully. By use of the software program GeoPIXE, it can easily exclude large grains of sand from the overall statistics, therefore limiting the error introduced by these non-uniform areas. **Figure 5.4.2** shows the elemental map as lighter spots for chloride as detected by PIXE. The outer rim of the sample is located on the left side of the map, visibly indicating a higher concentration of chloride in this region.

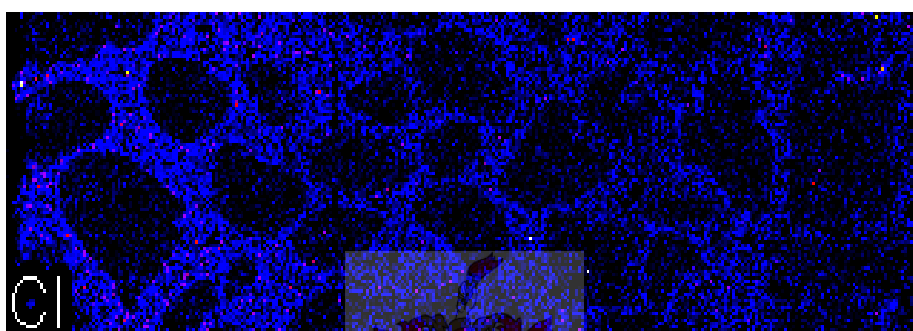


Figure 5.4.2: Elemental map for chloride as seen by PIXE detectors.

A single comparison between results is not nearly as reliable as multiple comparisons, equally in terms of sample- and instrumentation comparison. For this reason a random selection of samples were chosen for further PIXE analyses at iThemba Labs, South Africa under Dr. Wojciech Przybylowicz. It has to be stressed that all of the samples were exposed to similar chloride soaking solutions for similar time periods.

Instrumentation time was the biggest constraint in terms of the number of samples that could be effectively analysed, therefore only 5 more samples were completed. The samples were randomly picked and N1 (1000g fly ash A, 234.53g water, 23.99g NaOH, 50.5g KOH, 104.53g Na-silicate), N7 (150g slag/850g fly ash A), N13 (1000g fly ash B, 234.53g water, 23.99g NaOH, 50.5g KOH, 104.53g Na-silicate), N18 (194.53g water/1000g fly ash B) and N22 (2.1g sand/g fly ash B) were investigated.

Table 5.4.1: Chloride diffusion coefficient comparisons between values measured for PIXE and diffusion cell analyses.

Result Comparison		
Recipe	PIXE [cm ² /s]	Diffusion Cell [cm ² /s]
N1	3.467E-11	5.249E-14
N7	8.508E-14	2.678E-11
N13	2.171E-14	2.956E-13
N18	4.204E-14	2.053E-13
N22	2.015E-14	1.452E-13
N25	3.615E-15	1.433E-15

Table 5.4.1 presents a close relationship between the two analytical methods, excluding samples N1 and N7. On closer inspection, it was found that part of one of the PIXE maps for N7 was the edge of the sample ladder, which may have led to the low chloride concentration count. The discrepancy in coefficients for sample N1 may also be the result of PIXE calculations. Sample N1 was not analysed from the outer edge of the sample, but rather at 0.07 cm from that edge. The concentration at that point was analysed and used in the Fick Equation 2.5. Also, the data gathered from iThemba Labs relied on 5 point-based maps, opposed to the continuous flow produced by the CSIRO facilities. A combination of these factors most likely led to the dissimilarity in coefficients.

The specific accuracy of the coefficients may now be debatable; nevertheless, considering the fact that these independent methods produced results which remained in close range of each-other, it may be assumed that the order of magnitude in the diffusion cell determined coefficients to be reliable.

Jenneson et al. (1998) investigated the diffusion of chloride into OPC and OPC/fly ash blended samples. The samples were subjected to 0.5 wt % NaCl solution and then analysed with a PIXE micro-beam. The resulting diffusion coefficients were in the order of 1.7×10^{-7} cm²/s for OPC and 9.3×10^{-9} cm²/s for OPC/fly ash blends. Comparing these results with the geopolymer values shows that the OPC coefficients are at best 10^2 cm²/s higher and the blended OPC variants are up to 10^7 cm²/s larger. Conclusively, the superiority of geopolymeric material to resist chloride penetration is now verified.

5.5. Chloride diffusion and corrosion

Copper half cell potentials have been used by many former cement and concrete researchers as a method of indicating the existence and extent of corrosion to embedded rebars (**Ayala et al., 2000, Castro et al., 1997, Hossain & Lachemi, 2004**). This type of testing is uncommon to geopolymeric systems and it may even be used in future to determine the extent of other

reactions. This work will focus on the copper/copper-sulphate half cell potentials as a corrosion indication method.

The experimental set-up as discussed in **Chapter 3: Corrosion monitoring**, produced the voltage profiles revealed in **Figure 5.5.1**. Evident from these profiles is that pitting corrosion is the dominating type of active corrosion, which is expected when an excess of chloride ions are present. The voltage jump prominent between 75 and 85 days is normally associated with this type of corrosion (**Horváth & Schiller, 2003; Smulko et al., 2002**).

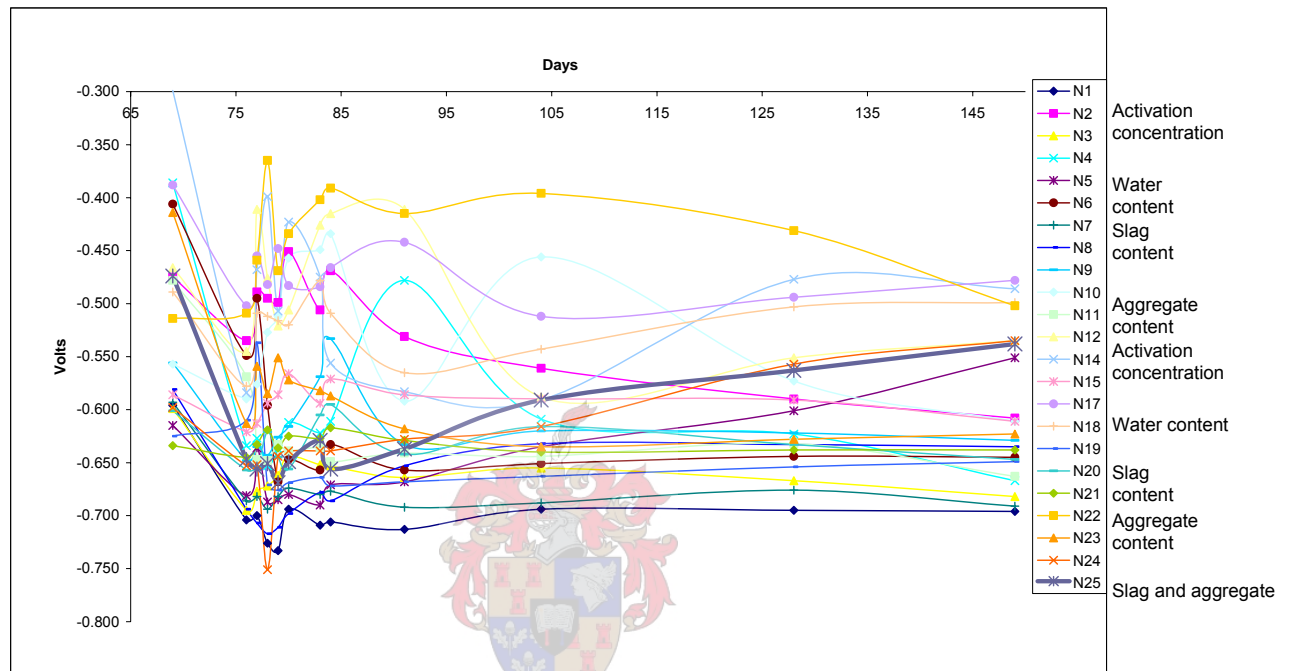


Figure 5.5.1: Half cell potential trends as found for the individual samples

The data relating to the trends in **Figure 5.5.1** were gathered over a period of nearly 3 months. Most of the prominent fluctuations are found within the first month of analysis, and seem to remain more stable thereafter. For this reason the average of the voltage trends was used to assign one specific representative value to the trends, especially when assessing them with other parameters as seen in **Chapter 4**.

Comparing these trends with published literature is seemingly more difficult than comparing chloride diffusion coefficients, largely because no unique value is assigned to represent this parameter. Also, unlike the chloride diffusion experiments, the literature did not make use of a single set of geometry, cover depth and external solution concentration guidelines (**Lui, 1996; Jolley, 2003; Hossain & Lachemi, 2004; Roskopf & Virnelson, 1985**). This section will therefore use a logical approach to compare the outcome of this experiment.

OPC corrosion profiles from **Lui (1996)** were higher in half cell potential than the geopolymeric profiles in **Figure 5.5.1**, suggesting that the extent of corrosion to the OPC

embedded rebar was lower than those found for the geopolymeric cover. On closer inspection it was found that the rebars embedded in the OPC samples were epoxy coated, also the cover depth was significantly larger than the geopolymeric sample equivalent. Considering both these facts, geopolymers may have performed equivalently, or even better, than the OPC mixtures. This can in no way be deduced solely from the half cell data, but in conjunction with the chloride diffusion coefficients it can safely be assumed that geopolymers resisted corrosion better than the OPC samples.

Jolley (2003) presented OPC half cell curves with significantly less oscillation than the geopolymer curves. The oscillations in the geopolymer half cell trends could originate from the measurement instrument, which was a simple hand held multi-meter. The same instrument was used throughout, therefore ensuring that if a measurement error occurred, it was a mutual error.

An investigation by **Hossain & Lachemi (2004)** presented results very similar to those found in this investigation. The only crucial difference is the cover depth of the OPC, which was significantly larger than the geopolymeric cover. **Roskopf & Virnelson (1985)** published results which are strikingly similar to the geopolymeric system, but the investigation was over a shorter time period and the external NaCl solution was at a lower concentration. All considered, it can reasonably be assumed that geopolymers do in fact resist chloride penetration better than normal and blended OPC. This reaffirms the chloride diffusion coefficient results presented in Section 5.3.

Considering the relative performance of the geopolymeric systems, some interesting aspects came to light. Samples with higher diffusion coefficients do not necessarily result in higher corrosion activity, **Figure 5.5.2**, especially when examining sample N22 (diffusion coefficient $1.5 \times 10^{-13} \text{ cm}^2/\text{s}$) and N1 (diffusion coefficient $5.2 \times 10^{-14} \text{ cm}^2/\text{s}$). N22 presents the lowest extent of corrosion, while N1 shows the highest corrosion activity though possessing a smaller diffusion coefficient.

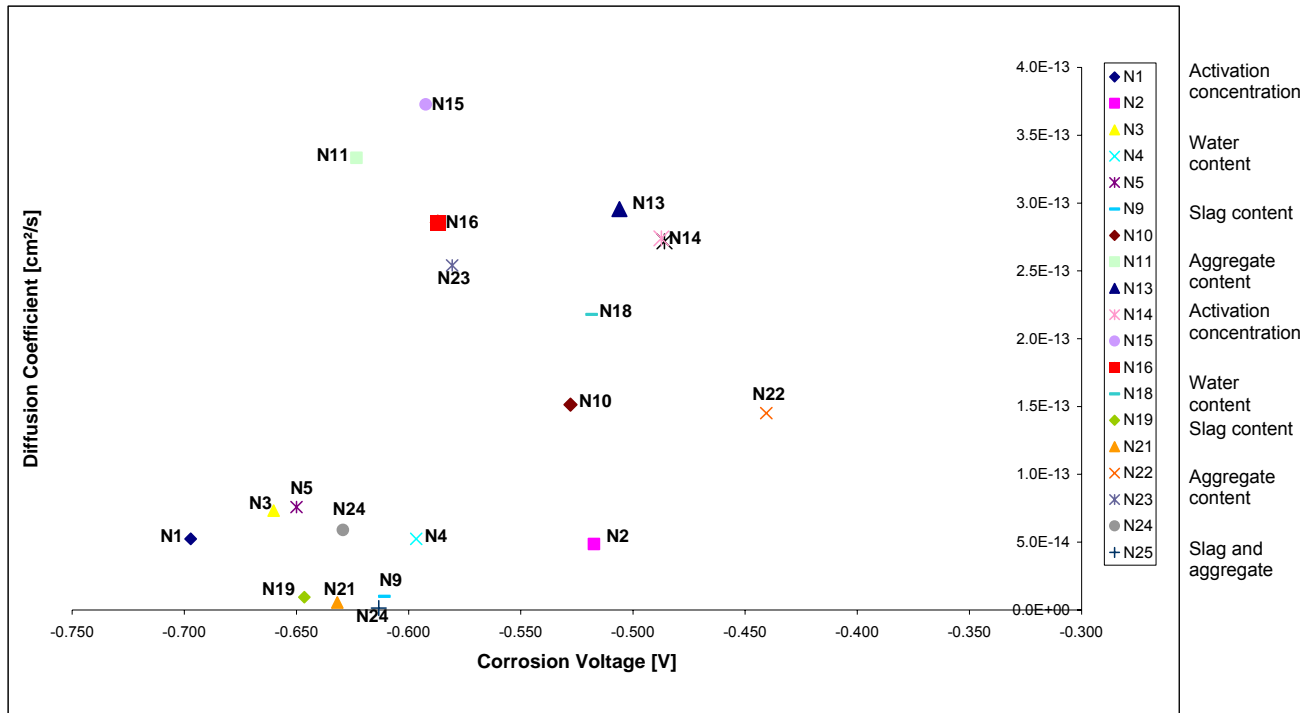


Figure 5.5.2: Chloride diffusion coefficients vs. copper-sulphate half cell voltages for the lower diffusion coefficient samples.

One of three possibilities can be the cause for this irregularity:

1. Although the bars were cleaned with diluted HCl prior to insertion, some corrosion may have been present on the bar due to unprotected exposure to ambient conditions. Once corrosion is activated, chloride acts as a catalyst to the corrosion process (Jolley, 2003 and Askeland, 1998) and the rate can no longer be determined by the rate of diffusing chloride ions. Also, if one bar was more corroded than the other, no direct comparison can be drawn from only the voltage values.
2. The rate of corrosion, or material resistance to corrosion, cannot be determined by solely looking at the chloride diffusion coefficients and the half cell voltages. Some other parameters may be needed to fully explain its behaviour when exposed to a chloride environment.
3. The epoxy coating at the interface of the external bar and the sample may have had some cavity bubbles. The chloride ions could have diffused more easily through these cavities due to the shorter diffusion distance. This option was ruled out after closer sample inspection. Macroscopic observations proved the epoxy coating to be more than adequate as covering layer.

Inevitably some degree of error was introduced to the half cell measurements, caused by the “sinking” of some of the mild steel bars to the bottom of the sample holder. This was largely because the geopolymer mixture was not viscous enough to support the extra weight at that time, which could have been avoided by prolonging the time between moulding the sample

and inserting the bar. Cases where this was especially significant were samples N6 (CDC = 1.16×10^{-11} and $V_{ave} = -0.604$), N7 (CDC = 1.68×10^{-11} and $V_{ave} = -0.676$) and N8 (CDC = 2.99×10^{-11} and $V_{ave} = -0.669$). The effect of the bar placement can now be debated, alongside the independent diffusion coefficients, where all three of the stated samples showed to have high diffusion coefficient values. It is therefore expected for these samples to show a higher extent of corrosion, which showed to be true. The bottom layer of epoxy coating therefore served its purpose and any discrepancies resulting from the bar position will be disregarded onwards.

The chosen cover depth of the samples may require more attention. Many of the samples showed some micro-cracks at the surface, which were not noticed for any of the other specimens from the same batch. An unfamiliar minimum cover depth was possibly not met and produced the excessive cracking as a result. This phenomenon was predominant for the geopolymeric pastes while the mortars showed no visible cracking. It is recommended that a study on the minimum cover depth of rebars, by geopolymeric materials, should be launched.

At first glance, the presence of visible cracks in the geopolymeric pastes eliminates the data as being trustworthy or indicative in any way. This is true when trying to compare the performance of the individual geopolymers, but upon considering comparisons to OPC performance, the geopolymeric mortars are the only logical recipes to compare. Geopolymer pastes are not considered to be an economical alternative to OPC, consequently the emphasis on a possible replacement formulation will definitely be a geopolymer mortar or geopolymer cement.

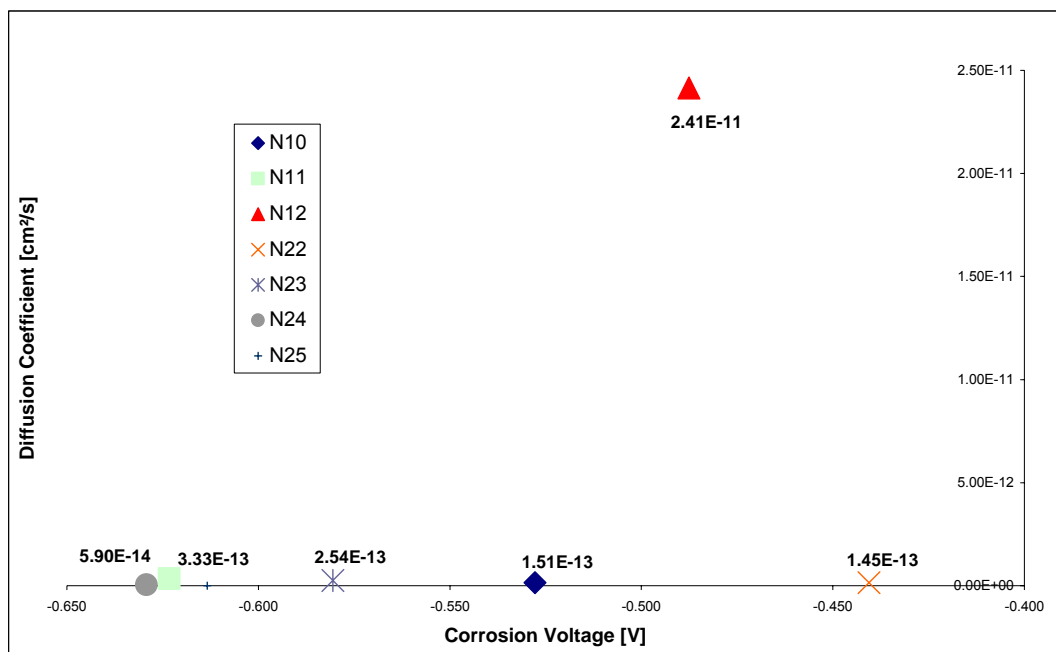
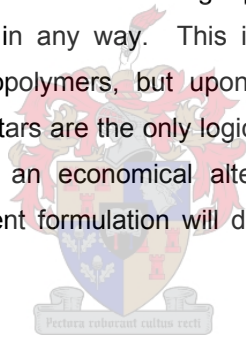


Figure 5.5.3: Chloride diffusion coefficients vs. copper-sulphate half cell voltages for the geopolymeric mortars only.

In order to predict values for samples N2 and N23, the trends from the opposing fly ash was used as basis. The average percentage difference is assumed to remain constant, where the same trends are expected for both fly ashes (concerning these specific samples).

A fair scatter of average half cell voltages is measured in **Figure 5.5.3**, confirming that the diffusion coefficient values are not the only indication for the expected extent of corrosion. Although sample N12 possesses the highest diffusion coefficient in **Figure 5.5.3**, it shows a low extent of active corrosion. Also, N10 and N22 possess nearly the same diffusion coefficient value, but show great differences in active corrosion. These observations agree with those discussed in **Chapter 4**.

5.6. Summary

The chapter commenced with an investigation on the effect of curing regimes on a property like specific pore volume. It was found that the two curing regimes do not influence this property significantly and it was decided to cure all the samples in this investigation according to the “short-cure” method.

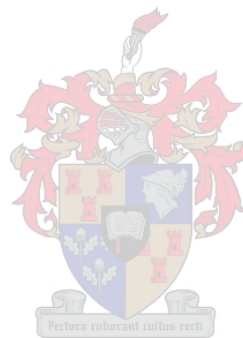
This chapter also introduced the behaviour of chloride penetrating a series of geopolymeric samples by looking at two different analytical techniques: Diffusion Cell and PIXE. PIXE was used only as confirmation to the results produced by the diffusion cell experiments. Excessive analytical time and costs associated with use of this technology limited the number of sample to be analysed. The results for these two techniques are surprisingly similar and it can be concluded that the results from the diffusion cell experiments are reliable. Also, comparing the measured results to those in published OPC literature confirmed that geopolymers will resist chloride penetration more effectively than OPC variants.

Once the chloride diffusion coefficients were established, the extent of active corrosion was determined by using a standard copper/copper-sulphate half cell. The half cell potential differences are an indication of the extent of active corrosion. All of the samples showed some extent of active corrosion after 5 months of exposure to a 560mM NaCl solution.

Published OPC literature lacked the basis for direct comparison as was established in the diffusion coefficients experimentation; however, a logical argument may prove that geopolymers are superior corrosion inhibitors.

It was concluded that chloride diffusion coefficients along with the appropriate half cell voltages cannot solely predict the extent of corrosion resistance exerted by a specific

geopolymeric recipe, whereas the pore characterisation discussed in **Chapter 4** may assist in further explaining certain phenomena.



Chapter 6.

INVESTIGATING GEOPOLYMER SULPHATE DIFFUSION COEFFICIENTS

Sulphate penetration into structures has some importance to OPC and OPC blended materials, but not for geopolymers, where solid proof of sulphate reacting with the geopolymer matrix is still lacking. Like chloride, sulphates may penetrate the high pH passive film protecting the metal rebar, activating corrosion.

It is therefore, to a lesser extent, advantageous to know the diffusive behaviour of a larger ion like sulphate through the geopolymeric matrix. The work in this chapter will specifically consider the diffusive behaviour of sulphates in an acidic medium, also attempting to demonstrate the superior acid resistance of geopolymer material.

The focus of this chapter is to support the previous findings where geopolymers proved to be a superior construction material, particularly when the aim is to minimise the penetration of chloride into the structure. The interest in geopolymers can be enhanced if it is shown that they resist sulphate penetration better than OPC, along with the added characteristic of resisting those ions in an acidic environment.

Initially only the sulphate diffusion coefficients (SDC) will be discussed in relative terms, thereafter the values will be compared with the equivalent sample CDC reported in **Chapter 5**. Similarities and discrepancies, if any, will then be discussed, aiding in the general characterisation of geopolymer durability and permeability outline.

6.1. Sulphate diffusion profiles and –coefficients

The behaviour of sulphate as diffusive-ion through all of the stated geopolymeric recipes will now be investigated. Continuing on this section, the resulting sulphate diffusion coefficients (SDC) will be compared with those measured for the chloride diffusion experiments, and any possible correlation will be examined.

Similar to the chloride diffusion coefficients, some of the results for the sulphate samples are lacking. The reason for this is that some of the samples were damaged during transit from Australia to South Africa, making it impossible to subject the samples to normal testing. Reconstructing the samples were also impractical, where the raw materials had to be imported from Australia (which is governed by strict quarantine regulations).

Overcoming this situation, the missing data were estimated by using the results for the other fly ash samples as basis, therefore using the results from the same formulation, but different fly ash. This method was also used where data were needed for the chloride diffusion coefficients. Care will be taken not to use any of these estimations in crucial discussions. The recipes referred to here are: N8, N12 and N24.

The experimental procedure was precisely as described for the CDC determination. The exact same equipment was not used, due to importing issues, but a replica was locally manufactured. A data table as presented in **Figure 6.1.1** was compiled for each formulation, from where the diffusion coefficient could directly be determined. Soft copies for each of these tables are included at the end of this thesis.

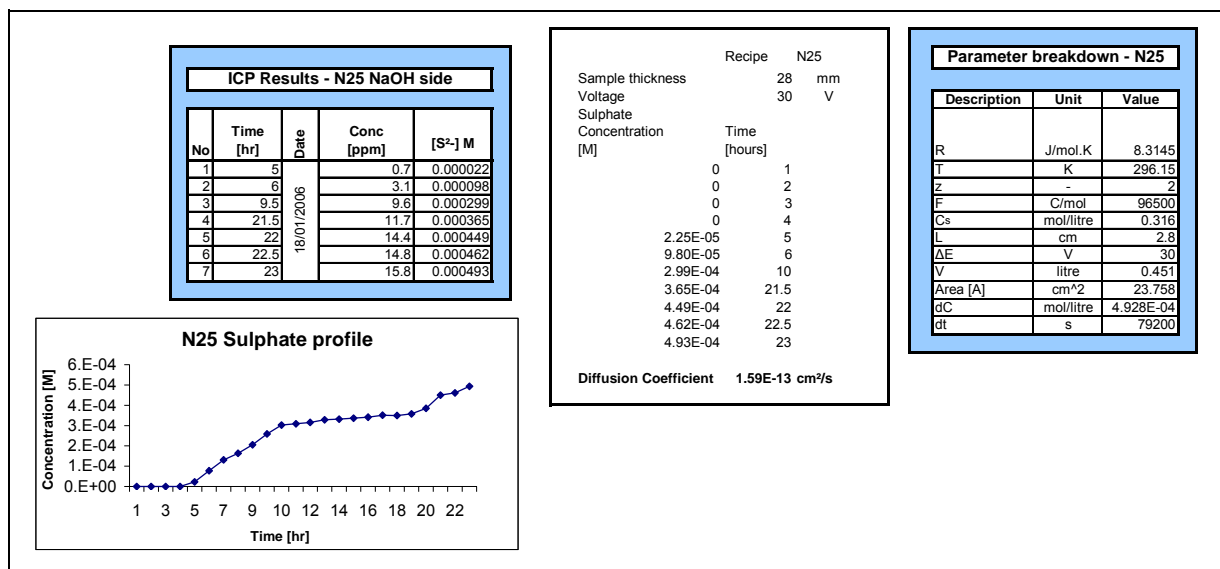


Figure 6.1.1: Data processing in determining SDC for sample N25.

It has to be stressed that the samples used in this testing originated from the same batch used for the CDC experimentation. No batch-to-batch deviations or discrepancies will be relevant in the data presented throughout this chapter.

One important difference to the CDC experiments is that the external sulphate medium was highly acidic. The reason for choosing such a harsh (nearly 0.3M) solution, was that normally sulphates do not significantly attack or bond with a geopolymeric matrix. Previous researchers (**Van Jaarsveld et al. 1998; Van Jaarsveld, 2000; Van Jaarsveld et al. 2002; Van Jaarsveld et al. 2003; Gokhale, 2000**) praised the excellent acid resistance exhibited by geopolymers, but without solid diffusive results to back their observations. The results presented later on may possibly assist to substantiate these speculations. **Figure 6.1.2** represents the lower value coefficients, which clearly demonstrates the importance of including either GGBFS and/or sand aggregate to the geopolymer mixture. Conveniently, it is the sample (N25) with both of these ingredients that resisted the penetration of sulphate most effectively. Sample N9 (50g slag/950g fly ash A) is not present in this figure as a result of its high SDC ($5.04 \times 10^{-11} \text{ cm}^2/\text{s}$) not covered in the scale of **Figure 6.1.2**.

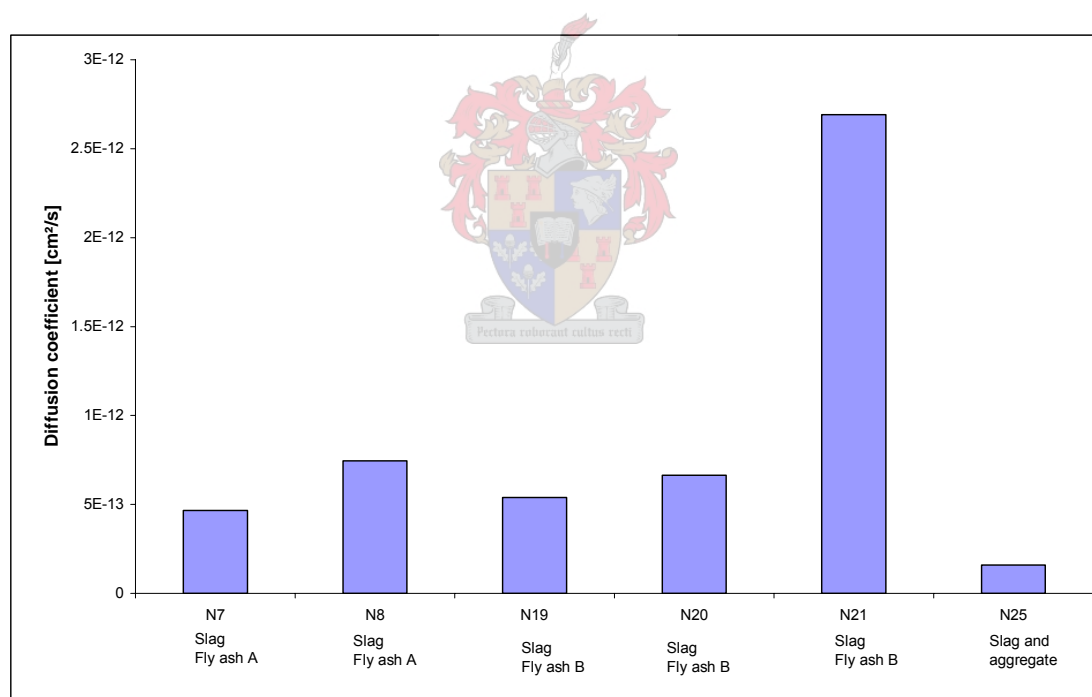


Figure 6.1.2: Sulphate diffusion coefficients for the lower value samples. Typically these samples contained either GGBFS or aggregate.

A distinctive increase in sulphate diffusion coefficient is found with a decrease in slag addition, especially when there is an addition of less than *ca* 7 wt %. This sharp increase in SDC is seen in both of the fly ashes (**Figure 6.1.3**), proposing that using less than *ca* 7 wt % GGBFS will not resist sulphates or acidic media effectively. Including this ingredient is crucial for the successful formulation of a commercially viable geopolymer. Similar results are discussed in **Chapter 5**.

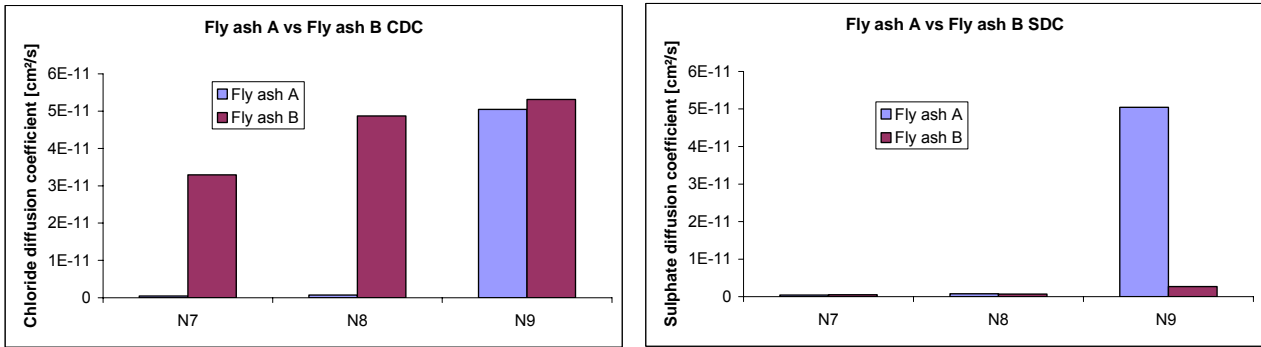


Figure 6.1.3: Diffusion coefficient trends for fly ash A and fly ash B on varying the slag content.

GGBFS (see **Appendix F**) is known to contain high amounts of reactive material (in the form of soluble glasses), therefore possibly decreasing the porosity and altering the pore size distribution altogether, elucidating the decrease in SDC with an increase in GGBFS addition. Furthermore, the calcium from the GGBFS source reacts spontaneously with sulphuric acid to produce gypsum. Not only does this reaction lessen the amount of free sulphates diffusing through the matrix, but the enlarged crystal products may bridge or even block cracks and pores to delay the diffusion process.

Aggregate has a lesser effect on the resulting SDC, although once the samples have completed their diffusion cell testing, a clear observation of the extent of the corrosive behaviour of the external H₂SO₄ solution on the sample surface can be made.



Figure 6.1.4: Minor surface decay of aggregate-added geopolymer sample (N22). Mortar samples showed severe cracking and aggressive surface decay.

Macroscopically the specimens with aggregate or slag showed the least amount of surface decay and cracking (**Figure 6.1.4**). It is therefore very clear why sample N25 performed so well under these extreme conditions.

A decrease in SDC is found for an increase in activation concentration for both ashes, but the values for fly ash A is generally higher than for fly ash B, making fly ash B less permeable to sulphates and more acid resistant. The decrease in SDC is expected, where the higher concentration of the activation solutions hypothetically produces more hydroxides in the pore-solutions, effectively lessening the attack of the acidic media through neutralisation reactions. The fact that fly ash B produced higher chloride diffusion coefficients than fly ash A for the corresponding formulations supports the theory of differences in the pore structures produced by the two ashes. Fly ash B has to consist of larger pores or a larger network of pores, elucidating the higher CDC and lower SDC.

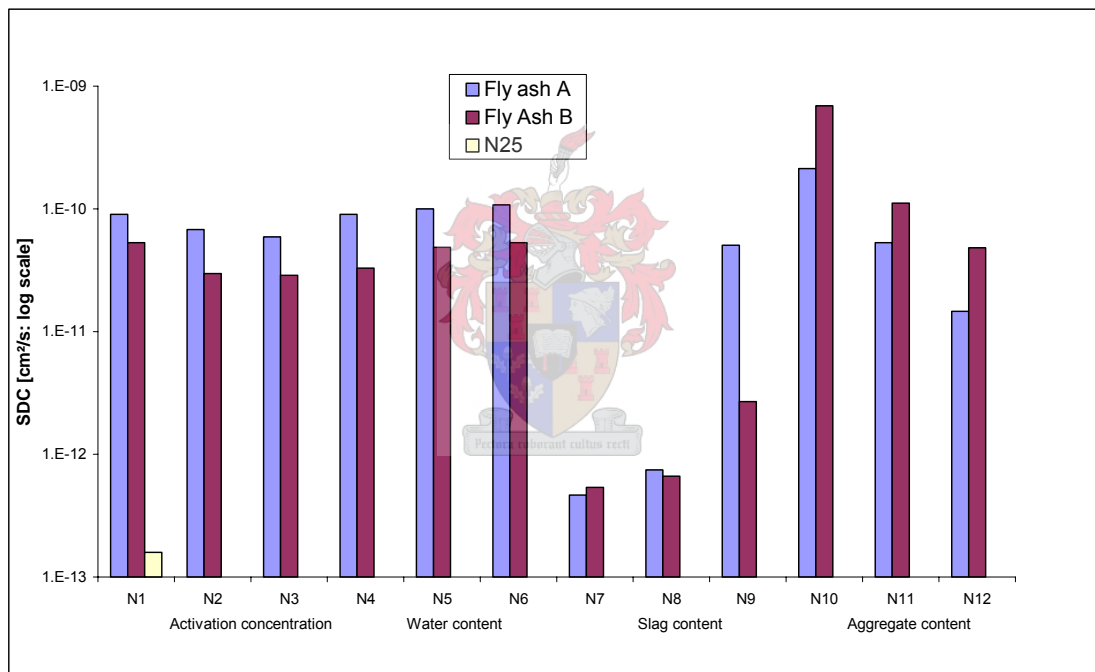


Figure 6.1.5: Comparing SDC for the two fly ashes on a logarithmic scale. Fly ash A produces larger SDC values, except for the mortar recipes.

A decrease in water content results in an increase in SDC (**Figure 6.1.5**). Once again, fly ash A generates higher SDC values. The same trend is observed for the CDC values, except that fly ash B produced higher values than the fly ash A formulations. This observation contradicts the findings discussed in **Chapter 5**, where a decrease in water content possibly gives rise to a network of longer and narrower pores. Fly ash B is assumed to have larger pores upon considering the heightened CDC values. This contradiction can possibly be explained by looking at the physical transformation of the matrix resulting from the acidic chemical reaction and/or the initial fly ash composition. Fly ash A (**Appendix B**) contains significantly more iron than fly ash B, which can readily react with sulphuric acid to produce iron-sulphate.

Equivalently to the effect of added GGBFS, the iron may reduce the transport of sulphates through the matrix considerably, resulting in the apparent contradiction.

Alternatively, an increase in aggregate results in a decreased SDC value. Also, fly ash B produces larger values than was found for fly ash A (**Figure 6.1.6**). Silica sand reduces the effective SDC by preventing cracking. Cracking was one of the most prominent features observed in samples containing no added slag or aggregate. Silica-oxide will not react with 0.3M sulphuric acid, therefore reducing the amount of geopolymeric paste in contact with the acidic medium. The volumetric contraction upon attack by acid is thus reduced accordingly, resulting in less tensile strain and a decrease in cracking. The decrease or even absence of cracks reduces the mobility of ions and effectively the diffusion rates are lower.

In terms of SDC, fly ash B is more permeable than fly ash A, with the reverse being true for the CDC values (**Figure 6.1.6**). Discussions in **Chapter 5** led towards the idea that pores of fly ash A were larger than those found in fly ash B, and the difference increased with an increase in added sand. Once more an apparent contradiction is crossed, where it will usually be expected for the diffusion trends for diverse ions to be similar. Similar to the results from the effect of water content on the geopolymer formulas, the difference in initial iron content in fly ash A can safeguard the matrix from sulphur attack. This hypothesis still needs to be verified on a microstructural scale.

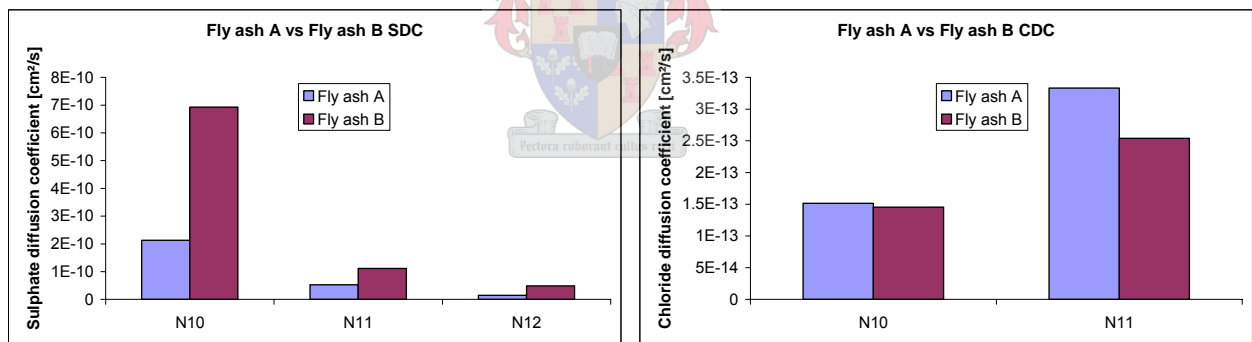


Figure 6.1.6: Diffusion coefficient trends for fly ash A and fly ash B. Sample N12 was omitted from the CDC chart due to its large order of magnitude. The trend for N12 continues as shown for the CDC chart, where fly ash A produces higher values than fly ash B.

Additionally, fly ash B illustrated considerably less surface deterioration than fly ash A, covering almost all of the formulations. Taking into account that both of these fly ashes are Class F ashes, they are expected to react similarly with outside reagents. Compressive strength data for fly ash B is also higher, suggesting that the particles are bonded more securely into the matrix. This implies that although the ashes react similarly, fly ash B requires a prolonged time of exposure to show the same amount of surface reaction.

6.2. Apparent geopolymer acid resistance

Continuing on the discussions in section 6.1, some interesting similarities and also irregularities are observed when comparing the SDC with the corresponding formulation CDC.

Plotting the SDC and the corresponding CDC on a bar graph, clearly exhibits the extent to which the SDC exceeds the CDC. This is expected when considering the highly acidic medium of the sulphate solution. The opposite would be expected if a sodium sulphate solution was used, where the movement of the larger ion will be more restricted in smaller pores. Time restrictions did not allow for the execution of these set of experiments, but may prove beneficial to future researchers.

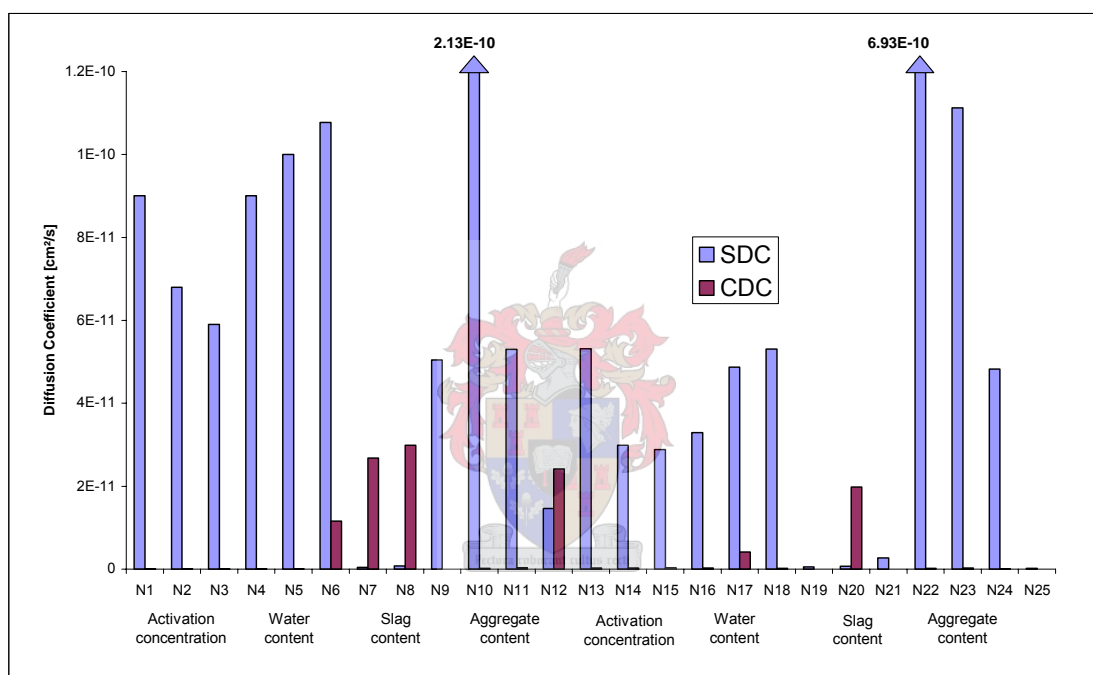


Figure 6.2.1: Comparing diffusion coefficients for the lower value. Clearly the SDC usually exceeds the CDC for similar recipes.

The recipes where the CDC exceeds the SDC (**Figure 6.2.1**) are N7 (150g slag/850g fly ash A), N8 (100g slag/900g fly ash A), N12 (4.2g sand/g fly ash A) and N20 (100g slag/900g fly ash B). Coincidentally, every one of these samples contains either slag or aggregate. More so, the trends described in **Chapter 5** for both cases of slag and aggregate samples are reversed for the SDC experiments. The chemical reactions involving slag and sand with sulphates alter the expected trends, reaffirming in some way that the diffusion of sulphates in this acidic medium is not purely determined by pore size and geometry.

Figure 6.2.1 demonstrates the importance of incorporating slag to a material exposed to a sulphate environment. The samples containing slag showed improved sulphate resistance, even compared with their chloride resistance. Aggregate addition appeared to be crucial for

maintaining a low CDC, but did not influence the SDC as dramatically. Hence, the material composed from both of these starting materials (i.e. N25) will undoubtedly be a superior choice of covering material for use in harsh environments.

Consequently, the geopolymers which demonstrated superb acid resistant properties were limited to the mortars and those containing slag, confirming observations by **Van Jaarsveld et al. (1998)**, **Van Jaarsveld (2000)**, **Yip & van Deventer (2005)** and others. Severe cracking was found in most of the pastes, so much so that slag-containing sample N7 cracked in both NaCl and acidic media. For sample N7 it is hard to believe that it could have failed under the compressive strain of the diffusion cell sealing-rods, particularly when considering it showed a compressive strength of 55.7 MPa. This formulation appears to be quite unstable, but is rigorously changed by introducing aggregate to the mixture (resulting in recipe N25). Irrefutably so, aggregate forms an integral part of the acid resistant properties exerted by geopolymers.

Some samples (N10 and N22) had a gel-like, yellow precipitate afloat in the H₂SO₄ side of the diffusion cell chamber. The precipitate consisted mainly of iron, which had to originate from the original fly ash, thus questioning the encapsulation abilities of these formulations in acidic environments. It is recommended to fully investigate this phenomenon prior to any scale of encapsulation application.

6.3. Comparing geopolymer SDC to cement literature

Quite a substantial number of cement and concrete researchers have spent their time investigating the effect of sulphate invasion to concrete structures. Most of the work was based on observations and comparisons between set blended variants, while very few of them concluded their work with diffusion coefficients. **Gospodinov et al. (1996)** following on work by **Cohen & Mathur (1991)**, determined an experimental sulphate diffusion coefficient of $3.35 \times 10^{-8} \text{ cm}^2/\text{s}$ for cement pastes.

Geopolymeric sample N25 produced a SDC of $1.59 \times 10^{-13} \text{ cm}^2/\text{s}$, while the “worst” performing geopolymer resulted in a $1.08 \times 10^{-10} \text{ cm}^2/\text{s}$ SDC. The latter is a geopolymeric paste. Bearing in mind the highly corrosive nature of the external liquid, as well as the high concentration of sulphates introduced, the geopolymer samples unmistakably outperform concrete material as a possible rebar corrosion inhibitor.

Bary & Béjaoui (2006) made use of “the multi-coated sphere model” for the theoretical calculation of the diffusion coefficients for OPC pastes. The model relies on a microstructure definition together with the hydrated cement products (portlandite, CSH, etc), simultaneously accounting for the physical properties of each phase and volume fraction. The outcome was

an average diffusion coefficient of $1.0 \times 10^{-8} \text{ cm}^2/\text{s}$ which was supported by experimental findings. This value remains well above those found for the geopolymeric material used in this investigation.

6.4. Summary

The emphasis of this chapter was to investigate the diffusive behaviour of sulphates through geopolymeric matrices.

The sulphate diffusion coefficients were experimentally determined by use of the same diffusion cell as described in **Chapter 5**. The extreme difference between the experiments is the acidic nature of the external sulphuric liquid (0.3 M H_2SO_4). Using such a harsh solute environment served a dual purpose: firstly to investigate the effect of sulphates penetrating the geopolymeric matrix and secondly investigating the resulting resistance of the material when exposed to acidic attack. Unlike OPC, geopolymers do not readily react with sulphates, consequently neutrally-based sulphates do not pose such a large threat to the expected durability. Also, the sulphate ion is much larger than a chloride ion, implying that the resulting SDC will be lower for the same formulation, therefore playing a minor role in the corrosive activity experienced by an embedded rebar. Investigating the effect of sulphates in an acidic medium can now substantiate the use of geopolymers in harsh environments, possibly areas with high acidic rain levels or even in applications such as sewerage lines.

The resulting formulation SDC from this study was higher in value than the corresponding CDC. Bearing in mind the acidic nature of the sulphate solution, this is quite expected. The importance of adding either GGBFS, aggregate or preferably both to the mixture is highlighted, where the samples not containing these raw materials showed excessive cracking or surface decay.

Comparing the measured SDC values with those in the cement- and concrete literature produced surprising results: Sulphate diffusion coefficients for geopolymers are significantly lower than those measured for OPC pastes subjected to a sodium-sulphate solution. The “worst” performing geopolymer remained $10^2 \text{ cm}^2/\text{s}$ lower than the best performing OPC sample, concluding that geopolymeric material is a far better selection for use in extreme applications.

Chapter 7.

DEFINING GEOPOLYMER ION MIGRATION RESISTANCE AND EXPECTED DURABILITY

The main focus of this chapter is to assemble all the information from preceding chapters, thereafter quantitatively defining the expected durability each of the geopolymer formulations will exhibit as possible construction materials. The concept of “durability” will be classified throughout this chapter by considering the performance of a formulation in terms of resisting chloride ion-, as well as sulphate ion penetration in an acidic medium.

Once all the measured parameters are gathered, the pore characterisation hypothesis discussed in **Chapter 4** will finally be defended or rejected and any discrepancies from the stated hypothesis will be discussed.

The chapter will conclude by comparing the hypothetical time-to-corrosion between concrete and geopolymer samples of the same thickness (cover depth). A Delphi-based interactive software programme will be included at the back of the thesis, where multiple comparisons on varying parameters can easily be conducted.

In essence, this chapter will serve as a broader “concluding” chapter in which the geopolymer superiority to OPC is highlighted.

7.1. Geopolymer diffusion coefficients

Chapters 5 and 6 discussed the diffusive behaviour the 25 geopolymer formulations presented in a chloride- and sulphate environment respectively. This section will concentrate on the final conclusions and comparisons to OPC literature. Also, the initial justification for use of geopolymers as construction material will be highlighted, whereas more extensive comparisons are covered later in this chapter.

7.1.1. Chloride diffusion coefficient (CDC)

Chloride induced corrosion to rebars embedded in concrete structures have been identified by numerous researchers as being the main deterioration factor. It is for this purpose that knowledge on the chloride diffusion coefficient for a specific material must be known, therefore assisting to successfully describe the durability of that material and its resistance to chloride penetration.

Extensive amounts of research time have gone into delaying the diffusion of chloride into OPC structures. Assuming a CDC of an unblended OPC sample of $ca\ 6.4 \times 10^{-8} \text{cm}^2/\text{s}$ (Thomas, 1996), coating the rebar with epoxy and adding a moisture inhibitor lowered the CDC to $ca\ 1.3 \times 10^{-8} \text{cm}^2/\text{s}$ (Berke et al., 2005), while adding 30% fly ash produced a CDC of $ca\ 5.8 \times 10^{-9} \text{cm}^2/\text{s}$ and other fillers like GGBFS and silica fume produced chloride diffusion coefficients of no less than $ca\ 0.5 \times 10^{-9} \text{cm}^2/\text{s}$ (Yeah & Kim, 2005; Berke et al., 2005; Jenneson et al., 1998).



Considering that the “worst” performing geopolymer samples did not produce a CDC above $3.0 \times 10^{-11} \text{cm}^2/\text{s}$, the best performing N25 formulation resulted in a CDC of $ca\ 1.4 \times 10^{-15} \text{cm}^2/\text{s}$. From this it is clearly expected for geopolymers to resist chloride penetration more effectively than any OPC variant. PIXE analyses substantiated the geopolymer CDC values by producing very similar results to those measured for the diffusion cell tests.

Acknowledging the fact that constructors are hesitant to incorporate a “new” technology for use in large projects, they may find it beneficial to embed geopolymer-coated rebars into a larger OPC frame. The effect (if any) of the geopolymer/OPC interface has not been laboratory tested as yet and future researchers may find it beneficial to look at this application as a stepping stone into the OPC monopoly. It is suggested, however, that a substantial coat (at least a cm) of geopolymer should be applied to the rebar. This recommendation is partly based on time-to-corrosion initiation findings presented later on in this chapter.

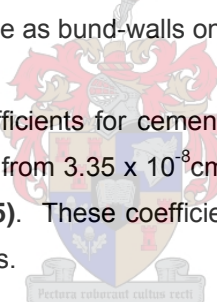
7.1.2. Acidic sulphate diffusion coefficient (SDC)

Sulphate induced deterioration has mainly been a consideration of sulphates reacting with the cement hydration products and consequently altering the durability of the OPC structures. Sulphates can, however, assist in the corrosion process in a similar way as chlorides do, but chlorides remain to be the main contributor to the eventual failing of the OPC structure.

Geopolymeric gel does not react as readily with sulphates as measured for OPC specimens (**Bakharev; 2003**), where the formation of cracks are the most prominent feature of durability deterioration. It has to be noted that Bakharev did not consider geopolymers blended with aggregate in her investigation and the samples were typically exposed to 5% sodium- and magnesium sulphate solutions for 5 months.

Due to the extended experimental times required for similar investigations on additional geopolymer formulations, it was decided to make use of the same diffusion accelerated test as used for the chloride diffusion investigation. More so, an acidic sulphate medium was chosen in order to additionally validate the resistance to acid attack by the geopolymeric material. This, in turn, introduces another possible application where structures need to resist high levels of acid rain or even for use as bund-walls on process plants.

Literature on sulphate diffusion coefficients for cement and cement stone is limited, but the work done produced results ranging from $3.35 \times 10^{-8} \text{cm}^2/\text{s}$ (**Gospodinov et al., 1996**) to $1.06 \times 10^{-8} \text{cm}^2/\text{s}$ (**Tumidajski et al., 1995**). These coefficients were obtained in sodium sulphate solutions by various soaking methods.



The geopolymer samples subjected to accelerated diffusion tests producing the highest coefficient (N22) ranged from $6.93 \times 10^{-10} \text{cm}^2/\text{s}$ to the sample with the lowest coefficient (N25) of $1.59 \times 10^{-13} \text{cm}^2/\text{s}$. Even in the highly acidic sulphate media ($0.3\text{M H}_2\text{SO}_4$) geopolymers outperformed the concrete specimens by a significant extent, subsequently proving that geopolymers do in fact resist sulphates more effectively. Also, it is proven that geopolymers are effective against acidic attack and a superior choice for use in applications where higher levels of acidity are expected.

7.2. Pore characterisation verification

The pore characterisation hypothesis discussed in **Chapter 4** has been a secondary topic of discussion throughout **Chapter 5**, with the emphasis on elucidating the migration of chloride through the geopolymer formulations. Due to the chemical reaction prominent in the highly acidic sulphate media in **Chapter 6**, the pore characterisation can no longer be applied nor compared with these systems although serving as a valuable indication of the independent acid resistance of each formulation.

Emphasis for this section will be on considering all the phenomena and finally concluding an acceptable pore geometry description. Throughout the discussion reference will be made to long/narrow or short/broad pores. These descriptions refer to the pores becoming more visible (short/broad) and eventually propagating into macro-pores/cracks, whereas long/narrow pores refer to the micro- and possibly capillary pores.

As part of the final comments in **Chapter 4**, it was concluded that certain ratios possibly gave rise to the following pore characteristics: A lower pore volume to surface area ratio favoured the formation of shorter/broader pores and a lower pore volume to compressive strength ratio favoured longer/narrower pores.

7.2.1. Varying activation concentrations

Pore volume (PV) to surface area (SA) and pore volume to compressive strength (CS) ratios suggested that the fly ash A specimens consist of both long/narrow pores and broad/short pores. Sample N2 (PV = $0.1215 \times 10^{-6} \text{ m}^3$, SA = $6.34 \text{ m}^2/\text{g}$, CS = 29 MPa) was believed to have less of the long/narrow pores than N3 (PV = $0.1018 \times 10^{-6} \text{ m}^3$, SA = $53.55 \text{ m}^2/\text{g}$, CS = 53.9 MPa), while N1 (PV = $0.1095 \times 10^{-6} \text{ m}^3$, SA = $16.41 \text{ m}^2/\text{g}$, CS = 19.8 MPa) possibly contain both variants. Fly ash B followed similar trends, but a higher PV/SA and lower PV/compressive strength was measured, suggesting a network of increased micro-pores.

Chloride diffusion coefficients (CDC) for sample N1 ($5.25 \times 10^{-14} \text{ cm}^2/\text{s}$) and N2 ($4.85 \times 10^{-14} \text{ cm}^2/\text{s}$) remained fairly constant, while N3 ($7.33 \times 10^{-14} \text{ cm}^2/\text{s}$) was slightly higher, suggesting the formation of continuous pores with increasing activation solution. The fly ash B variants once again showed a similar trend, but with higher CDC values.

Hydrostatic variation for sample N1 (exact same formulation as N4) to N3 seemed to decrease with an increase in activation concentration, suggesting that a direct link from the external surface to the sensing pad becomes less prominent. The only fly ash B specimen available for testing produced a large hydrostatic variation, suggesting a more continuous pathway from the outer rim to the sensing pad.

Copper/copper-sulphate half cell voltages indicated that N1 ($V_{\text{ave}} = -0.697\text{Volt}$) was significantly more corroded than sample N2 ($V_{\text{ave}} = -0.517\text{Volt}$) and N3 ($V_{\text{ave}} = -0.660\text{Volt}$). The possible formation of more prominent macro-pores in sample N1 when introduced with an inserted object (MS bar or sensor) could explain the high hydrostatic variation and high corrosive activity. Considering all the experimental constraints (limitation of samples) it may be concluded that an increase in activation solution possibly favours the formation of more continuous macro-pores. More work, however, needs to be done to draw an absolute conclusion in this regard.

Half cell potentials for the fly ash B formulations showed similar trends to the fly ash A variants, although producing lower voltages. This observation contradicts all of the other observations where an increased in chloride permeability was expected and therefore increased corrosive activity. Along with the significantly larger compressive strengths exerted by these formulations, it will be concluded that fly ash B formulations generally consist of a network of increased micro-pores, hence disregarding the half cell values.

7.2.2. Varying water content

From the PV to BET and PV to compressive strength ratios it was concluded that a decrease in water promotes the formation of micro-pores (Water: N4, N16 > N5, N17 > N6, N18), with fly ash B possibly containing more of these pores.

CDC values showed an increase in chloride permeability with a decrease in added water to the formulation. Fly ash B once again produced lower values, therefore being more permeable to chloride penetration.

High hydrostatic variation was measured for samples N4 (PV = 0.1095 m³, SA = 23.82 m²/g, CS = 19.8 MPa) and N6 (PV = 0.1209 m³, SA = 23.17 m²/g, CS = 29.2 MPa), while varying very little in value it suggests a network of continuous pores. The Fly ash B samples (N17 and N18) seemed to produce large hydrostatic variations, but decreases with decreasing water.

The extent of corrosion seemed to increase from sample N4 ($V_{ave} = -0.597$ Volt) to N5 ($V_{ave} = -0.650$ Volt), with N6 ($V_{ave} = -0.604$ Volt) showing similar corrosive activity as N4. Decreasing the water content possibly results in longer pores, but less of them. Fly ash B specimens (N16 to N18) showed lower half cell voltages, suggesting lower corrosive activity.

Once more the corrosion half cell potentials for fly ash B contradict other findings and will be disregarded from the pore characterisation hypothesis, which indicates an increase in the formation of macro-pores with decreasing water. The number of these pores per unit sample is also assumed to decrease with decreasing water.

The half cell potentials deviated from the pore characterisation hypothesis for especially the fly ash B specimens upon varying the activation concentration and water content. Considering the amount of potassium and sodium present in both ashes, it may be the effect of fly ash B containing larger quantities of this element and therefore producing more a more basic mixture than fly ash A. A more basic mixture will result in higher alkali concentration pore liquids, therefore resisting corrosion more readily by maintaining a high pH for longer.

7.2.3. Varying GGBFS content

The fly ash A specimens showed very similar pore volume values, while deviating significantly in terms of BET surface area (**N7**: PV = 0.1226 m³; SA = 55.64 m²/g; CS = 55.7 MPa, **N8**: PV = 0.1331 m³, SA = 34.46 m²/g, CS = 25.7 MPa, **N9**: PV = 0.1365 m³, SA = 27.42 m²/g, CS = 21.6 MPa). Yet again, a decrease in added slag produced an increase in PV/SA ratio and a sharp increase in PV/CS. Slag favours the formation of longer/narrower micro-pores, partly elucidating the increase in compressive strength with an increase in slag addition.

Fly ash B specimens (**N19**: PV = 0.1381 m³; SA = 15.33 m²/g; CS = 77 MPa, **N20**: PV = 0.1735 m³, SA = 39.75 m²/g, CS = 69.8 MPa, **N21**: PV = 0.1408 m³, SA = 29.14 m²/g, CS = 68.7 MPa) showed comparable trends to the fly ash A variants, except for producing lower PV/compressive strength values; suggesting the formation of extended micro-pores. Although not fully substantiated in **Chapter 4**, it was suggested that the fly ash B samples result in a network of entangled micro-pores, therefore lacking the expected continuous pathway.

The chloride diffusion coefficients measured for samples N7 ($2.68 \times 10^{-11} \text{cm}^2/\text{s}$), N8 ($2.99 \times 10^{-11} \text{cm}^2/\text{s}$) to N9 ($9.93 \times 10^{-15} \text{cm}^2/\text{s}$) showed a decrease in chloride permeability with a decrease in added slag, hence advocating the formation of continuous micro-pores with increasing slag. Samples N19 ($9.47 \times 10^{-15} \text{cm}^2/\text{s}$) to N21 ($5.57 \times 10^{-15} \text{cm}^2/\text{s}$) did not follow the trends as shown for the fly ash A-based formulations. A sharp increase in CDC value for sample N20 ($1.98 \times 10^{-11} \text{cm}^2/\text{s}$) suggested that a “threshold” may be present upon adding 7 wt% slag to the mixture or an experimental error has occurred. Samples N19 and N21 produced CDC values well below those found for the equivalent fly ash A types, suggesting the increased formation of micro-pores.

A high variation on hydrostatic pressure was found for sample N8, suggesting a continuous pore structure from the outer sample rim to the inner embedded sensing pad. N19 produced very low hydrostatic variation, therefore possibly lacking a network of continuous pores. This reinforces the idea that the fly ash B samples favour the formation of interlinked network of micro-pores.

The half cell potentials indicated a decrease in extent of corrosive activity for a decrease in added slag for both ashes (N7 = -0.676Volt, N8 = -0.669Volt, N9 = -0.611Volt). The fly ash B specimens showed a lower extent of corrosive activity (N19 = -0.647Volt, N20 = -0.631Volt, N21 = -0.632Volt), therefore suggesting a more interlinked micro-pore network.

All of the parameters suggest the GGBFS addition favours the formation of micro-pores, whereas the fly ash B formulations generally produce an interlinked pore network.

7.2.4. Varying aggregate content

Increased quantities of aggregate undeniably transform the pore structure of any probable geopolymer matrix (**N10**: PV = 0.0506 m³; SA = 5.93 m²/g; CS = 19.8 MPa, **N11**: PV = 0.0252 m³, SA = 5.07 m²/g, CS = 17.5 MPa, **N12**: PV = 0.0230 m³, SA = 3.31 m²/g, CS = 16 MPa), where an increase of aggregate results in broader/shorter macro-pores for both ashes. Fly ash B (**N22**: PV = 0.0554 m³; SA = 5.12 m²/g; CS = 40.3 MPa, **N23**: PV = 0.0459 m³, SA = 2.95 m²/g, CS = 33.6 MPa, **N24**: PV = 0.0300 m³, SA = 3.03 m²/g, CS = 34.7 MPa) demonstrates lower PV/SA and higher PV/compressive strength values, indicating that the pores of these samples are generally larger. These results are comparable to those found for adding GGBFS, possibly implying that once again the fly ash B formulations produces a tangled pore network.

Chloride diffusion values resulted in an increased CDC for an increase in aggregate (N10 CDC = 1.51 x 10⁻¹³ cm²/s, N11 CDC = 3.33 x 10⁻¹³ cm²/s, N12 CDC = 2.41 x 10⁻¹¹ cm²/s) to the fly ash A formulation, proposing that the material becomes more porous as the aggregate content increases. Surprisingly, the fly ash B specimens show a decrease in CDC with increasing aggregate (N22 CDC = 1.45 x 10⁻¹³ cm²/s, N23 CDC = 2.54 x 10⁻¹³ cm²/s, N24 CDC = 5.90 x 10⁻¹⁴ cm²/s). The only plausible explanation for this phenomenon may be the required water for each ash to polymerise, where fly ash B possibly requires less water.

Some extent of hydrostatic variation for sample N10 was evident. Considering the fact sample N10 effectively is sample N4 with 2.1 (wt) parts aggregate, it may be concluded that aggregate (up to a point) promotes a less porous geopolymer. Sample N22 produced very low variation in hydrostatic variation, suggesting a network of non-continuous pores.

The corrosion indicative half cell voltages were largely affected by the formation of visible macro-cracks once the MS-embedded samples were cured and removed from the plastic mould (N10 = -0.528Volt, N11 = -0.623Volt, N12 = -0.488Volt). Sample N22 (-0.441Volt) was the least corroded out of all the formulations, while possessing a high compressive strength, suggesting a distribution of tangled micro-pores (N23 = -0.581Volt, N24 = -0.629Volt). As discussed in **Chapter 4**, aggregate addition may possibly affect the pore width more than it does the length, where an increase in pore width is associated with an increase in aggregate.

7.2.5. Samples containing both aggregate and GGBFS

The only sample that contained both aggregate and slag is sample N25 (PV = 0.0741 m³, SA = 5.82 m²/g, CS = 55.7 MPa). This is a fly ash A based sample, mixed from the N7 (PV = 0.1226 m³, SA = 55.64 m²/g) formulation, with added 60 (wt) % aggregate.

The PV/SA for sample N25 is appreciably larger than for N7, therefore possibly indicating an increased network of micro-pores, whereas the larger PV to compressive strength ratio for N25 further strengthens the assumption.

The CDC for these two samples showed a significant decrease in chloride permeability with addition of aggregate. Sample N25 with a coefficient of $1.4 \times 10^{-15} \text{ cm}^2/\text{s}$ showed 4 orders of magnitude improvement to the coefficient of sample N7 ($2.7 \times 10^{-11} \text{ cm}^2/\text{s}$).

Copper/copper-sulphate half cell potentials for these two samples also point out the superior corrosion resistance of sample N25 compared with the performance of N7, supporting the hypothesis that N25 is a much less porous material than N7.

Therefore, it can be concluded that the N25 geopolymer formulation will be the most sensible replacement material for construction OPC applications.

7.2.6. Theoretical time-to-corrosion comparisons

Directly comparing time-to-corrosion data between OPC and geopolymer specimens is quite a difficult task, where the threshold chloride concentration value for OPC has been widely debated by cement and concrete researchers (**Glass & Buenfeld, 1997; Trejo & Pillai, 2004**).

Zhang & Lounis (2006) conducted sensitivity analyses on the parameters modelling the corrosion of reinforcing steel in concrete specimens. It is from this work that a simplified solution to the Tuutti corrosion model, given in Equation 7.1, was obtained:

$$T_i = f(C_s; C_{th}; D; d_c) = \frac{d_c^2}{4D} \sum_{m=0}^{12} A_m \left[\frac{C_{th}}{C_s} \right]^m \quad (7.1)$$

Where T_i = time-to-corrosion [seconds],

C_s = External, constant chloride concentration [M],

C_{th} = Threshold chloride concentration to initiate corrosion [M],

D = material chloride diffusion coefficient [cm^2/s]

and d_c = material cover depth [cm].

The solution of the Tuutti model given in Equation 7.1 is that of a 12th order polynomial fit from an error function, with coefficients A_0 to A_{12} presented in **Table 7.2.1**:

Table 7.2.1: Function coefficients for the 12th order polynomial fit

A0	1.70E+00
A1	-7.59E-01
A2	1.85E-03
A3	2.40E-04
A4	1.95E-05
A5	-1.04E-06
A6	3.87E-06
A7	-9.90E-06
A8	1.75E-07
A9	2.11E-07
A10	1.66E-07
A11	-7.45E-06
A12	1.50E-06
Residu	1.00E-06

Although no threshold chloride concentration values for geopolymers are available as yet, the time-to-corrosion comparisons cannot be excluded as an essential tool to evaluate its overall performance in terms of durability.

It is for this reason that a simplistic Delphi7-based program (assisted by **Charl Maree**) was created. The parameters presented in Equation 7.1 can now effortlessly be changed in order to fit any geopolymer formulation and experimentally acquired chloride concentration thresholds. This may prove to be an extremely beneficial tool for commercial geopolymeric-material users to qualitatively compare various formulations; alternatively, future users may decide on a specific time-to-corrosion and choose a suited geopolymer formulation on the basis of the obtained CDC.



Theoretical comparisons can now be made, where the chloride concentration threshold (C_{th}) will be assumed to remain constant for both geopolymeric and OPC material. This assumption, however, is not trustworthy in any sense because the passivity layer formed by each material is significantly different in terms of composition and pH and may require significantly higher chloride concentrations to initiate corrosion. **Trejo & Pillai (2004)** reported mean C_{th} values for carbon steel to SS316LN. Considering these values of 0.52kg/m^3 and 10.8kg/m^3 respectively, the value of mild steel will undoubtedly fall within these boundaries and only the two external conditions need to be investigated.

Extended times for chloride-induced corrosion is not uncommon in the OPC literature: **Thomas (1996)** indicated that the time-to-corrosion initiation for an unblended OPC specimen with a cover of 60mm and a constant 4% external chloride source will be in the order of 5 years, providing a CDC of $6.4 \times 10^{-8} \text{ cm}^2/\text{s}$. Incorporating the values into Equation 7.1 yields a value of 7.89 years, which is almost double the original estimation. This difference could be the cause of the fact that **Thomas (1996)** made use of the electrical gradient in concrete to predict the diffusion coefficients, possibly creating circular referencing. He does, however;

also state that by blending the concrete with 30% Fly ash can extend the time to corrosion initiation to almost 43 years. Using the DiffCoeff Delphi program, **Figure 7.2.1**, yields a value of 4.6 years, which is much closer to the Thomas values, suggesting that the correlation in Equation 7.1 is not as accurate as the original error function in Equation 7.2.

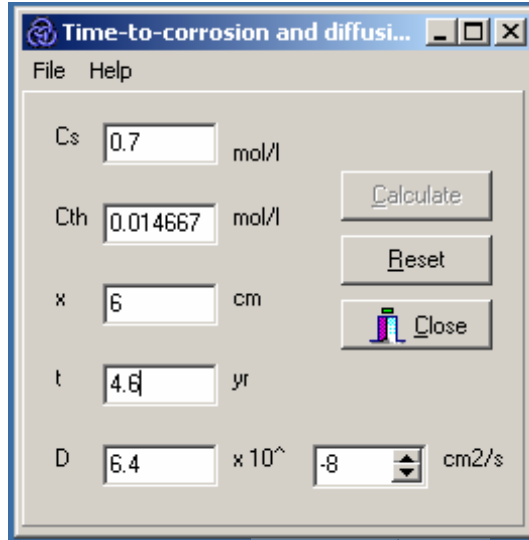


Figure 7.2.1: DiffCoeff-Program supporting results presented by **Thomas (1996)**. Users of the programme are advised to ensure dimensional consistency as presented next to each parameter.

Berke et al. (2005) also made use of a Fickian model and concluded that a 65mm coating of OPC/slag blend could last *ca* 74 years before chloride-induced corrosion is initiated. Berke made use of a chloride build-up model, with no specification or reference to the chloride concentration from an external source, therefore making it impracticable to compare the results with those obtained by use of Equation 7.1 or the DiffCoeff-software.

Incorporating the results of Equation 7.1 for geopolymers similar to the OPC conditions set out by **Thomas (1996)**, the geopolymeric formulation N25 produces a T_i of nearly 3.5×10^8 years! Upon closer inspection into the time-to-corrosion formulation, it seems to be mostly affected by the low diffusion coefficient of the geopolymer sample. Whether or not this falls beyond the boundaries of the original error function is not entirely clear, although unlikely, seeing that the error function is only dependent on the surface concentration (C_s) and threshold concentration (C_{th}) in Equation 7.2.

$$1 - \frac{C_{th}}{C_s} = \text{erf}\left(\frac{d_c}{2\sqrt{D \cdot t}}\right) \quad (7.2)$$

Effectively Equation 7.1 is a fitted model for Equation 7.2, which is a transformed version of the Crank's solution on Fickian diffusion, providing a constant diffusion coefficient and constant surface chloride content (**Zhang & Lounis, 2006; Crank, 1975**). All of the boundary

conditions for the solution were met, but still an astronomical result for the geopolymeric system indicates that corrosion will in actual fact never occur, which is not likely. Also, varying the values of C_{th} and d_c does not greatly influence the outcome of the result, suggesting that the low diffusion coefficients obtained for geopolymeric samples may fall beyond the restrictions of fitted model of Equation 7.1. There is no reason, however, not to use the model for higher diffusion coefficients of particularly geopolymer pastes.

The DiffCoeff-program, once again assuming the Thomas values, yields a time-to-corrosion of 20.5×10^6 years for sample N25. Although a significant difference is noted between the results from Equation 7.1 and 7.2, exorbitant values are obtained. The program also restricts the input of values beyond the error-function limitations, therefore ensuring calculation stability. It is therefore not clear at this point whether or not the very low geopolymer diffusion coefficient values can solely predict the time-to-corrosion characteristics expected for a particular structure, but even if only in a very elementary sense it shows that geopolymeric material will resist chloride-induced corrosion more effectively than OPC.

DiffCoeff was dually written to also be used for “reverse” calculations, where the diffusion coefficient can be calculated if all the other parameters are known. This function may aid to choose a specific formulation if the durability requirements (i.e. time to corrosion) are known or estimated.

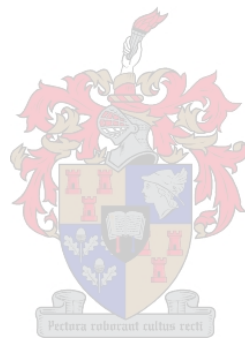
7.3. Summary

This chapter focussed on the summation of results and to provide rounded proof and sensible comparisons in order to successfully illustrate the superior chloride, sulphate and acid resistance exhibited by geopolymeric material.

The pore characterisation hypothesis set out in earlier chapters is once more considered, this time under the light of all the relating results, therefore providing final justification to the hypothesis. Importantly, the characterisation hypothesis assisted in the elucidation of diffusive behaviour shown by varying geopolymeric formulations. Further experimental and analytical data may be required to fully prove the hypothesis.

The chapter is concluded by looking at time-to-corrosion literature and applications set out by previous cement- and concrete investigators. A Microsoft Windows compatible program was compiled in order to further compare data not covered in this work. The program is adaptable to both geopolymer and OPC data and may prove to be a valuable tool for future researchers and commercial geopolymer implementers. Due to the large values shown in the calculations for the time to corrosion regarding the geopolymer samples, future researchers may find it beneficial to look at other diffusive models, where Fick’s laws may not describe the

diffusion characteristics exhibited by these materials effectively. This holds for both OPC and geopolymeric material, where comparative data for different diffusion models may provide some extent of clarity on the true time to corrosion expected for a specific covering material.



Chapter 8.

CONCLUSIONS AND RECOMMENDATIONS

This project aimed to address questions raised in terms of the durability that can be expected from geopolymer applications, resulting in the generation of new experimental methods and – data, initiating a durability description. In particular, this work presents data resulting from accelerated tests commonly used in cement- and concrete investigations, including investigations with half cell potentials and embedded sensors.

A thorough literature review in the geopolymer field was required, not only as basis for the work, but more importantly to rapidly establish a series of geopolymer formulations which may accomplish as robust an investigation as possible. Seeing that no prior work on geopolymer durability has been published, a qualitative assessment on concrete literature was also required to provide a solid knowledge base that can serve as a starting point for reliable comparisons between the two materials, the aim remaining to facilitate the wider use of concepts relating to geopolymers as superior corrosion and deterioration inhibitor.

Early in the investigation, particularly during the overview of cement- and concrete literature, it became clear that the basis for proving the superiority of geopolymers most probably lies in the permeability this material expresses towards chloride penetration. This is one of the major “shortcomings” in the cement- and concrete technology, where very costly reconstructive work is essential on a continuous basis. Chloride diffusion coefficient comparisons between the 25 geopolymer formulations and OPC blends proved that even the worst performing geopolymer exhibited lower diffusion coefficients than the best OPC/Silica-Fume/GGBFS variants. This work therefore suggests that geopolymers may not only be a more economical replacement for OPC, but also possesses huge durability advantages.

Sulphate induced corrosion to OPC structures has been identified as not being a major contributor to the overall structure deterioration, but may in some cases accelerate the process by reacting with the cement hydration products. Sulphates do not react with the geopolymeric matrix as readily, therefore this work introduced sulphates in a highly acidic medium to all of the geopolymer formulations. The resulting sulphate diffusion coefficient comparisons between the materials showed that once again geopolymers resisted sulphate penetration more readily than OPC and OPC blends. The geopolymer formulations mixed with slag or aggregate (preferably both) showed impressive acid resistance and compressive

strengths above its excellent sulphate and chloride resistance. These findings introduced another level of possible geopolymer applications, especially for use in acidic environments, including acid rain, processing bund walls and sewerage lines.

Further investigations were undertaken to determine the possible pore characterisation or varying formulations, which was then correlated to the findings in corrosive activity, diffusion coefficients and other physical properties. Although the pore geometric (variation of pore length and width) hypothesis is justified in the majority of cases, some future analytical work may be required to completely verify the hypothesis. A pore characterisation basis is provided in this work, while extensions to this topic may prove to be a valuable tool in tailoring a geopolymer formulation for a specific application.

This thesis concludes by highlighting the improved durability the geopolymer formulations exhibited by both Class F fly ashes. A theoretical time-to-corrosion software tool was developed and included in this work in an effort to assist future researchers and possible commercial users to compare formulations not included in this investigation.

The following recommendations may be useful to future researchers in this field:

Sample N18 produced a very low diffusion coefficient, as well as other unexpected physical properties. Inadequate mixing may have caused the anomalous result, which introduced an error that propagated into each analytical method. The effect of batch-to-batch deviations should be investigated, as well as repetition to test specimens.

The number of available samples limited the investigation in some areas, where the raw materials originated from Australia. Repeating certain analyses was impossible due to importing issues, suggesting that the experimental phase should be conducted on a single continent.

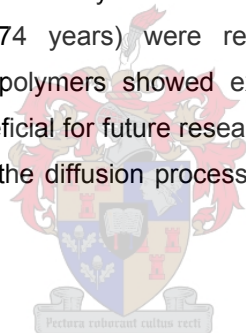
The number of elemental iron originally present in each fly ash may have a significant effect on the total diffusive behaviour for that sample. Further investigation into this phenomenon may point towards certain ashes for greater performance.

Corrosion half cell testing could be improved by increasing the geopolymer cover thickness. A significant number of samples cracked upon introducing an embedded object (mild steel bar or sensor). The severity of cracking only became evident once the samples were completely cured. Also, some cracking may have occurred during transit from Melbourne to Stellenbosch.

Even though valuable acid resistance indications resulted from use of H_2SO_4 as sulphate source, more about the pore geometry can be learned through knowledge on the sulphate diffusion coefficient obtained from Na_2SO_4 solution for Diffusion Cell experiments.

The mechanisms may be debated on how the diffusion is taking place (i.e. means of mass transfer), but the overall coefficient is only there to indicate how well a certain cover of material will resist the penetration of a certain ion. The mechanism now becomes irrelevant, whereas the embedded rebar is only concerned with the amount of corrosive ions that will eventually lead to the failure of the structure. Although invaluable to a fundamental explanation of the geopolymer resistance potential, the work is not covered in this thesis.

The success of the Delphi7™ program relies on accurate chloride threshold concentrations, which are not available for geopolymeric species. Although this value did not influence the outcome of the calculation significantly, it may become crucial for geopolymers with higher chloride diffusion coefficients. The large values obtained for the time-to-corrosion for the geopolymer samples may suggest these materials do not follow Fick's diffusion laws as readily as was assumed early on. This may also be true for concrete samples, where large time-to-corrosion values (up to 74 years) were recorded, but not substantiated by experimental data. Although geopolymers showed extended corrosion resistive periods based on Fick's law, it may be beneficial for future researchers to look into a range of models that can more accurately describe the diffusion process present in both of these composite materials.



REFERENCES:

Askeland, D. R., **“The Science and Engineering of Materials,”** *Third S.I. Edition, Stanley Thornes (Publishers) Ltd. UK. 1998. 350 pages.*

Auer, S., Kuzel, H. J., Pollmann, H., Sorrentino, F., **“Investigation on MSW fly ash treatment by reactive calcium aluminates and phases formed,”** *Cement and Concrete Research*, 25, No. 6. 1995. pp 1347-1359.

Ayala, V., Ingalls, A., Genesca, J., **“Mathematical Modelling of Rebar Corrosion in Seawater,”** *Dpto. Ingeniería Metalúrgica. Facultad Química. Ciudad Universitaria. Mexico. 2000. 12 pages.*

Bary, B., Béjaoui, **“Assessment of diffusive and mechanical properties of hardened cement pastes using a multi-coated sphere assemblage model,”** *Cement and concrete research. Volume 36, 2006. pp 245-258.*

Bakharev, T., **“Durability of geopolymer materials in sodium and magnesium sulphate solutions,”** *Cement and concrete research. Volume 35, 2005. pp 1233-1246.*

Berke, N. S., Hicks, M. C., Malone, J., Rieder, K. L., **“Concrete Durability,”** *Concrete International. Farmington Hills. Aug 2005, page 63.*

Breese, B. M. H., Jamieson, D. N., **“Material analysis using a Nuclear Microprobe,”** John Wiley and Sons, 1996. 300 pages.

Brimblecombe, P., **“Air composition and chemistry,”** Cambridge; New York. *Cambridge University Press*, 1996. 220 pages.

Broken, H. J. P., **“Moisture transport in brick masonry: The grey area between bricks,”** *Thesis at the Eindhoven University of Technology*, 1998. 170 pages.

Castro, P., Véleva, L., Balancán, M., **“Corrosion of reinforced concrete in a tropical marine environment and in accelerated tests,”** *Construction and Building Materials*, Vol. 11, No. 2. 1997. pp 75-81

Cioffi, R., Marroccoli, M., Mascolo, G., "On permeation effects of aqueous solutions through non-mature pastes of portland-pozzolana cement," *Cement and Concrete Research*, Vol. 19, 1989. pp 189-193

Cohen, M. D., Mathur, B., "Sulphate attack on concrete," *ACI Material Journal*. Issue 88, 1991. pp 62-69.

Cullity, B. D., Stock, S. R., "Elements of XRD," *Upper saddle river, N. J: Prentice Hall*, London, 3rd edition, 2001. 250 pages.

Crank, J., "The mathematics of diffusion," *Clarendon Press*. Second Edition, Oxford. 1975. 200 pages.

Dhir, R. K., Jones, M. R., Ahmed, H. E. H., Seneviratne, A. M. G., "Rapid estimation of chloride diffusion coefficient in concrete," *Magazine of Concrete Research*, 42, No. 152. 1990. pp 177-185.

Dickerson, N. P., Simonen, J. T., Andringa, M. M., Wood, S. L., Neikirk, D. P., "Wireless low-cost corrosion sensors for reinforced concrete structures," *Department of Electrical and Computer Engineering, University of Texas, Austin, TX, USA 78712*. www.ece.utexas.edu/~andringa/resume.html.

Deventer, J.S.J., "The effect of alkali cations on aluminium incorporation in geopolymeric gels," *Industrial & Engineering Chemistry Research*, 44. No. 4, 2005 (a). pp 832-839.

Duxson, P., Provis, J.L., Lukey, G.C., Separovic, F. & Van Deventer, J.S.J., "²⁹Si NMR study of structural ordering in aluminosilicate geopolymer gels," *Langmuir*, 21. No. 7, 2005(b) pp 3028-3036.

Duxson, P., Provis, J.L., Lukey, Mallicoat, S. W., Kriven, W. M., & Van Deventer, J.S.J., "Understanding the relationship between geopolymer composition, microstructure and mechanical properties," *Colloids and surfaces A – Physicochemical and Engineering Aspect*, 269, No. 1-3, 2005. pp 47-58.

Engineering News. **Cement Surge**. *Creamer Media*. Vol 25, No. 35, September 9-15, 2005. page 16.

Faimon, J.: **“Oscillatory silicon and aluminium aqueous concentrations during experimental aluminosilicate weathering”**. *Geochimica et Cosmochimica Acta*, 60, 1996. pp 2901-2907.

Feng, D., Tan, H. & Van Deventer, J.S.J., **“Ultrasound enhanced geopolymerisation,”** *Journal of Materials Science*, vol. 39, no.2, 2004, pp. 571-580.

Fritz, J. S., Gjerde, D. T., **“Ion Chromatography,”** Weinheim. *Wiley-VCH*. 2000. 254 pages.

Glass, G. K., Buenfeld, N. R., **“Presentation of the chloride threshold level for corrosion of steel in concrete,”** *Corrosion Science*, Volume 39, No. 5, May 1997. pp 1001-1013.

Gokhale, C. **“The immobilisation of organic waste through geopolymerisation.”** *Masters thesis*, November 2001. University of Stellenbosch. 169 pages.

Goretta, K.C., Chen, N., Gutierrez-Mora, F., Routbort, J.L., Lukey, G.C. & Van Deventer, J.S.J., **“Solid-particle erosion of a geopolymer containing fly ash and blast-furnace slag,”** *Wear*, vol. 256, 2004, pp. 714-719.

Gospodinov, P., Kazandjiev, R., Mironova, M., **“The effect of Sulphate ion diffusion on the structure of cement stone,”** *Cement and Concrete composites*. Issue 18, 1997. pp 401-407.

Groot, C., **“Effects of water on mortar-brick bond,”** *Thesis Technische Universiteit Delft*, The Netherlands, 1993. 183 pages.

Horváth, Á, Schiller, R. **“Rescaled range analysis of the corrosion potential noise,”** *Corrosion Science* 45, 2003. pp 597-609.

Halamickova, P., Detwiler, R. J., **“Water permeability and chloride ion diffusion in Portland cement Mortars: Relationship to sand content and critical pore diameter,”** *Cement and Concrete Research*, Vol. 25, No. 4, 1995. pp 790-802

Hossain, K. M. A., Lachemi, M., **“Corrosion resistance and chloride diffusivity of volcanic ash blended cement mortar,”** *Cement and Concrete Research* 34, 2004. pp 695-702.

Jenneson, P.M., Clough, A. S., Hollands, R., Mulheron, M. J., Jeynes, C. **“Profiling chloride diffusion into ordinary Portland cement and pulverised fuel ash pastes using scanning MeV proton micro-PIXE,”** *Department of Physics, Civil Engineering and Electrical and Electronic Engineering, University of Surrey, Guildford, Surrey, GU2 5XH, UK. 1998.* www.ph.surrey.ac.uk. 6 pages.

Jolley, M. J., **“Evaluation of Corrosion-Resistant Steel Reinforcement,”** *Iowa State University, October 2003.* 18 pages.

Keyte, L.M., Lukey, G.C., van Deventer, J.S.J: **“The effect of Coal Ash Chemistry on the tailored design of waste-based geopolymeric products”** *Department of Chemical and Biomolecular Engineering, The University of Melbourne, Victoria 3010, Australia.* 2005

Keyte, L. M: **Private Communication/Discussion.** University of Melbourne, Australia. 2005

Lee, W.K.W & Van Deventer, J.S.J., **“The effect of ionic contaminants on the early-age properties of alkali-activated fly ash-based cements”**, *Cement and Concrete Research*, vol. 32, 2002(a). pp 577-584.



Lee, W.K.W. & Van Deventer, J.S.J., **“Effects of anions on the formation of aluminosilicate gel in geopolymers,”** *Industrial & Engineering Chemistry Research*, vol. 41, no. 18, 2002(b). pp 4550-4558.

Lee, W.K.W. & Van Deventer, J.S.J., **“Structural reorganisation of class F fly ash in alkaline silicate solutions,”** *Colloids and Surfaces A*, vol. 211, no. 1, 2002(c). pp 49-66.

Lee, W.K.W. & Van Deventer, J.S.J., **“The effects of inorganic salt contamination on the strength and durability of geopolymers,”** *Colloids and Surfaces A*, vol. 211, nos. 2-3, 2002(d). pp 115-126.

Lee, W.K.W. & Van Deventer, J.S.J., **“The use of infrared spectroscopy to study geopolymerisation of heterogeneous amorphous aluminosilicates,”** *Langmuir*, vol. 19, no. 21, 2003. pp 8726-8734.

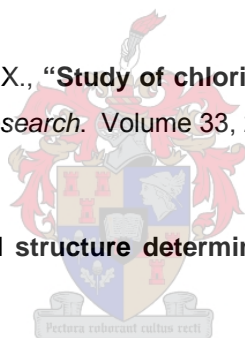
Lee, W.K.W. & Van Deventer, J.S.J., **“The interface between natural siliceous aggregates and geopolymers,”** *Cement and Concrete Research*, vol. 34, no. 2, 2004. pp 195-206.

Liu, Y., **“Modeling the Time-to-Corrosion cracking of the Cover Concrete in Chloride Contaminated Reinforced Concrete Structures,”** *PhD Thesis*. Faculty of the Virginia Polytechnic Institute and State University. October 1996. 117 pages.

Lloyd, R. R., & Van Deventer, J.S.J., **“The microstructure of geopolymers synthesised from industrial wastes,”** *Department of Chemical and Biomolecular Engineering, The University of Melbourne, Victoria 3010, Australia*. 2005. Conference paper. 8 pages.

Luo, R., Cai, Y., Wang, C., Huang, X., **“Study of chloride binding and diffusion in GGBS concrete,”** *Cement and concrete research*. Volume 33, 2003. Pages 1 to 7.

Massa, W., Gould, R. O., **“Crystal structure determination,”** Berlin, *Springer*. 2004. 210 pages.



McGrath, P. F., Hooton, R. D., **“Influence of Voltage on Chloride diffusion coefficients form chloride migration tests,”** *Cement and Concrete Research*, vol. 26, no. 8, 1996. pp 1239-1244.

Mindess, S., Young, J. F., **“Concrete,”** *Prentice-Hall Inc*. London. 1981. 350 pages.

Neville, A. M., **“Properties of Concrete,”** *Longman*, Harlow. 1995. 181 pages.

Nölte, J., **“ICP emission spectrometry: a practical guide,”** *Weinheim, Wiley-VCH*. 2003. 267 pages.

Novak, L. J., Grizzle, K. M., Wood, S. L., Neikirk, D. P., **“Development of state sensors for civil engineering structures,”** *Proceedings of SPIE, Smart Structures and Materials 2003: Smart Systems and Non-destructive Evaluation for Civil Infrastructures*, Vol. 5057, 2003. pp 358-363.

Oh, B. H., Jang, S. Y., **“Prediction of diffusivity of concrete based on simple analytic equations,”** *Cement and Concrete Research* 34, 2004. pp 463-480.

Phair, J.W. & Van Deventer, J.S.J., **“Effect of silicate activator pH on the leaching and material characteristics of waste-based inorganic polymers”**, *Minerals Engineering*, vol. 14, No. 3, 2001(a). pp 289-304.

Phair, J.W., Van Deventer, J.S.J. & Smith, J.D., **“Interaction of sodium silicate with zirconia and its consequences for polysialation”**, *Colloids and Surfaces A*, vol. 182, No. 1-3, 2001(b). pp 143-159.

Phair, J.W. & Van Deventer, J.S.J., **“Effect of silicate activator pH on the microstructural characteristics of waste-based geopolymers”**, *International Journal of Mineral Processing*, vol. 66, No. 1-4, 2002(a). pp 121-143.

Phair, J.W. & Van Deventer, J.S.J., **“Characterization of fly ash-based geopolymeric binders activated with sodium aluminate”**, *Industrial & Engineering Chemistry Research*, vol. 41, No. 17, 2002(b). pp 4242-4251.

Phair, J.W., Smith, J.D. & Van Deventer, J.S.J., **“Characteristics of aluminosilicate hydrogels related to commercial ‘Geopolymers,’** *Materials Letters*, vol. 57, no. 28, 2003, pp 4356-4367.

Phair, J.W., Smith, J.D. & Van Deventer, J.S.J., **“Mechanism of polysialation in the incorporation of zirconia into fly ash-based geopolymers”** *Industrial & Engineering Chemistry Research*, vol. 39, No. 8, 2000. pp 2925-2934.

Phair, J.W., **“Compositional Effects and Microstructure of Fly ash-Based Geopolymers,”** *PhD Thesis*, Department of Chemical Engineering. The University of Melbourne, Australia. September 2001. 350 pages.

Popovics, S., **“Concrete Making Materials,”** McGraw-Hill, Sydney. 1979. 181 pages.

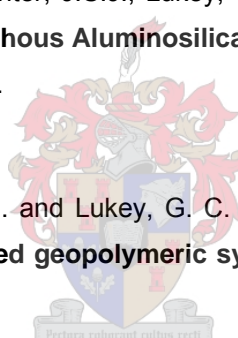
Postek, M. T., **“Scanning electron microscopy: a student’s handbook,”** Ladd Research Industries, 1980. 305 pages.

Provis, J.L., Lukey, G.C., Van Deventer, J.S.J. **“Do geopolymers actually contain noncrystalline zeolites – A re-examination of existing results.”** *Chemistry of Materials*, Volume 17, No. 1, 2005(a). pp 3075-3085.

Provis, J.L., Duxson, P., Van Deventer, J.S.J. **“The role of mathematical modelling and gel chemistry in advancing geopolymer technology”.** *Chemical Engineering Research & Design*,. Volume 83, No. A7, 2005(b). pp 853-860.

Provis, J.L., Duxson, P., Van Deventer, J.S.J., Lukey, G.C. **“A statistical Thermodynamic Model for Si/Al ordering in Amorphous Aluminosilicates”.** *Chemistry of Materials*, Volume 17, No. 11, 2005(c). pp. 2976-2986.

Provis, J. L., van Deventer, J. S. J. and Lukey, G. C. **"A conceptual model for solid-gel transformations in partially reacted geopolymeric systems."** *Ceramic Transactions*, 165, 2005(d). pp 49-70.



Roskopf, P. A., Virnelson, R. C., **“Laboratory Tests for Corrosion of Steel in Concrete,”** *Laboratory Corrosion Tests and Standards, ASTM STP 866*, American Society for Testing and Materials, Philadelphia, 1985. pp 275-284.

Simonen, J. T., Andringa, M. M., Grizzle, K. M., Wood, S. L., Neikirk, D. P., **“Wireless sensors for monitoring corrosion in reinforced concrete members,”** *Proceedings of SPIE, Smart Structures and Materials 2004: Smart Systems and Non-destructive Evaluation for Civil Infrastructures*, Vol 5391, 2004. pp 587-596.

Smulko, J., Darowicki, K., Zicliński, A. **“Detection of random transients caused by pitting corrosion,”** *Electrochimica Acta*, Vol 47, Issue 8, 2002. pp 1297-1303.

Stuart, B., **"Infrared spectroscopy: Fundamentals and applications,"** England, *John Wiley and Sons*. 2004. 224 pages.

Swaddle, T. W., **"Silicate complexes of aluminium (III) in aqueous systems,"** *Coordination Chemistry Reviews*, 219-221, 2001. pp 665 – 686.

Trejo, D., Pillai, R. G., **"Accelerated Chloride threshold testing Part II: Corrosion-resistant reinforcement,"** *ACI material journal*, Volume 101, No. 1, 2004. pp 57-64.

Thomas, M. D. A., **"Author's reply to discussion of paper – Chloride thresholds in marine concrete – by David B. McDonald,"** *Cement and Concrete Research*, Vol. 26, No. 10, 1996. pp 1603-1604.

Tumidajski, P. J., Chan, G. W., Philipose, K. E., **"An effective diffusivity for Sulphate transport into concrete,"** *Cement and Concrete Research*, Vol. 25, N. 6, 1995. pp 1159-1163.

Van Jaarsveld, J.G.S., Van Deventer, J.S.J. & Lorenzen, L., **"Factors affecting the immobilization of metals in geopolymerized fly ash,"** *Metallurgical and Materials Transactions B*, Vol. 29B, 1998. pp 283-291.



Van Jaarsveld, J.G.S., Van Deventer, J.S.J. & Lukey, G.C., **"The effect of composition and temperature on the properties of fly ash- and kaolinite-based geopolymers,"** *The Chemical Engineering Journal*, Vol. 89, Nos. 1-3, 2002. pp 63-73.

Van Jaarsveld, J.G.S., Van Deventer, J.S.J. & Lukey, G.C., **"The characterisation of source materials in fly ash based geopolymers,"** *Materials Letters*, Vol. 57, 2003. pp 1272-1280.

Van Jaarsveld, J.G.S., Van Deventer, J.S.J. & Lukey, G.C., **"A comparative study of kaolinite versus metakaolinite in fly ash based geopolymers containing immobilised metals,"** *Chemical Engineering Communications*, Vol. 191, No. 4, 2004. pp 531-549.

Van Jaarsveld, J.G.S. **“The physical and Chemical Characterisation of Fly ash Based Geopolymers”**. *PhD Thesis*, Department of Chemical Engineering. The University of Melbourne, Australia. March 2000. 381 pages.

Yeau, Y. K., Kim, E. K., **“An experimental study on corrosion resistance of concrete with ground granulated blast furnace slag,”** *Cement and Concrete Research*, Vol. 35, 2005. pp 1391-1399.

Yip, C.K. & Van Deventer, J.S.J., **“Microanalysis of calcium silicate hydrate gel formed within a geopolymeric binder,”** *Journal of Materials Science*, Vol. 38, No.18, 2003. pp 3851-3860.

Yip, C.K., Lukey, G.C. & Van Deventer, J.S.J. **“Effect of blast furnace slag addition on microstructure and properties of metakaolinite geopolymeric materials”**. *Ceramic Transactions*, Vol. 153 (Advances in Ceramic Matrix Composites IX), 2003. pp187-209.

Yip, C.K. & Van Deventer, J.S.J., **“The coexistence of geopolymeric gel and calcium silicate hydrate at the early stage of alkaline activation,”** *Cement and Concrete Research*, Vol. 25, No. 9, 2005. pp 1688-1697.

Xu, H., Van Deventer, J.S.J. & Lukey, G.C., **“Effect of alkali metals on the preferential geopolymerisation of stilbite/kaolinite mixtures”**, *Industrial & Engineering Chemistry Research*, Vol. 40, 2001. pp 3749-3756.

Xu, H. & Van Deventer, J.S.J., **“Factors affecting the geopolymerisation of alkali-feldspars”**, *Minerals and Metallurgical Processing*, Vol. 19, No. 4, 2002(a). pp 209-214.

Xu, H. & Van Deventer, J.S.J., **“Geopolymerisation of multiple minerals,”** *Minerals Engineering*, Vol. 15, No. 12, 2002(b). pp 1131-1139.

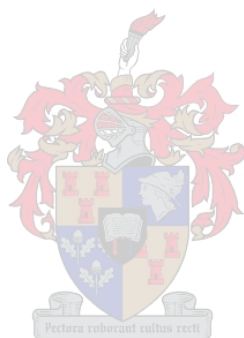
Xu, H. & Van Deventer, J.S.J., **“The effect of alkali metals on the formation of geopolymeric gels from alkali-feldspars,”** *Colloids and Surfaces A*, Vol. 216, 2003(a). pp 27-44.

Xu, H. & Van Deventer, J.S.J., “**Effect of source materials on geopolymerisation,**” *Industrial & Engineering Chemistry Research*, Vol. 42, 2003(b). pp 1698-1706.

Xu, H., Van Deventer, J.S.J., Roszak, S. & Leszczynski, J., “**Ab Initio study of dissolution reactions of five-membered aluminosilicate framework rings**”, *International Journal of Quantum Chemistry*, Vol. 96, No. 4, 2004. pp 365-373.

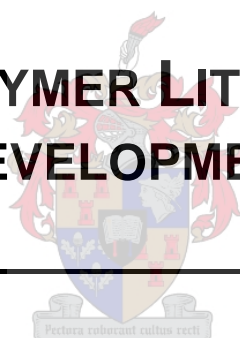
Xu, H., Lukey, G.C. & Van Deventer, J.S.J., “**The effect of Ca on activation of class C, class F-fly ash and blast furnace slag,**” *Cement and Concrete Research*, Received 9 March 2004; accepted 6 February 2005. Available online 28 July 2006.

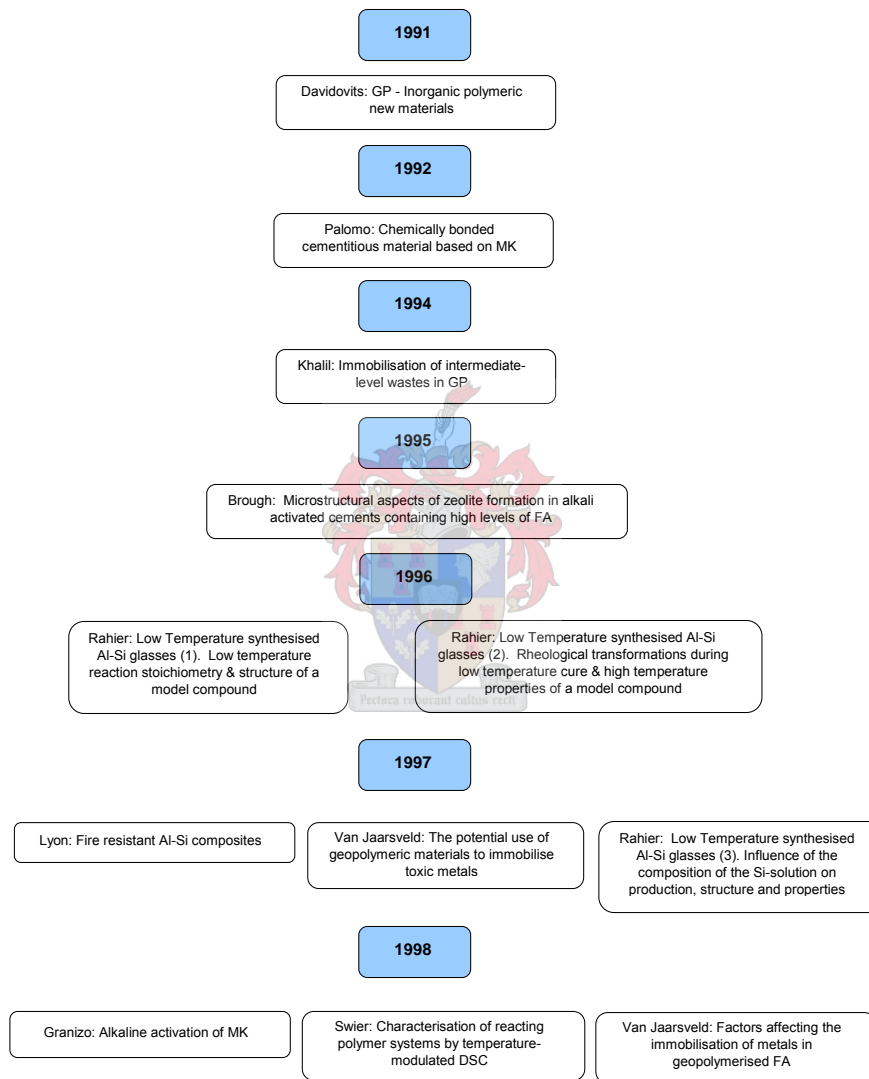
Zhang, J., Lounis, Z., “**Sensitivity analysis of simplified diffusion-based corrosion initiation model of concrete structures exposed to chlorides,**” *Cement and Concrete research*. Vol 36, Issue 7 , July 2006. pp 1312-1323.

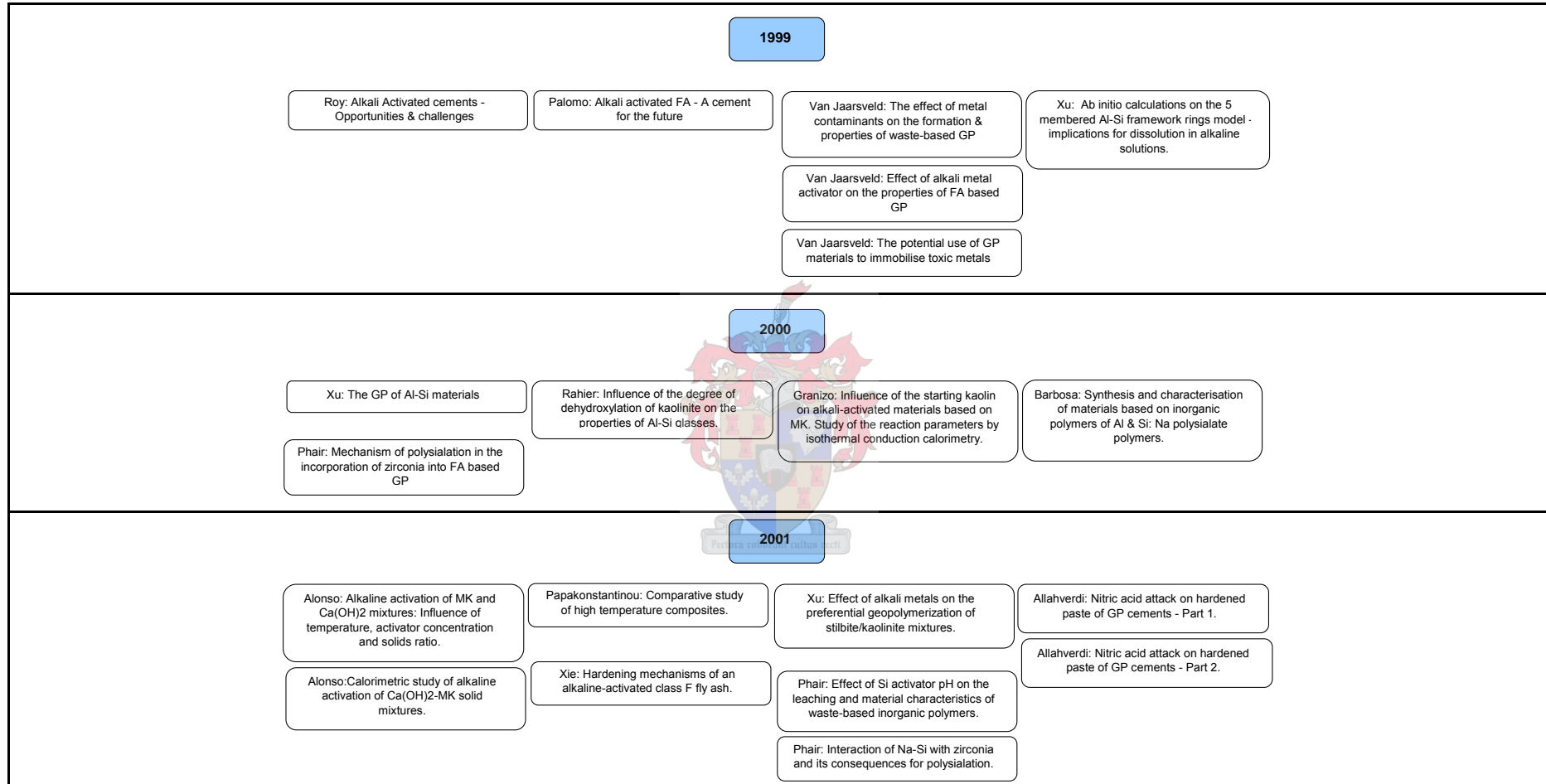


APPENDIX A

GEOPOLYMER LITERATURE DEVELOPMENT







2002

Hos: Investigation of a synthetic aluminosilicate inorganic polymer.

Granizo: Alkaline activation of MK: Effect of Ca(OH)₂ in the products of reaction.

Phair: Characterization of FA based GP binders activated with Na-Al

Van Jaarsveld: The effect of composition and temperature on the properties of FA- & kaolinite-based GP.

Lee: The effect of ionic contaminants on the early-age properties of alkali-activated FA-based cements.

Xu: Factors affecting the geopolymerization of alkali-feldspars.

Swanepoel: Utilisation of FA in a geopolymeric material.

Phair: Effect of the Si activator pH on the microstructural characteristics of waste-based GP.

Lee: Effects of anions on the formation of Al-Si gel in GP.

Xu: Geopolymerisation of multiple minerals.

Lee: The effects of inorganic salt contamination on the strength and

Xu: Microstructural characterisation of GP synthesised from kaolinite/stilbite

Lee: Structural reorganisation of class F FA in alkaline Si solutions.

2003

Buchwald: Alkali-activated binders and pozzolan cement binders - Compete binder reaction or 2 sides of the same story?

Palomo: Alkali-activated cementitious materials: Alternative matrices for the immobilisation of hazardous wastes - Part I. Stabilisation of boron.

Van Jaarsveld: The characterisation of source materials in FA-based GP.

Rowles: Chemical optimisation of the compressive strength of Al-Si GP synthesised by Na Si activation of MK.

Xu: The effect of alkali metals on the formation of GP gels from alkali-feldspars.

Cioffi: Optimization of GP synthesis by calcination & polycondensation of a kaolinitic residue.

Bao: Binders for radioactive waste forms made from pretreated calcined Na bearing waste.

Palomo: Alkali-activated cementitious materials: Alternative matrices for the immobilisation of hazardous wastes - Part II. Stabilisation of Cr & Pb.

Phair: Characteristics of Al-Si hydrogels related to commercial "Geopolymers".

Comrie: Composite cold ceramic GP in a refractory application.

Xu: Effect of source materials on geopolymerization.

Lecomte: Synthesis and characterization of new inorganic polymeric composites based on kaolin or white clay and on GGBFS.

Fernández-Jiménez: Characterisation of fly ashes.

Rahier: Low-temperature synthesized aluminosilicate glasses. Part IV. Modulated DSC study on the effect of particle size of MK on the production of

Phair: Investigation of the microstructure of alkali-activated cements by neutron scattering.

Donaldson: Evaluation of the reaction kinetics parameters for a Na-PSDS GP using DCS.

Yip: Effect of blast furnace slag addition on microstructure and properties of MK geopolymeric materials.

Barbosa: Synthesis and thermal behaviour of Na-sialate geopolymers.

Silva: Fibre reinforcement and fracture response in geopolymeric mortars.

Rahier: Low-temperature synthesized aluminosilicate glasses. Part IV. Modulated DSC study on the effect of particle size of MK on the production of

Lee: The use of infrared spectroscopy to study GP of heterogeneous amorphous Al-Si.

Gourley: Geopolymers; Opportunities for environmentally friendly construction materials.

Yip: Microanalysis of CSH gel formed within a GP binder.

Barbosa: Thermal behaviour of inorganic geopolymers and composites derived from Na polysialate.

Cheng: Fire-resistant geopolymer produced by GGBFS.

Chervonnyi: Geopolymeric agent for immobilization of radioactive ashes after biomass burning.

Kriven: Microstructure and microchemistry of fully-reacted GP & geopolymer matrix composites.

Yip: Microstructure and properties of slag/MK GP materials.

2004

Palacios: Alkali-activated FA matrices for Pb immobilisation: A comparison of different leaching tests.

Li: Development of sustainable cementitious materials.

Van Jaarsveld: A comparative study of kaolinite versus MK in FA based GP containing immobilized metals.

Kriven: Effect of alkali choice on GP properties

Hardjito: Brief review of development of GP concrete.

Bankowski: Reduction of metal leaching in brown coal FA using GP.

Palomo: Alkaline activation of FA: NMR study of the reaction products.

Wei: In situ monitoring of the hydration process of K-PS GP cement with ESEM.

Xu: Ab initio study of dissolution reactions of 5-membered Al-Si framework rings.

Kriven: GP refractories for the glass manufacturing industry.

Hardjito: FA-based GP concrete, construction material for sustainable development.

Bankowski: Using inorganic polymer to reduce leach rates of metals from brown coal FA.

Fernández-Jiménez: Microstructural characterisation of alkali-activated PFA matrices for waste immobilisation.

Zhang: Novel modification method for inorganic GP by using water soluble organic polymers.

Phair: Effect of Al source and alkali activation on Pb and Cu immobilization in FA based "GP".

Kriven: GP: Nanoparticulate, nanoporous ceramics made under ambient conditions.

Hardjito: On the development of FA-based GP concrete.

Kirschner: Investigation of GP binders with respect to their application for building materials.

Perera: Geopolymers made using New Zealand FA.

Keyte: The effect of coal ash composition on the properties of waste-based GP.

Bell: Nanoporosity in Al-Si, GP cements.

Hussain: Investigation of thermal and fire performance of novel hybrid GP composites

Kirschner: Investigation of GP binders with respect to their application for building materials.

Grutzeck: Zeolite formation in alkali-activated cementitious systems.

Singh: Outstanding problems posed by nonpolymeric particulates in the synthesis of a well-structured GP material.

Lee: The interface between natural siliceous aggregates and GP.

Goretta: Solid-particle erosion of a GP containing FA and GGBFS.

Feng: Ultrasound enhanced geopolymerisation.

2005

Wagh: Chemically bonded phosphate ceramics - A novel class of GP.

Stevenson: Relationships between composition, structure and strength of inorganic polymers. Part 1 - MK-derived inorganic polymers.

Yip: The coexistence of GP gel and calcium Si-hydrate at the early stage of alkaline activation.

Criado: Alkali activation of FA. Part 1: Effect of curing conditions on the carbonation of the reaction products.

Gordon: Comparison of naturally and synthetically derived, K-based GP.

Bakharev: Durability of GP materials in Na and Mg-sulfate solutions.

Wagh: Reduction in wear of MK-based GP composite through filling of PTFE.

Stevenson: Relationships between composition, structure, and strength of inorganic polymers. Part 2. FA-derived inorganic polymers.

Duxson: The effect of alkali cations on Al incorporation in GP gels.

Fernández-Jiménez: Composition and microstructure of alkali activated fly ash binder: Effect of the activator.

Duxson: Understanding the relationship between GP composition, microstructure and mechanical

Bakharev: GP materials prepared using Class F FA & elevated temperature curing.

Wagh: Synthesis and mechanical properties of MK-based GP.

Wagh: Synthesis and tribological behavior of MK-based GP composites.

Keyte: The effect of coal ash glass chemistry on the tailored design of waste-based GP products.

Fernández-Jiménez: Fixing arsenic in alkali-activated cementitious matrices.

Bell: Use of GP cements as a refractory adhesive for metal and ceramic joins.

Bakharev: Resistance of GP materials to acid attack.

Vance: Solid state chemistry phenomena in GP with Si/Al-2.

Feng: Preparation of GP materials from fly ash filler by steam curing with special reference to binder products.

Weng: Effects of Al on the formation of GP.

Zang: Hydration process of interfacial transition in K polysialate (K-PSDS) GP concrete.

Zang: Hydration process of K polysialate (K-PSDS) cement.

Bao: Preparation and properties of hydroceramic waste forms made with simulated Hanford low-activity waste.

Perera: Immobilization of Pb in a GP matrix.

Škvára: GP materials based on FA

Oudadesse: Infrared and NMR structural studies vs. thermal treatment of GP/biphasic Ca-phosphates.

Duxson: Microstructural characterisation of MK-based GP.

Lloyd: The microstructure of GP synthesised from industrial wastes.

Provis: Modeling chemical ordering in Al-Si and subsequent prediction of cation immobilisation efficiency.

Duxson: The characterization of nanostructure and structural ordering in Al-Si GP gels.

Duxson: 29Si NMR study of structural ordering in Al-Si GP gels.

Provis: A conceptual model for solid-gel transformations in partially reacted GP systems.

Provis: A statistical thermodynamic model for Si/Al ordering in amorphous Al-Si.

Provis: Do GP actually contain nanocrystalline zeolites? - A reexamination of existing results.

Provis: The role of mathematical modelling and gel chemistry in advancing GP technology.

Provis: Modeling speciation in highly concentrated alkaline silicate solutions.

Fernández-Jiménez: Immobilization of Cs in alkaline activated FA matrix.

Fernández-Jiménez: Microstructure development of alkali-activated FA cement: A descriptive model.

Fernández-Jiménez: Mid-infrared spectroscopic studies of alkali-activated FA structure.

Palomo: Properties of alkali-activated FA determined from rheological measurements.

Dias: Fracture toughness of GP concretes reinforced with basalt fibers.

Hussain: Synthesis and thermal behavior of inorganic-organic hybrid GP composites.

Fletcher: The composition range of Al-Si GP.

Schmücker: Microstructure of Na polysialate siloxo GP.

Allahverdi: Sulfuric acid attack on hardened paste of GP cements. Part 1. Mechanism of corrosion at relatively high concentrations.

Singh: Structural studies of geopolymers by 29Si and 27Al MAS-NMR.

Singh: Geopolymer formation processes at room temperature studied by 29Si and 27Al MAS-NMR.

2006

Lecomte: (Micro)-structural comparison between geopolymers, alkali-activated slag cement and Portland cement.

Xu: Study on the factors of affecting the immobilization of heavy metals in FA-based GP.

Duxson: The effect of alkali and Si/Al ratio on the development of mechanical properties of MK-based GP.

Fernández-Jiménez: The role played by the active Al content in the alkaline activation of FA.

Provis: Silica nanoparticle formation in the system TPAOH-TEOS-H₂O: A population balance model.

Provis: Modeling Si/Al ordering in MK-based GP.

Van Deventer: Reaction mechanisms in the geopolymeric conversion of inorganic waste to useful products.

APPENDIX B

CHARACTERISATION OF RAW MATERIALS

B.1 XRF for Fly ash A

Na ₂ O	0.36
MgO	1.33
Al ₂ O ₃	26.79
SiO ₂	45.83
P ₂ O ₅	1.57
SO ₃	0.12
K ₂ O	0.84
CaO	4.16
TiO ₂	1.21
MnO	0.17
Fe ₂ O ₃	11.62
LOI	6
SUM	100

Figures presented in mass%.

B.2 XRF for Fly ash B

Na ₂ O	3.23
MgO	2.11
Al ₂ O ₃	30.1
SiO ₂	48.16
P ₂ O ₅	1.04
SO ₃	0.09
K ₂ O	1.55
CaO	4.74
TiO ₂	1.59
MnO	0.05
Fe ₂ O ₃	3.82
LOI	3.52
SUM	100

Figures presented in mass%.

B.3 XRF for GGBS

Na ₂ O (%)	0.2590
MgO (%)	6.0480
Al ₂ O ₃ (%)	13.2000
SiO ₂ (%)	33.0320
SO ₃ (%)	3.3300
K ₂ O (%)	0.3220
CaO (%)	40.0050
TiO ₂ (%)	0.6640
V ₂ O ₅	0.0270
MnO (%)	0.4020
Fe ₂ O ₃ (%)	0.4290
CuO	0.0130
SrO	0.0665
Y ₂ O ₃	0.0100
ZrO ₂	0.0332
LOI	2.1593
SUM	100.0000

Figures presented in mass%.

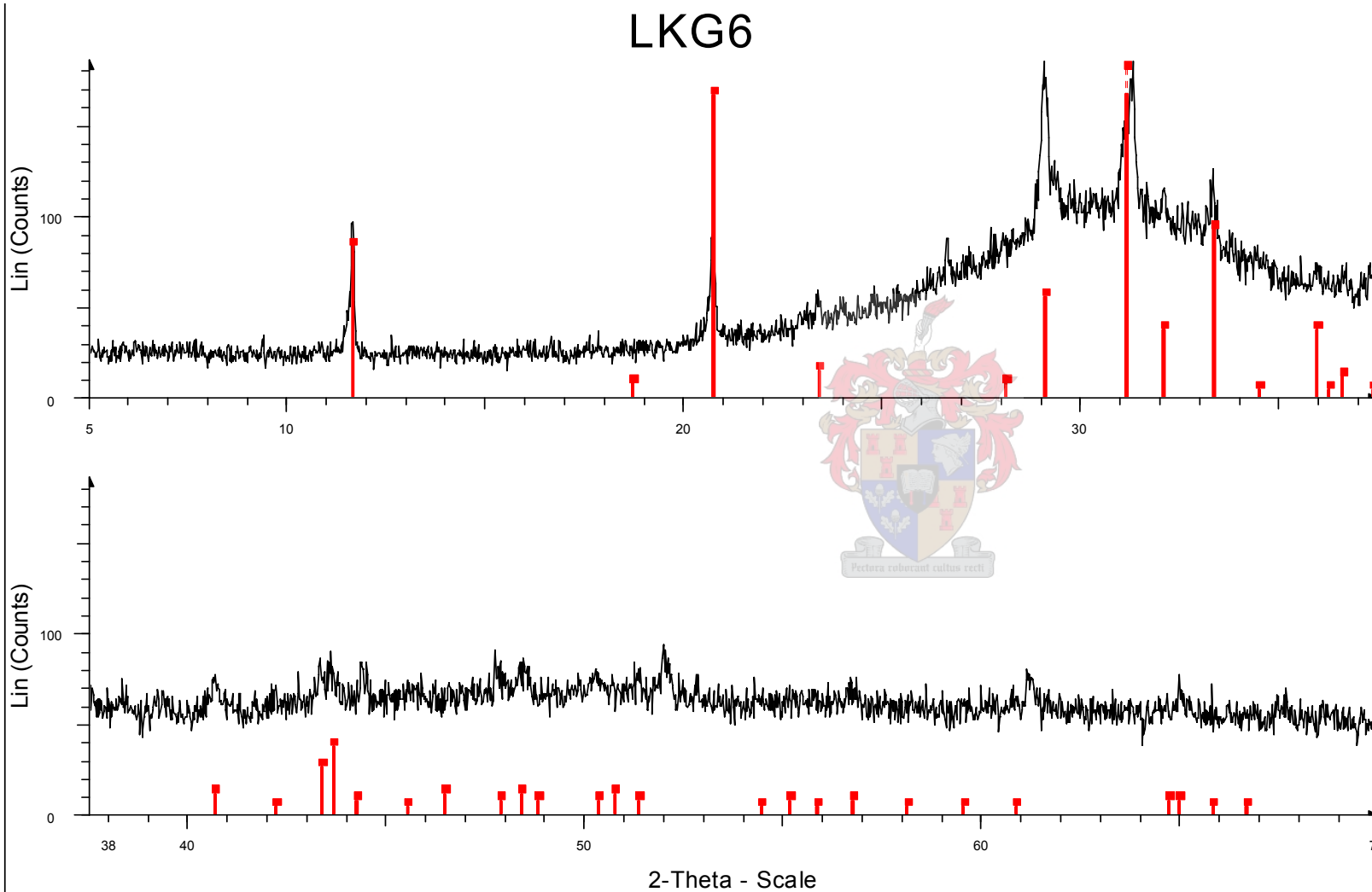
B.4 Q-XRD for Fly ash A and Fly ash B

Fly Ash	Mullite	Quartz	Maghemite	Calcite	Hematite
A	12	4	4	0.5	0
B	23	11	0	0	0

Values are given in crystalline phase concentrations of fly ash A and B (wt %), as determined by Q-XRD ($\pm 5\%$).

B.5 Q-XRD for GGBFS

LKG6



Sample appears to be mainly Gypsum and possibly amorphous material present.

- Original sample Amorphous Content = 5%
- Gypsum = 95%

LKG6 - File: LKG6.raw - Type: 2Th/Th locked - Start: 5.000 ° - End: 70.000 ° - Step: 0.020 ° - Step time: 1.2 s - Temp.: 25 °C (Room) - Time Started: 0 s - 2-Theta: 5.000 ° - Theta: 2.500 ° - Chi
Operations: Import
00-021-0816 (*) - Gypsum - CaSO4·2H2O

APPENDIX C

SAMPLE RECIPES

C.1 Nomenclature and Sample Recipes

Ash A

Effect of Activating Concentrations				
		N1	N2	N3
Ash A	g	1000	1000	1000
Water	g	234.53	234.53	169.31
NaOH	g	23.99	46.49	17.99
KOH	g	50.5	82.06	58.92
NaSilicate	g	104.53	104.53	209.06

Ash B

Effect of Activating Concentrations				
		N13	N14	N15
Ash B	g	1000	1000	1000
Water	g	234.53	234.53	169.31
NaOH	g	23.99	46.49	17.99
KOH	g	50.5	82.06	58.92
NaSilicate	g	104.53	104.53	209.06

Effect of Water Content				
		N4	N5	N6
Ash A	g	1000	1000	1000
Water	g	234.53	214.53	194.53
NaOH	g	23.99	23.99	23.99
KOH	g	50.5	50.5	50.5
NaSilicate	g	104.53	104.53	104.53

Effect of Water Content				
		N16	N17	N18
Ash B	g	1000	1000	1000
Water	g	234.53	214.53	194.53
NaOH	g	23.99	23.99	23.99
KOH	g	50.5	50.5	50.5
NaSilicate	g	104.53	104.53	104.53

Effect of Slag addition and Content				
		N7	N8	N9
Ash A	g	850	900	950
Slag	g	150	100	50
Water	g	234.53	234.53	234.53
NaOH	g	23.99	23.99	23.99
KOH	g	50.5	50.5	50.5
NaSilicate	g	104.53	104.53	104.53

Effect of Slag addition and Content				
		N19	N20	N21
Ash B	g	850	900	950
Slag	g	150	100	50
Water	g	234.53	234.53	234.53
NaOH	g	23.99	23.99	23.99
KOH	g	50.5	50.5	50.5
NaSilicate	g	104.53	104.53	104.53

Effect of Sand addition as Aggregate				
		N10	N11	N12
Ash A	g	1000	1000	1000
Sand	g	2100	3150	4200
Water	g	234.53	234.53	234.53
NaOH	g	23.99	23.99	23.99
KOH	g	50.5	50.5	50.5
NaSilicate	g	104.53	104.53	104.53

Effect of Sand addition as Aggregate				
		N22	N23	N24
Ash B	g	1000	1000	1000
Sand	g	2100	3150	4200
Water	g	234.53	234.53	234.53
NaOH	g	23.99	23.99	23.99
KOH	g	50.5	50.5	50.5
NaSilicate	g	104.53	104.53	104.53

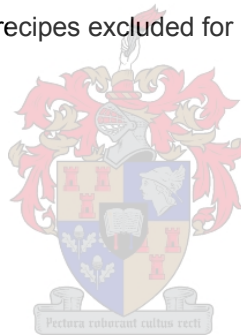
C.2 Nomenclature and recipe for sample used in PIXE (Melbourne) analysis:

Commercial Geopolymer Recipe - N25	
Ingredient	Amount [grams]
Fly Ash A	850
Ground Slag	150
Sand (Optional)	2100
Water	234.53
Sodium Hydroxide	23.99
Potassium Hydroxide	50.5
Sodium Silicate solution	104.53

C.3 Nomenclature for samples used for PIXE (South Africa) analysis:

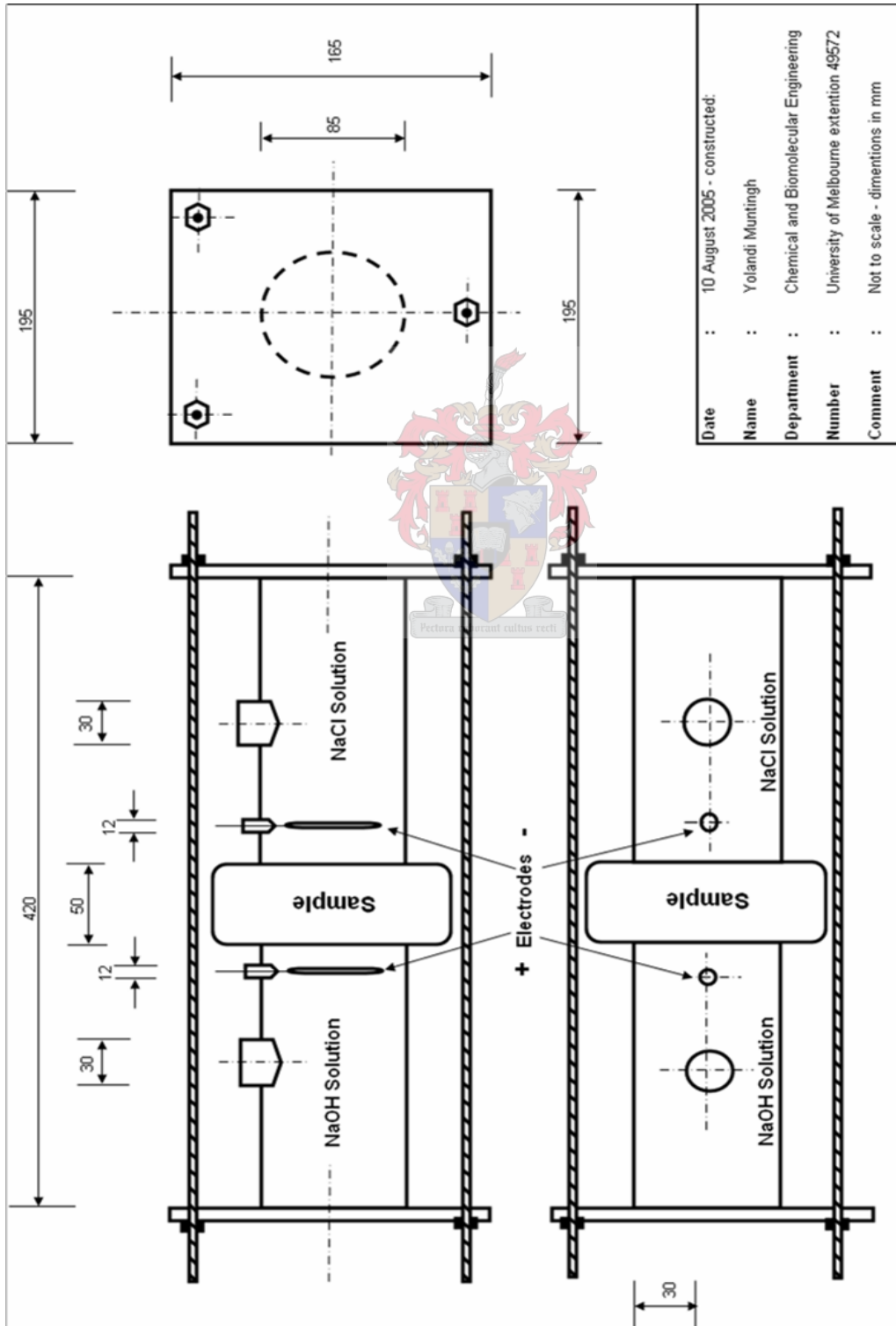
Referring back to Appendix B1, the recipes excluded for PIXE analyses is given as:

- N1
- N7
- N13
- N18
- N22



APPENDIX D

DIFFUSION CELL DESIGN



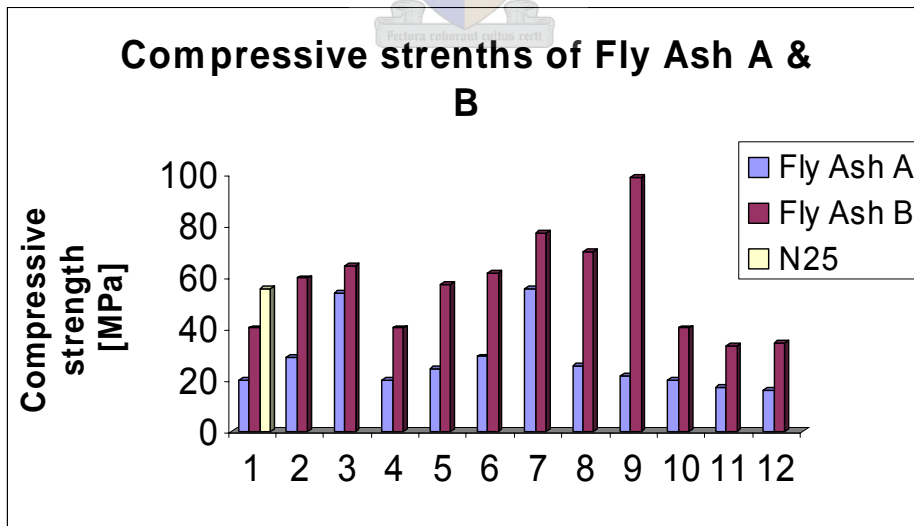
APPENDIX E

COMPRESSIVE STRENGTH RESULTS

E.1 Tabular Compressive strengths data

Compressive Strengths			
Recipe	MPa	Recipe	MPa
N1	19.8	N13	40.3
N2	29	N14	59.7
N3	53.9	N15	64.5
N4	19.8	N16	40.3
N5	24.5	N17	57
N6	29.2	N18	61.9
N7	55.7	N19	77
N8	25.7	N20	69.8
N9	21.6	N21	98.7
N10	19.8	N22	40.3
N11	17.5	N23	33.6
N12	16	N24	34.7
		N25	55.7

E.2 Compressive Strength Bar Graph:

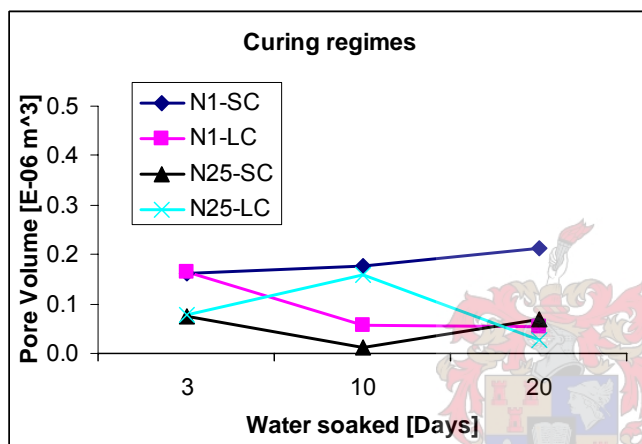


A relative comparison between the two types of fly ashes is given here. Fly ash A is represented by the light-coloured bars, while those of fly ash B are the darker bars. Those corresponding recipes are grouped together, so if the recipe for fly ash B is required, it can be traced by use of **Appendix C1**.

APPENDIX F

AUXILIARY TABLES & FIGURES

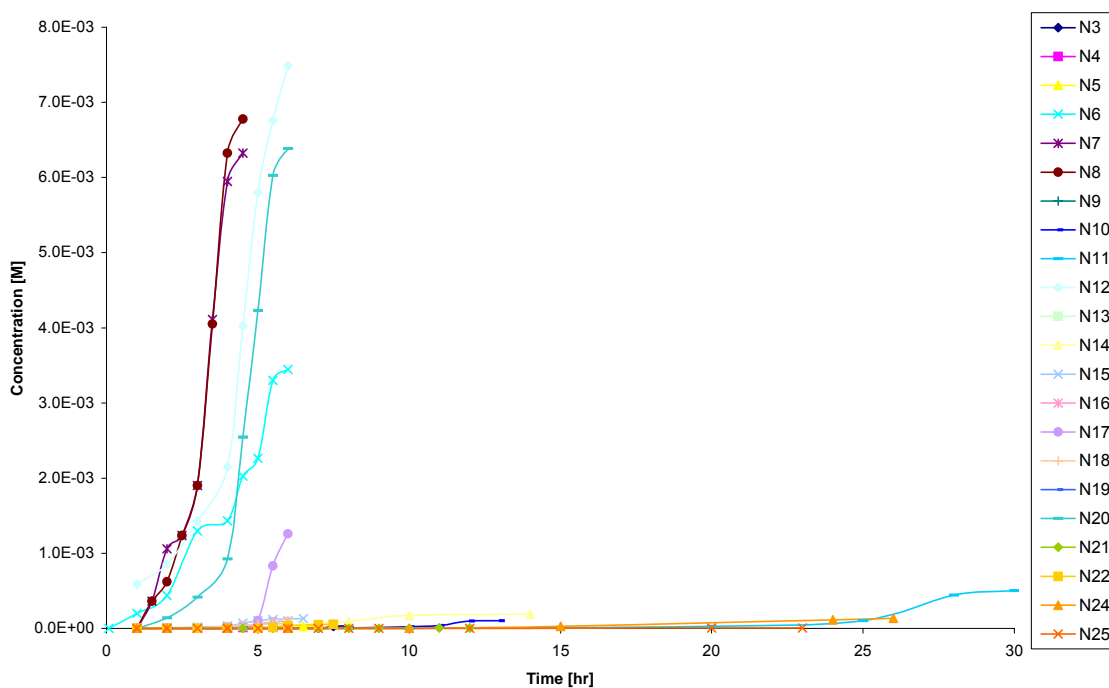
F.1: Pore volume variation for the extended soaked samples.



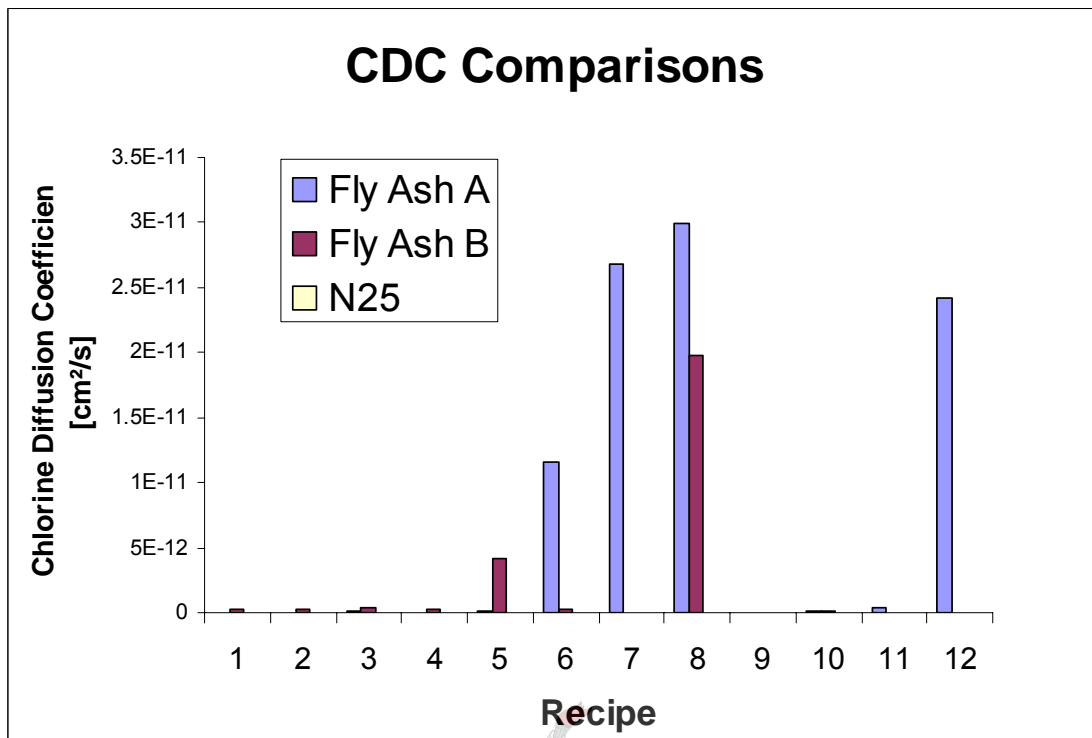
Some variation in the pore volume is measured for the extended soaked samples. These variations can be considered negligible due to the small scale of deviation.

F.2: Chloride Profiles as found during Diffusion Cell Testing

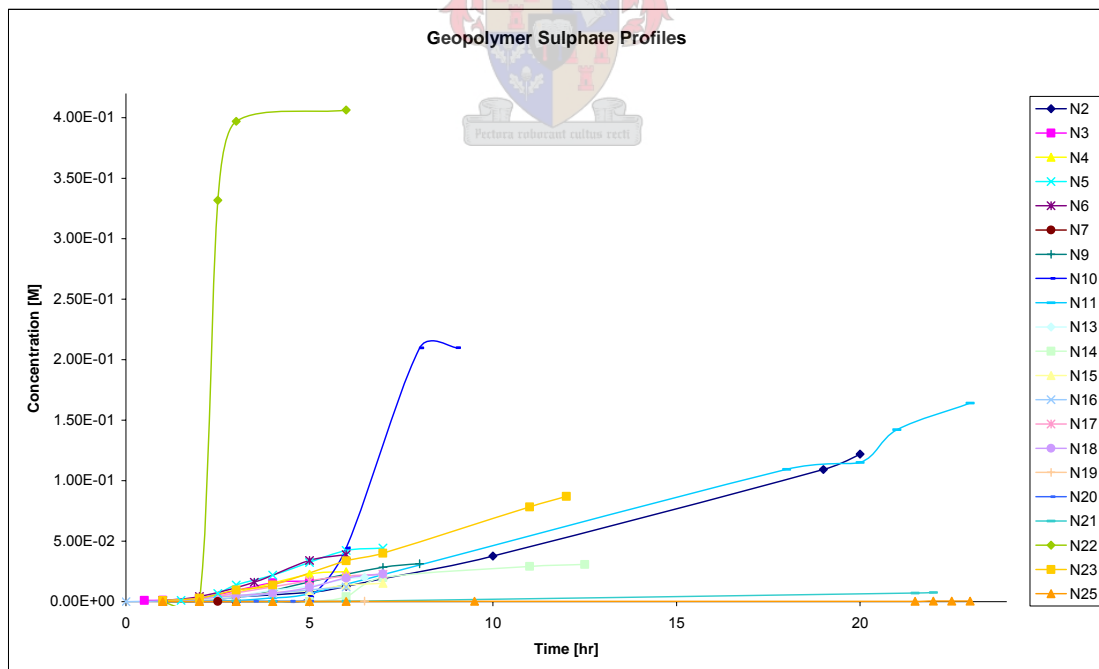
Geopolymer Chloride Profile



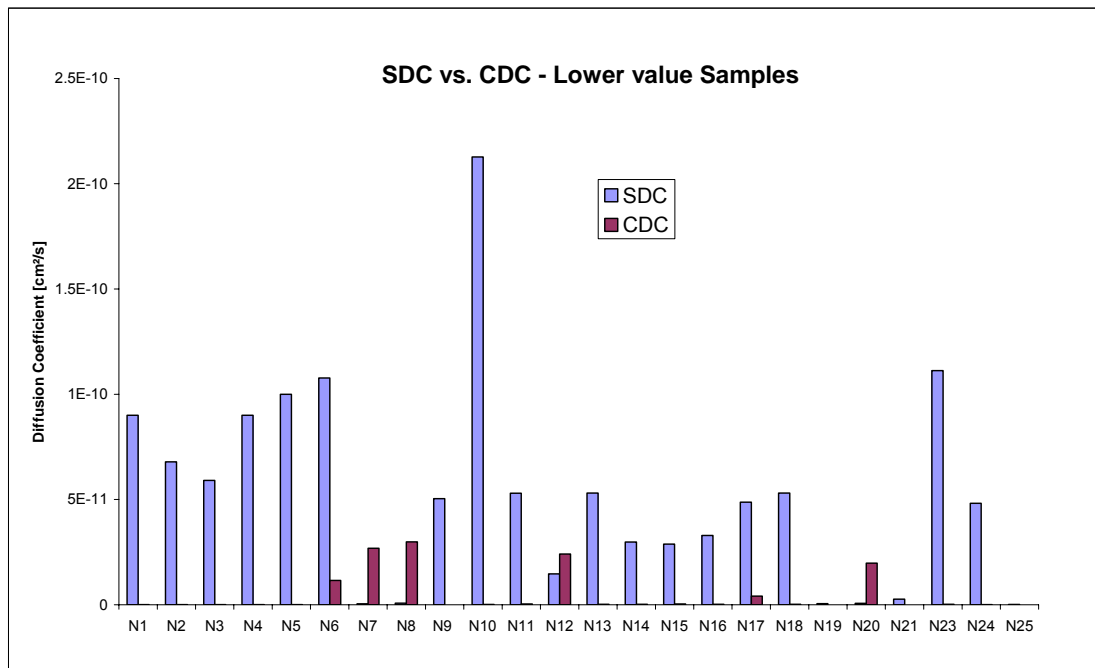
F.3: CDC Comparison between the two ashes:



F.4: Sulphate Profiles as found during Diffusion Cell Testing:



F.5: Lower value SDC vs. CDC for all of the formulations:

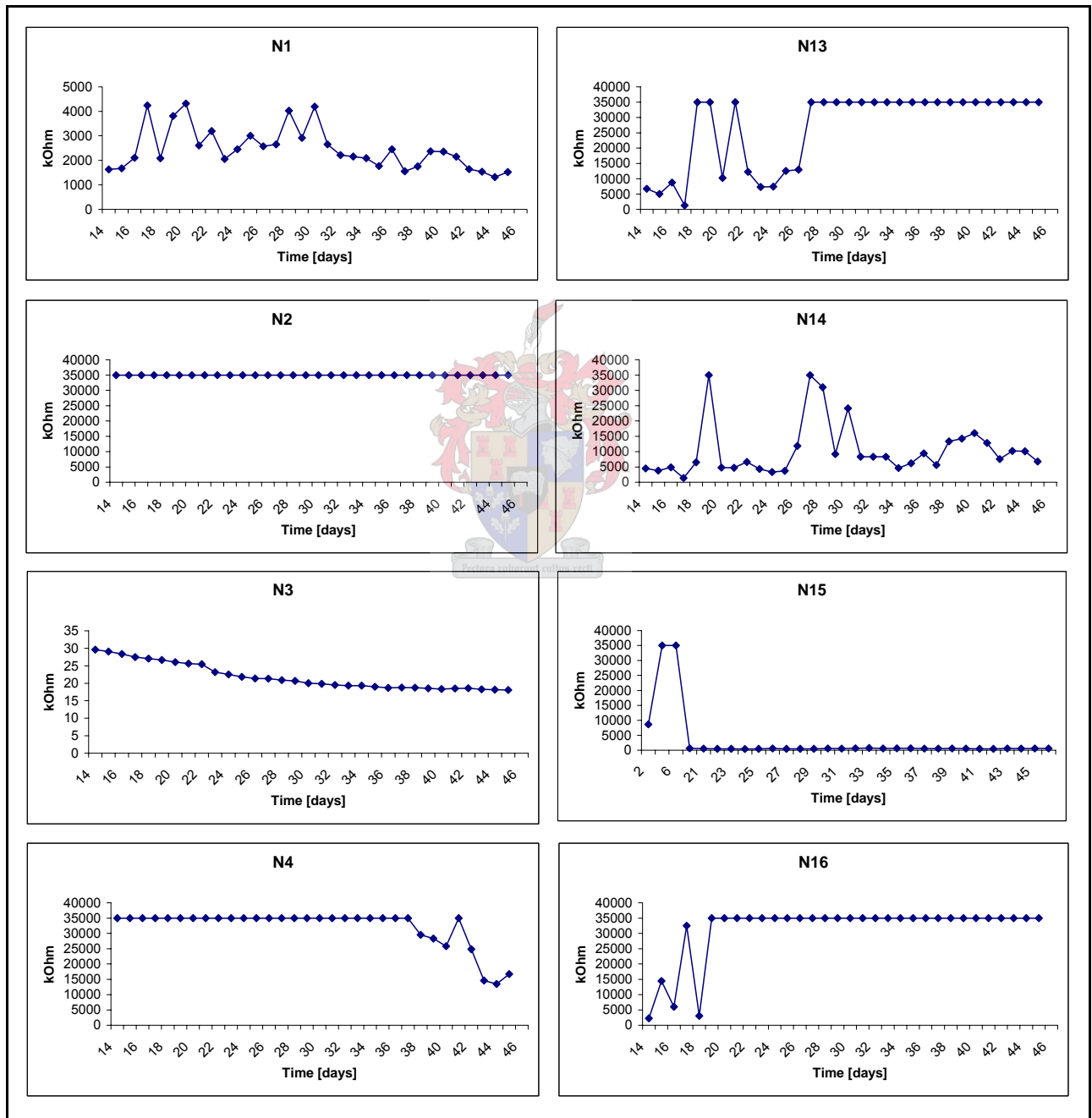


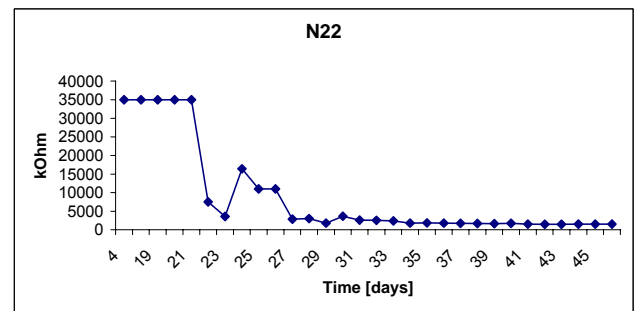
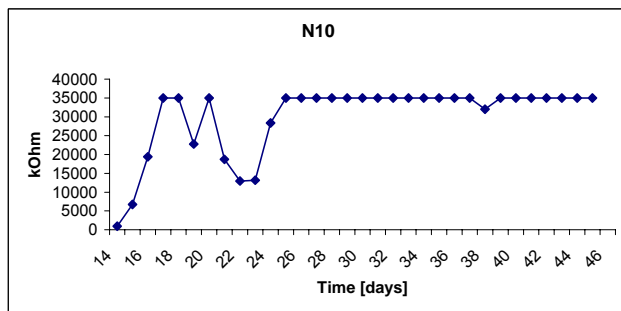
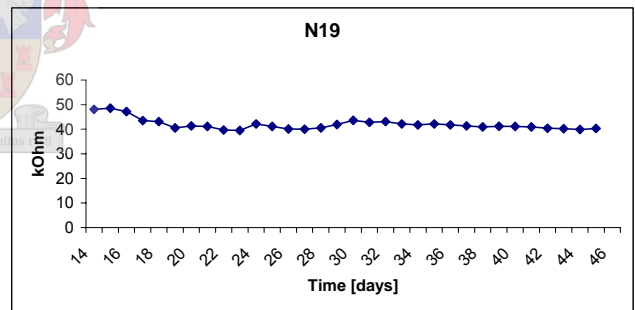
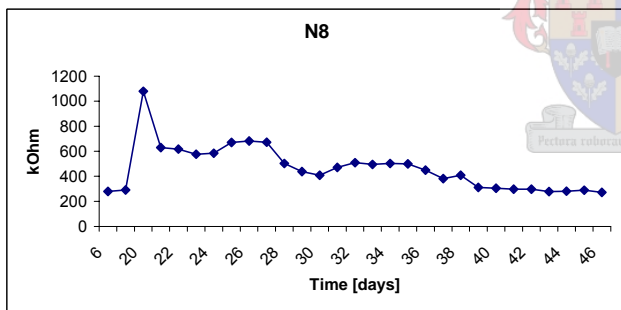
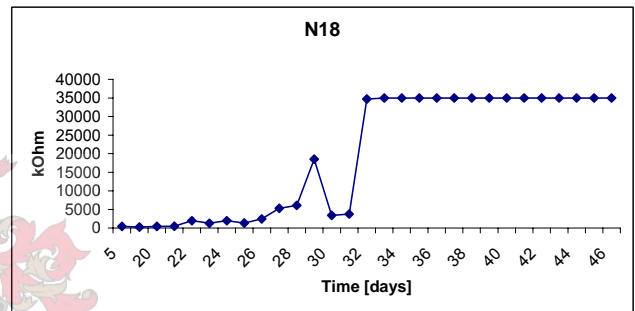
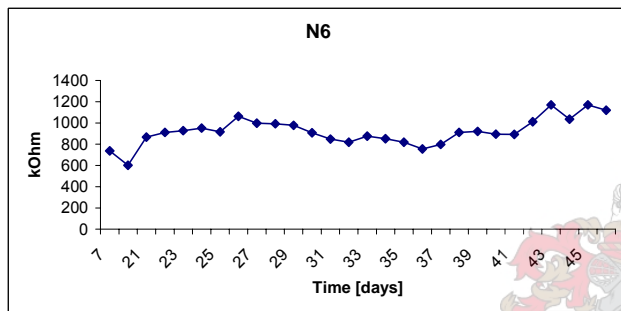
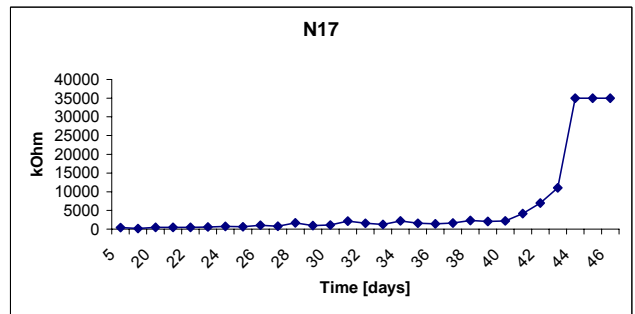
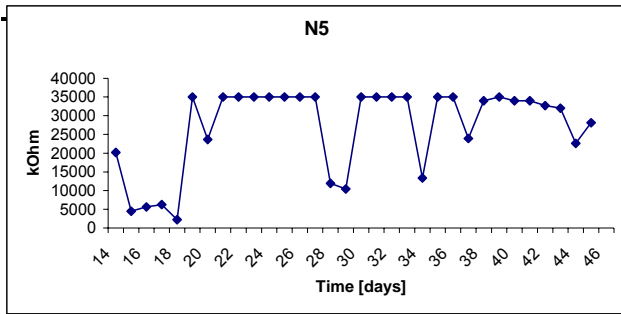
F.5: Parameter summary for each formulation:

Formulation Parameter Summary						
Sample	Pore Volume [E-06 m³/g]	BET [m²/g]	Compressive Strength [MPa]	Average Voltage [V]	CDC [cm²/s]	SDC [cm²/s]
N1	0.1210	16.41	19.8	-0.697	5.25E-14	9.00E-11
N2	0.1215	6.34	29.0	-0.517	4.85E-14	6.80E-11
N3	0.1018	53.55	53.9	-0.660	7.33E-14	5.90E-11
N4	0.1095	23.82	19.8	-0.597	5.25E-14	9.00E-11
N5	0.1159	23.12	24.5	-0.650	7.59E-14	1.00E-10
N6	0.1209	23.17	29.2	-0.604	1.16E-11	1.08E-10
N7	0.1226	55.64	55.7	-0.676	2.68E-11	4.65E-13
N8	0.1331	34.46	25.7	-0.669	2.99E-11	7.46E-13
N9	0.1365	27.42	21.6	-0.611	9.93E-15	5.04E-11
N10	0.0506	5.93	19.8	-0.528	1.51E-13	2.13E-10
N11	0.0252	5.07	17.5	-0.623	3.33E-13	5.30E-11
N12	0.0230	3.31	16.0	-0.488	2.41E-11	1.47E-11
N13	0.1271	14.94	40.3	-0.506	2.96E-13	5.31E-11
N14	0.1227	4.24	59.7	-0.487	2.74E-13	2.98E-11
N15	0.1098	36.48	64.5	-0.592	3.73E-13	2.88E-11
N16	0.1395	15.72	40.3	-0.587	2.86E-13	3.29E-11
N17	0.1406	16.09	57.0	-0.470	4.14E-12	4.87E-11
N18	0.1191	17.38	61.9	-0.518	2.18E-13	5.31E-11
N19	0.1381	15.33	77.0	-0.647	9.47E-15	5.40E-13
N20	0.1735	39.75	69.8	-0.631	1.98E-11	6.64E-13
N21	0.1408	29.14	68.7	-0.632	5.57E-15	2.69E-12
N22	0.0554	5.12	40.3	-0.441	1.45E-13	6.93E-10
N23	0.0459	2.95	33.6	-0.581	2.54E-13	1.11E-10
N24	0.0300	3.03	34.7	-0.629	5.90E-14	4.82E-11
N25	0.0741	5.82	55.7	-0.613	1.43E-15	1.59E-13

APPENDIX G

SENSOR READINGS - CURING



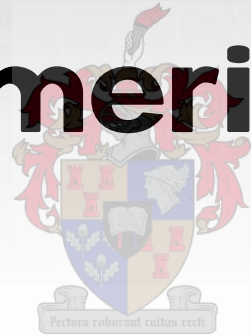






FAKULTEIT INGENIEURSWESE
FACULTY OF ENGINEERING

Durability and Diffusive Behaviour Evaluation of Geopolymeric Material



Yolandi Muntingh

Department of Process Engineering

October 2006



UNIVERSITEIT
STELLENBOSCH
UNIVERSITY

Agenda

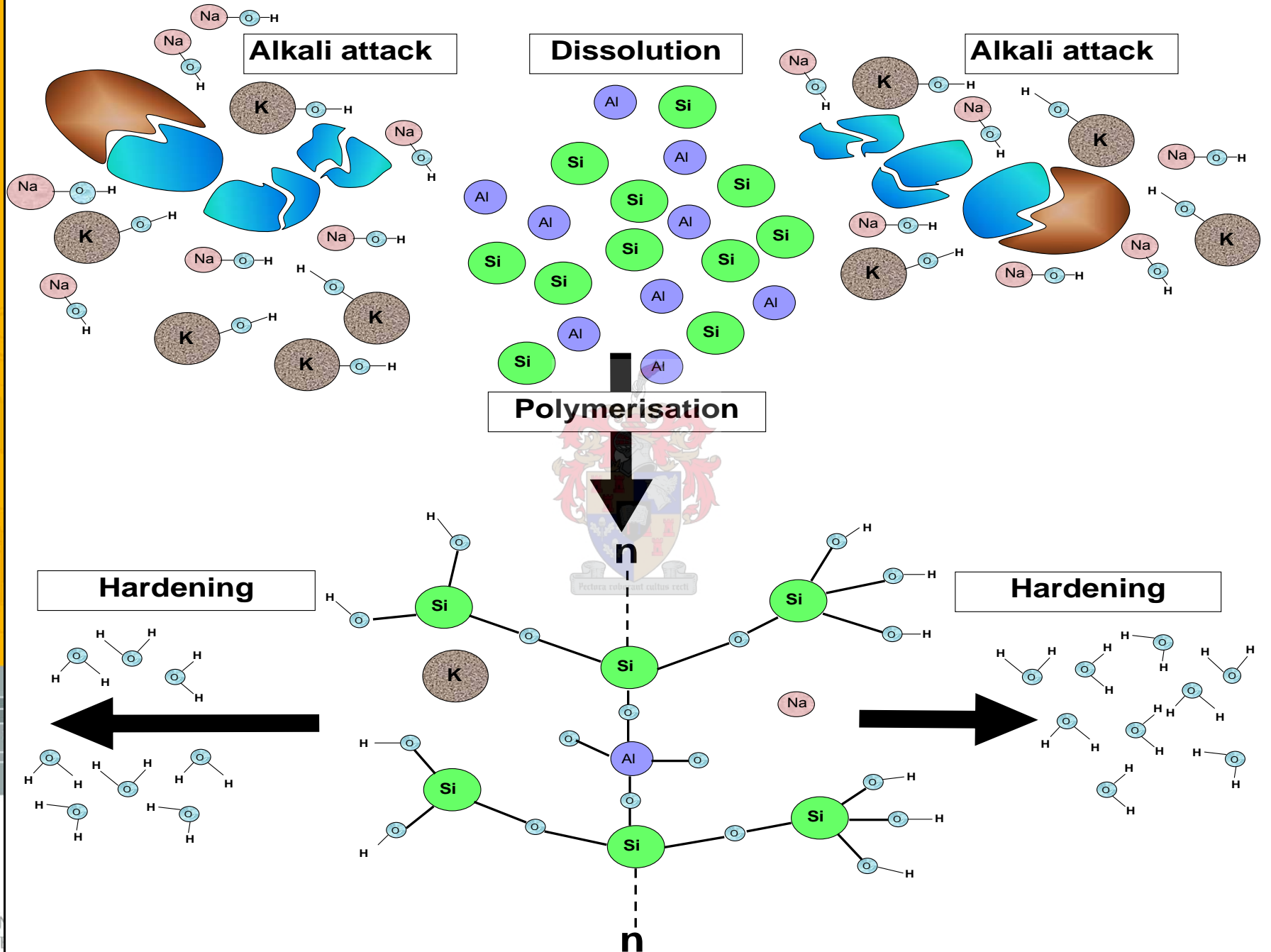
- Geopolymer?
- Durability Issues
- Cement and Concrete
- Chloride Diffusion Coefficient (CDC)
- Sulphate Diffusion Coefficient (SDC)
- Cement and Concrete CDC & SDC
- Pore Characterisation
- Conclusions
- Future Applications

Introduction

- Durability: Ancient Construction materials
- Cost Competitive alternative to OPC
- Valuable waste management
- Largely developed by Davidovits in France
- Current wider understanding: both macro & microscopically

Scope of Project

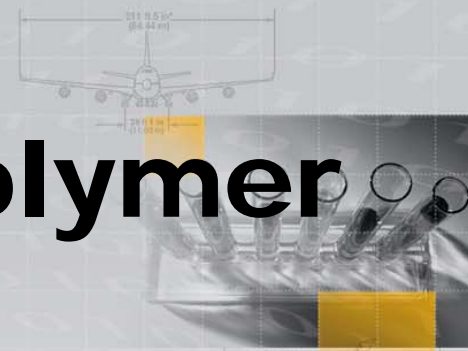
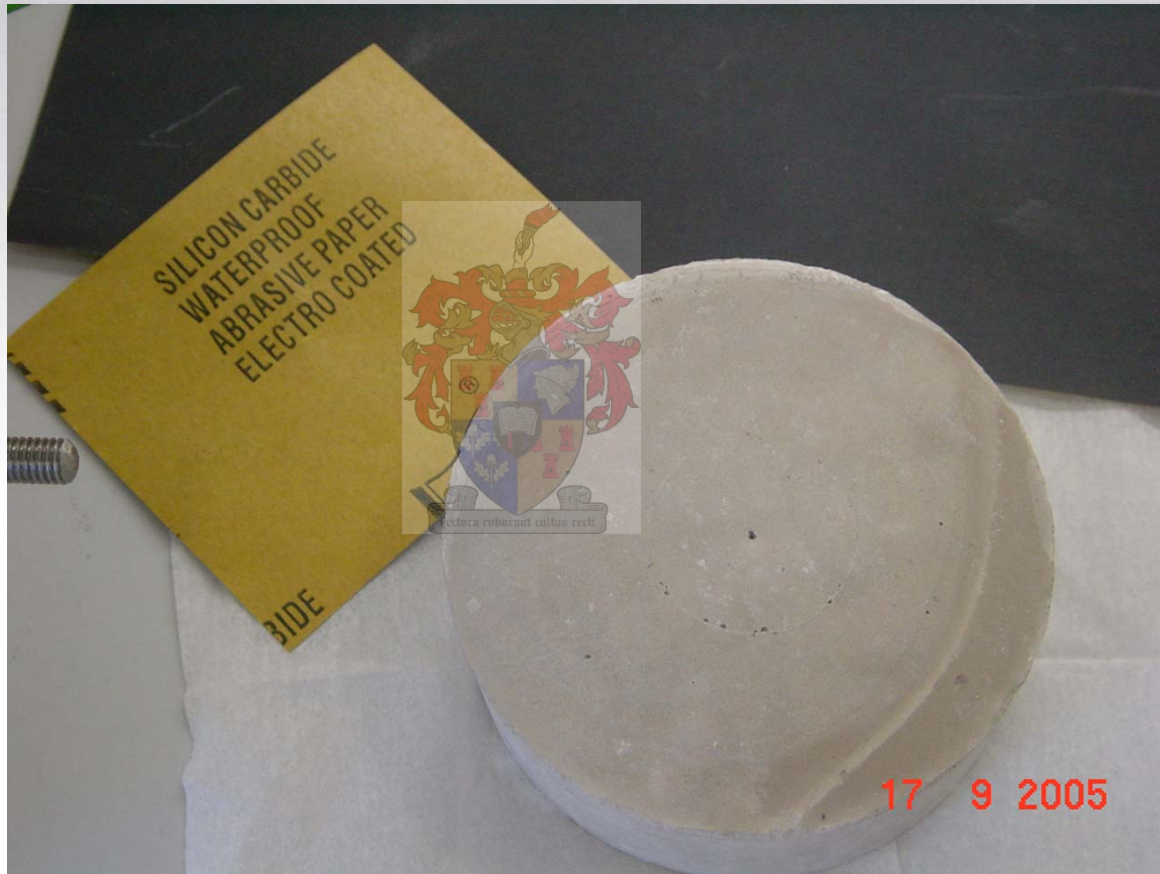
- Investigate Geopolymer durability
- Assist in commercial incorporation
- Determine diffusive behaviour
- Compare with OPC
- Selection of techniques employed:
- DC, PIXE, BET, SEM, IR, IC, ICP-OES, compressive strength, etc





FAKULTEIT INGENIEURSWESE
FACULTY OF ENGINEERING

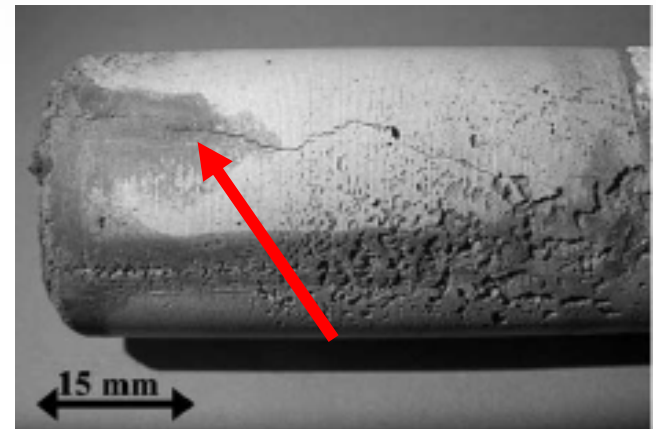
Fly ash-based Geopolymer



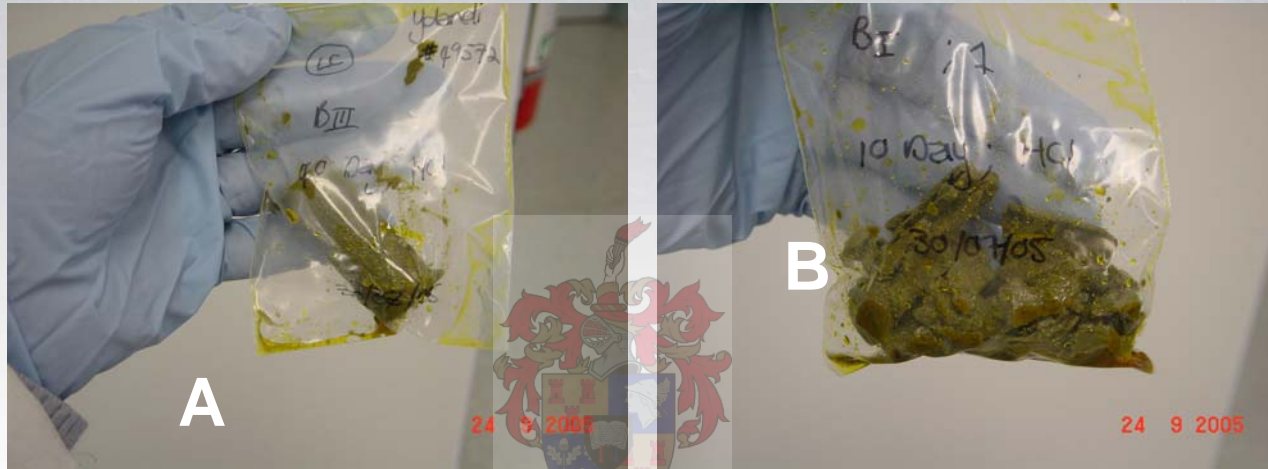
UNIVERSITEIT
STELLENBOSCH
UNIVERSITY

Durability Issues:

- Chloride Corrosion to OPC
- Costly and frequent restorations
- Compare diffusive properties



Apparent Differences



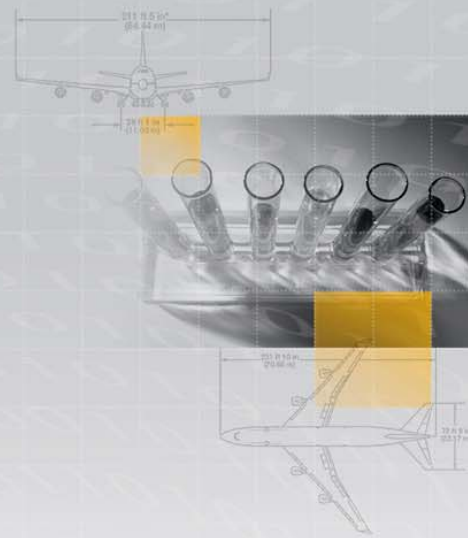
- Concentrated HCl soaking solution
- A = GP with aggregate
- B = GP (water:binder of 0.3)

Formulation

- Over a decade of research
- Compressive Strength orientated
- Decided on 25 formulations
- Covering 2 Class F fly ashes:
 - Activation concentration
 - Water
 - Slag
 - Aggregate

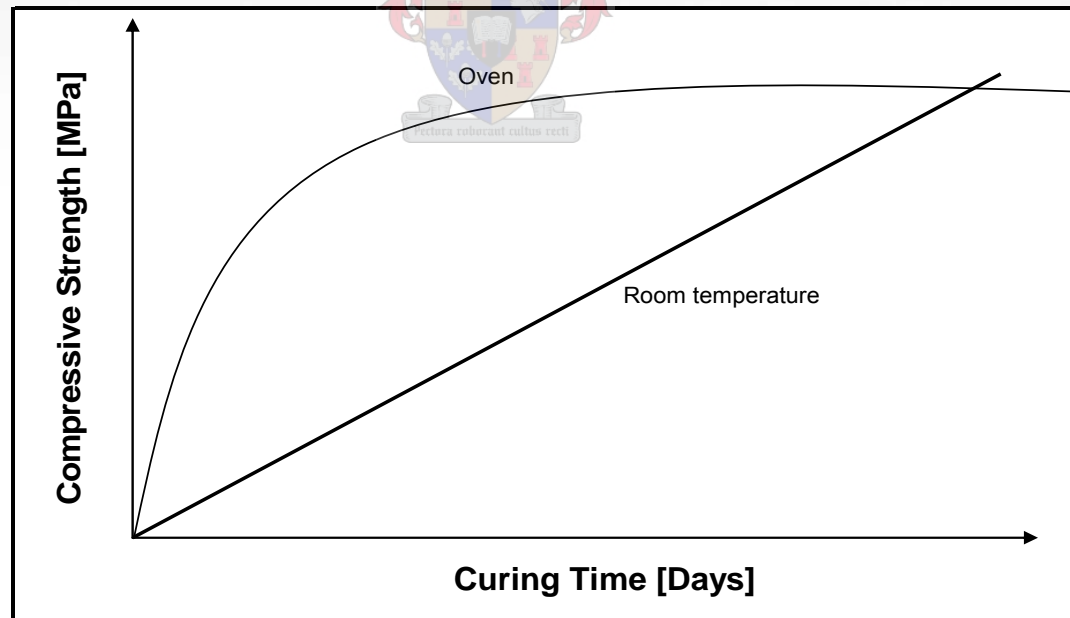
Synthesis

- Prepare activation solution
- Cool to room temperature
- Add dry raw materials
- Mechanical shaker
- PVC moulds
- Cure



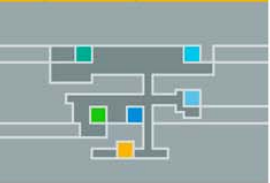
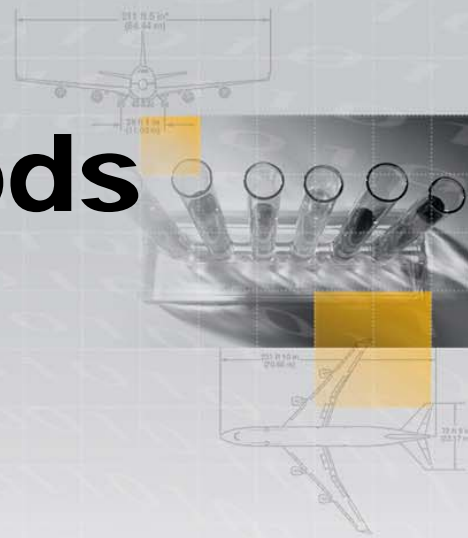
Curing

- Two curing methods
- SC (Short Cure): Oven
- LC (Long Cure): Room Temperature
- LC most probable industrial method



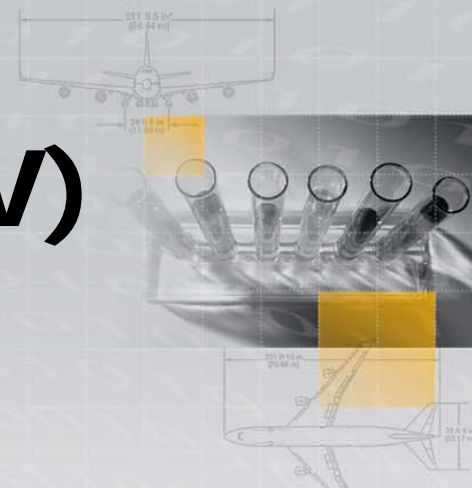
Experimental Methods

- Pore Characterisation:
 - BET
 - Pore Volume
 - Hydrostatic Potential
- Compressive Strength
- Test for corrosion (SEM)
- Diffusion Cell
- Half Cell Potential
- Time to Corrosion



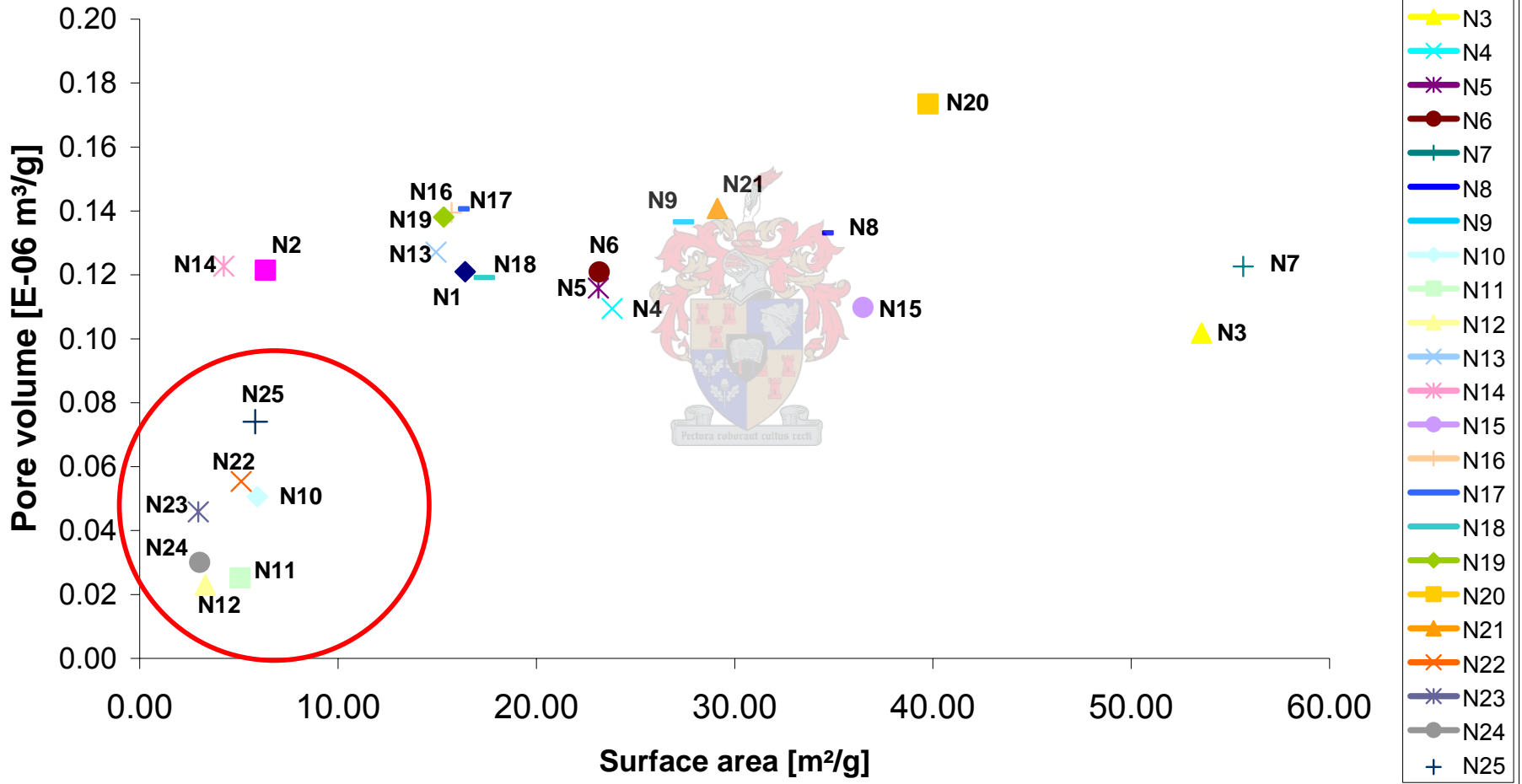
Pore Volumes (PV)

- Small samples of each formulation
- Weighed₁
- Dried @ 100°C for 48 hours
- Weighed₂
- $\Delta\text{mass} = \text{Pore Volume}$





Surface Area vs Pore volume



Pore Characterisation

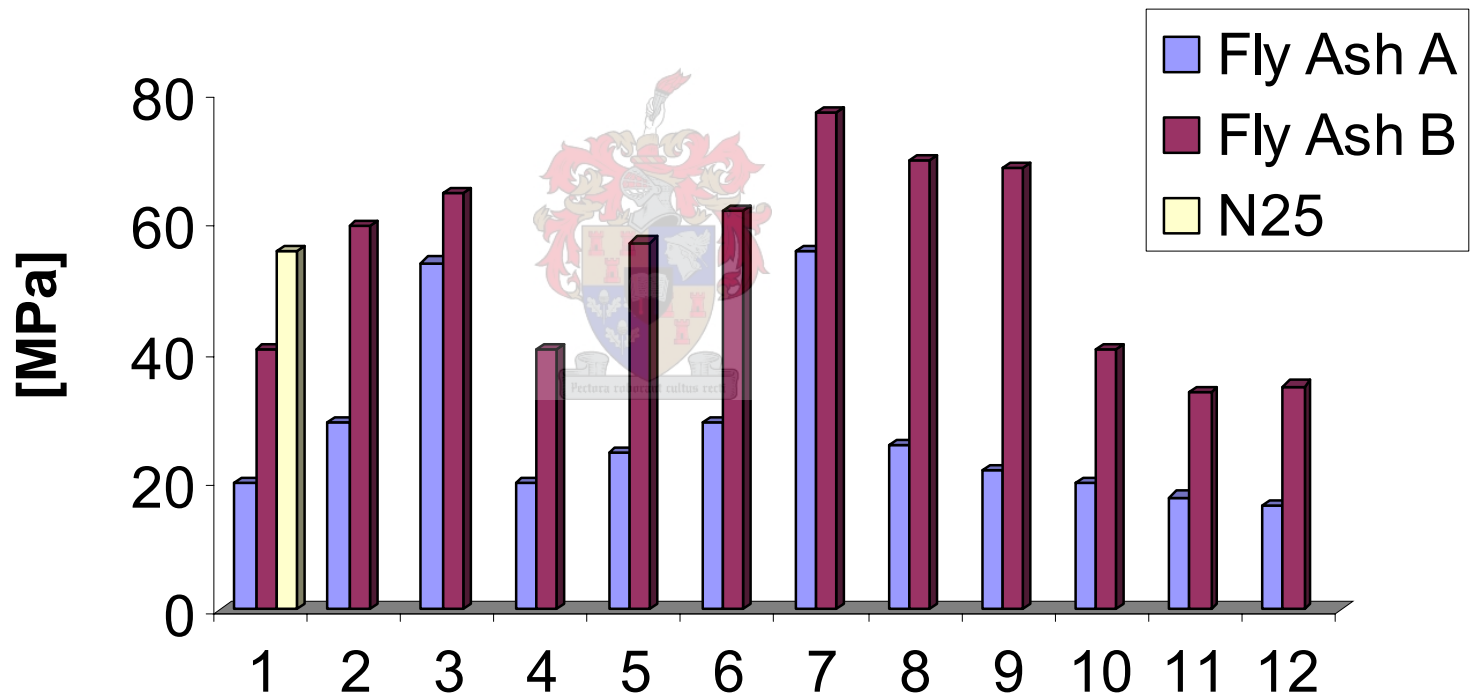
- Decrease in PV/BET for Fly ash A
- Decrease in PV/BET for Fly ash B
- As PV/BET pores must become:
 - Narrower or
 - Shorter
- Deciding which requires Compressive Strength results



Compressive Strengths



Compressive strengths of Fly Ash A & B

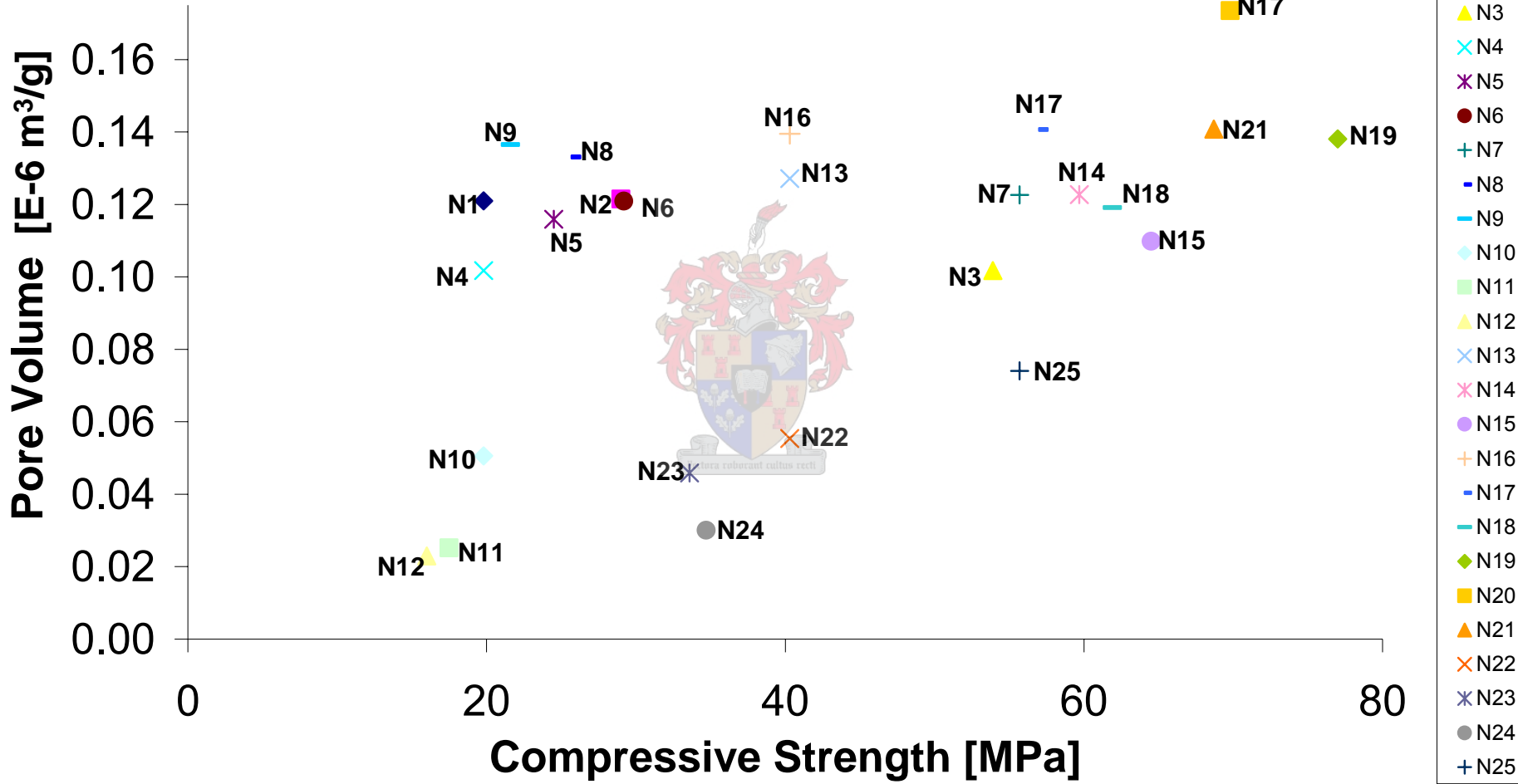


Compressive Strength

- Different water requirements by the two ashes produce the Δ CS
- Supported by PSD
- Askeland: Brittle material with micro cracks are generally stronger
- Thus: High CS samples will contain narrower pores



Compressive strength vs Pore Volume

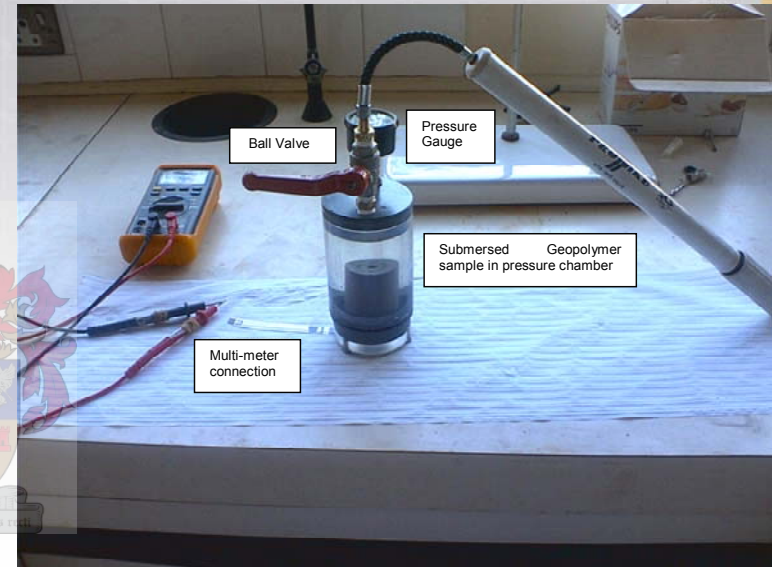




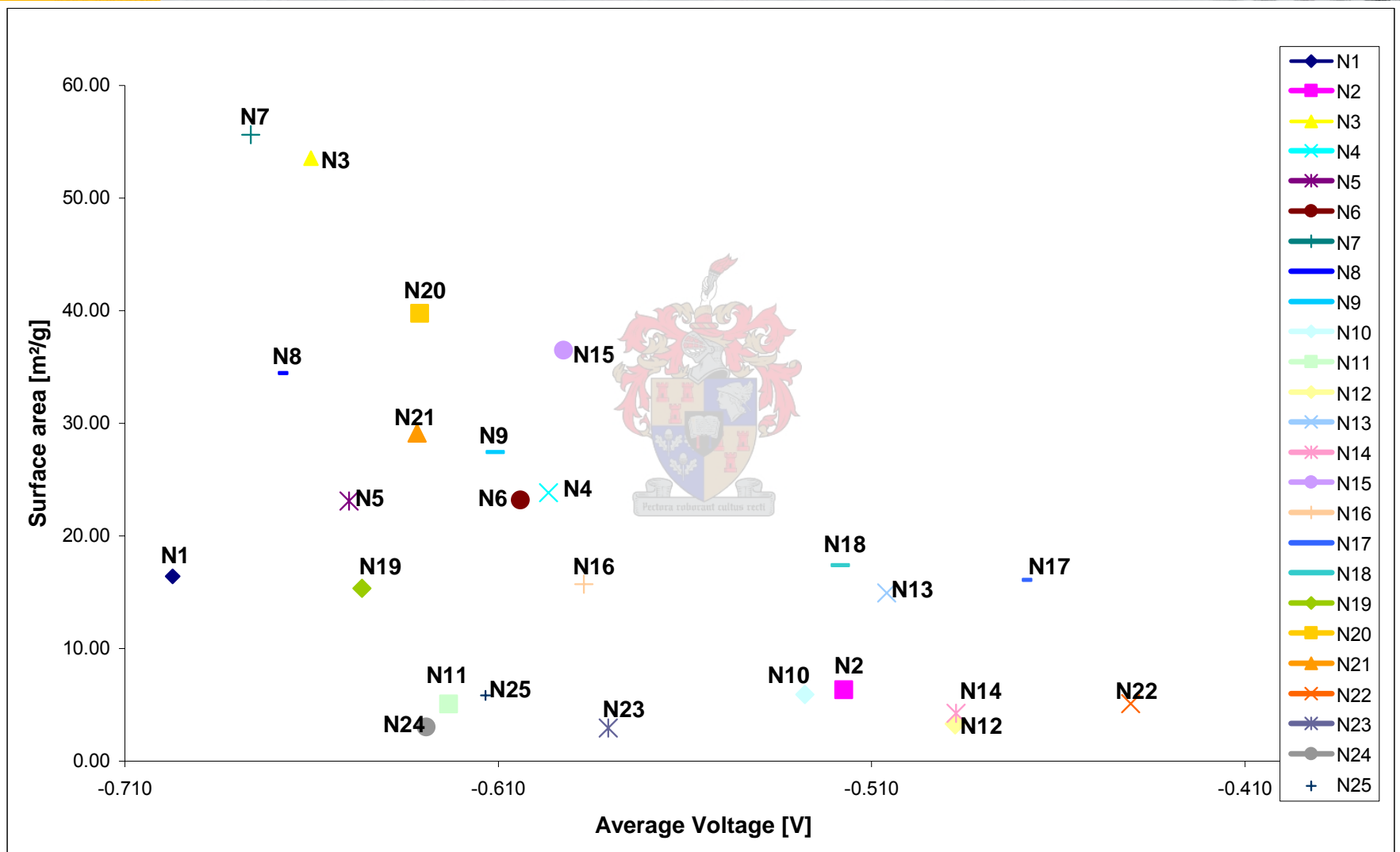
Pectora cultorum ciliis cecit

Hydrostatic Potential

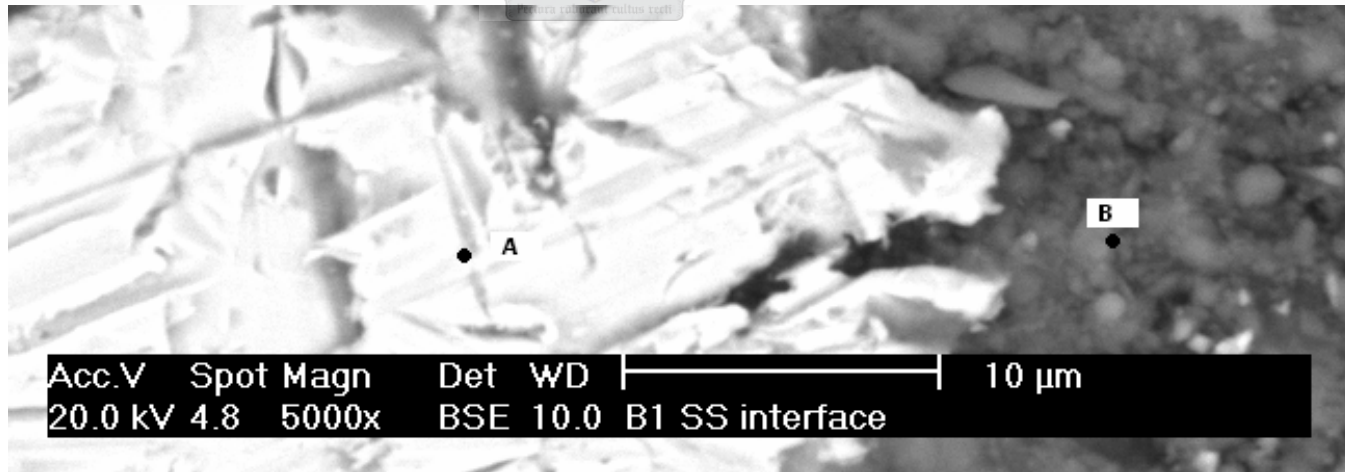
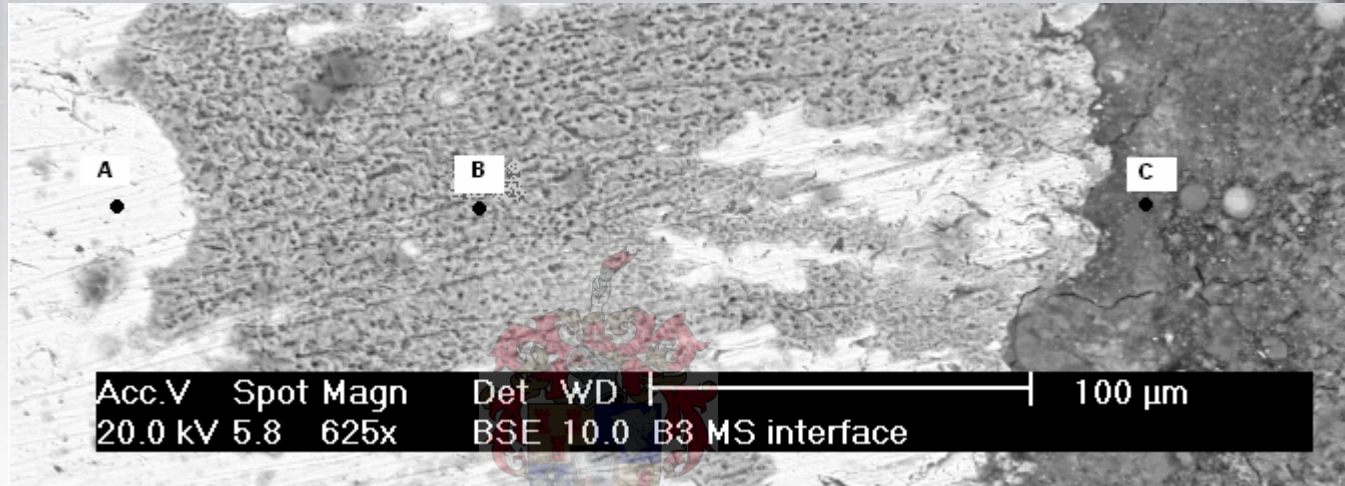
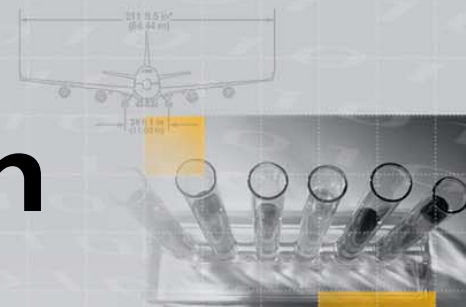
- Need to verify this Hypothesis
- Use HP at low pressure
- Check variations on Embedded sensor.



Half Cell Potential

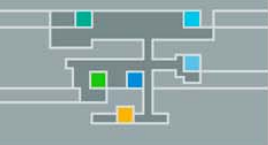


Test for corrosion

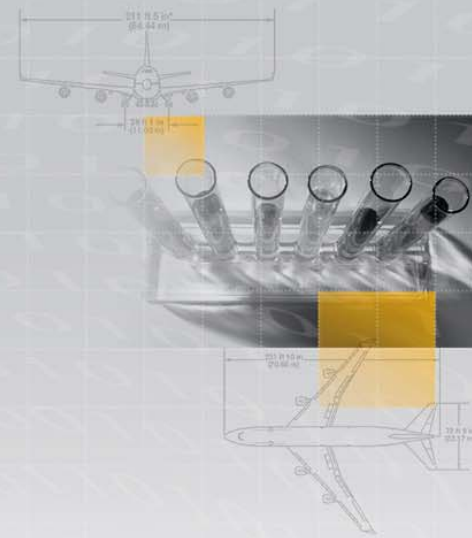




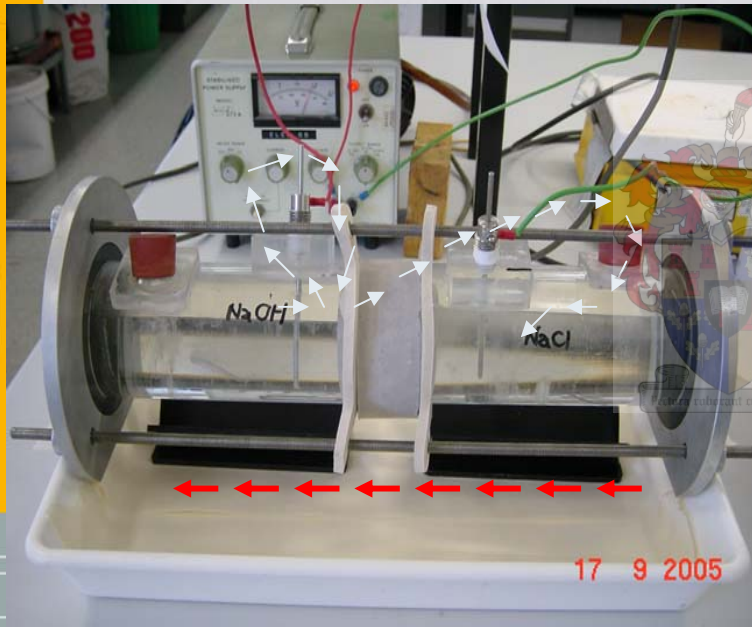
FAKULTEIT INGENIEURSWESE
FACULTY OF ENGINEERING



UNIVERSITEIT
STELLENBOSCH
UNIVERSITY

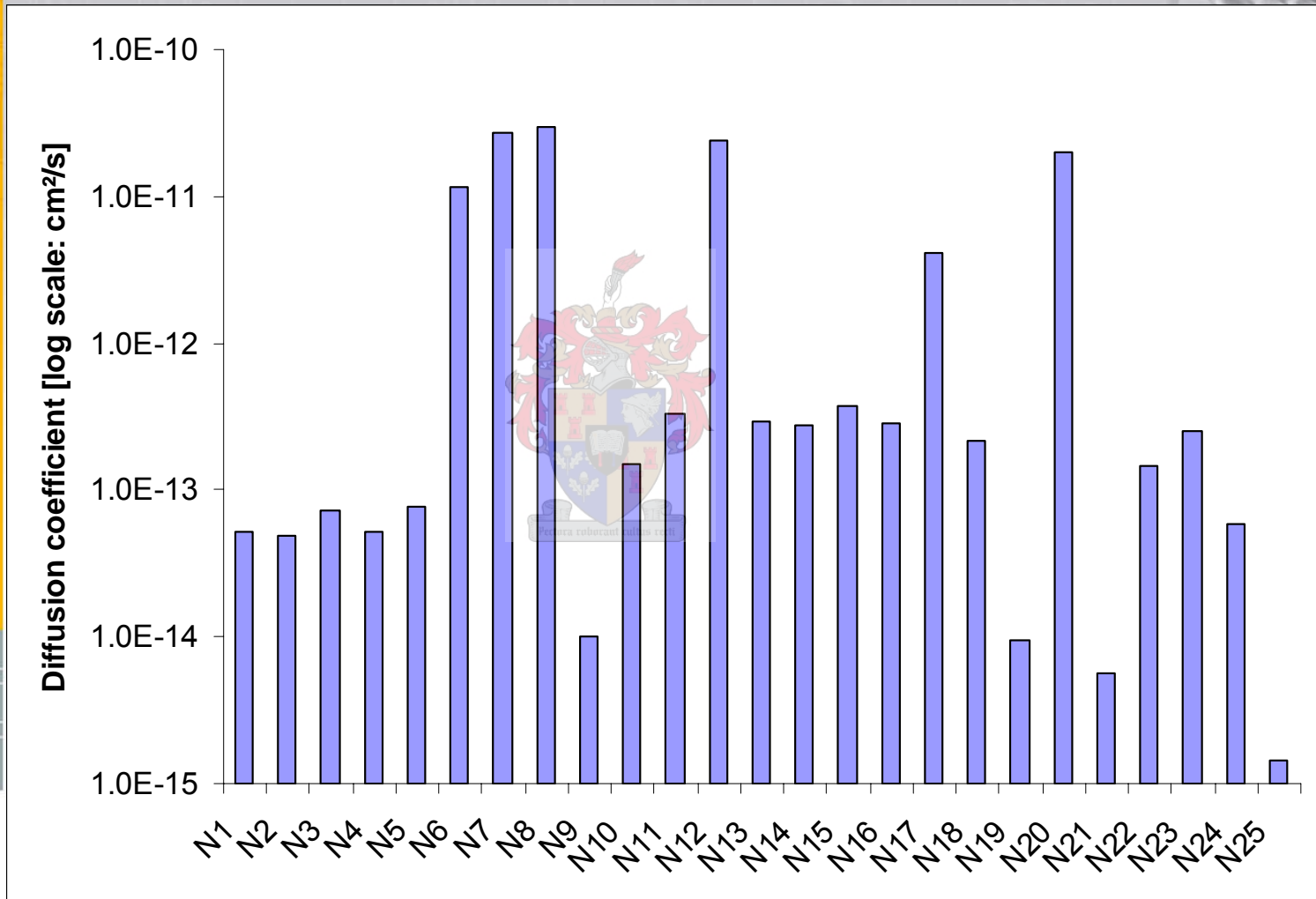


Chloride Diffusion Coefficient (CDC):



- ACID test
- Cl⁻ profiles in diffusion equation.
- Conforms to **ASTM C1202**
- Direct comparison

Geopolymer CDC



Comparative CDC

	OPC	GP
Compressive strength [MPa]	55.9	55.7
CDC [cm ² /s]	5.0E-09	1.43E-15
Curing [days]	56	28
Added Slag (wt %)	55	4.3
Fly ash (wt %)	0	24

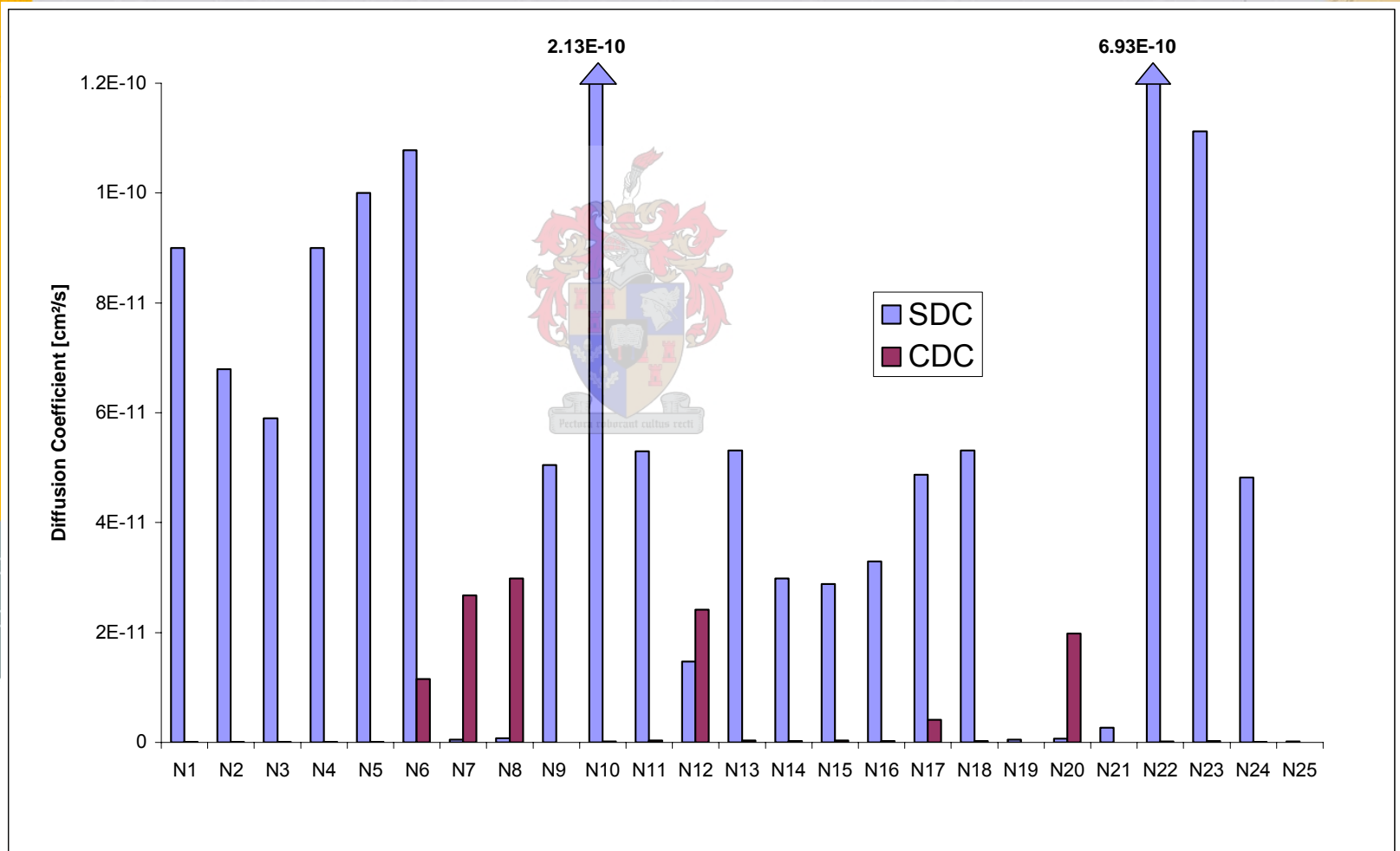
- CDC (Geopolymer) = 1.4×10^{-15} cm²/s
- CDC (OPC) = 5.0×10^{-9} cm²/s

Credible CDC Results?

- PIXE analyses (CSIRO Melbourne & iThemba labs South Africa)

Result Comparison		
Recipe	PIXE [cm ² /s]	Diffusion Cell [cm ² /s]
N1	5.030E-08	5.249E-14
N7	2.266E-13	2.678E-11
N13	3.160E-14	2.956E-13
N18	1.600E-13	2.053E-13
N22	3.289E-14	1.452E-13
N25	3.615E-15	1.433E-15

Sulphate Diffusion Coefficient (SDC)



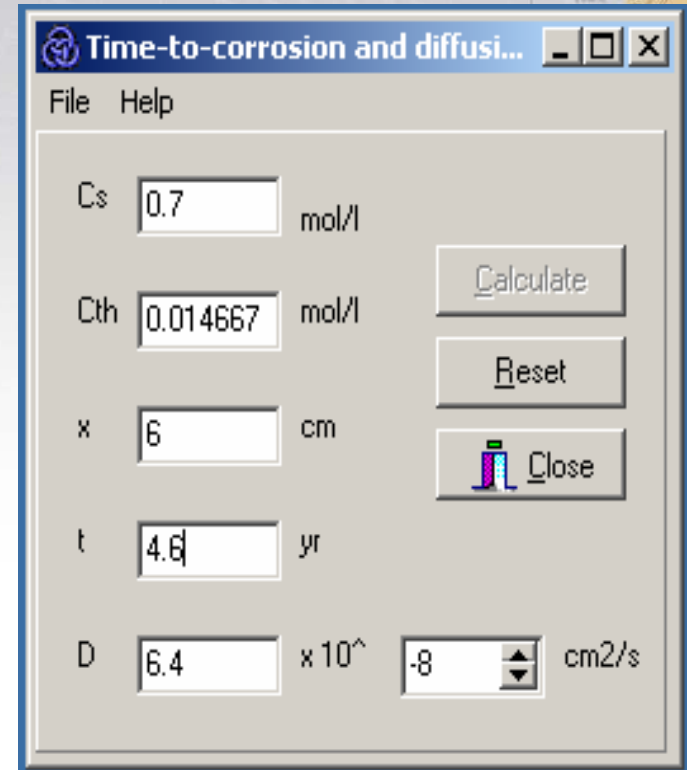
Comparative SDC

- Little literature on SDC values
- **Gospodinov et al. (1996)** following on work by **Cohen & Mathur (1991)** = 3.35×10^{-8} cm²/s for cement pastes
- **Bary & Béjaoui (2006)** = 1.0×10^{-8} cm²/s
- N25 produced a SDC of 1.59×10^{-13} cm²/s
- “Worst” performing geopolymer = 1.08×10^{-10} cm²/s.

Time-to-corrosion

- **Trejo & Pillai (2004):**
 $0.52\text{kg/m}^3 < C_{th} < 10.8\text{kg/m}^3$.
- **Thomas (1996) = 5 years**
 (providing CDC 6.4×10^{-8} cm^2/s , cover of 60mm & constant 4% external Cl-source)
- Geopolymer C_{th} unknown
- N25: $T_i = 20.5 \times 10^6$ years

$$1 - \frac{C_{th}}{C_s} = \text{erf} \left(\frac{d_c}{2\sqrt{D \cdot t}} \right)$$



Time-to-corrosion and diffusi...

File Help

Cs mol/l

Cth mol/l

x cm

t yr

D x 10⁻⁸ cm²/s

Calculate

Reset

Close

Conclusions

- GP resist Cl^- & SO_4^{2-} more effectively than OPC blends
- Enormous range of possible applications:
 - General Construction (marine area)
 - Low cost housing
 - Process Plants (bund walls)
 - Sewerage systems



Pectora roburant cultus...

Acknowledgements:

- Prof. Leon Lorenzen
- University of Melbourne
(Prof Jannie van Deventer)
- NRF (D.o.L) Scarce Skills
- NRF Mobility Fund



THE UNIVERSITY OF
MELBOURNE





??Questions??